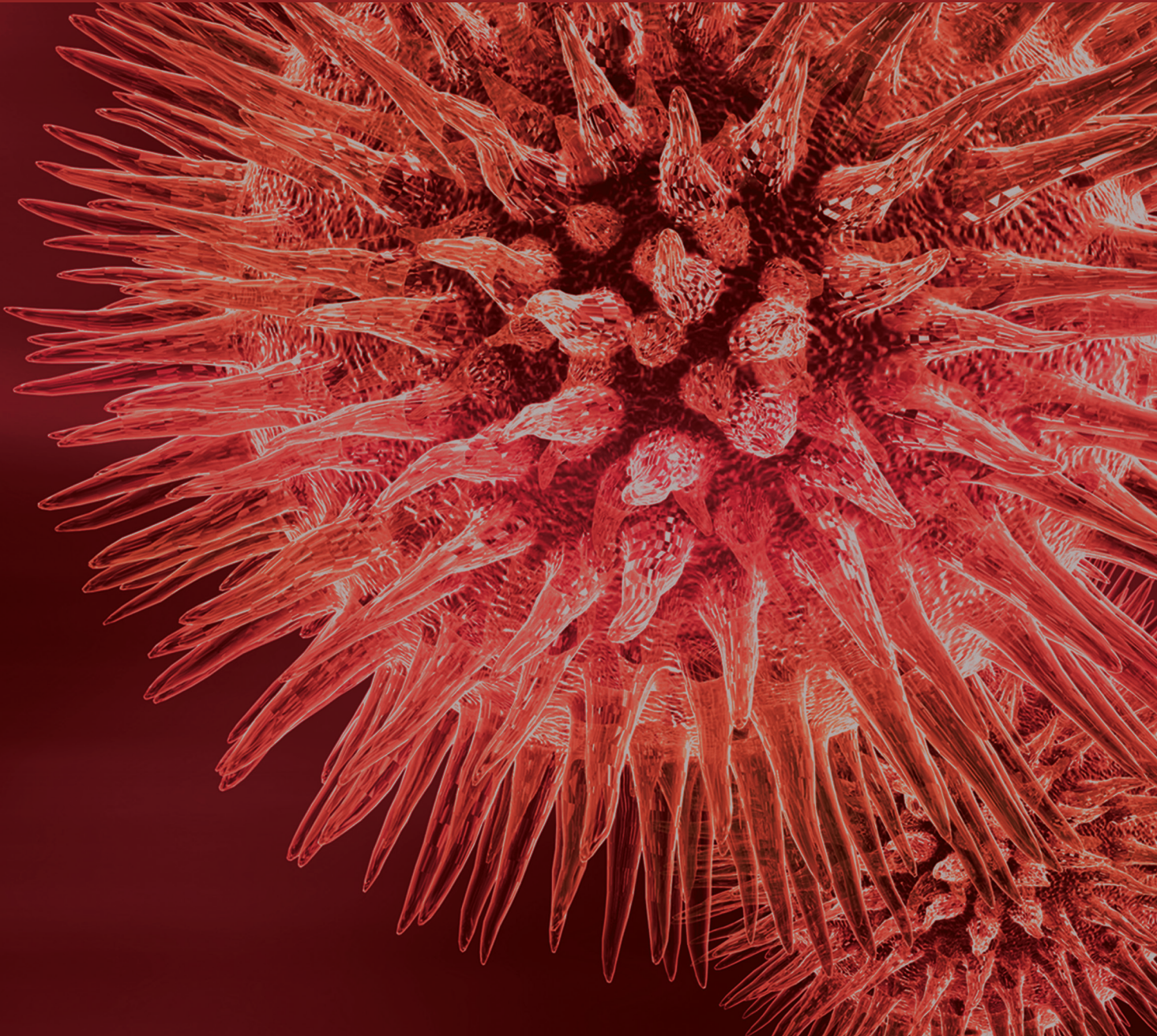# Toward a Meta-Analytic Synthesis of the Resting-State fMRI Literature for Clinical Populations

Guest Editors: Yu-Feng Zang, Xi-Nian Zuo, Micheal Milham, and Mark Hallett

Toward a Meta-Analytic Synthesis of the Resting-State fMRI Literature for Clinical Populations

Toward a Meta-Analytic Synthesis of the Resting-State fMRI Literature for Clinical Populations

Guest Editors: Yu-Feng Zang, Xi-Nian Zuo, Micheal Milham, and Mark Hallett

Contents

Editorial

Toward a Meta-Analytic Synthesis of the Resting-State fMRI Literature for Clinical Populations

Yu-Feng Zang,[1,2] Xi-Nian Zuo,[3] Michael Milham,[4,5] and Mark Hallett[6]

[1] *Center for Cognition and Brain Disorders, Hangzhou Normal University, Hangzhou 310015, China*

[2] *Zhejiang Key Laboratory for Research in Assessment of Cognitive Impairments, Hangzhou Normal University, Hangzhou 310015, China*

[3] *Key Laboratory of Behavioral Science and Magnetic Resonance Imaging Research Center, Institute of Psychology, Chinese Academy of Sciences, Beijing 100101, China*

[4] *Center for the Developing Brain, Child Mind Institute, New York, NY 10022, USA*

[5] *Center for Biomedical Imaging and Neuromodulation, Nathan S. Kline Institute for Psychiatric Research, Orangeburg, NY 10962, USA*

[6] *Human Motor Control Section, National Institute of Neurological Disorders and Stroke, NIH, Bethesda, MD 20892, USA*

Correspondence should be addressed to Yu-Feng Zang; zangyf@gmail.com

Received 10 May 2015; Accepted 10 May 2015

Coordinate-based meta-analysis (CB-meta) is playing an important role in identifying spatially consistent findings for targeted questions in the neuroimaging literature, by quantitatively aggregating independent results reported in a standard coordinate space [1]. CB-meta has been widely used in voxel-based magnetic resonance imaging (MRI) studies, including task functional MRI (fMRI), where either patterns of within-group activation or patterns of between-group activation differences can be aggregated across studies. Given that variations in task design can introduce confounds into such pursuits, researchers work to limit any effort to the inclusion of studies using highly similar tasks. Task fMRI CB-meta papers have been published in most brain disorders.

Resting-state fMRI (RS-fMRI) does not require cognitive task probes, and its design is inherently similar across studies. From this perspective, it is ideally suited for CB-meta. However, while an array of analytic methods have emerged to characterize different aspects of resting brain activity, not all of them are suitable for CB-meta. This likely explains the relatively small number of RS-fMRI based CB-meta published to date [2–8].

The analytic methods for RS-fMRI can be divided into two categories, one for depicting functional relationships between remote brain regions and another for local activity (for a systematic review, see [9]). The widely used methods in the former category include seed-based functional connectivity, spatial independent component analysis (sICA), and graph theory. The latter has two widely used methods, namely, regional homogeneity (ReHo) and amplitude of low frequency fluctuation (ALFF)/fractional ALFF (fALFF).

Seed-based functional connectivity is one of the most widely used analytic methods in RS-fMRI studies. Typically, a region of interest (ROI) is predefined and then linear correlation or linear regression analysis is performed between the mean time series of this ROI and the time series of each voxel in the brain. The results are of course dependent on the location of seed ROIs and therefore are not suitable for CB-meta. Most of the 8 CB-meta RS-fMRI papers aforementioned did not include seed-based functional connectivity studies.

Spatial independent component analysis (sICA) decomposes the RS-fMRI data into multiple networks (components), among which only about 10 networks are psychophysiologically interpretable [10]. "Spatial independent" means spatially nonoverlapping. Therefore, sICA papers should not be taken into a CB-meta study, unless different papers have focused on the same component (e.g., the default mode network). A few CB-meta RS-fMRI studies have included

sICA RS-fMRI papers [2, 4, 6, 8]. However, few explicitly mentioned the limitation of sICA for CB-meta.

Graph theory has been widely used for exploring the topological organization of complex brain networks in RS-fMRI studies. Unlike seed-based functional connectivity and sICA, which focus on a specific functional system(s), graph theory usually explores the topological properties, such as small-world, modular structure and highly connected hubs, of the entire brain. From this point of view, RS-fMRI studies using graph theory are also well suitable for meta-analysis. However, due to the high computational cost, most graph-based RS-fMRI studies have chosen a limited number of brain regions or ROIs, rather than brain voxels, as network nodes. Such results do not provide the coordinate information needed to support CB-meta. Degree centrality is one of the simplest and least computation-demanding measures for graph theory complex networks. Several RS-fMRI toolboxes (e.g., DPARSF (http://www.restfmri.net/; http://rfmri.org/) and Gretna (https://www.nitrc.org/projects/gretna/)) have included voxel-based degree centrality measurement [11, 12]. Some studies have applied voxel-based centrality to brain disorders including depression [13–15] and Alzheimer's disease [16]. In light of recent increases in computational capacity, more complicated measurements of graph theory will be implemented in a voxel-wise manner, thereby increasing the suitability of graph theory for CB-meta.

ReHo and ALFF are two methods widely used for characterizing local spontaneous activity of RS-fMRI data. ReHo measures the local synchronization of the time series of neighboring voxels [17] whereas ALFF/fALFF measures the amplitude of time series fluctuations at each voxel [18, 19]. Although both ReHo and ALFF/fALFF measure the local activity of each voxel, many studies used the two measurements and suggested that the two methods reveal different aspects of brain function and abnormalities arising in clinical populations [20–23]. For nearly all of the existing CB-meta RS-fMRI studies, researchers have combined across these methods for characterizing local activity (ReHo and/or ALFF), despite known differences in their properties. A CB-meta RS-fMRI study of depression by Iwabuchi and colleagues for the first time included RS-fMRI papers using the same analytic method (ReHo) [5]. This approach markedly reduces discrepancies in analytic methods. However, only 10 of the 200+ RS-fMRI papers on depression to date met the inclusion criteria of that CB-meta study.

Clinical studies always face the challenges of high heterogeneity and limited sample size in patient groups. Therefore, meta-analysis is critical for drawing congruent conclusion across studies carried out with similar settings and techniques. Few techniques for clinical studies enable the application of the broad range of analytic methods that RS-fMRI does in an effort to reveal the functional complexity of the human brain from multiple aspects. Although some analytic methods are not suitable for CB-meta, the strength of RS-fMRI is that its design is inherently similar across studies. Therefore, each dataset could be reanalyzed by using analytic methods being suitable to perform CB-meta. The current special issue was launched to encourage RS-fMRI studies on brain disorders by reanalyzing the published data with methods supporting future CB-meta.

In the current issue, a paper from Dr. Chunshui Yu's group in Tianjin Medical University is of particular interest (see Y. Xu et al., "Altered Spontaneous Brain Activity in Schizophrenia: A Meta-Analysis and a Large-Sample Study"). The authors not only performed two CB-meta RS-fMRI studies, in which only RS-fMRI papers using methods for local activity (ReHo and ALFF, resp.) were included, but they also validated the CB-meta results in their own dataset obtained from a relatively large sample of schizophrenia patients. One of the congruent results was that ALFF was reduced in the primary visual and primary sensorimotor cortex (see details in Y. Xu et al. "Altered Spontaneous Brain Activity in Schizophrenia: A Meta-Analysis and a Large-Sample Study"). The limitation of this study, like other CB-meta RS-fMRI studies, is the small number of eligible RS-fMRI papers. Only 6 ALFF papers and 4 ReHo RS-fMRI papers were included.

We hope this special issue will draw attention to the need for and value of CB-meta in the RS-fMRI research field. If your dataset has not been analyzed with a method that facilitates future CB-meta, please try it. Future CB-meta efforts need large numbers of studies for inclusion to enable more definitive conclusions, upon which models for the prediction or diagnosis of brain disorders can be developed. Additionally, accurate localization of abnormal spontaneous brain activity may help to guide intervention therapies (e.g., deep brain stimulation, transcranial magnetic stimulation, or transcranial ultrasound stimulation).

Yu-Feng Zang
Xi-Nian Zuo
Michael Milham
Mark Hallett

References

[1] S. B. Eickhoff, A. R. Laird, C. Grefkes, L. E. Wang, K. Zilles, and P. T. Fox, "Coordinate-based activation likelihood estimation meta-analysis of neuroimaging data: a random-effects approach based on empirical estimates of spatial uncertainty," *Human Brain Mapping*, vol. 30, no. 9, pp. 2907–2926, 2009.

[2] S. Kühn and J. Gallinat, "Resting-state brain activity in schizophrenia and major depression: a quantitative meta-analysis," *Schizophrenia Bulletin*, vol. 39, no. 2, pp. 358–365, 2013.

[3] J. Graham, G. Salimi-Khorshidi, C. Hagan et al., "Meta-analytic evidence for neuroimaging models of depression: state or trait?" *Journal of Affective Disorders*, vol. 151, no. 2, pp. 423–431, 2013.

[4] B. Sundermann, M. L. Beverborg, and B. Pfleiderer, "Toward literature-based feature selection for diagnostic classification: a meta-analysis of resting-state fMRI in depression," *Frontiers in Human Neuroscience*, vol. 8, article 692, 2014.

[5] S. J. Iwabuchi, R. Krishnadas, C. Li, D. P. Auer, J. Radua, and L. Palaniyappan, "Localized connectivity in depression: a meta-analysis of resting state functional imaging studies," *Neuroscience & Biobehavioral Reviews*, vol. 51, pp. 77–86, 2015.

[6] S. M. Palmer, S. G. Crewther, L. M. Carey, and START Project Team, "A meta-analysis of changes in brain activity in clinical depression," *Journal of Frontiers in Human Neuroscience*, vol. 8, article 1045, 2015.

[7] Z. Q. Chen, M. Y. Du, Y. J. Zhao et al., "Voxel-wise meta-analyses of brain blood flow and local synchrony abnormalities in medication-free patients with major depressive disorder," *Journal of Psychiatry & Neuroscience*, vol. 40, no. 2, Article ID 140119, 2015.

[8] Y. Hannawi, M. A. Lindquist, B. S. Caffo, H. I. Sair, and R. D. Stevens, "Resting brain activity in disorders of consciousness: a systematic review and meta-analysis," *Neurology*, vol. 84, no. 12, pp. 1272–1280, 2015.

[9] X. Zuo and X. Xing, "Test-retest reliabilities of resting-state FMRI measurements in human brain functional connectomics: a systems neuroscience perspective," *Neuroscience & Biobehavioral Reviews*, vol. 45, pp. 100–118, 2014.

[10] J. S. Damoiseaux, S. A. R. B. Rombouts, F. Barkhof et al., "Consistent resting-state networks across healthy subjects," *Proceedings of the National Academy of Sciences of the United States of America*, vol. 103, no. 37, pp. 13848–13853, 2006.

[11] Y. Chao-Gan and Z. Yu-Feng, "DPARSF: a MATLAB toolbox for 'pipeline' data analysis of resting-state fMRI," *Frontiers in System Neuroscience*, vol. 4, article 13, 2010.

[12] T. Xu, Z. Yang, L. Jiang, X.-X. Xing, and X.-N. Zuo, "A connectome computation system for discovery science of brain," *Science Bulletin*, vol. 60, no. 1, pp. 86–95, 2015.

[13] L. Wang, Z. Dai, H. Peng et al., "Overlapping and segregated resting-state functional connectivity in patients with major depressive disorder with and without childhood neglect," *Human Brain Mapping*, vol. 35, no. 4, pp. 1154–1166, 2014.

[14] L. Wang, M. Xia, K. Li et al., "The effects of antidepressant treatment on resting-state functional brain networks in patients with major depressive disorder," *Human Brain Mapping*, vol. 36, no. 2, pp. 768–778, 2015.

[15] Y. Shen, J. Yao, X. Jiang et al., "Sub-hubs of baseline functional brain networks are related to early improvement following two-week pharmacological therapy for major depressive disorder," *Human Brain Mapping*, 2015.

[16] Z. Dai, C. Yan, K. Li et al., "Identifying and mapping connectivity patterns of brain network hubs in Alzheimer's disease," *Cerebral Cortex*, 2014.

[17] Y. Zang, T. Jiang, Y. Lu, Y. He, and L. Tian, "Regional homogeneity approach to fMRI data analysis," *NeuroImage*, vol. 22, no. 1, pp. 394–400, 2004.

[18] Y. F. Zang, Y. He, C. Z. Zhu et al., "Altered baseline brain activity in children with ADHD revealed by resting-state functional MRI," *Brain & Development*, vol. 29, no. 2, pp. 83–91, 2007.

[19] Q. H. Zou, C. Z. Zhu, Y. Yang et al., "An improved approach to detection of amplitude of low-frequency fluctuation (ALFF) for resting-state fMRI: fractional ALFF," *Journal of Neuroscience Methods*, vol. 172, no. 1, pp. 137–141, 2008.

[20] D. Lei, J. Ma, X. Du, G. Shen, M. Tian, and G. Li, "Spontaneous brain activity changes in children with primary monosymptomatic nocturnal enuresis: a resting-state fMRI study," *Neurourology and Urodynamics*, vol. 31, no. 1, pp. 99–104, 2012.

[21] L. An, Q.-J. Cao, M.-Q. Sui et al., "Local synchronization and amplitude of the fluctuation of spontaneous brain activity in attention-deficit/hyperactivity disorder: a resting-state fMRI study," *Neuroscience Bulletin*, vol. 29, no. 5, pp. 603–613, 2013.

[22] E. Premi, F. Cauda, R. Gasparotti et al., "Multimodal FMRI resting-state functional connectivity in *Granulin* mutations: the case of fronto-parietal dementia," *PLoS ONE*, vol. 9, no. 9, Article ID e106500, 2014.

[23] L. Han, L. Zhaohui, Y. Fei et al., "Disrupted neural activity in unilateral vascular pulsatile tinnitus patients in the early stage of disease: evidence from resting-state fMRI," *Progress in Neuro-Psychopharmacology and Biological Psychiatry*, vol. 59, pp. 91–99, 2015.

Research Article

Decreased Resting-State Interhemispheric Functional Connectivity in Parkinson's Disease

ChunYan Luo,[1] XiaoYan Guo,[1] Wei Song,[1] Bi Zhao,[1] Bei Cao,[1] Jing Yang,[1] QiYong Gong,[2] and Hui-Fang Shang[1]

[1] *Department of Neurology, West China Hospital, Sichuan University, Chengdu, Sichuan 610041, China*
[2] *Huaxi MR Research Center (HMRRC), Department of Radiology, West China Hospital, Sichuan University, No. 37 Guo Xue Xiang Chengdu, Sichuan 610041, China*

Correspondence should be addressed to QiYong Gong; huaxi_gong@126.com and Hui-Fang Shang; hfshang2002@126.com

Background. Abnormalities in white matter integrity and specific functional network alterations have been increasingly reported in patients with Parkinson's disease (PD). However, little is known about the inter-hemispheric interaction in PD. *Methods.* Fifty-one drug naive patients with PD and 51 age- and gender-matched healthy subjects underwent resting-state functional magnetic resonance imaging (rs-fMRI) scans. We compared the inter-hemispheric resting-state functional connectivity between patients with PD and healthy controls, using the voxel-mirrored homotopic connectivity (VMHC) approach. Then, we correlated the results from VMHC and clinical features in PD patients. *Results.* Relative to healthy subject, patients exhibited significantly lower VMHC in putamen and cortical regions associated with sensory processing and motor control (involving sensorimotor and supramarginal cortex), which have been verified to play a critical role in PD. In addition, there were inverse relationships between the UPDRS motor scores and VMHC in the sensorimotor, and between the illness duration and VMHC in the supramarginal gyrus in PD patients. *Conclusions.* Our results suggest that the functional coordination between homotopic brain regions is impaired in PD patients, extending previous notions about the disconnection of corticostriatal circuit by providing new evidence supporting a disturbance in inter-hemispheric connections in PD.

1. Introduction

Parkinson's disease (PD), the second most common neurodegenerative disease worldwide, is characterized by cardinal motor symptoms including tremor, rigidity, bradykinesia, and postural instability. It has been suggested that some motor symptoms in PD might result from impaired sensorimotor integration, in which both deficient afferent external information and high-order cognitive process might play an important role [1, 2]. Some progressive impairment in PD might be a reflection of alterations in integrity of distributed brain networks with resultant reduced information integration capacity between brain regions.

Previous studies have demonstrated that human with sectioned corpus callosum had deficits in the sensory, motor, and cognitive processing [3–6], highlighting the importance of inter-hemispheric coordination to human behaviors. Inter-hemispheric coordination especially is needed for the execution of complex tasks [7, 8]. However, the inter-hemispheric coordination in PD is still an unexplored field. PD is usually of unilateral onset, providing evidence of inter-hemispheric dissociations and an imbalance between activity of the left and right hemisphere [9]. Abnormalities in the corpus callosum and widely impaired white matter integrity in the frontal, temporal, and parietal lobes have been reported in PD patients, which may affect inter-hemispheric functional coordination [10–12]. In addition, preliminary evidence from electroencephalography (EEG) study has suggested impaired inter-hemispheric coordination in patients with PD [13]. Given the importance of bihemispheric coordination for

sensory, motor and cognitive processing, and the core motor symptoms in PD, it is reasonable to expect that inter-hemispheric interaction deficits played a key role in the pathophysiology of PD. Therefore, it would be meaningful to examine the inter-hemispheric coordination in PD.

Resting-state fMRI (rs-fMRI), which captures the patterns of coherent spontaneous fluctuations of blood oxygen level dependent (BOLD) signals [14] during rest, can be used to measure the inter-hemispheric coordination. Functional homotopy, defined as the high degree of synchrony in spontaneous activity between geometrically corresponding inter-hemispheric regions, has been suggested to be a key characteristic of the brain's intrinsic functional architecture [15, 16]. Thus, homotopic resting-state functional connectivity (RSFC) may be a sensitive index for detecting the PD-related inter-hemispheric coordination alterations. Here, we examined homotopic RSFC in patients PD using a recently validated approach named "voxel-mirrored homotopic connectivity (VMHC) [17]." Different strengths of VMHC between different symmetric regions could represent different characteristics of hemispheric specialization in the information processing, sensory integration, and motor coordination [16]. Using the VMHC method, abnormal homotopic RSFC has been demonstrated in schizophrenia [18], autism [19], depression [20, 21], and cocaine addiction [22].

In neurodegenerative diseases, as a diseases process evokes a cascade of pathophysiologic changes, it is important to examine an early stage of the disease that is minimally affected by other confounding factors such as treatment. To minimize the effect of such confounding factors, only drug naive patients with PD were recruited in the present study. Given the extensive evidence of functional disconnections and asymmetry in PD, we hypothesized that an impairment of inter-hemispheric functional coordination may be involved in the pathogenesis of PD, which would be reflected as reduced homotopic RSFC in PD patients. In addition, the values of VMHC might be correlated with the severity of PD symptoms. The greater symptom severity will be associated with lower VMHC values.

2. Methods

2.1. Participant. Patients with PD were recruited from Movement Disorders Outpatient Clinic of West China Hospital of Sichuan University from January 2010 to February 2012. All PD patients were diagnosed based on the UK PD Society Brain Bank Clinical Diagnostic Criteria. Patients with secondary Parkinsonism and Parkinson-plus syndrome were excluded from this study. At the inclusion to the study, all the patients should have never been treated with anti-Parkinson medications at the initial visit. Patients were excluded if they had (1) moderate-severe head tremor; (2) H-Y stage ≥ 3; (3) disease duration ≥ 4 years; (4) a history of head injury, stroke, or other neurological diseases; (5) dementia; (6) any disorder that interfered with the assessment of the manifestation of PD. In addition, patients with poor response to dopaminergic medication or emergence of non-Parkinsonism symptoms during follow-up period (rang from 12 months to 36 months) will be excluded from the study. Finally, 51 PD patients were

TABLE 1: Demographic and clinical characteristics for Parkinson's disease.

	PD ($N = 51$)	Control ($N = 51$)
Age (years)	52.83 ± 8.68	52.24 ± 8.66
Handedness for writing (R : L)	51 : 0	51 : 0
Gender (female : male)	24 : 27	24 : 27
Disease duration (years)	1.68 ± 1.02	—
H & Y stage	1.82 ± 0.62	—
UPDRS scores		
Part I—nM-EDL	2.28 ± 2.15	—
Part II—M-EDL	7.96 ± 4.45	—
Part III—motor examination	24.39 ± 11.62	—
Part IV—motor complications	0	—
Total UPDRS scores	34.43 ± 16.60	—
MMSE scores	27.67 ± 2.67	—

Data are presented as mean ± SD. H & Y = Hoehn & Yahr staging; MMSE = Mini-Mental State Exam; UPDRS = Unified Parkinson's Disease Rating Scale; nM-EDL: Nonmotor Aspects of Experiences of Daily Living; M-EDL: Motor Aspects of Experiences of Daily Living.

included in the study. Most of those subjects are from the same cohort that we used in another recently published work [23]. Functional images were also acquired at initial visit of these patients. The demographic features and clinical data, including age, age of onset, gender, diagnostic delay, and disease duration were collected using a standard questionnaire by a movement disorder specialist during face-to-face interviews at the initial visit. The Unified PD Rating Scale (UPDRS) part III was used to assess the motor disability, and Hoehn and Yahr (H&Y) stage was used to evaluate disease severity. Mini-Mental State Exam (MMSE) was used to evaluate cognition. The ratings were performed blinded to the MRI dataset.

Additionally, 51 right-handed healthy control subjects were recruited from local area by poster advertisements. Control subjects will be excluded if they have (1) any neurological illness, as assessed according to clinical evaluations and medical records and (2) organic brain defects on T1 or T2 images. All the controls were matched for age and sex to patients with PD. The demographic and clinical characteristics of the enrolled subjects are summarized in Table 1. The local research ethics committee approved this study, and written informed consent was obtained from all subjects.

2.2. MRI Acquisition. MRI was performed on a 3.0 Tesla (T) MR imaging system (Excite; GE, Milwaukee, WI) by using an eight-channel phased-array head coil. High-resolution T1-weighted images were acquired via a volumetric three-dimensional spoiled gradient recall sequence (TR = 8.5 msec, echo time = 3.4 msec, flip angle = 12°, slice thickness = 1 mm). Field of view (240×240 mm^2) was used with an acquisition matrix comprising 256 readings of 128 phase encoding steps that produced 156 contiguous coronal slices, with a slice thickness of 1.0 mm. The final matrix size of T1-weighted images was automatically interpolated in-plane to 512×512, which yielded an in-plane resolution of 0.47×0.47 mm^2.

MR images sensitive to changes in BOLD signal levels (TR = 2000 msec, echo time = 30 msec, flip angle = 90°) were obtained via a gradient-echo echo-planar imaging sequence (EPI). The slice thickness was 5 mm (no slice gap) with a matrix size of 64 × 64 and a field of view of 240 × 240 mm^2, resulting in a voxel size of $3.75 \times 3.75 \times 5$ mm^3. Each brain volume comprised 30 axial slices and one functional run contained 200 image volumes. The fMRI scanning was performed in darkness, and the participants were explicitly instructed to relax and close their eyes and not to fall asleep (confirmed by subjects immediately after the experiment) during the resting-state MR acquisition. Earplugs were used to reduce scanner noise, and head motion was minimized by stabilizing the head with cushions.

2.3. Preprocessing of fMRI Data Analysis. R-fMRI data preprocessing was then conducted by SPM8 software package (http://www.fil.ion.ucl.ac.uk/spm/), REST (http://restfmri .net/forum/rest) and Data Processing Assistant for Resting-State fMRI (DPARSF) [24]. Briefly, the preprocessing steps included the following steps: (1) removal of first 10 time points due to allowing for magnetization equilibrium and the subjects' adaptation to the environment; (2) correction for differences in the image acquisition time between slices; (3) six parameter rigid body spatial transformation to correct for head motion during data acquisition; (4) coregistration of the T1 image to the mean EPI scans; (5) grey and white matter segmentation using "New Segment" and spatial normalization of the structural image to a standard template (Montreal Neurological Institute) by DARTEL "normalization"; (6) spatial normalization of the EPI images using the normalization parameters estimated in the previous preprocessing step and resampling to $3 \times 3 \times 3$ mm^3; (7) spatial smoothing with a 6 mm full width half maximum Gaussian kernel; (8) temporally bandpass filtering (0.01–0.08 Hz) and linearly detrended removal; (9) regressing eight nuisance covariates, including the white matter signal, the cerebral spinal fluid signal, and six head motion parameters, to remove the possible variances from time course of each voxel.

According to the record of head motions within each fMRI run, all participants had less than 1.5 mm maximum displacement in the x, y, or z plane and less than 1.5° of angular rotation about each axis. We also calculated the mean head translation, mean head rotation, and framewise displacement (FD) [25, 26] for each group. Analysis of those head motion parameters did not reveal differences between the control group and the patient group ($P > 0.05$).

2.4. Voxel-Mirrored Homotopic Connectivity Computation. VMHC assumes symmetric morphology between hemispheres. To account for differences in the geometric configuration of the cerebral hemispheres, we firstly averaged the normalized T1 images of all subjects to create a mean normalized T1 image. This image was then averaged with its left-right mirrored version to generate a group-specific symmetrical T1 template. After that, the individual T1 images in MNI space were nonlinearly registered to the symmetrical T1 template and those transformations were applied to the above

processed functional data. The VMHC computation was performed with software REST. For each participant, the homotopic RSFC was computed as the Pearson correlation coefficient between each voxel's residual time series and that of its symmetrical inter-hemispheric counterpart. Correlation values were then Fisher z-transformed to improve the normality. The resultant values were referred to as the VMHC and were applied for the group comparisons.

2.5. Statistical Analysis. When appropriate, two-sample t-test and Chi-square tests were performed to assess the differences in demographic and clinical data between PD patients and controls. A two-tailed P value of 0.05 was deemed significant. To test for regional group differences in VMHC, individual-level VHMC maps were entered into a group-level voxelwise t-test. Significant differences of VMHC between PD patients and controls were set at the threshold of voxelwise $P < 0.001$ and cluster level of cluster size >100 voxel and $P < 0.05$ corrected by familywise error (FWE) correction.

Once significant group differences were observed in any brain areas, we further assessed the relationships between these VMHC values and clinical variables (disease duration and UPDRS-III scores). Pearson correlation analyses were performed, and the significance was set at $P < 0.05$ (two-tailed).

3. Results

3.1. Demographic and Clinical Characteristics. Age, sex, and handedness were not significantly different between the patients group and the healthy control group. Patients were at early stage of PD with mean disease duration of 1.68 ± 1.02 years (defined as the time since symptom onset). The average H&Y stage was 1.82 ± 0.62. The average motor score on the UPDRS was 24.39 ± 11.62. The clinical data of PD patients are shown in Table 1.

3.2. Regional Variation in Voxel-Mirrored Homotopic Connectivity. Homotopic RSFC was a robust global brain phenomenon, with regional differences in strength (Figure S1 in the Supplementary Material available online at http://dx.doi .org/10.1155/2015/692684), which is consistent with previous work [17]. Group comparisons revealed that patients exhibited lower VMHC than healthy subjects in putamen, sensorimotor cortex (involving precentral, postcentral gyrus and paracentral lobe), and the supramarginal cortex. No region showed greater VMHC in the patient group than in the control group. Figure 1 and Table 2 showed the group comparisons of VMHC values between patients and healthy subjects.

3.3. Correlations between VMHC and Clinical Characteristics. The mean VMHC values were extracted in the three regions with significant group differences. Pearson correlations were performed between VMHC and UPDRS motor scores and duration in the patient group. Significantly negative correlation was observed between VMHC in the primary sensorimotor cortex and the UPDRS motor scores ($P < 0.01$) (Figure 2). A trend of negative correlation between VMHC
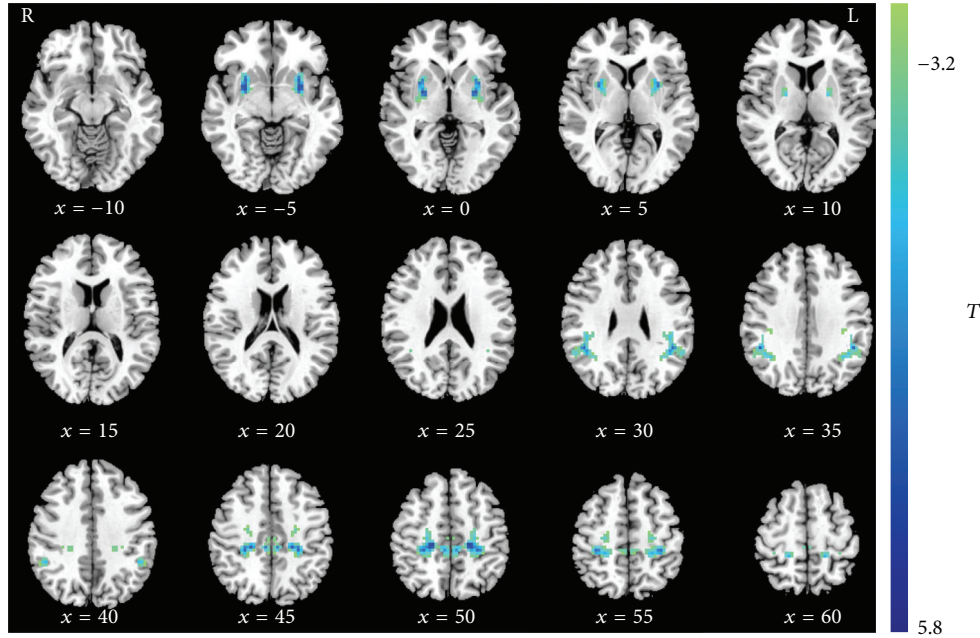
FIGURE 1: Regions showing significant differences in VMHC between PD patients and healthy controls. Blue colors indicate reduced VMHC in patients compared to the controls. The threshold was set at a corrected $P < 0.001$. The color bar indicates the T value from t-test between groups. VMHC = voxel-mirrored homotopic connectivity.

TABLE 2: Regions showing significant differences in VMHC between PD patients and healthy controls.

Cluster location	Peak MNI coordinates			Cluster voxels	Peak T
	X	Y	Z		
Putamen	±27	−3	−3	141	5.8
Sensorimotor cortex	±18	−27	48	235	5.44
Supramarginal gyrus	±48	−45	33	104	4.77

in supramarginal cortex and the UPDRS motor scores was also observed ($P = 0.06$). In addition, VMHC in the supramarginal cortex was also negatively correlated with disease duration ($P = 0.02$) (Figure 2). No significant correlation was found between VMHC in putamen and clinical variables.

4. Discussion

Homotopic RSFC is one of the most salient characteristics of the brain's intrinsic functional architecture, and many R-fMRI studies have noted the striking degree of homotopic RSFC [15, 16, 27–29]. Stronger and weaker homotopic RSFC are interpreted as indexing tendencies toward inter-hemispheric coordinated or independent processing, respectively [17]. Here, VMHC was applied for the first time to investigate inter-hemispheric RSFC in PD. Relative to healthy subject, patients exhibited lower VMHC in putamen and cortical regions associated with sensory processing and motor control, which have been verified to play a critical role in the pathology of PD. In addition, there were inverse relationships between the degree of motor disability and VMHC in the sensorimotor regions and between the illness duration and VMHC of the supramarginal gyrus in PD patients.

Parkinson's disease (PD) is characterized by a degeneration of dopaminergic cells in the substantia nigra (SN) pars compacta, which leads to dopamine depletion in the striatum. Putamen is the striatal structure that suffers most from nigro-striatal dopamine depletion. Consistent with its important role in the pathology of PD, we demonstrate lower VMHC value in putamen in patients with PD relative to healthy controls. PD patient typically has a unilateral motor onset, and although the disease becomes bilateral, the initial side commonly remains more afflicted than the later-involved side. This is associated with uneven degeneration of dopaminergic neurons in the nigrostriatal pathway [30]. PD patients with moderate to severe bilateral motor disability still show considerable asymmetry in the putamen and caudate, with relatively reduced DA activity contralateral to the initial motor symptom side [31]. The decreased homotopic RSFC in putamen detected by our study is likely to be associated with the asymmetrical dopamine depletion in putamen.

We also observed a decrease in inter-hemispheric RSFC in some cortical regions, involving primary somatosensory, motor, and supramarginal cortex. Primary sensorimotor cortex is the key structure of sensorimotor circuits, the dysfunction of which has been recognized as a crucial reason
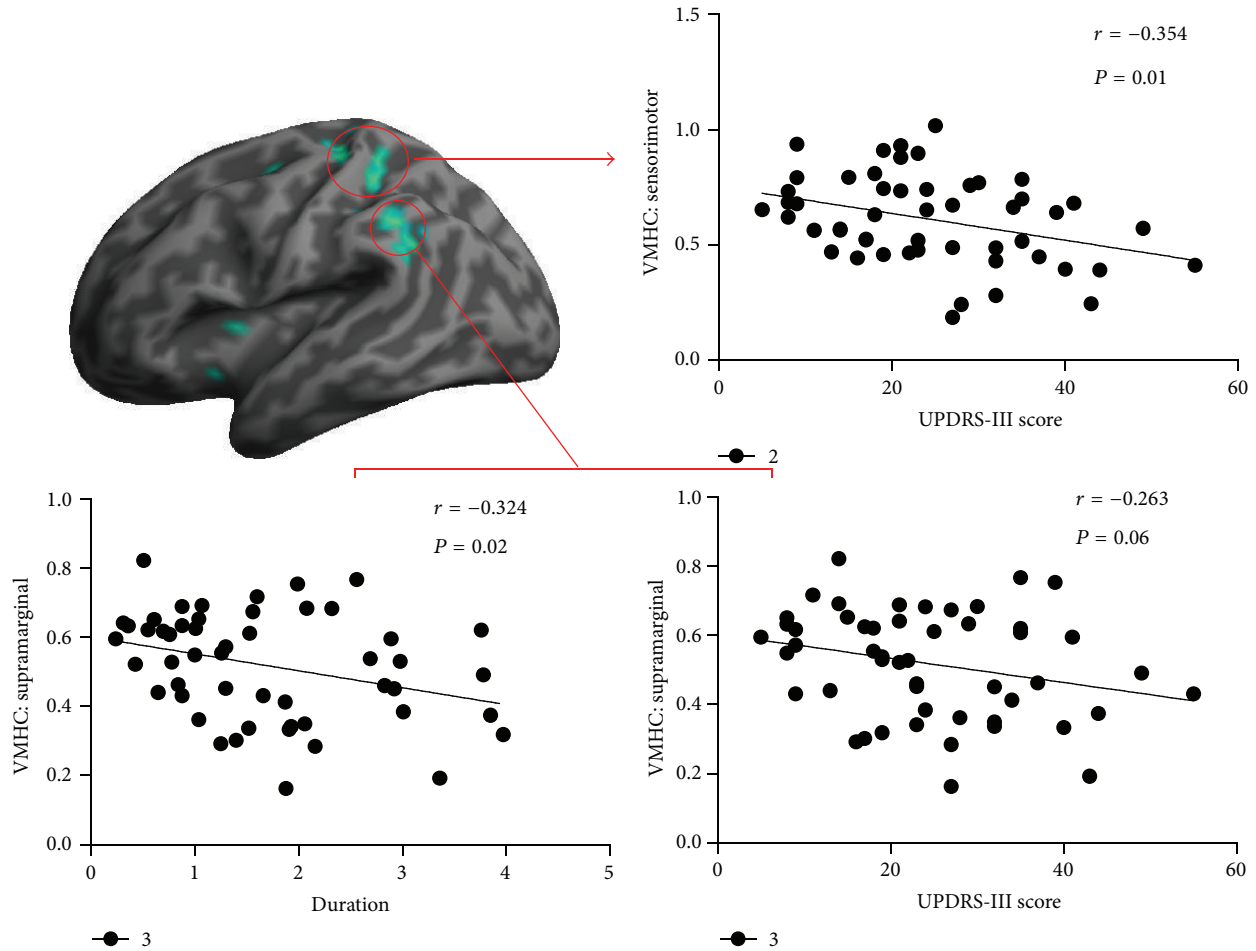
FIGURE 2: Correlations between the VMHC values and clinical measures in the patient group. VMHC = voxel-mirrored homotopic connectivity; UPDRS = Unified Parkinson's Disease Rating Scale.

for motor difficulties in PD [32]. Abnormal blood oxygenation level dependent (BOLD) fMRI activation and baseline metabolism/perfusion have been reported previously in primary sensorimotor regions in patients with PD [33–37]. Inferior parietal cortex (including supramarginal cortex) is known to be a high-order sensory association area [38, 39] that receives multimdoal sensory afferents and contributes to prception of body scheme and the sensorimtor integration [40, 41]. Disturbed activity and connectivity in this area have also been reported during rest and task-related processes in PD patients [42, 43]. Besides, structural difference in sensorimotor and supramarginal cortex have also been reported in PD [11, 44, 45]. Our results are consistent with the previous finding.

In healthy subjects, the brain motor networks must maintain a dynamic equilibrium during the resting state to integrate bilateral sensory/motor information and be ready to perform a future motor task [46], which requires relatively stringent inter-hemispheric interaction. Accordingly, sensory/motor regions have been demonstrated to exhibited stronger homotopic RSFC than hemispherically specialized frontal and parietal association cortex [16] and increased homotopic RSFC with developmental maturation [17]. Generally, it can be more efficient for the two hemispheres to interact than for one hemisphere to perform all of the processing [47]. If the inter-hemispheric interaction between sensorimotor cortex is disrupted in the resting state, it might lead to deficient inter-hemispheric cooperation, lack of ability to handle complex tasks, and disturbances of sensory processing, and sensorimotor integration, thus contributing to motor impairment. Supporting this, one rs-fMRI study [48] demonstrates that loss and recovery of sensorimotor function decline were paralleled by deterioration and subsequent retrieval of inter-hemispheric functional connectivity within the sensorimotor system in poststroke patients. Consistent with the previous study, our study found a negative correlation between UPDRS motor scores and VMHC in the primary sensorimotor and supramarginal cortex, suggesting deficient inter-hemispheric interaction as a potential mechanism for motor impairment in PD.

A negative correlation was also found between the disease duration and VMHC in the supramarginal cortex, suggesting

that this region may have a role in the chronicity of PD. In accordance with our study, a previously published study found an inverse correlation between the cortical thinning of bilateral supramarginal gyrus and illness duration/UPDRS motor score in PD patients [45]. Given that all patients in this study were in early stage with relatively short disease durations, this finding needs to be confirmed in patients with longer illness duration.

It is of interest to speculate on the potential underlying mechanisms of the VMHC deficits which we have demonstrated. They could be related to widespread white matter integrity abnormalities observed in PD. Particularly, deficits in white matter integrity of corpus callosum, the major white matter tract connecting homologous regions of the left and right hemisphere, could disrupt the synchrony between homotopically connected regions. Although the callosum is the largest conduit for information transfer and coordination between the hemispheres, alternative pathways (e.g., subcortical) exist. Homotopic regions with few monosynaptic callosal connections also demonstrated strong resting-state FC [49, 50]. Even studies on split-brain patients have found that a normal complement of resting-state networks and intact functional coupling between hemispheres can emerge in the absence of the corpus callosum [51]. Thus, though with few callosal connections, putamen exhibited decreased interhemispheric RSFC in PD which is congruent with the above findings. Anotherexplanation, not mutually exclusive, is that asymmetrical dysregulation of the striatum may in turn lead to further asymmetrical dysfunction of neural circuits that include the basal ganglia and cortical areas. The neurochemical alteration in the basal ganglia impairs neuronal processing and could propagate, through the dense corticostriatal connections, to altered activity in cortical regions. Therefore, the VMHC deficits in sensorimotor regions and putamen could both be related to asymmetrical dopamine depletion in putamen. Further studies are needed to elucidate the mechanism underlying the VMHC alterations in PD.

Several other limitations should be noted. First, there are existing asymmetries in cortical structure. We attempted to mitigate these issues by using a symmetric template. However, the effects of methodological symmetry could not be completely eliminated. Also, the cross-sectional design might limit the interpretations of our results. Whether these regions with abnormal VMHC change dynamically needs to be explored in further longitudinal study. Finally, we recruited only drug naïve patients to reduce effects of confounding factors such as treatment. For the same reason, the present findings might be compounded by a selection bias since drug naive subjects are generally in their early stage.

In summary, we found reduced inter-hemispheric functional connectivity in the key regions of corticostriatal circuit in patients with PD during resting state. This finding extends previous notions about the disconnection of corticostriatal circuit in PD by providing new evidence supporting a disturbance in inter-hemispheric connections in PD. Furthermore, the inverse relations between the motor ability and VMHC of the sensorimotor regions observed in our patients suggest potential clinical implication of VMHC measure for PD.

Conflict of Interests

The authors declare that there is no conflict of interests regarding the publication of this paper.

References

[1] N. Georgiou, R. Iansek, J. L. Bradshaw, J. G. Phillips, J. B. Mattingley, and J. A. Bradshaw, "An evaluation of the role of internal cues in the pathogenesis of parkinsonian hypokinesia," *Brain*, vol. 116, part 6, pp. 1575–1587, 1993.

[2] T. Bäumer, P. P. Pramstaller, H. R. Siebner et al., "Sensorimotor integration is abnormal in asymptomatic Parkin mutation carriers: a TMS study," *Neurology*, vol. 69, no. 21, pp. 1976–1981, 2007.

[3] S. J. Dimond, "Tactual and auditory vigilance in split-brain man," *Journal of Neurology Neurosurgery and Psychiatry*, vol. 42, no. 1, pp. 70–74, 1979.

[4] S. J. Dimond, "Performance by split-brain humans on lateralized vigilance tasks," *Cortex*, vol. 15, no. 1, pp. 43–50, 1979.

[5] H. C. Sauerwein and M. Lassonde, "Cognitive and sensorimotor functioning in the absence of the corpus callosum: neuropsychological studies in callosal agenesis and callosotomized patients," *Behavioural Brain Research*, vol. 64, no. 1-2, pp. 229–240, 1994.

[6] H. C. Sauerwein and M. Lassonde, "Neuropsychological alterations after split-brain surgery," *Journal of Neurosurgical Sciences*, vol. 41, no. 1, pp. 59–66, 1997.

[7] D. H. Weissman and M. T. Banich, "The cerebral hemispheres cooperate to perform complex but not simple tasks," *Neuropsychology*, vol. 14, no. 1, pp. 41–59, 2000.

[8] A. Belger and M. T. Banich, "Interhemispheric interaction affected by computational complexity," *Neuropsychologia*, vol. 30, no. 10, pp. 923–929, 1992.

[9] A. Cronin-Golomb, "Parkinson's disease as a disconnection syndrome," *Neuropsychology Review*, vol. 20, no. 2, pp. 191–208, 2010.

[10] T. R. Melzer, R. Watts, M. R. Macaskill et al., "White matter microstructure deteriorates across cognitive stages in Parkinson disease," *Neurology*, vol. 80, no. 20, pp. 1841–1849, 2013.

[11] H. J. Kim, S. J. Kim, H. S. Kim et al., "Alterations of mean diffusivity in brain white matter and deep gray matter in Parkinson's disease," *Neuroscience Letters*, vol. 550, pp. 64–68, 2013.

[12] G. Gattellaro, L. Minati, M. Grisoli et al., "White matter involvement in idiopathic Parkinson disease: a diffusion tensor imaging study," *The American Journal of Neuroradiology*, vol. 30, no. 6, pp. 1222–1226, 2009.

[13] R. Yuvaraj, M. Murugappan, N. M. Ibrahim et al., "Interhemispheric EEG coherence analysis in Parkinson's disease: assessing brain activity during emotion processing," *Journal of Neural Transmission*, 2014.

[14] M. D. Fox and M. E. Raichle, "Spontaneous fluctuations in brain activity observed with functional magnetic resonance imaging," *Nature Reviews Neuroscience*, vol. 8, no. 9, pp. 700–711, 2007.

[15] R. Salvador, J. Suckling, M. R. Coleman, J. D. Pickard, D. Menon, and E. Bullmore, "Neurophysiological architecture of functional magnetic resonance images of human brain," *Cerebral Cortex*, vol. 15, no. 9, pp. 1332–1342, 2005.

[16] D. E. Stark, D. S. Margulies, Z. E. Shehzad et al., "Regional variation in interhemispheric coordination of intrinsic hemodynamic fluctuations," *The Journal of Neuroscience*, vol. 28, no. 51, pp. 13754–13764, 2008.

[17] X. N. Zuo, C. Kelly, A. di Martino et al., "Growing together and growing apart: regional and sex differences in the lifespan developmental trajectories of functional homotopy," *Journal of Neuroscience*, vol. 30, no. 45, pp. 15034–15043, 2010.

[18] M. J. Hoptman, X.-N. Zuo, D. D'Angelo et al., "Decreased interhemispheric coordination in schizophrenia: a resting state fMRI study," *Schizophrenia Research*, vol. 141, no. 1, pp. 1–7, 2012.

[19] J. S. Anderson, T. J. Druzgal, A. Froehlich et al., "Decreased interhemispheric functional connectivity in autism," *Cerebral Cortex*, vol. 21, no. 5, pp. 1134–1146, 2011.

[20] L. Wang, K. Li, Q.-E. Zhang et al., "Interhemispheric functional connectivity and its relationships with clinical characteristics in major depressive disorder: a resting state fMRI study," *PLoS ONE*, vol. 8, no. 3, Article ID e60191, 2013.

[21] W. Guo, F. Liu, Y. Dai et al., "Decreased interhemispheric resting-state functional connectivity in first-episode, drug-naive major depressive disorder," *Progress in Neuro-Psychopharmacology and Biological Psychiatry*, vol. 41, pp. 24–29, 2013.

[22] C. Kelly, X. N. Zuo, K. Gotimer et al., "Reduced interhemispheric resting state functional connectivity in cocaine addiction," *Biological Psychiatry*, vol. 69, no. 7, pp. 684–692, 2011.

[23] C. Luo, W. Song, Q. Chen et al., "Reduced functional connectivity in early-stage drug-naive Parkinson's disease: a resting-state fMRI study," *Neurobiology of Aging*, vol. 35, no. 2, pp. 431–441, 2014.

[24] Y. Chao-Gan and Z. Yu-Feng, "DPARSF: a MATLAB toolbox for "pipeline" data analysis of resting-state fMRI," *Frontiers in Systems Neuroscience*, vol. 4, article 13, 2010.

[25] J. D. Power, K. A. Barnes, A. Z. Snyder, B. L. Schlaggar, and S. E. Petersen, "Spurious but systematic correlations in functional connectivity MRI networks arise from subject motion," *NeuroImage*, vol. 59, no. 3, pp. 2142–2154, 2012.

[26] K. R. A. van Dijk, M. R. Sabuncu, and R. L. Buckner, "The influence of head motion on intrinsic functional connectivity MRI," *NeuroImage*, vol. 59, no. 1, pp. 431–438, 2012.

[27] B. Biswal, F. Z. Yetkin, V. M. Haughton, and J. S. Hyde, "Functional connectivity in the motor cortex of resting human brain using echo-planar MRI," *Magnetic Resonance in Medicine*, vol. 34, no. 4, pp. 537–541, 1995.

[28] S. M. Smith, P. T. Fox, K. L. Miller et al., "Correspondence of the brain's functional architecture during activation and rest," *Proceedings of the National Academy of Sciences of the United States of America*, vol. 106, no. 31, pp. 13040–13045, 2009.

[29] H. Liu, S. M. Stufflebeam, J. Sepulcre, T. Hedden, and R. L. Buckner, "Evidence from intrinsic activity that asymmetry of the human brain is controlled by multiple factors," *Proceedings of the National Academy of Sciences of the United States of America*, vol. 106, no. 48, pp. 20499–20503, 2009.

[30] P. A. Kempster, W. R. G. Gibb, G. M. Stern, and A. J. Lees, "Asymmetry of substantia nigra neuronal loss in Parkinson's disease and its relevance to the mechanism of levodopa related motor fluctuations," *Journal of Neurology Neurosurgery and Psychiatry*, vol. 52, no. 1, pp. 72–76, 1989.

[31] A. Antonini, P. Vontobel, M. Psylla et al., "Complementary positron emission tomographic studies of the striatal dopaminergic system in Parkinson's disease," *Archives of Neurology*, vol. 52, no. 12, pp. 1183–1190, 1995.

[32] S. T. Grafton, R. S. Turner, M. Desmurget et al., "Normalizing motor-related brain activity: subthalamic nucleus stimulation in Parkinson disease," *Neurology*, vol. 66, no. 8, pp. 1192–1199, 2006.

[33] R. C. Helmich, B. R. Bloem, and I. Toni, "Motor imagery evokes increased somatosensory activity in parkinson's disease patients with tremor," *Human Brain Mapping*, vol. 33, no. 8, pp. 1763–1779, 2012.

[34] A. Maillet, A. Krainik, B. Debû et al., "Levodopa effects on hand and speech movements in patients with Parkinson's disease: a FMRI study," *PLoS ONE*, vol. 7, no. 10, Article ID e46541, 2012.

[35] S. Thobois, P. F. Dominey, J. Decety et al., "Motor imagery in normal subjects and in asymmetrical Parkinson's disease: a PET study," *Neurology*, vol. 55, no. 7, pp. 996–1002, 2000.

[36] U. Sabatini, K. Boulanouar, N. Fabre et al., "Cortical motor reorganization in akinetic patients with Parkinson's disease. A functional MRI study," *Brain*, vol. 123, no. 2, pp. 394–403, 2000.

[37] A. Nagano-Saito, T. Kato, Y. Arahata et al., "Cognitive- and motor-related regions in Parkinson's disease: FDOPA and FDG PET studies," *NeuroImage*, vol. 22, no. 2, pp. 553–561, 2004.

[38] L. B. Hinkley, L. A. Krubitzer, S. S. Nagarajan, and E. A. Disbrow, "Sensorimotor integration in S2, PV, and parietal rostroventral areas of the human Sylvian fissure," *Journal of Neurophysiology*, vol. 97, no. 2, pp. 1288–1297, 2007.

[39] L. Fogassi and G. Luppino, "Motor functions of the parietal lobe," *Current Opinion in Neurobiology*, vol. 15, no. 6, pp. 626–631, 2005.

[40] R. A. Andersen and C. A. Buneo, "Intentional maps in posterior parietal cortex," *Annual Review of Neuroscience*, vol. 25, pp. 189–220, 2002.

[41] G. Rizzolatti, G. Luppino, and M. Matelli, "The organization of the cortical motor system: new concepts," *Electroencephalography and Clinical Neurophysiology*, vol. 106, no. 4, pp. 283–296, 1998.

[42] M. Samuel, A. O. Ceballos-Baumann, J. Blin et al., "Evidence for lateral premotor and parietal overactivity in Parkinson's disease during sequential and bimanual movements. A PET study," *Brain*, vol. 120, no. 6, pp. 963–976, 1997.

[43] R. C. Helmich, L. C. Derikx, M. Bakker, R. Scheeringa, B. R. Bloem, and I. Toni, "Spatial remapping of cortico-striatal connectivity in parkinson's disease," *Cerebral Cortex*, vol. 20, no. 5, pp. 1175–1186, 2010.

[44] L. L. Chan, K. M. Ng, H. Rumpel, S. Fook-Chong, H. H. Li, and E. K. Tan, "Transcallosal diffusion tensor abnormalities in predominant gait disorder parkinsonism," *Parkinsonism and Related Disorders*, vol. 20, no. 1, pp. 53–59, 2014.

[45] C. H. Lyoo, Y. H. Ryu, and M. S. Lee, "Cerebral cortical areas in which thickness correlates with severity of motor deficits of Parkinson's disease," *Journal of Neurology*, vol. 258, no. 10, pp. 1871–1876, 2011.

[46] S. L. Bressler and J. A. S. Kelso, "Cortical coordination dynamics and cognition," *Trends in Cognitive Sciences*, vol. 5, no. 1, pp. 26–36, 2001.

[47] M. T. Banich and D. L. Karol, "The sum of the parts does not equal the whole: evidence from bihemispheric processing," *Journal of Experimental Psychology: Human Perception and Performance*, vol. 18, no. 3, pp. 763–784, 1992.

[48] M. P. A. van Meer, K. van der Marel, K. Wang et al., "Recovery of sensorimotor function after experimental stroke correlates with restoration of resting-state interhemispheric functional connectivity," *Journal of Neuroscience*, vol. 30, no. 11, pp. 3964–3972, 2010.

[49] A. K. Roy, Z. Shehzad, D. S. Margulies et al., "Functional connectivity of the human amygdala using resting state fMRI," *NeuroImage*, vol. 45, no. 2, pp. 614–626, 2009.

[50] A. Di Martino, A. Scheres, D. S. Margulies et al., "Functional connectivity of human striatum: a resting state fMRI study," *Cerebral Cortex*, vol. 18, no. 12, pp. 2735–2747, 2008.

[51] L. Q. Uddin, E. Mooshagian, E. Zaidel et al., "Residual functional connectivity in the split-brain revealed with resting-state functional MRI," *NeuroReport*, vol. 19, no. 7, pp. 703–709, 2008.

Research Article

Altered Synchronizations among Neural Networks in Geriatric Depression

Lihong Wang,[1,2,3] Ying-Hui Chou,[2,3] Guy G. Potter,[2] and David C. Steffens[1,2]

[1]*Department of Psychiatry, University of Connecticut Health Center, 263 Farmington, CT 06119, USA*
[2]*Department of Psychiatry and Behavioral Sciences, Duke University, Durham, NC, USA*
[3]*Brain Imaging and Analysis Center, Duke University, Durham, NC, USA*

Correspondence should be addressed to Lihong Wang; lihong001@gmail.com

Although major depression has been considered as a manifestation of discoordinated activity between affective and cognitive neural networks, only a few studies have examined the relationships among neural networks directly. Because of the known disconnection theory, geriatric depression could be a useful model in studying the interactions among different networks. In the present study, using independent component analysis to identify intrinsically connected neural networks, we investigated the alterations in synchronizations among neural networks in geriatric depression to better understand the underlying neural mechanisms. Resting-state fMRI data was collected from thirty-two patients with geriatric depression and thirty-two age-matched never-depressed controls. We compared the resting-state activities between the two groups in the default-mode, central executive, attention, salience, and affective networks as well as correlations among these networks. The depression group showed stronger activity than the controls in an affective network, specifically within the orbitofrontal region. However, unlike the never-depressed controls, geriatric depression group lacked synchronized/antisynchronized activity between the affective network and the other networks. Those depressed patients with lower executive function has greater synchronization between the salience network with the executive and affective networks. Our results demonstrate the effectiveness of the between-network analyses in examining neural models for geriatric depression.

1. Introduction

It has long been postulated that major depression may be a consequence of failed coordination between the central executive system and affective processing system [1]. While a great number of studies [2, 3] have identified abnormal activation in the regions subserving executive function (e.g., dorsolateral prefrontal cortex (dlPFC) and dorsal anterior cingulate (dACC)) and affective processing (e.g., ventromedial prefrontal cortex (vmPFC), orbitofrontal cortex (OFC), and amygdala), only a few studies have examined coordination between the executive system and affective processing system directly at a network level in major depression.

In addition to the executive and affective processing systems, the abnormalities in the default-mode network (DMN, primarily including the anterior and posterior cingulate, and bilateral lateral parietal cortex areas) and salience network

(including the dorsal anterior cingulate and insula cortices) in major depression have also been identified [4]. A number of studies have reported an increased activity of the DMN in major depression during resting state [5, 6] and persistent activity of the DMN during tasks [4, 7]. Northoff and Sibille [8] have suggested hyperactivity of the DMN as one of the endophenotypes of major depression, which could predispose individuals with this endophenotype to depression, whereas Marchetti and colleagues [9] hypothesized that the increased DMN activity could be a depressive scar resulting from a dysfunctional switch between internally and externally oriented attention. Meanwhile, there are also reports about decreased function in the executive system [2, 3, 10] that some authors refer to as task-positive deficiency [9, 11]. Interestingly, Hamilton and colleagues [4] have reported a task-negative (i.e., DMN) dominance over task-positive

network dominance during resting state in major depression using an index to quantify the number of time periods when the DMN signal is stronger than the signal from the task-positive network. They also proposed that the right anterior insula might be a driver subserving the switch between internal and external attentions. They found that while in healthy controls the anterior insula activity was increased when task-positive activity was at the peak, in patients with major depression the anterior insula activity was increased when the DMN activity was at the peak. The anterior insula as a key node of the salience network (SN) has recently gained lots of attention in the neuroimaging research field and has been found also involved in major depression by many other authors [12–14]. van Tol et al. [13] reported decreased functional connectivity of the salience network with the medial prefrontal cortex, ventrolateral prefrontal cortex, and ventral striatum. Manoliu and colleagues [12] recently also found decreased connectivity between the insula and dorsal anterior cingulate (dACC) within the salience network, which was associated with the severity of symptoms and aberrant DMN/CEN interactions as well. Furthermore, Yuen and colleagues [14] found the decreased right anterior insular-dACC connectivity and increased insular-dorsolateral prefrontal cortex (dlPFC) connectivity in older major depression patients who had apathy symptoms. Therefore, it is necessary to clarify the relationships among the affective, executive, DMN, attention, and salient systems in major depression.

Major depression in individuals who had the first depression episode at their older ages (typically older than 50 years) is often referred as geriatric depression. Different from major depression in younger adults, geriatric depression has frequently been found in those with cerebrovascular disorders [15, 16], such as white matter hyperintensities, which are associated with disconnections/low blood supplies in white matters and gray matters. Because of the disconnection pathology, geriatric depression could serve as an interesting model in studying the alteration of the interactions among different neural networks. However, so far, there is only one study in geriatric depression which has investigated the interaction between regions from different neural networks. That study was focused only on the differences of the insular connectivity between those who had high ($n = 7$) versus low ($n = 9$) apathy symptoms, which needs further confirmation in a larger sample. Therefore, more studies in geriatric depression are very necessary.

In recent years, with the development of various analyzing methods on task-related and task-free functional magnetic resonance imaging (fMRI) data, analyzing fMRI data at a neural network level becomes a reality. One of the widely used techniques to identify neural networks is the independent component analysis (ICA). Unlike the seed-based functional connectivity analysis which is dependent on the location and size of a seed, the ICA approach is data driven. It identifies independent components (ICs) based on the spatial and temporal distribution patterns [17]. Since the regions within an IC are temporally synchronized and are commonly activated during a certain cognitive processing simultaneously, these regions within an IC are often considered to be within the same neural network. A number of studies [18–20] have identified intrinsically connected neural networks by comparing ICs with task-activated brain regions through meta-analysis. With the identified neural networks, we can further investigate the properties of the neural networks and the relationships among different neural networks.

The majority of previous studies in the literature have examined the association of regional activity or connectivity between two regions with depression severity [4, 6, 21, 22]. Although there are some reports on interactions among regions from different neural networks [23], few studies have examined the interactions among different neural networks by evaluating the synchronization of an entire network. The advantage of evaluating the synchronization of an entire network over the region-to-region synchronization analysis is that the former would allow us to compute/understand a neural model for a mental disorder more easily. To examine the interactions between neural networks in geriatric depression, we conducted an ICA and identified the default-mode, executive, attention, affective, and salience networks by comparing each component with the template of Laird and colleagues [19] using the goodness of fit analysis. Then we computed the significant differences between the depressed and healthy control groups in the correlations among these networks. Regression analyses between the network synchronizations with depression severity were also conducted. Since geriatric depression typically has executive dysfunction, we conducted the study in geriatric depression to examine the influence of network interactions on depressive symptoms and executive function. We hypothesized that the correlation/coordination between or among networks rather than in a single network has a strong association to depressive symptoms and executive dysfunction.

2. Materials and Methods

2.1. Participants. Thirty-two individuals who had been diagnosed with major depressive disorder (19 females, mean ± SD age: 68 ± 6.5 years) and thirty-two healthy never-depressed volunteers (18 females, mean ± SD age: 72 ± 8.2 years) participated in this study. Participants were recruited from the neurocognitive outcomes of depression in the elderly study (NCODE). All depressed patients met DSM-IV criteria for major depression. They were either in a remitted state ($n = 21$) or in an actively depressed state ($n = 11$) with the Montgomery-Åsberg Depression Rating Scale (MADRS) mean ± SD score of 2.1 ± 1.8 for the remitted and 17.4 ± 9.2 for the actively depressed patients. The exclusion criteria for depressed subjects included (1) another major psychiatric illness, including bipolar disorder, schizophrenia, or dementia; (2) alcohol or drug abuse or dependence; (3) neurological illness, including dementia, stroke, and epilepsy; (4) medical illness, medication use, or disability that would prevent the participant from completing neuropsychological testing; and (5) contraindications to MRI. All never-depressed subjects were cognitively intact and had no history or clinical evidence of dementia, and they all scored 28 or more on the minimal state examination. Among the 32 depressed

participants, 9 were receiving antidepressant monotherapy (4 on selective serotonin reuptake inhibitors (SSRIs), 2 on serotonin antagonist and reuptake inhibitors (SARIs), 1 on serotonin-norepinephrine reuptake inhibitors (SNRIs), and 2 on an tricyclic), 9 were receiving combination treatment (4 on two SSRIs, 2 on SSRI combined with either SARI or norepinephrine-dopamine reuptake inhibitors (NDRIs), 2 on SARI and NDRI, and 1 on SNRI and NDRI), and 14 were not on medication (Table 1).

Prior to the fMRI, all subjects completed the Stroop Color and Word Test to examine the executive function. The study received approval by Duke School of Medicine Institutional Review Board. All subjects gave verbal and written consent after being explained the purpose and procedures to be used in the study.

2.2. Neuroimaging Acquisition. All participants were scanned using a research-dedicated 3.0 T GE EXCITE HD scanner (GE Medical Systems, Milwaukee, Wisconsin). First, high-resolution T1-weighted structural images in coronel view were acquired with slice thickness of 1 mm without a gap (matrix = $256 \times 256 \times 216$). We then obtained 5-minute resting fMRI scans for each participant. Participants were instructed to rest without moving, keep their eyes open, and focus on a fixation cross-presented in the center of the screen inside the scanner. Inward spiral sequence functional images in the axial view were acquired using the following parameters: TR = 2000 ms, TE = 31 ms, FOV = 24 cm, flip angle = $90°$, and matrix = $64 \times 64 \times 34$.

2.3. Data Analyses. Data were preprocessed using the Duke BIAC resting state pipeline based on the tools from the FSL analysis package (FMRIB Software Library, http://fsl.fmrib.ox.ac.uk/fsl/fslwiki/, Version 5.98) and locally developed MATLAB code (MathWorks, Natick, MA), including slice-timing alignment, motion correction, coregistration, nonbrain voxel extraction, and normalization. We also regressed out six-parameter rigid body head motion, the signal averaged over the white matter, and signal averaged over the cerebrospinal fluid regions [24]. Frequencies less than 0.08 Hz were retained [25]. The group independent component analysis (ICA) was conducted using melodic and dual regression program following the instructions on FslWiki (http://fsl.fmrib.ox.ac.uk/fsl/fslwiki/DualRegression). Briefly, we first concatenated all subjects' data including both the patient and control groups and calculated the group-averaged independent components (IC) by limited the ICs to twenty components to match the study of Laird and colleagues [19]. Next, we identified the default-mode network (DMN), central executive network (CEN), central attentional network (CAN), salience network (SN), and affective network (AN) by using the goodness of fit test (GOF) [5] to best match the networks provided by Laird and colleagues [19]. In the case that the second largest GOF value was close to the first largest GOF value, we kept the component as a component of interest as well. Next, we regressed spatial ICs into each subject's 4D data to generate both subject-specific component time courses and subject-specific spatial maps as

outputs [26]. Specifically, as described in the FSL webpage (http://fsl.fmrib.ox.ac.uk/fsl/fslwiki/DualRegression), "for each subject, the group-average set of spatial maps is regressed (as spatial regressors in a multiple regression) into the subject's 4D space-time dataset. This results in a set of subject-specific timeseries [sic], one per group-level spatial map. Next, those timeseries [sic] are regressed (as temporal regressors, again in a multiple regression) into the same 4D dataset, resulting in a set of subject-specific spatial maps, one per group-level spatial map." The z-score for every voxel was estimated by normalizing each voxel's intensity with respect to intensity of all the voxels in each individual IC. The IC maps were then compared between groups on a voxelwise basis for statistical tests using FSL's randomize permutation-testing tool. Finally, pairwise Pearson's correlation coefficient analyses were conducted to compute the interaction between any two networks as listed above.

2.4. Statistical Analyses. To identify group difference between the depression patients and controls in each component identified as DMN, CEN, CAN, SN, and AN and the inter-IC correlations between any two networks, voxelwise two-sample t-tests were computed. Two-sample t-tests were conducted to test group differences in inter-IC correlations. Age was used as a regressor to control the aging effect. To examine the interactions between network activity strength and clinical status, we also conducted regression analyses using MADRS score (depression severity) and executive function as measured by the color-word interference condition of the Stroop task. The measures of the Stroop task were converted into standardized score based on age, gender, and race. Significant level was determined using threshold of $Z > 2.3$, $P < 0.05$ with cluster correction. For the interactions between networks, the significance was determined using $P < 0.05$ based on the Monte-Carlo simulation. Specifically, similar to the network-based statistics [27], our multiple comparisons were corrected based on nonrandom data distribution patterns. The first step was to identify a set of correlations that exhibited a P value less than 0.05. Second, among the set of correlations, we determined whether a cluster of correlations was significant based on the size of the cluster. The size of the cluster was determined by 10,000 Monte-Carlo simulations.

3. Results

3.1. Clinical Profile of the Participants. We summarize the demographic details, clinical profile, and performance of participants on the Stroop task in Table 1. Given a non-significant trend for age difference between the two groups, with the control group relatively older than the depression group, we included age as a covariate in subsequent group comparison analyses. For executive function, the depression group showed a relatively lower score than the control group in performing the Stroop task; however, there was not a significant difference between the two groups (Table 1).

3.2. Differences in Resting-State Activity within and between Neural Networks between Depression and Control Groups.

TABLE 1: The clinical profiles of the participants.

	Depression ($n = 32$)	Control ($n = 32$)	P value
Gender (F/M)	18/14	19/13	0.80[+]
Age	68.3 (6.5)	71.8 (8.2)	0.06
Years of education	14.9 (3.1)	16.0 (2.5)	0.11
MADRS	7.0 (9.2)	0.0 (0.9)	<0.001[*]
Number medicated for hypotension	11	8	0.40[+]
Number medicated for antidepressants	18	0	
Monotherapy			
SSRI	4		
SARI	2		
SNRI	1		
Tricyclic	2		
Combined treatment			
Two SSRIs	4		
SSRI with either SARI or NDRI	2		
SARI & NDRI	2		
SNRI & NDRI	1		
Executive function (Stroop task)	−0.10 (0.82)	0.24 (0.71)	0.08

[+] Chi-square test, and the rests were two-sample t-tests; [*] significant results with $P < 0.05$. SSRI = selective serotonin reuptake inhibitor; SARIs = serotonin antagonist and reuptake inhibitors; SNRIs = serotonin-norepinephrine reuptake inhibitors; NDRIs = norepinephrine-dopamine reuptake inhibitors.

FIGURE 1: The ICA components which correspond to different neural networks according to the goodness-of-fit analysis using the templates of Laird et al. AN = affective network; CAN = central attentional network; CEN = central executive network; DMN = default-mode network; SN = salience network.

Our aim was to examine whether we can identify altered interactions among networks that are related to depressive symptoms and cognitive dysfunctions in geriatric depression. To achieve this goal, using the results from Laird and colleagues [19] as templates, first we identified the components that were best matched to the default-mode network (DMN, IC1, corresponding to Laird et al.'s IC13), central executive network (CEN, IC4, and IC6 corresponding to Laird et al.'s IC15 and IC18, resp.), central attentional network (CAN, IC7 corresponding to Larid et al.'s IC7), salience network (SN, IC10, corresponding to Laird et al.'s IC4), and affective

work (AN, IC12, and IC18, corresponding to Laid et al.'s IC2; the IC18 was also matched to Laird et al.'s IC1). Figure 1 shows the matched components between the ICs in our study with Larid et al.'s. The detailed coverage for each component is listed in Table 2 and Figure 2. More detailed coverage of each component is shown in axial views in supplementary sFigure 1 in Supplementary Material available online at http://dx.doi.org/10.1155/2015/343720.

When comparing each individual network between patients and controls using two-sample t-tests, we found significantly increased IC12 (one of the affective networks, ANs)

TABLE 2: The clusters of each IC component identified matches the CEN, CAN, DMN, AN, and SN, respectively.

Network	IC	Clusters	Peak coordinate (MNI X, Y, Z)
DMN	IC1	Bilateral medial prefrontal cortex	[4, 59, −2]
		Bilateral posterior cingulate	[−7, −55, 19]; [1, 59, −5]
		Bilateral lateral parietal cortex	[−42, −65, 36]; [45, −63, 32]
AN	IC12	Bilateral dorsomedial prefrontal cortex	[−21, 35, 38]; [28, 42, 40]
		Rostral anterior cingulate	[6, 47, −4]
		Bilateral subgenual cingulate	[4, 41, −11]
	IC18	Bilateral subgenual cingulate	[13, 24, −18]
		Bilateral rostral anterior cingulate	[0, 61, 13]
		Bilateral ventrolateral prefrontal cortex	[−36, 37, 4]; [48, 32, 6]
		Bilateral orbitofrontal cortex	[−38, 34, −16]; [29, 36, −19]
		Bilateral amygdala	[−28, −1, −16]; [34, −3, −15]
		Bilateral caudate	[−6, 2, 8]; [10, 10, −2]
CEN	IC6	Left dorsolateral prefrontal cortex	[−46, 27, 19];
		Left dorsomedial prefrontal cortex	[−2, 23, 48]
		Bilateral superior parietal cortex	[−33, −50, 44]; [30, −58, 46]
		Right inferior temporal cortex	[−58, −43, −13]
		Left anterior part of posterior cingulate	[−5, −38, 38]
		Right cerebellum	[31, −69, −47]
	IC4	Right dorsolateral prefrontal cortex	[42, 22, 44]
		Right dorsomedial prefrontal cortex	[6, 27, 41]
		Bilateral superior parietal cortex	[−46, −50, 46]; [42, −58, 47]
		Right inferior temporal cortex	[61, −28, −6]
		Right anterior part of posterior cingulate	[5, −47, 40]
		Left cerebellum	[−39, −68, −45]
CAN	IC7	Bilateral frontal eye field	[−21, 2, 53]; [26, 2, 49]
		Bilateral precuneus	[−11, −69, 56]; [11, −65, 56]
		Bilateral parieto-occipital fissure	[−28, −82, 29]; [38, −73, 23]
		Bilateral lingual gyrus	[−13, −58, 11]; [18, −58, 15]
SN	IC10	Bilateral dorsal cingulate	[3, 27, 20];
		Bilateral insula	[−38, −14, 6]; [41, −12, 8]
		Bilateral parieto-occipital fissure	[−13, −62, 15]; [19, −57, 11]

activity specifically in the cerebellar vermis in the depression group relative to the control group. In fact, the cerebellar vermis was not represented in the IC12 when we use the threshold of $Z > 2.3$, $P < 0.05$ with cluster correction. However, the IC12 of the depressed group did have a cluster in the cerebellar vermis when using the threshold of $Z > 2.3$, $P < 0.001$ without cluster correction (Figure 3).

When comparing correlations among networks between the two groups (pairwise correlations), it was the IC12 that showed a significant group difference in the synchronizations between this network with several other networks (Table 3). Specifically, we found a positive correlation in the IC12 with IC6 (one of the CENs) in the control group; however, the correlation was significantly reduced (no significant correlation existed) in the depression group. We also found a significantly increased correlation (less negative) in the depression group relative to the control group in the IC12 with IC7 (CAN, mainly in the precuneus region) and the IC12 with IC10 (the salience network, SN) (Figure 4).

3.3. Correlation with Depression Severity and Executive Function. We did not find any significant correlation of the severity of depressive symptoms with any of the networks or interactions between any two networks. However, as shown in Figure 5, we found a negative correlation between the Stroop task performance and the interactions between the IC10 (SN) and IC6 (one of the CENs) and between IC10 (SN) and IC18 (one of the AN) in the depression group but not in the control group. In other words, in the depression group, those who had higher synchronization between the salience network and the central executive network and affective networks were the ones who had poor task performance on the Stroop task.

3.4. Depression-State Related Alteration. Given the fact that we had a fair number of patients in a remitted state, we suspected that the reason that we did not find a significant correlation between neural activity and depression severity might be because their relationship is nonlinear; that is, it might be a depression-state dependent rather than a linear

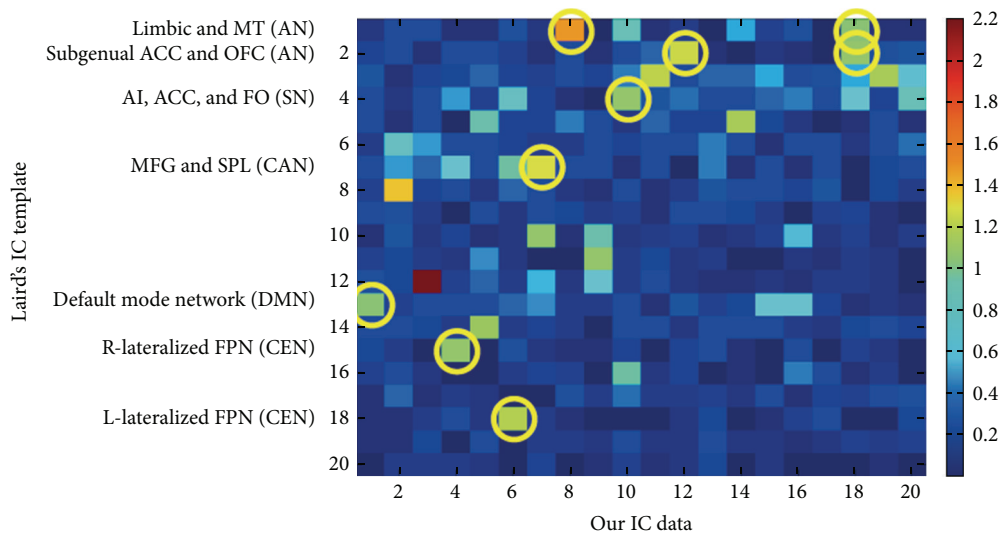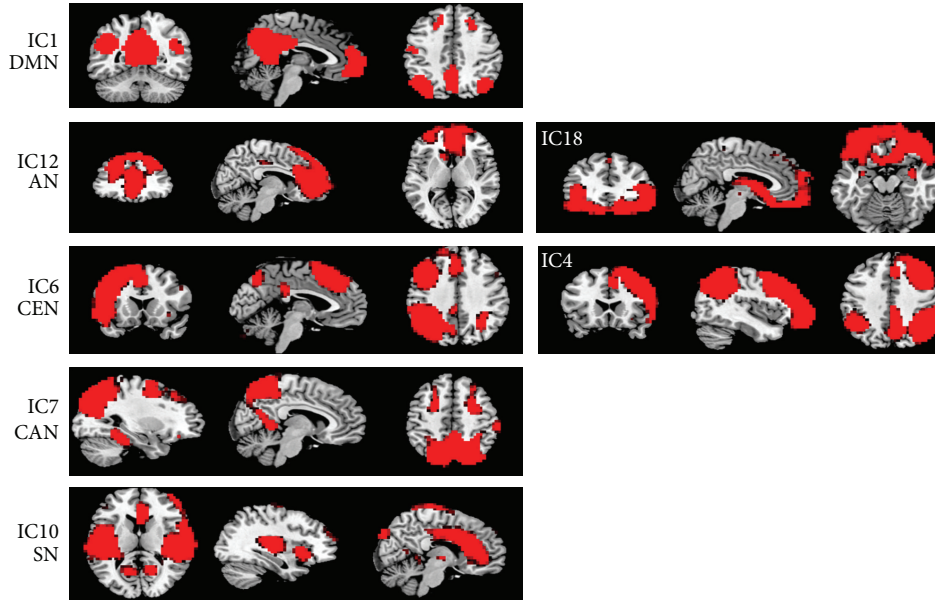FIGURE 2: The locations of each IC component which correspond to different neural networks according to the goodness-of-fit analysis using the templates of Laird et al. The IC components were computed using dual regression analysis by combining the data from both the depression and never-depressed control group ($Z > 2.3$, $P < 0.05$ with cluster correction).

TABLE 3: Mean (SD) inter-IC correlations that showed significant group differences and that correlated with performance of the Stroop task.

	Control	Depression	P value
IC12(AN)-IC6(CEN) correlation	0.30 (0.28)	0.15 (0.26)	0.03
IC12(AN)-IC7(CAN) correlation	−0.39 (0.33)	−0.22 (0.32)	0.04
IC12(AN)-IC10(SN) correlation	−0.18 (0.29)	−0.02 (0.32)	0.04
Stroop performance with IC10(SN)-IC6(CEN) correlation		$r = -0.34$	0.05
Stroop performance with IC10(SN)-IC18(AN) correlation		$r = -0.51$	0.003

relationship. Therefore, we subsequently examined the differences in neural networks and interactions of networks between the remitted versus the actively depressed groups and between the remitted versus the control groups. As shown in Figures 3(c) and 3(d), the increased cerebellar vermis activity shown in the pooled depression group relative to controls was mainly driven by the remitted group in comparison with controls. The increased cerebellar vermis activity was not found in the actively depressed group in comparison with the control group. Instead, we found significantly increased resting activity of IC18 (another AN) in the left orbitofrontal cortex and ventromedial prefrontal cortex in the actively depressed group compared with both the control group and the remitted patient group (Figure 6). Therefore, we believe the increased orbitofrontal cortex of AN should be a depression-state effect.

We also examined the group differences in network synchronizations between the actively depressed versus control, actively depressed versus remitted, and remitted versus control groups. The analyses confirmed the network interaction results in the combined patient sample, in that the significant positive correlation between IC10 (SN) and IC6 (CEN) and the negative correlation between IC10 (SN) and IC7 (CAN)

in the control group were significantly less positive or less negative in the actively depressed group. There were no significant group differences between the actively depressed and remitted groups or between the remitted and control groups among the network interactions.

4. Discussion

We investigated the interactions among different intrinsic connectivity networks in patients with both acute and remitted geriatric depression and found that depression patients had significant alterations in the synchronizations/antisynchronizations between the affective network with other networks including the central executive network, attentional network, and the salience network. In addition, we found depressive-state specific increase in the orbitofrontal area of the affective network. Although these changes were not correlated with depression severity, the significant differences confirmed in the acutely depressed group indicate an importance of the interactions between networks as the neuropathology of major depression.

It is interesting that the depression group mainly had altered correlations between the component of the affective
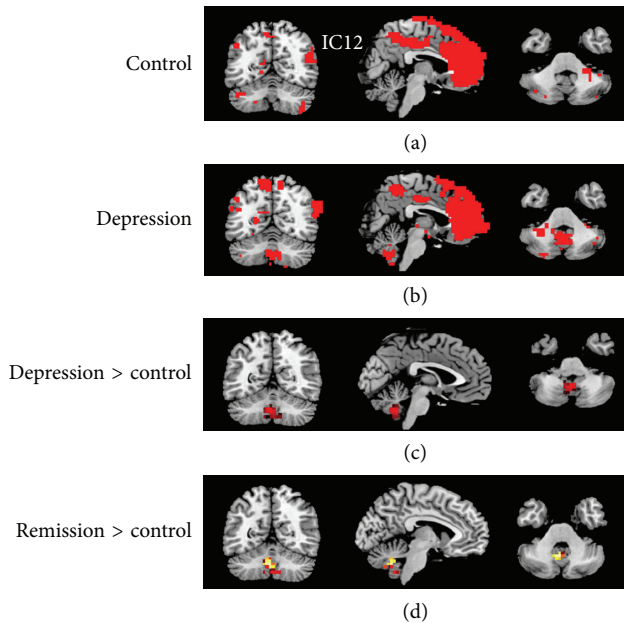
FIGURE 3: (a) Component 12 (IC12), one of the affective networks, in the control group; (b) IC12 in the depression group. To show the voxels in the cerebellum, (a) and (b) were based on threshold of $Z > 2.3$, $P < 0.001$ without cluster correction. (c) Regions within IC12 which showed significantly increased activity in the depression group (all patients) related to the control group; (d) regions within IC12 which showed significantly increased activity in subjects remitted from depression (part of patients in the depression group) related to the controls. (c) and (d) were based on threshold of $Z > 2.3$, $P < 0.05$ with cluster correction.

network (including the orbitofrontal, subgenual cingulate, and the dorsomedial prefrontal cortex) with other neural networks. This component best matched component 2 (subgenual cingulate and orbitofrontal cortex) of Laird and colleagues' study and the authors indicated its role in "olfaction, gustation, and emotion" [19]. Previous studies in the literature using task-related fMRI have frequently found activation in the orbitofrontal and the dorsomedial prefrontal cortex during emotion related tasks, particularly in tasks related to emotion expectation and emotional learning [28–30]. It is hypothesized that medial prefrontal cortex (mPFC) may use the inputs from the orbitofrontal cortex (OFC) as signals of internal states to select appropriate behaviors during automatic cognitive change paradigms [31]. In fact, in the model of Phillips and colleagues [31], the OFC, mPFC, and subgenual cingulate, together with the hippocampus and parahippocampus, could function as an automatic emotion regulation system. They also proposed the central executive system including dorsolateral prefrontal cortex, dorsomedial prefrontal cortex, and dorsal anterior cingulate as voluntary emotion regulation system. Phillips and colleagues pointed that the voluntary emotion regulation system function may be mediated by the OFC and subgenual cingulate [31]. Consistently, we found a positive correlation between the automatic emotion regulation system (IC12) and the voluntary emotion regulation system (IC6) in the healthy

control group, the correlation did not exist in the depression group, suggesting that emotion regulation requires good coordination/synchronization between the automatic and voluntary systems. That is, the synchronization between the two systems was broken in depressed patients, which could result in depressive symptoms.

We also found a negative correlation between the IC12 with IC7 and IC10 in the healthy control group and the correlation become less negative in the depressed group. The IC7 located at the frontal eye area and the precuneus areas and best matched the IC7 of Laird's study which should be an attentional network, whereas IC10 matched the IC4 of Laird's study (the bilateral anterior insula/frontal opercula and ACC) which should be the salience network. The salience network recently has been hypothesized to play an important role in facilitating attentional transition between cognition and emotion/interoception [32, 33]. Negative correlations between the automatic emotional regulation system with the attentional system and the salient system suggest that when the automatic emotional regulation system was working, attention to affective stimuli and attentional transition from cognition to emotion/interoception would be suppressed, which could be a consequence of successful automatic emotional regulation. However, the network interactions disappeared in the depressed group. Together with the discoordination of the automatic emotion regulation system with the voluntary emotion regulation system, we speculate that the major deficits in our depression group were the discoordination between the affective (automatic emotion regulation) system and the other neural systems (central executive network, cognitive attention, and attention transition between cognition and emotion/interoception). Although we did not find a significantly linear correlation between the network interactions with depression severity, the subgroup analysis confirmed the results were more significant in the currently depressed group than the remitted group. Although our study sample was older adults, our findings are largely in consistent with Mayberg [1] and Philips's neuroscience model of depression and emotion.

Since we mainly found a discoordination between the affective networks with other networks, we speculate that the primary deficits in depression could be in the automatic emotion regulation system of the affective network which have resulted in the interaction deficits between this network and other networks. Indeed, we found increased activity in the left orbitofrontal cortex area (although not IC12 but IC18 instead) in depression, especially in the actively depressed group relative to both the remitted depression group and healthy control group (suggesting a depressive state-related alteration). As shown in the results, there are some spatial overlaps in the ventromedial prefrontal and orbitofrontal regions between the IC18 and IC12. Similar to IC12, the IC18 also matched the IC2 as well as IC1 of Lairds' study, but the IC18 also included the limbic and brainstem regions, all of which should also be part of the automatic emotion regulation network. The pathological deficit in the orbitofrontal cortex in depression has long been well documented [28]. Rajkowska et al. [34] found a decrease in cortical thickness of orbitofrontal cortex in depressed patients. In older adults,

(a)

(b)
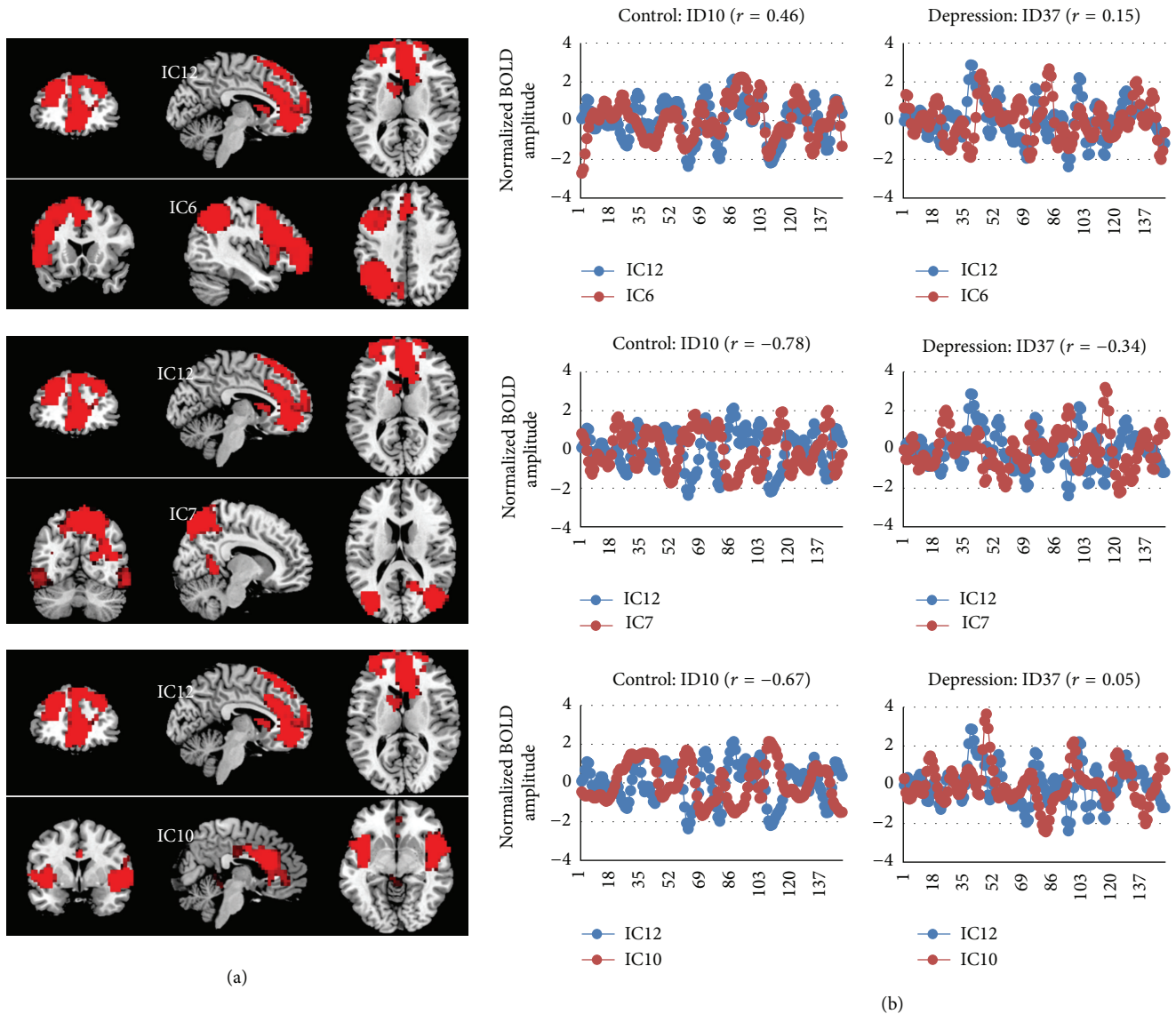
FIGURE 4: (a) Neural network pairs which revealed significant correlations in the control group. (b) The plots of time course of each network in a control subject (ID10) and a depression subject (ID37) to illustrate the interaction effect between each paired neural networks. The significance was tested using Monte-Carlo simulation.

decreased volume of the orbitofrontal cortex has been reported in many studies [35–37]. Increased metabolism or regional cerebral blood flow (rCBF) of the orbitofrontal cortex has been shown in unmedicated depressive patients [38] although decreased orbitofrontal activation was found associated with anxiety symptoms [39]. Therefore, in consistent with Drevets and colleagues' theory [28], increased resting activity in the orbitofrontal area of the automatic emotion regulation network could be a core deficit in depression.

In this study, we also found a negative correlation between the Stroop task performance and the synchronization of the salience network (IC10) with the central executive network/voluntary emotion regulation network (IC6) as well as the synchronization of the salience network with the automatic emotion regulation network (IC18) in the depression

group but not in the control group. In other words, those patients, who had poor performance in the Stroop task, had stronger synchronization between the salience network and the emotional regulation (both voluntary and automatic) networks. The results may implicate that, those whose salience network and emotional regulation networks are positively synchronized, may be more easily to reallocate their attention to emotional events, which then could distract them from ongoing cognitive tasks and result in poor performance in the executive tasks such as the Stroop task. Supportively, in the control group, the salience network was negatively correlated with the automatic emotion regulation network (IC12 though). However, it is difficult to explain why those who had poor performance during the Stroop task had a positive correlation between the salience network and the

(a)

(b)
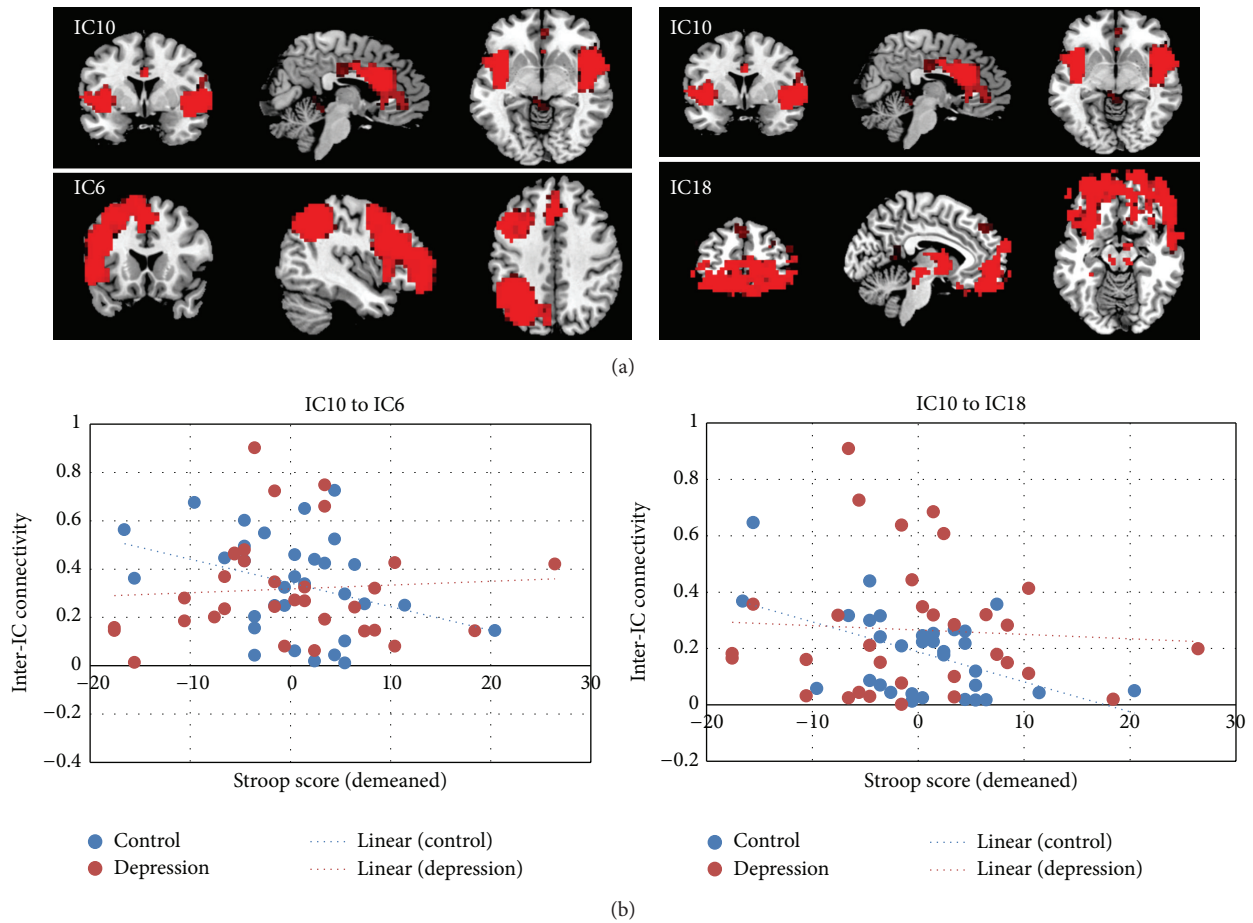
FIGURE 5: (a) Neural network pairs that their correlation or anticorrelation was correlated with the Stroop task performance in depression patients. (b) The correlation plots in the patient group (red) and control group (blue).
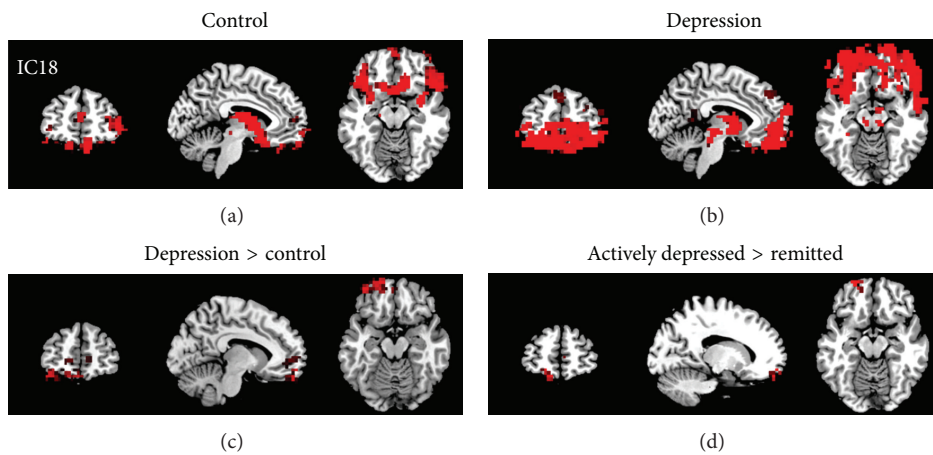
FIGURE 6: Upper: the IC18 in the control group (a) and depression group. (b) Lower: the regions within IC18 that revealed significantly increased activity in the depressed patients than controls (c) and in the actively depressed patients than the remitted patients (d) ($Z > 2.3$, $P < 0.05$ with cluster correction).

voluntary emotional regulation network. While it might be a compensatory effect, future studies to investigate the synchronization between the salience network and the voluntary emotional regulation (central executive) network during performing the Stroop task scan is necessary to explain the phenomenon.

There are a couple of technical issues that need to be discussed here. First of all, we conducted motion correction during preprocessing which has not been frequently reported in the literature in ICA analyses. We rationale that for the majority of functional connectivity analysis (e.g., seed-based connectivity analysis), in addition to the slice-time correction, motion correction, and normalization, filtering and regressing out covariates (such as six motion parameters, white matter signal, and CSF signal) are also essential during data preprocessing [40]. Regressing out estimated motion parameters and physiological signals can largely increase the gray matter temporal signal to noise [41]. We believe that it makes sense to include these preprocessing steps before ICA. We expect that performing ICA without these preprocessing steps would probably increase some independent components of noise. Secondly, one may concern how our interested components were influenced by the template which we used in the study. It is worth to note that the template provided by Laird and colleagues was based on a metadata set associated with 8637 functional brain imaging experiments across 31,724 subjects. We believe the key elements of each network do not deviate much from the template of other datasets [20], although the naming of the components is relatively different (e.g., the affective network that we named here was referred as "limbic" by Yeo and colleague). The number of ICs should have some influences on our results. How to describe/present neural networks and label their functions is one of the hot research areas and an ideal solution for mapping brain function may arrive in the very near future. In addition, the networks we are discussing in this study have covered several subnetworks. For example, our salience network included the bilateral insula and dorsal anterior cingulate. As indicated by Menon and Uddin [33], the anterior insula has different roles from the posterior insula. The anterior insula, not the posterior one, should be part of the salience network. Similarly, the function of subcomponents within DMN is also different [18], which could be the reason why we did not find a significant change in the DMN in depression patients compared with the controls. Therefore, instead of 20 components in the ICA analysis, using a larger number of components to define neural networks in a fine scale might leads to different conclusions.

In addition, we only studied the interactions between any two neural networks at a time. Using more complicated models that calculate the interactions among the networks simultaneously is necessary to confirm our results. We studied the internetwork correlations in geriatric depression because there have been known pathological disconnections in geriatric depression. Thus, our results cannot be generalized to younger depression patients. Because different regions might be involved in the pathology of geriatric depression due to large variations of outcomes from cerebrovascular diseases, further studies should be conducted to examine whether and how different cerebrovascular deficits affect our findings.

This study is also limited by the small sample size and different medications of the depression patients. The small number of actively depressed patients may impact on the robustness of the significance of our results. This might explain why we only found significant alterations in the affective network but not in the executive network. Based on the results from the small number of patients, perhaps what we may conclude here is that at least deficits in the affective network were more robust and obvious than those in the executive network in the actively depressed group. Future replication studies in unmedicated patients with geriatric depression in a larger sample are warranted to confirm our conclusions.

While deficits of resting activity in depression have been reported in a number of studies in major depression, the aberrant interactions among intrinsic neural networks have not been demonstrated previously. Although our current study cannot determine which was the primary deficit in major depression firmly, the altered network activity, or the interactions among networks, we were able to examine the interactions between networks directly using the ICA approach. Our results have demonstrated that hyperactivity within the affective network (the automatic emotion regulation system), in particular the orbitofrontal cortex, in conjunction with sparse correlation among the central executive network, attentional network, and the salience network, is the core dysfunction of older depression patients during resting state. The results are in consistent with several depression models proposed in the literature and indicated that studying the correlations among networks is an effective approach in revealing neural mechanisms of depression.

Conflict of Interests

The authors declare that there is no conflict of interests regarding the publication of this paper.

Acknowledgments

References

[1] H. S. Mayberg, "Limbic-cortical dysregulation: a proposed model of depression," *The Journal of Neuropsychiatry and Clinical Neurosciences*, vol. 9, no. 3, pp. 471–481, 1997.

[2] P. B. Fitzgerald, A. R. Laird, J. Maller, and Z. J. Daskalakis, "A meta-analytic study of changes in brain activation in depression," *Human Brain Mapping*, vol. 29, no. 6, pp. 683–695, 2008.

[3] N. A. Groenewold, E. M. Opmeer, P. de Jonge, A. Aleman, and S. G. Costafreda, "Emotional valence modulates brain functional abnormalities in depression: evidence from a meta-analysis of fMRI studies," *Neuroscience and Biobehavioral Reviews*, vol. 37, no. 2, pp. 152–163, 2013.

[4] J. P. Hamilton, D. J. Furman, C. Chang, M. E. Thomason, E. Dennis, and I. H. Gotlib, "Default-mode and task-positive network activity in major depressive disorder: implications for adaptive and maladaptive rumination," *Biological Psychiatry*, vol. 70, no. 4, pp. 327–333, 2011.

[5] M. D. Greicius, B. H. Flores, V. Menon et al., "Resting-state functional connectivity in major depression: abnormally increased contributions from subgenual cingulate cortex and thalamus," *Biological Psychiatry*, vol. 62, no. 5, pp. 429–437, 2007.

[6] J. Zhang, J. Wang, Q. Wu et al., "Disrupted brain connectivity networks in drug-naive, first-episode major depressive disorder," *Biological Psychiatry*, vol. 70, no. 4, pp. 334–342, 2011.

[7] Y. I. Sheline, D. M. Barch, J. L. Price et al., "The default mode network and self-referential processes in depression," *Proceedings of the National Academy of Sciences of the United States of America*, vol. 106, no. 6, pp. 1942–1947, 2009.

[8] G. Northoff and E. Sibille, "Why are cortical GABA neurons relevant to internal focus in depression? A cross-level model linking cellular, biochemical and neural network findings," *Molecular Psychiatry*, vol. 19, no. 9, pp. 966–977, 2014.

[9] I. Marchetti, E. H. W. Koster, E. J. Sonuga-Barke, and R. De Raedt, "The Default Mode Network and recurrent depression: a neurobiological model of cognitive risk factors," *Neuropsychology Review*, vol. 22, no. 3, pp. 229–251, 2012.

[10] L. Wang, K. S. LaBar, M. Smoski et al., "Prefrontal mechanisms for executive control over emotional distraction are altered in major depression," *Psychiatry Research—Neuroimaging*, vol. 163, no. 2, pp. 143–155, 2008.

[11] L. Leyman, R. de Raedt, M.-A. Vanderhasselt, and C. Baeken, "Effects of repetitive transcranial magnetic stimulation of the dorsolateral prefrontal cortex on the attentional processing of emotional information in major depression: a pilot study," *Psychiatry Research*, vol. 185, no. 1-2, pp. 102–107, 2011.

[12] A. Manoliu, C. Meng, F. Brandl et al., "Insular dysfunction within the salience network is associated with severity of symptoms and aberrant inter-network connectivity in major depressive disorder," *Frontiers in Human Neuroscience*, vol. 7, article 930, 2014.

[13] M.-J. van Tol, I. M. Veer, N. J. A. van der Wee et al., "Whole-brain functional connectivity during emotional word classification in medication-free Major Depressive Disorder: abnormal salience circuitry and relations to positive emotionality," *NeuroImage: Clinical*, vol. 2, no. 1, pp. 790–796, 2013.

[14] G. S. Yuen, F. M. Gunning-Dixon, M. J. Hoptman et al., "The salience network in the apathy of late-life depression," *International Journal of Geriatric Psychiatry*, vol. 29, no. 11, pp. 1116–1124, 2014.

[15] W. D. Taylor, H. J. Aizenstein, and G. S. Alexopoulos, "The vascular depression hypothesis: mechanisms linking vascular disease with depression," *Molecular Psychiatry*, vol. 18, no. 9, pp. 963–974, 2013.

[16] M. Wu, C. Rosano, M. Butters et al., "A fully automated method for quantifying and localizing white matter hyperintensities on MR images," *Psychiatry Research—Neuroimaging*, vol. 148, no. 2-3, pp. 133–142, 2006.

[17] C. F. Beckmann and S. M. Smith, "Probabilistic independent component analysis for functional magnetic resonance imaging," *IEEE Transactions on Medical Imaging*, vol. 23, no. 2, pp. 137–152, 2004.

[18] R. F. Betzel, L. Byrge, Y. He, J. Goñi, X.-N. Zuo, and O. Sporns, "Changes in structural and functional connectivity among resting-state networks across the human lifespan," *NeuroImage*, vol. 102, part 2, pp. 345–357, 2014.

[19] A. R. Laird, P. M. Fox, S. B. Eickhoff et al., "Behavioral interpretations of intrinsic connectivity networks," *Journal of Cognitive Neuroscience*, vol. 23, no. 12, pp. 4022–4037, 2011.

[20] B. T. Thomas Yeo, F. M. Krienen, J. Sepulcre et al., "The organization of the human cerebral cortex estimated by intrinsic functional connectivity," *Journal of Neurophysiology*, vol. 106, no. 3, pp. 1125–1165, 2011.

[21] C. H. Y. Fu, H. Steiner, and S. G. Costafreda, "Predictive neural biomarkers of clinical response in depression: a meta-analysis of functional and structural neuroimaging studies of pharmacological and psychological therapies," *Neurobiology of Disease*, vol. 52, pp. 75–83, 2013.

[22] I. M. Veer, C. F. Beckmann, M.-J. van Tol et al., "Whole brain resting-state analysis reveals decreased functional connectivity in major depression," *Frontiers in Systems Neuroscience*, vol. 4, article 41, 2010.

[23] M. J. Jafri, G. D. Pearlson, M. Stevens, and V. D. Calhoun, "A method for functional network connectivity among spatially independent resting-state components in schizophrenia," *NeuroImage*, vol. 39, no. 4, pp. 1666–1681, 2008.

[24] M. D. Fox, D. Zhang, A. Z. Snyder, and M. E. Raichle, "The global signal and observed anticorrelated resting state brain networks," *Journal of Neurophysiology*, vol. 101, no. 6, pp. 3270–3283, 2009.

[25] B. Biswal, F. Z. Yetkin, V. M. Haughton, and J. S. Hyde, "Functional connectivity in the motor cortex of resting human brain using echo-planar MRI," *Magnetic Resonance in Medicine*, vol. 34, no. 4, pp. 537–541, 1995.

[26] C. F. Beckmann, C. E. Mackay, N. Filippini, and S. M. Smith, "Group comparison of resting-state FMRI data using multi-subject ICA and dual regression," in *Proceedings of the 15th Annual Meeting of the Organization of Human Brain Mapping (HBM '09)*, San Francisco, Calif, USA, June 2009.

[27] A. Zalesky, A. Fornito, and E. T. Bullmore, "Network-based statistic: identifying differences in brain networks," *NeuroImage*, vol. 53, no. 4, pp. 1197–1207, 2010.

[28] W. C. Drevets, "Orbitofrontal cortex function and structure in depression," *Annals of the New York Academy of Sciences*, vol. 1121, pp. 499–527, 2007.

[29] J. N. Felder, M. J. Smoski, R. V. Kozink et al., "Neural mechanisms of subclinical depressive symptoms in women: a pilot functional brain imaging study," *BMC Psychiatry*, vol. 12, article 152, 2012.

[30] A. K. Y. Mak, Z.-G. Hu, J. X. X. Zhang, Z. Xiao, and T. M. C. Lee, "Sex-related differences in neural activity during emotion regulation," *Neuropsychologia*, vol. 47, no. 13, pp. 2900–2908, 2009.

[31] M. L. Phillips, C. D. Ladouceur, and W. C. Drevets, "A neural model of voluntary and automatic emotion regulation: implications for understanding the pathophysiology and neurodevelopment of bipolar disorder," *Molecular Psychiatry*, vol. 13, no. 9, pp. 833–857, 2008.

[32] V. Menon, "Large-scale brain networks and psychopathology: a unifying triple network model," *Trends in Cognitive Sciences*, vol. 15, no. 10, pp. 483–506, 2011.

[33] V. Menon and L. Q. Uddin, "Saliency, switching, attention and control: a network model of insula function," *Brain Structure & Function*, vol. 214, no. 5-6, pp. 655–667, 2010.

[34] G. Rajkowska, J. J. Miguel-Hidalgo, J. Wei et al., "Morphometric evidence for neuronal and glial prefrontal cell pathology in major depression," *Biological Psychiatry*, vol. 45, no. 9, pp. 1085–1098, 1999.

[35] J. D. Bremner, M. Vythilingam, E. Vermetten et al., "Reduced volume of orbitofrontal cortex in major depression," *Biological Psychiatry*, vol. 51, no. 4, pp. 273–279, 2002.

[36] A. L. T. Lacerda, A. Y. Hardan, O. Yorbik, and M. S. Keshavan, "Measurement of the orbitofrontal cortex: a validation study of a new method," *NeuroImage*, vol. 19, no. 3, pp. 665–673, 2003.

[37] T.-J. Lai, M. E. Payne, C. E. Byrum, D. C. Steffens, and K. R. R. Krishnan, "Reduction of orbital frontal cortex volume in geriatric depression," *Biological Psychiatry*, vol. 48, no. 10, pp. 971–975, 2000.

[38] F. Biver, S. Goldman, V. Delvenne et al., "Frontal and parietal metabolic disturbances in unipolar depression," *Biological Psychiatry*, vol. 36, no. 6, pp. 381–388, 1994.

[39] J. D. Townsend, N. K. Eberhart, S. Y. Bookheimer et al., "FMRI activation in the amygdala and the orbitofrontal cortex in unmedicated subjects with major depressive disorder," *Psychiatry Research—Neuroimaging*, vol. 183, no. 3, pp. 209–217, 2010.

[40] J. R. Andrews-Hanna, A. Z. Snyder, J. L. Vincent et al., "Disruption of large-scale brain systems in advanced aging," *Neuron*, vol. 56, no. 5, pp. 924–935, 2007.

[41] R. M. Birn, K. Murphy, J. Bodurka, and P. A. Bandettini, "The use of multiple physiologic parameter regression increases gray matter temporal signal to noise by up to 50%," in *Proceedings of the 14th Scientific Meeting of the International Society for Magnetic Resonance in Medicine*, p. 1091, Seattle, Wash, USA, 2006.

Research Article

The Altered Triple Networks Interaction in Depression under Resting State Based on Graph Theory

Hongna Zheng,[1] Lele Xu,[1] Fufang Xie,[1] Xiaojuan Guo,[1] Jiacai Zhang,[1] Li Yao,[1,2,3] and Xia Wu[1,2,3,4]

[1] *College of Information Science and Technology, Beijing Normal University, No. 19 Xin Jie Kou Wai Da Jie, Beijing 100875, China*

[2] *State Key Laboratory of Cognitive Neuroscience and Learning and IDG/McGovern Institute for Brain Research, Beijing Normal University, Beijing 100875, China*

[3] *Center for Collaboration and Innovation in Brain and Learning Sciences, Beijing Normal University, Beijing 100875, China*

[4] *State Key Laboratories of Transducer Technology, Chinese Academy of Sciences, Shanghai 200050, China*

Correspondence should be addressed to Xia Wu; wuxia@bnu.edu.cn

The triple network model (Menon, 2011) has been proposed, which helps with finding a common framework for understanding the dysfunction in core neurocognitive network across multiple disorders. The alteration of the triple networks in the major depression disorder (MDD) is not clear. In our study, the altered interaction of the triple networks, which include default model network (DMN), central executive network (CEN), and salience network (SN), was examined in the MDD by graph theory method. The results showed that the connectivity degree of right anterior insula (rAI) significantly increased in MDD compared with healthy control (HC), and the connectivity degree between DMN and CEN significantly decreased in MDD. These results not only supported the proposal of the triple network model, but also prompted us to understand the dysfunction of neural mechanism in MDD.

1. Introduction

Human brain is a complex neural network; many psychological and neurological disorders are associated with the dysfunction of multiple brain regions or networks [1–4]. Based on that, Menon proposed a triple network model which helps in finding a common framework for understanding cognitive and affection disorders [4]. Major depression disorder (MDD), as one of the main kinds of affection disorders, is characterized by stable, pervasive depressive mood, guilt, disinterest, worthlessness, and even tendency of suicide [5]. It seriously impacts the daily lives of patients as well as their family and also brings about significant economic and professional functioning burdens to society [6]. It is important to investigate the altered interaction of the triple networks in MDD, which will help to understand the neural mechanism of MDD.

Three networks, default model network (DMN), central executive network (CEN), and the salience network (SN), are included in the triple network model. DMN decreases neural activity when performing task and increases activity in the resting [1]; CEN is responsible for high-level cognitive functions and external information procession [4] and the SN keeps homeostatic interoception and external stimulus [7]. In particular, anterior insula (AI) within SN is a hub of the large scale brain networks and is applied to accommodate the dynamic interaction between the internal self-perception and external orient stimulus [4, 8]. In recent years, dysfunction of the three cognitive networks has remarkably occurred in many mental and neurological disorders [2, 9–12]. For instance, the intraintrinsic functional connectivity (intra-iFC) was altered in patients' DMN, CEN, and SN and the interintrinsic functional connectivity (inter-iFC) between the SN and CEN was increased in schizophrenia [12]. All of these

studies suggested that the triple network model may offer a new insight to understand the brain mechanism of MDD.

The study of Sheline et al. (2010, PNAS) in MDD was to explore the altered connectivity between the dorsal medial prefrontal cortex region and the three important networks: the cognitive control networks, default mode network, and affective network. They determined significant differences using the three a priori seed regions by mean correlation coefficients between the MDD and HC [10]. In Manoliu et al.'s study the participants' spatial maps were compared by two-sample t-test among the interested networks (anterior DMN, inferior posterior DMN, superior posterior DMN, SN, left ventral CEN, right ventral CEN, and dorsal CEN); patient with MDD showed decreased intra-iFC within SN right AI. The decreased inter-iFC between the DMN and CEN and increased inter-iFC between the SN and DMN after the subjects' specific time courses were used to analyze the inter-iFC among these interested networks [13]. Furthermore, many studies based on functional magnetic resonance imaging (fMRI) have reported that the abnormality of the functional connectivity in the intrinsic brain neural mechanism contributes to the MDD [14]. Yuen et al.'s study showed that resting state functional connectivity between the right anterior insula (rAI) and right posterior parietal cortex (rPPC) increased in the apathy of late-life depression [15]; the research of Lemogne et al. indicated that patients in depression displayed an increasing functional connectivity between the medial frontal gyrus (MFG), dorsal anterior cingulate cortex (dACC), and the dorsolateral prefrontal cortex (dlPFC) [16], and Strigo et al. reported that the depression subjects showed lower rAI activity related to anticipatory shift in stimulus intensity [17]. However, the interaction among networks of the nodes in the triple networks of MDD is not clear.

In this study, functional connectivity of the nodes and the interaction between the triple networks (DMN, CEN, and SN) in MDD and HC under the resting state fMRI were examined by graph theory method, which has been applied to the multiple brain regions functional connectivity in both the resting state and the motor task [18].

2. Materials and Methods

2.1. Participants. Sixteen MDD (four males, mean age 33.13 years) and sixteen age-, sex-, and education-matched HC participated in this study. The MDD were recruited from the Anding Hospital, Capital Medical University, while the participants in the HC group were recruited through newspaper advertisements. All the subjects in MDD met the American Psychiatric Association DSM-IV diagnostic criteria of depression, and HC were interviewed using the Structured Clinical Interview for DSM-IV, nonpatient edition. Before experiment, all of the subjects wrote informed consent by themselves. The clinical characteristics of MDD and HC were shown in Table 1.

2.2. fMRI Data Acquisition. All the resting state functional images scans were acquired on a 3.0-Tesla scanner (Siemens,

Erlangen, Germany) in the National Key Laboratory for Cognitive Neuroscience and Learning, Beijing Normal University, using a single-shot T2* weighted gradient echo-planar imaging (EPI) sequence, with the following parameters: repetition time (TR) = 2000 ms, echo time (TE) = 30 ms, flip angle (FA) = 90°, matrix size = 64 × 64, field of view (FOV) = 220 mm × 220 mm, total 240 volumes, slice thickness = 3.5 mm, skip = 0.6 mm, and slices number 33. All participants were kept in resting state, remained quiet, without moving, eyes closed, no sleeping, and no system thinking activities during functional MRI scanning.

2.3. Data Preprocessing. Firstly, the data preprocessing was performed based on the software of SPM8 (statistical Parametric Mapping 8, http://www.fil.ion.ucl.ac.uk/spm). Each fMRI scan contained a total of 240 times points; the first 10 volumes were discarded due to signal stabilization and subjects' adaptation to the scanner's noise.

After that, slicing timing and realignment, spatially normalized into standard stereotaxic space and smoothing image volumes with an 8 × 8 × 8 full-width at half maximum (FWHM) Gaussian kernel, were performed.

Finally, the images of all subjects were done with detrend in order to remove linear trend, filtered in the bandwidth of 0.01~0.08 Hz to reduce the high-frequency interference with the Resting State fMRI Data Analysis Toolkit (REST, http://resting-fmri.sourceforge.net).

2.4. Defining the Nodes. Independent component analysis (ICA) has been reported as an appropriate method to explore the fMRI data in functional connectivity analysis [19] and has been well used in the resting state fMRI analysis [20]. In this study we used the group ICA of fMRI toolbox (GroupICAT v2.oc, http://icatb.sourceforge.net/) to obtain the brain spatial pattern maps.

In order to make sure the same components were identified in each subject, group ICA treated all subjects as one group [21]. In the current study, 22 components were chosen according to the minimum description length (MDL) method. Furthermore, the components of DMN, CEN, and SN were selected according to the previous studies about the triple networks through visual inspection [4]. After that, the spatial patterns of DMN, CEN, and SN were generated by one sample t-test with the software of SPM8.

In our study, the nodes were defined based on the spatial pattern maps. As reported in previous studies, the critical brain regions for DMN are posterior cingulate cortex (PCC), ventral medial prefrontal cortex (vmPFC), and angular gyrus (Ang) [22]. CEN mainly includes the dorsolateral prefrontal cortex (dlPFC) and posterior parietal cortex (PPC) [23]. SN consists of dorsolateral anterior cingulate cortex (dACC) and anterior insula (AI) [7]. The coordinates were determined according to the highest T-value in the spatial pattern maps shown in Table 2 in detail. After that, we defined spheres with radius of 3 mm for each node as the masks, centered on the coordinates of each node determined. Then, the associated average time series of each node was extracted for each subject.

TABLE 1: Demographic and clinical characteristics.

Variables (mean ± SD)	MDD ($n = 16$)	HC ($n = 16$)	P value[a]
Gender (M : F)	4 : 12	4 : 12	1
Age (years)	33.13 ± 8.29	39.13 ± 10.22	0.10
Education level (years)	13.75 ± 3.01	12.93 ± 2.40	0.61
Age range	21–57	21–55	
Duration of illness (years)	7.66 ± 8.29	—	
Number of depressive episodes	2.63 ± 1.26	—	
HAMD	21.44 ± 3.97	—	
HAMA	16.00 ± 9.61	—	

MDD: major depressions disorder; HC: healthy controls; SD: standard deviation; HAMD: Hamilton Depression Rating Scale.
[a]P value for the two-sample t-test of MDD and HC.

TABLE 2: Spatial coordinates of the nodes among the triple networks.

Network	Brain region	BA	Coordinates (MNI)			T
			x	y	z	
DMN	lAng	39	−48	−67	34	8.94
	rAng	39	54	−61	30	5.58
	PCC	30	0	−52	18	13.90
	vmPFC	10	−1	56	10	5.05
CEN	lPPC	7	−33	−70	50	7.73
	rPPC	7	42	−62	50	7.56
	ldlPFC	6	−27	20	58	6.03
	rdlPFC	6	27	20	62	3.60
SN	dACC	32	2	34	25	3.27
	lAI	45	−34	23	4	4.46
	rAI	45	34	23	5	3.50

BA: Brodmann areas; MNI: Montreal Neurological Institute spatial array coordinates; T: t-value.

2.5. Functional Connectivity Analyses.

For the graph theory method, the nodes are denoted by nodes in a graph and the links between the nodes represent the functional connectivity between them. The interregional connectivity degree between nodes i and j was defined as

$$\eta_{ij} = e^{-\xi d_{ij}}, \tag{1}$$

where ξ is a positive real constant; here we set it equal to 2 and it indicates how the interregional connectivity changes with the distance between the two nodes [18]. d_{ij} denotes the distance between nodes i and j calculated by Golay et al. 1998 [24], defined as

$$d_{ij} = \frac{\left(1 - c_{ij}\right)}{\left(1 + c_{ij}\right)}, \tag{2}$$

where c_{ij} represents the Pearson correlation coefficient between the two time series of nodes i and j:

$$c_{ij} = \frac{\text{cov}(i, j)}{\sigma_i \sigma_j}. \tag{3}$$

The larger the value of η means the closer the interaction between the two brain regions.

In this study, in order to explore the dynamic interaction between the three networks of the patients with depression in rest we defined two formulas with the graph theory method. One is for the intrinsic functional connectivity of all the nodes included in the three networks (DMN, CEN, and SN). The other is for the investigation of internetwork intrinsic functional connectivity between the three cognitive networks of DMN, CEN, and SN, which help to further understand the relationship between the three networks. The specific formulas are as follows.

2.5.1. The Degree of the Node.

We define the sum of all the functional interregional connectivities η between i and all other nodes in the three networks

$$\Gamma_i = \sum_{j=1}^{n} \eta_{ij} \tag{4}$$

as the connectivity degree of the node i in a graph. In this study, during the graph theory calculation, we put all the 11 nodes in one graph to obtain the degree of each node. This means that the larger the degree of node i the more the importance of node i in the graph, which also means that the greater the impact of node i on other brain regions in the network. Then we normalized the Γ_i:

$$\overline{\Gamma_i} = \frac{\Gamma_i}{\sum_{j=1}^{n} \Gamma_j}; \tag{5}$$
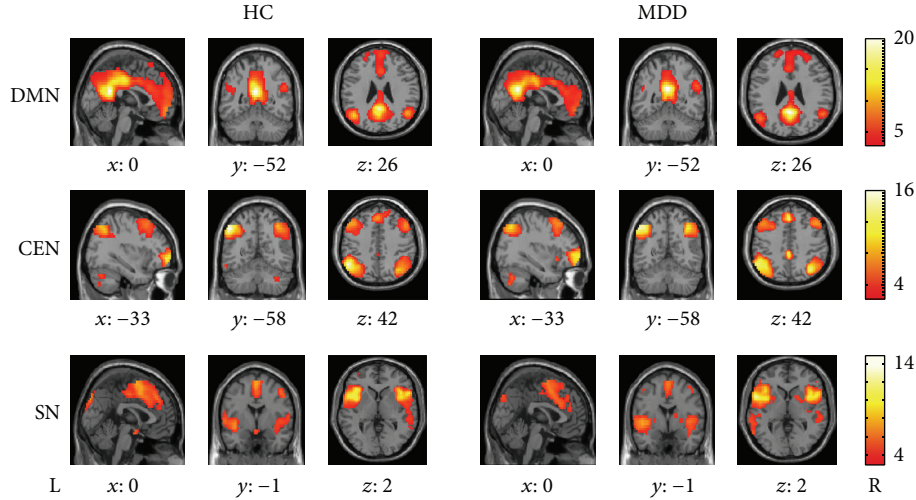
FIGURE 1: The DMN, CEN, and SN spatial pattern maps of HC and MDD. The statistical maps displaying one sample t-test of the two groups, with the color scale representing the ranges of t-values.

in this study the $\overline{\Gamma_i}$ presents the functional connectivity of the node i with the other nodes in the three networks. For each node the alteration of $\overline{\Gamma}$ between the two groups was tested using two-sample t-test.

Moreover, it is necessary to investigate the significantly altered interregional connectivity that related to the node i. Thus, the nodes were significantly altered in $\overline{\Gamma}$; further exploration on the interregional connectivity η between two nodes was carried out. In particular, for each node i, the interregional connectivity $\eta_{ij} = e^{-\xi d_{ij}}$ for each $j \neq i$ was analyzed statistically by two-sample t-test between depression and HC.

2.5.2. Connectivity Degree of the Network. In order to further explore the functional connectivity between the three networks, we defined a calculation for the network analysis as follows:

$$\Gamma_{MN} = \sum_{i=1}^{n} \sum_{j=1}^{m} \eta_{ij}, \qquad (6)$$

where Γ_{MN} is the connectivity degree between the two networks M and N; m and n denote the number of nodes in the networks M and N, respectively; η_{ij} denotes the interregional connectivity between nodes i and j, defined as $\eta_{ij} = e^{-\xi d_{ij}}$; the i represents the node of the network M; and the j is the node in the network N. The larger the value of Γ_{MN}, the closer the functional connectivity between the two networks. The two-sample t-test was used to analyze the alteration of Γ_{MN} for each network between the two group subjects.

3. Result

3.1. Spatial Pattern of the Triple Networks. In our study the nodes of DMN were PCC, vmPFC, right Ang (rAng), and left Ang (lAng). CEN mainly included the right dlPFC (rdlPFC), left dlPFC (ldlPFC), right (rPPC), and left PPC (lPPC). SN consisted of dACC, right AI (rAI), and left AI (lAI). The

group spatial pattern maps of the DMN, CEN, and SN were shown in Figure 1. The coordinates determined according to the highest T-value were shown in Table 2.

3.2. Alteration of Connectivity Degree of Nodes. After the two-sample t-test for each node between MDD and HC, significant increase in the connectivity degree of the rAI was detected in MDD ($P < 0.05$). The alteration also existed in other brain regions though not significant statistically. For MDD, the mean connectivity degree of lAI and dACC increased and the mean degree for vmPFC, PCC, bilateral angular gyrus (rAng and lAng), bilateral dlPFC (rdlPFC and rdlPFC), and bilateral PPC (rPPC and lPPC) decreased compared with HC (Figure 2).

3.3. Alterations of Interregional Connectivity between Nodes. The degree of rAI significantly increased in MDD compared to the HC just as above shown (Figure 2). Therefore the interregional connectivity (η) between the rAI and other nodes was measured in further analysis. For MDD, the η between rAI and vmPFC, rdlPFC, ldlPFC, rPPC, lPPC, PCC, rAng, and lAng was larger than HC although the alteration was not significant after the statistical analysis by two-sample t-test. The result is shown in Figure 3.

3.4. Alterations of Connectivity Degree between Networks. After the investigation of the connectivity degree between networks with $\Gamma_{MN} = \sum_{i=1}^{n} \sum_{j=1}^{m} \eta_{ij}$ and two-sample t-test, the result showed that the connectivity degree between the DMN and CEN significantly decreased in MDD (two-sample t-test, $P < 0.05$). The interaction degree of the networks DMN and SN, CEN, and SN increased in MDD. The details are shown in Table 3 and Figure 4.

4. Discussion

To investigate the relationship among the important cognitive and affective related brain regions of the triple networks (DMN, CEN, and SN) in MDD, the functional connectivity
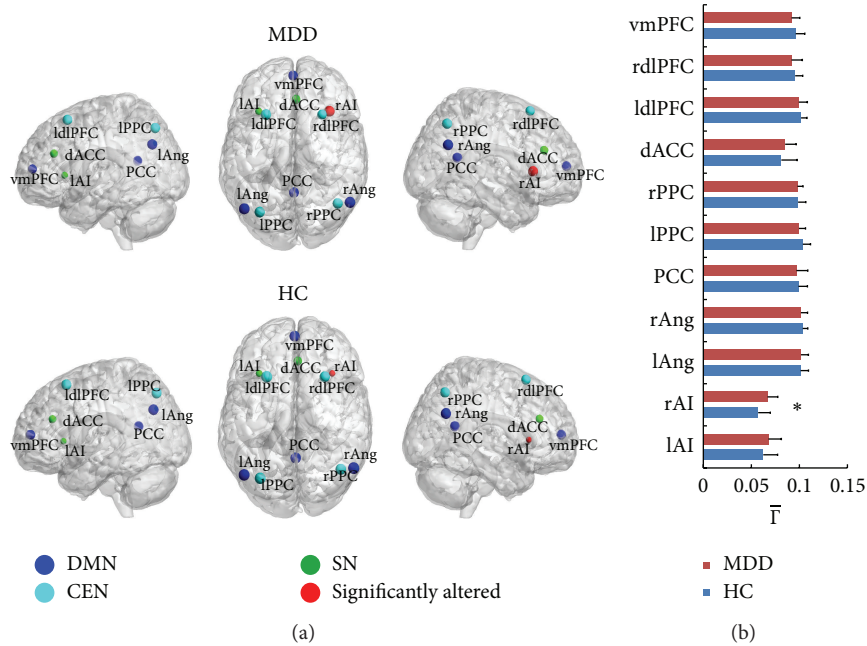
FIGURE 2: The region connectivity degree of MDD and HC. In (a) the size of the node visualizes the value of the connectivity degree $\bar{\Gamma}$ of all the 11 nodes. Red dot indicates the nodes that significantly altered for the MDD compared to HC; the other colored dots mean "not significant." The blue dots are the nodes in DMN and dark green dots in CEN; bright green dots indicate the nodes in SN. (b) shows the $\bar{\Gamma}$ of all the 11 nodes (∗ represents significance with $P < 0.05$).

TABLE 3: The connectivity degree between networks and the P value by two-sample t-test.

Variables (mean ± SD)	MDD	HC	P value (MDD versus HC)
DMN-CEN	7.15 ± 2.72	9.27 ± 1.57	0.01*
DMN-SN	1.63 ± 3.16	0.73 ± 2.72	0.40
CEN-SN	2.70 ± 2.87	2.19 ± 2.74	0.61

*Significant by two-sample t-test.

of the nodes and the altered interaction of the triple networks (DMN, CEN, and SN) were examined by using the graph theory method in the resting state fMRI. The results demonstrated the significantly increased degree of rAI in MDD and the significantly decreased interaction degree between the DMN and CEN in MDD.

4.1. Aberrance of Connectivity Degree in Nodes. Increased degree of rAI is found in MDD, which means the interactivity between the rAI and the other brain regions increases in MDD during resting state. This suggested that the aberrance of rAI contributes to the cognitive impairment of depression in rest. The deficit of rAI was found in the literature in MDD [13]. Meanwhile, some researches have proved that rAI, which is an important brain region of SN [7], is associated with neural cognition, interoception, affection process, and subjective and autonomic function [25], which are all associated with depression [5]. The aberrance of rAI contributes to the dysfunction switch of the DMN and CEN in resting state [13, 26]. The disorder of the connectivity degree of rAI between other regions in the triple network model suggested

that more activity is needed to keep the normal regulation in the MDD.

4.2. Aberrance of Interregional Connectivity. The alteration of interregional connectivity between the rAI and the other regions in the triple networks was detected. The interregional connectivity η increases occurred in the vmPFC, rdlPFC, ldlPFC, rPPC, lPPC, PCC, rAng, and lAng brain regions. All these increasing η contributed to the significantly increased connectivity degree of the rAI and further proved the important role of the AI in MDD. The other brain regions are all important for the neurocognition, such as the research showing that the brain regions of PCC and Ang are related to the episodic memory retrieval [27], autobiographical memory [28], and semantic memory related to internal thought [29]. The vmPFC is associated with self-related and social cognitive processes [30], value-based decision making [31], and emotion regulation [32]. The decreased function of dlPFC in MDD has been detected in resting [33], which matches the result of our study shown in **Figure 2**. Though the CEN is composed of portion of prefrontal lobe and parietal lobe,
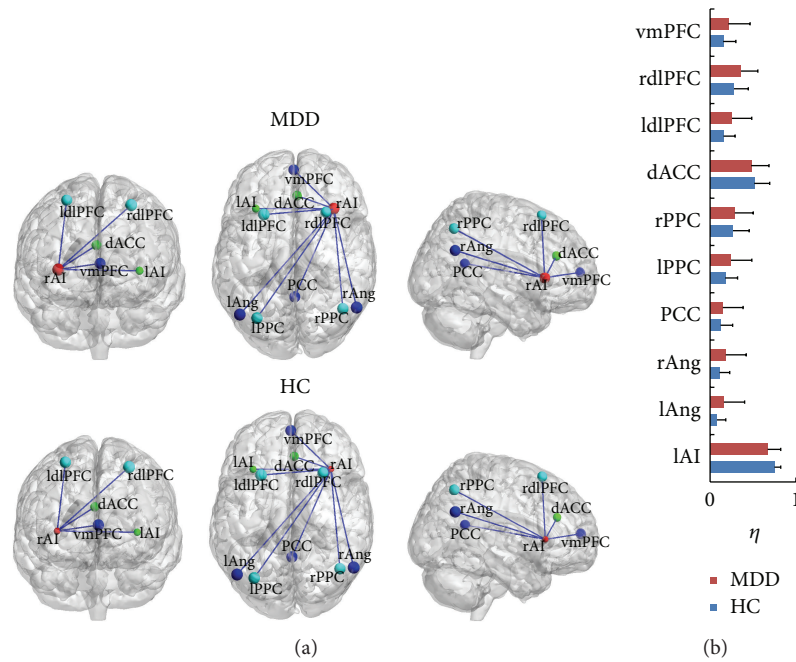
FIGURE 3: The interregional connection η between rAI and other brain regions in MDD and HC. (a) The lines showed the visualization of η. (b) shows the value η between the rAI and all the other nodes.
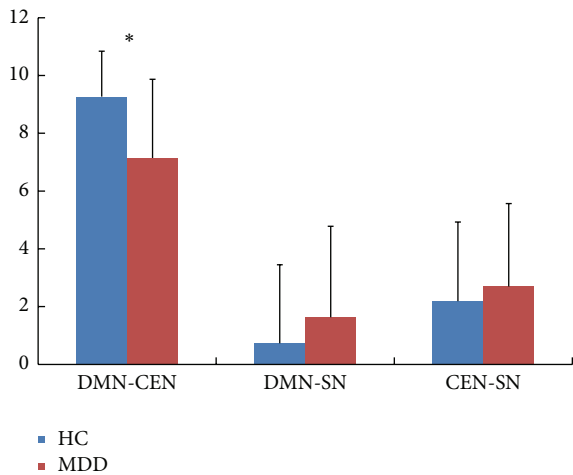
FIGURE 4: The connectivity degree Γ between the networks. Γ is the functional connectivity degree between the networks for the two groups ($*$ represents significance by two-sample t-test).

a lot of investigations show the main abnormal functional connection of several psychiatric disorders associated with the aberrance of dlPFC, including the depression [4, 34, 35].

4.3. Aberrance of Networks. For MDD, the functional connectivity degree between the DMN and CEN significantly decreases compared with the HC in the current study. The network DMN is involved in self-referential oriented process, which is active in the resting state [36] and is deactivated during goal-directed tasks [9]. The CEN is responsible for the high-level external cognitive tasks and modulation of

mood reaction [37] in both of resting state [34] and stimulus task [35] in major depression. The investigations have found dysfunction in both of the two cognitive networks in MDD [38]. The results suggested the decreased functional interaction between the DMN and CEN of the MDD in the resting state. Our findings couple with the statement of the aberrant network connectivity in major depression [10, 39]. The results might suggest that the patients with MDD cannot normally regulate the switching between the internal self-reference, working memory, autobiography, decision making and the external stimulus, orientation tasks, and demand cognitive action in rest.

According to the triple model proposed by Menon [4], it is mentioned that SN has a core role in mediating the conversion of the functional connectivity between the DMN, which is related to the self-referential cognition [36], and CEN, which is related to the external oriented task [37], especially the region rAI which is part of SN [4, 26]. A lot of researches demonstrate that the rAI occupies an important position in the interaction between the DMN and CEN in the HC [26] and MDD [8] and also in other psychogenic disorders. Recently, Manoliu et al. found that the aberrance of the rAI may be associated with the disorder interaction between DMN and CEN in schizophrenia [2, 12] and major depression [13]. In our study, patients with MDD could not well modulate the dynamic interaction between the DMN and CEN. All of these researches provided evidence for the assumption of the triple network model, which might be a common frame for understanding dysfunction in the three core networks of variety in cognitive disorders and supported the proposal of the triple network model. It showed the contribution of the rAI to the depression and suggested a

link between the MDD and the dysfunction interaction of the DMN and CEN.

5. Conclusion

The results showed that increased connectivity degree occurred in right anterior insula (rAI) in MDD compared with HC and decreased connectivity degree between DMN and CEN in MDD. These abnormalities may indicate that the functional connectivity increased between the SN and CEN for MDD and the dynamic interaction between the DMN and CEN decreased for MDD. All the results provided new insights into our understanding of depression.

Conflict of Interests

The authors declare that there is no conflict of interests regarding the publication of this paper.

Acknowledgments

References

[1] M. D. Greicius, B. Krasnow, A. L. Reiss, and V. Menon, "Functional connectivity in the resting brain: a network analysis of the default mode hypothesis," *Proceedings of the National Academy of Sciences of the United States of America*, vol. 100, no. 1, pp. 253–258, 2003.

[2] A. Manoliu, V. Riedl, A. Zherdin et al., "Aberrant dependence of default mode/central executive network interactions on anterior insular salience network activity in schizophrenia," *Schizophrenia Bulletin*, vol. 40, no. 2, pp. 428–437, 2014.

[3] F. X. Castellanos and E. Proal, "Large-scale brain systems in ADHD: beyond the prefrontal-striatal model," *Trends in Cognitive Sciences*, vol. 16, no. 1, pp. 17–26, 2012.

[4] V. Menon, "Large-scale brain networks and psychopathology: a unifying triple network model," *Trends in Cognitive Sciences*, vol. 15, no. 10, pp. 483–506, 2011.

[5] American Psychiatric Association, *Diagnostic And Statistical Manual Of Mental Disorders DSM-IV-TR*, American Psychiatric Association, 4th edition, 2000.

[6] A. D. Lopez, C. D. Mathers, M. Ezzati, D. T. Jamison, and C. J. Murray, "Global and regional burden of disease and risk factors, 2001: systematic analysis of population health data," *The Lancet*, vol. 367, no. 9524, pp. 1747–1757, 2006.

[7] N. Goulden, A. Khusnulina, N. J. Davis et al., "The salience network is responsible for switching between the default mode network and the central executive network: replication from DCM," *NeuroImage*, vol. 99, pp. 180–190, 2014.

[8] V. Menon and L. Q. Uddin, "Saliency, switching, attention and control: a network model of insula function," *Brain Structure and Function*, vol. 214, no. 5-6, pp. 655–667, 2010.

[9] Y. I. Sheline, D. M. Barch, J. L. Price et al., "The default mode network and self-referential processes in depression," *Proceedings of the National Academy of Sciences of the United States of America*, vol. 106, no. 6, pp. 1942–1947, 2009.

[10] Y. I. Sheline, J. L. Price, Z. Yan, and M. A. Mintun, "Resting-state functional MRI in depression unmasks increased connectivity between networks via the dorsal nexus," *Proceedings of the National Academy of Sciences of the United States of America*, vol. 107, no. 24, pp. 11020–11025, 2010.

[11] C. Rosano, H. J. Aizenstein, J. L. Cochran et al., "Event-related functional magnetic resonance imaging investigation of executive control in very old individuals with mild cognitive impairment," *Biological Psychiatry*, vol. 57, no. 7, pp. 761–767, 2005.

[12] A. Manoliu, V. Riedl, A. Doll et al., "Insular dysfunction reflects altered between-network connectivity and severity of negative symptoms in schizophrenia during psychotic remission," *Frontiers in Human Neuroscience*, vol. 7, 2013.

[13] A. Manoliu, C. Meng, F. Brandl et al., "Insular dysfunction within the salience network is associated with severity of symptoms and aberrant inter-network connectivity in major depressive disorder," *Frontiers in Human Neuroscience*, vol. 7, article 930, 2014.

[14] C. Lemogne, P. Delaveau, M. Freton, S. Guionnet, and P. Fossati, "Medial prefrontal cortex and the self in major depression," *Journal of Affective Disorders*, vol. 136, no. 1, pp. e1–e11, 2012.

[15] G. S. Yuen, F. M. Gunning-Dixon, M. J. Hoptman et al., "The salience network in the apathy of late-life depression," *International Journal of Geriatric Psychiatry*, vol. 29, no. 11, pp. 1116–1124, 2014.

[16] C. Lemogne, G. le Bastard, H. Mayberg et al., "In search of the depressive self: extended medial prefrontal network during self-referential processing in major depression," *Social Cognitive and Affective Neuroscience*, vol. 4, no. 3, pp. 305–312, 2009.

[17] I. A. Strigo, S. C. Matthews, and A. N. Simmons, "Right anterior insula hypoactivity during anticipation of homeostatic shifts in major depressive disorder," *Psychosomatic Medicine*, vol. 72, no. 3, pp. 316–323, 2010.

[18] T. Jiang, Y. He, Y. Zang, and X. Weng, "Modulation of functional connectivity during the resting state and the motor task," *Human Brain Mapping*, vol. 22, no. 1, pp. 63–71, 2004.

[19] M. J. McKeown and T. J. Sejnowski, "Independent component analysis of fMRI data: examining the assumptions," *Human Brain Mapping*, vol. 6, no. 5-6, pp. 368–372, 1998.

[20] V. G. van de Ven, E. Formisano, D. Prvulovic, C. H. Roeder, and D. E. J. Linden, "Functional connectivity as revealed by spatial independent component analysis of fMRI measurements during rest," *Human Brain Mapping*, vol. 22, no. 3, pp. 165–178, 2004.

[21] S. H. A. Chen, C.-Y. Wu, R.-P. Lua, M. Miyakoshi, and T. Nakai, "Age-related changes in resting-state and task-activated functional MRI networks," in *Proceedings of the 7th International Symposium on Medical Information and Communication Technology (ISMICT '13)*, pp. 218–222, IEEE, March 2013.

[22] R. L. Buckner, J. R. Andrews-Hanna, and D. L. Schacter, "The brain's default network: anatomy, function, and relevance to disease," *Annals of the New York Academy of Sciences*, vol. 1124, pp. 1–38, 2008.

[23] W. W. Seeley, V. Menon, A. F. Schatzberg et al., "Dissociable intrinsic connectivity networks for salience processing and executive control," *The Journal of Neuroscience*, vol. 27, no. 9, pp. 2349–2356, 2007.

[24] X. Golay, S. Kollias, G. Stoll, D. Meier, A. Valavanis, and P. Boesiger, "A new correlation-based fuzzy logic clustering algorithm for fMRI," *Magnetic Resonance in Medicine*, vol. 40, no. 2, pp. 249–260, 1998.

[25] A. Ibañez, E. Gleichgerrcht, and F. Manes, "Clinical effects of insular damage in humans," *Brain Structure and Function*, vol. 214, no. 5-6, pp. 397–410, 2010.

[26] D. Sridharan, D. J. Levitin, and V. Menon, "A critical role for the right fronto-insular cortex in switching between central-executive and default-mode networks," *Proceedings of the National Academy of Sciences of the United States of America*, vol. 105, no. 34, pp. 12569–12574, 2008.

[27] C. Sestieri, M. Corbetta, G. L. Romani, and G. L. Shulman, "Episodic memory retrieval, parietal cortex, and the default mode network: functional and topographic analyses," *Journal of Neuroscience*, vol. 31, no. 12, pp. 4407–4420, 2011.

[28] R. N. Spreng, R. A. Mar, and A. S. N. Kim, "The common neural basis of autobiographical memory, prospection, navigation, theory of mind, and the default mode: a quantitative meta-analysis," *Journal of Cognitive Neuroscience*, vol. 21, no. 3, pp. 489–510, 2009.

[29] J. R. Binder, R. H. Desai, W. W. Graves, and L. L. Conant, "Where is the semantic system? A critical review and meta-analysis of 120 functional neuroimaging studies," *Cerebral Cortex*, vol. 19, no. 12, pp. 2767–2796, 2009.

[30] D. M. Amodio and C. D. Frith, "Meeting of minds: the medial frontal cortex and social cognition," *Nature Reviews Neuroscience*, vol. 7, no. 4, pp. 268–277, 2006.

[31] A. Rangel, C. Camerer, and P. R. Montague, "A framework for studying the neurobiology of value-based decision making," *Nature Reviews Neuroscience*, vol. 9, no. 7, pp. 545–556, 2008.

[32] A. Etkin, T. Egner, and R. Kalisch, "Emotional processing in anterior cingulate and medial prefrontal cortex," *Trends in Cognitive Sciences*, vol. 15, no. 2, pp. 85–93, 2011.

[33] C. J. Bench, K. J. Friston, R. G. Brown, L. C. Scott, R. S. J. Frackowiak, and R. J. Dolan, "The anatomy of melancholia—focal abnormalities of cerebral blood flow in major depression," *Psychological Medicine*, vol. 22, no. 3, pp. 607–615, 1992.

[34] P. B. Fitzgerald, A. R. Laird, J. Maller, and Z. J. Daskalakis, "A meta-analytic study of changes in brain activation in depression," *Human Brain Mapping*, vol. 29, no. 6, pp. 683–695, 2008.

[35] P. B. Fitzgerald, A. Srithiran, J. Benitez et al., "An fMRI study of prefrontal brain activation during multiple tasks in patients with major depressive disorder," *Human Brain Mapping*, vol. 29, no. 4, pp. 490–501, 2008.

[36] M. D. Greicius, B. H. Flores, V. Menon et al., "Resting-state functional connectivity in major depression: abnormally increased contributions from subgenual cingulate cortex and thalamus," *Biological Psychiatry*, vol. 62, no. 5, pp. 429–437, 2007.

[37] M. D. Fox and M. E. Raichle, "Spontaneous fluctuations in brain activity observed with functional magnetic resonance imaging," *Nature Reviews Neuroscience*, vol. 8, no. 9, pp. 700–711, 2007.

[38] J. P. Hamilton, M. C. Chen, and I. H. Gotlib, "Neural systems approaches to understanding major depressive disorder: an intrinsic functional organization perspective," *Neurobiology of Disease*, vol. 52, pp. 4–11, 2013.

[39] G. S. Alexopoulos, M. J. Hoptman, G. Yuen et al., "Functional connectivity in apathy of late-life depression: a preliminary study," *Journal of Affective Disorders*, vol. 149, no. 1–3, pp. 398–405, 2013.

Research Article

An fMRI Study of Local Synchronization in Different Subfrequency Bands during the Continuous Feedback of Finger Force

Hang Zhang,[1,2,3] Zhong-Zhan Gao,[2,3] and Yu-Feng Zang[1,2,3]

[1]*Paul C. Lauterbur Research Center for Biomedical Imaging, Shenzhen Institutes of Advanced Technology,*
 Chinese Academy of Sciences, Shenzhen 518055, China
[2]*Center for Cognition and Brain Disorders and the Affiliated Hospital, Hangzhou Normal University, Hangzhou 310015, China*
[3]*Zhejiang Key Laboratory for Research in Assessment of Cognitive Impairments, Hangzhou 310015, China*

Correspondence should be addressed to Hang Zhang; hang.zhang@siat.ac.cn

Conventional functional magnetic resonance imaging (fMRI) studies on motor feedback employ periodical blocked paradigm which does not allow frequency analysis of brain activity. Here, we carried out an fMRI study by using a continuous paradigm, that is, continuous (8 min) feedback of finger force. Borrowing an analytic method widely used in resting-state fMRI studies, that is, regional homogeneity (ReHo), we compared the local synchronization in some subfrequency bands between real and sham feedback, and the subbands were defined as Slow-6 (0.0–0.01 Hz), Slow-5 (0.01–0.027 Hz), Slow-4 (0.027–0.073 Hz), Slow-3 (0.073–0.198 Hz), and Slow-2 (0.198–0.25 Hz). Our results revealed that the five subfrequency bands of brain activity contributed to the changes of ReHo between real and sham feedback differently, and, more importantly, the changes in basal ganglia were only manifested in Slow-6, implicating the fact that ReHo in ultraslow band may be associated with the functional significance of BG, that is, motor control. These findings provide novel insights into the neural substrate underlying motor feedback, and properties of the ultraslow band of local synchronization deserve more attention in future explorations.

1. Introduction

The motor feedback is a technique that enables participants to effectively regulate some kinetic parameters such as muscle force [1], speed [2], and gestures [3]. It exhibits benefits in improving some motor functions like the stand balance [4], finger force [5], and bimanual coordination [6] and also subserves the motor function rehabilitation for the patients with brain disorders of Parkinson disease [7], brain damage [8], chronic stroke [9], and so forth. These clinical values prompt more and more investigations on the neural substrates underlying the motor feedback.

Neuroimaging investigations intensively indicate that the motor feedback involves intricate brain activity. Results from functional magnetic resonance imagining mostly revealed that the motor cortices (e.g., precentral gyrus and postcentral gyrus) [10, 11], basal ganglia [12], and visual cortices [13, 14] exhibit functional prominence for varied experimental conditions of motor feedback, such as precision versus power force grip [10, 13], force magnitude [15], duration of maintained force [16], feedback frequency [17], and maturation of force control [18]. The involvement of these brain areas mainly came from the investigations on a block paradigm which is intermitted periodically (such as 30 s); however, the motor feedback in practice, for example, when driving a car, usually lasts for several minutes/hours. During such long-lasting feedback, sustained attention also plays important roles in motor control [19, 20]. Thus, Dong and his colleagues proposed a continuous performing paradigm for the fMRI investigation of the motor feedback and revealed the altered

brain activity in the visual cortex and the areas of the default mode network, for example, posterior cingulate cortex, while comparing real and sham feedback conditions [21].

Recently, frequency-dependent characteristics of brain activity have been reported by more and more fMRI investigations [22–25]. Some separate frequency bands of brain activity such as Slow-6 (0.0–0.01 Hz) [22], Slow-5 (0.01–0.027 Hz), Slow-4 (0.027–0.073 Hz), Slow-3 (0.073–0.198 Hz) [23, 24], and Slow-2 (0.198–0.25 Hz) [23] are generated with specific properties and physiological functions. The frequency-dependent analysis of brain activity exhibits clinical usefulness for quantification and detection of the functional pathological changes in brain disorders such as Parkinson's disease [25]. Although these brain disorders could be treated clinically with the motor feedback, the brain activity of motor feedback remains to be understood in different subfrequency bands.

Brain activity measured with the fMRI signal exhibits the local synchronization of the time courses of neighboring voxels, which could be assessed through the measurement of regional homogeneity (ReHo). Therefore, the present study aims to examine the local synchronization in the subfrequency bands of Slow-6, Slow-5, Slow-4, Slow-3, and Slow-2 during motor feedback. Conventional block paradigm involves the periodical intermission that does not allow frequency-dependent analysis. Thus, we performed the fMRI experiment by employing a continuous paradigm, that is, continuous feedback of finger force. Then, the differences in ReHo between real and sham feedback conditions were investigated in the subfrequency bands.

2. Materials and Methods

2.1. Participants.
Forty-three right-handed college students participated in the study (22.7 ± 1.6 years, range 19–25; 23 females). No participant had the histories of brain injury, neurological illness, or psychiatric disorders. Five subjects were excluded due to the malfunction of experimental equipment or excessive head motion (head motion was >2 mm translation or >2° rotation in any direction), and, at last, data from 38 subjects (mean age, 22.3 ± 1.6 years; 19 females) were involved in the further analysis. All experiments conducted in this study were approved by the Institutional Review Board of the National Key Laboratory of Cognitive Neuroscience, Beijing Normal University. All of the subjects gave written informed before scanning.

2.2. Experimental Design.
The experimental procedure has been reported in our recent study [21]. Each participant first underwent a scanning of resting state for adapting to the fMRI environment. Then, two scanning sessions, one for continuous real feedback and one for continuous sham feedback, were performed. Each session lasted for 8 min, and the order of the two sessions was counterbalanced across all participants. In the session of real feedback, the participants gripped a pressure sensor between the right index finger and thumb. This sensor is one module of an MRI-compatible physiological multichannel analyzer (model MP150, BIOPAC Systems,

Inc., Goleta, CA). The sampling frequency was 250 Hz and the pressure sensitivity was 0.01 cm H_2O. The pressure was recorded by a sensor via an airtight tube, and the force of pressure was synchronously fed back to the participant via a projector. At the same time, each participant was requested to continuously maintain the pinch force at 20 cm H_2O as far as possible according to the visual feedback. This target force was set in order to reduce the possibility of muscular fatigue for each subject [26]. In the session of sham feedback, participants were also asked to maintain the pinch force at 20 cm H_2O as far as possible, and the visual feedback they received came from the performance of another participant in the session of real feedback. The aim of this procedure was to minimize the difference in visual presentation between real and sham feedback sessions. Because sham feedback of pinch force could be easily detected by the subject, we informed participants of this fact in advance and requested them to watch the feedback while keeping their own performance unaffected. Before each session, the participants had a short training period.

2.3. Image Acquisition.
Brain scans were performed at the MRI Center of Beijing Normal University using a 3.0-T Siemens whole-body MRI scanner. A single-shot $T2^*$-weighted, gradient-echo EPI sequence was used for functional imaging acquisition with the following parameters: TR/TE/flip angle = 2000 ms/30 ms/90°, acquisition matrix = 64 × 64, field of view (FOV) = 200 × 200 mm^2, and thickness/gap = 3.5/0.7 mm. Thirty-three axial slices parallel to the AC-PC line were obtained in an interleaved order to cover the entire cerebrum and cerebellum. Then a T1-weighted sagittal three-dimensional magnetization-prepared rapid gradient-echo (MPRAGE) sequence was acquired (128 sagittal slices, thickness/gap = 1.33/0 mm, in-plane resolution = 256 × 192, TR = 2530 ms, TE = 3.39 ms, inversion time = 1100 ms, flip angle = 7°, and FOV = 256 × 256 mm^2).

2.4. Data Analysis

2.4.1. Preprocessing.
The preprocessing was carried out using the Data Processing Assistant for Resting-State fMRI (DPARSF) [27] which is based on the Statistical Parametric Mapping (SPM8) (http://www.fil.ion.ucl.ac.uk/spm/) and Resting-State fMRI Data Analysis Toolkit (REST) [28] (http://www.restfmri.net/). For each subject, the first 10 time points of the functional data of real/sham feedback were discarded to allow for signal stabilization. These images were further corrected for intravolume acquisition time delay between slices and intervolume geometrical displacement due to head movement. Then, all images were normalized to the standard Montreal Neurological Institute (MNI) template (resampled into 3 × 3 × 3 mm^3) via parameters of individual structural image spatial normalization based on unified segmentation [29]. Six head motion parameters (three rigid body translations and three rotations) were regressed out from the fMRI data, and the linear trends were removed from the time courses of the voxels in each image. According to previous

TABLE 1: Clusters showing significant main effect for the feedback condition. The statistical threshold was set at $P < 0.005$, cluster size >98.

Brain regions	L/R	BA	Peak MNI coordinates			
			x	y	z	$F(1, 370)$
Inferior/middle occipital Gyrus/calcarine	L/R	17/18	12	−90	0	78.86
PCC	L/R	31	0	−45	33	28.31
mPFC	L/R	9	−6	48	27	18.36
BG	L		−24	−12	12	13.39

investigations [22–25], we used band-pass filtering to subdivide the whole detectable frequency range (0–0.25 Hz) into five subfrequency bands, namely, Slow-6 (0.0–0.01 Hz), Slow-5 (0.01–0.027 Hz), Slow-4 (0.027–0.073 Hz), Slow-3 (0.073–0.198 Hz), and Slow-2 (0.198–0.25 Hz). Then, for each subfrequency band, the filtered functional data were further assessed through a voxelwise measurement of the regional homogeneity (ReHo).

2.4.2. Regional Homogeneity (ReHo) Analysis. ReHo is an analytic method widely used in resting-state fMRI studies. It is a voxelwise measure of the brain activity by examining the synchronization of the time courses of a certain voxel and its adjacent neighboring voxels [30].

The ReHo analysis employs Kendall's coefficient of concordance (KCC) to measure the local synchronization of the time courses of neighboring voxels as follows [30]:

$$W = \frac{\sum (R_i)^2 - n\left(\overline{R}\right)^2}{(1/12) K^2 \left(n^3 - n\right)}, \tag{1}$$

where W is the KCC among given voxels, ranged from 0 to 1; R_i is the sum rank of the ith time point; $\overline{R} = ((n + 1)K/2)$ is the mean of the R_i's; K is the number of time courses within a measured cluster (here, $K = 27$, one given voxel plus the number of its neighbors); n is the number of ranks. The KCC was calculated for each 27 nearest neighboring voxels in a voxelwise manner and the KCC value was assigned to the central voxel of each 27-voxel cluster. For each subfrequency band, the ReHo analysis was conducted using DPARSFA. Individual ReHo image during real/sham feedback was generated within a whole-brain mask and nonbrain areas are excluded. The whole-brain mask was provided in REST [28]. The individual ReHo image for each frequency band during real/sham feedback was then smoothed with a $6 \times 6 \times 6$ mm full-width-at-half-maximum (FWHM) Gaussian kernel. Then, a two-way repeated measures analysis of variance (ANOVA) was performed with factors of the feedback condition (2 levels, real and sham) and the frequency band (5 levels, i.e., Slow-6, Slow-5, Slow-4, Slow-3, and Slow-2). Then, the resultant F-maps were corrected for multiple comparisons with the threshold of $P < 0.005$ and cluster size >98 voxels, corresponding to a corrected P value of <0.05 as determined by AlphaSim (http://afni.nimh.nih.gov/pub/dist/doc/manual/AlphaSim.pdf). For clusters showing significance in the main effect of the feedback condition factor, region of interest (ROI) was defined with a sphere of 6 mm radius which was centered at the peak coordinate. Then, for each ROI, the mean ReHo across all subfrequency bands and subjects was

calculated for real and sham feedback conditions, respectively. For clusters showing significant interaction effect between factors of the feedback condition and the frequency band, we also defined ROIs with a sphere of 6 mm radius which was centered at the peak coordinate. ReHo of each ROI was extracted based on the frequency band and the feedback condition of every subject. Then, for each ROI, paired t-tests were further performed to examine the difference of ReHo between real and sham feedback in each subfrequency band. The tested results were corrected for multiple comparisons to a significant level of $P < 0.05$ (Bonferroni correction across the five frequency bands).

3. Result

According to the main effect of the feedback condition factor, differences of ReHo between real and sham feedback were distributed in four clusters, including bilateral visual cortex (containing bilateral inferior occipital gyrus, bilateral middle occipital gyrus, and bilateral calcarine), bilateral posterior cingulate cortex (PCC), bilateral medial prefrontal cortex (mPFC), and left BG (mainly located in putamen) (Table 1 and Figure 1(a)). For these clusters, the mean ReHo across all investigated subfrequency bands and subjects were shown in Figures 1(b)–1(e). Visual cortex showed lower ReHo while comparing real feedback with sham feedback (Figure 1(b)). As Figure 1(c) shows, ReHo for the mPFC was greater in real feedback than it was in sham feedback. As to the PCC, real feedback recruited greater ReHo than sham feedback (Figure 1(d)), and, for the left BG, greater ReHo was observed in real feedback as compared with that in sham feedback (Figure 1(e)). The main effect of the frequency band factor was similar to the findings of the previous study [23], and it was not presented here because it is not the focus of the current study.

The interaction effect between factors of the feedback condition and the frequency band was observed in three clusters, that is, the bilateral PCC and both of the left and right basal ganglia (BG) (mainly containing putamen and caudate) (Figure 2(a) and Table 2). For the PCC, real feedback exhibited greater ReHo in the Slow-5 ($t(37) = 3.71$, $P < 0.005$) and Slow-4 ($t(37) = 3.75$, $P < 0.005$) than sham feedback (Figure 2(d)). As Figures 2(b) and 2(c) show, real feedback recruited greater ReHo in the left and right BG than sham feedback and these significant differences were only manifested in Slow-6 ($t(37) = 4.38$, $P < 0.005$ for the left BG and $t(37) = 4.29$, $P < 0.005$ for the right BG).

(a)

(b)

(c)

(d)

(e)
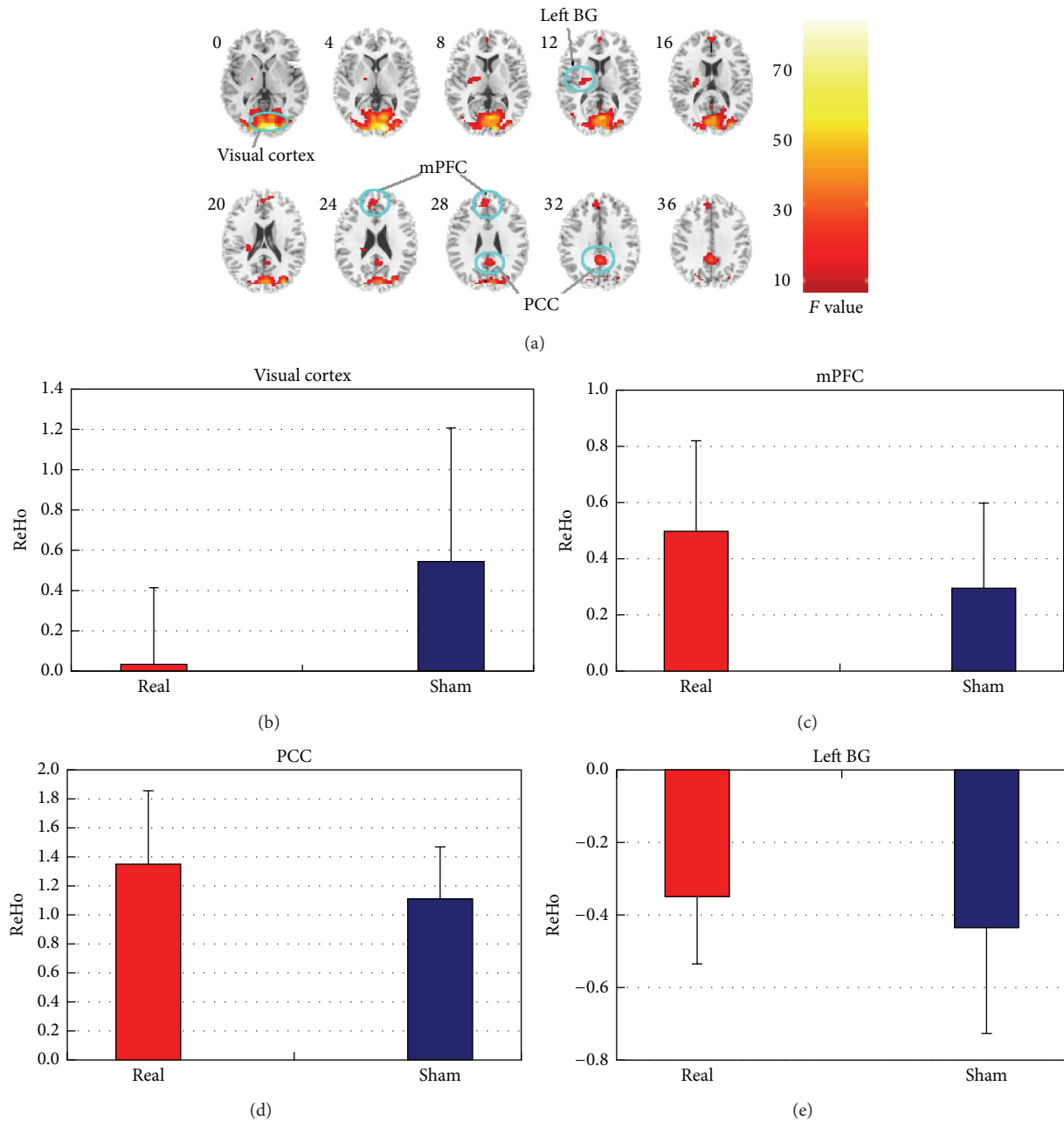
FIGURE 1: Clusters showing significant main effect of the feedback condition and ReHo of each cluster in all subfrequency bands for real/sham feedback. (a) Slice views of the spatial maps for the main effect of the feedback condition. (b) ReHo of the visual cortex in all subfrequency bands for real/sham feedback; (c) ReHo of the mPFC in all subfrequency bands for real/sham feedback; (d) ReHo of the PCC in all subfrequency bands for real/sham feedback; (e) ReHo of the left BG in all subfrequency bands for real/sham feedback. Red represents real feedback and blue represents sham feedback.

TABLE 2: Clusters showing significant interaction effect between the feedback condition and the frequency band. The statistical threshold was set at $P < 0.005$, cluster size >98.

Brain regions	L/R	BA	Peak MNI coordinates			
			x	y	z	$F(4, 370)$
PCC	L/R	7/31	0	−66	33	10.08
BG	L		−30	3	0	7.32
BG	R		33	3	6	7.79

(a)

(b)

(c)

(d)
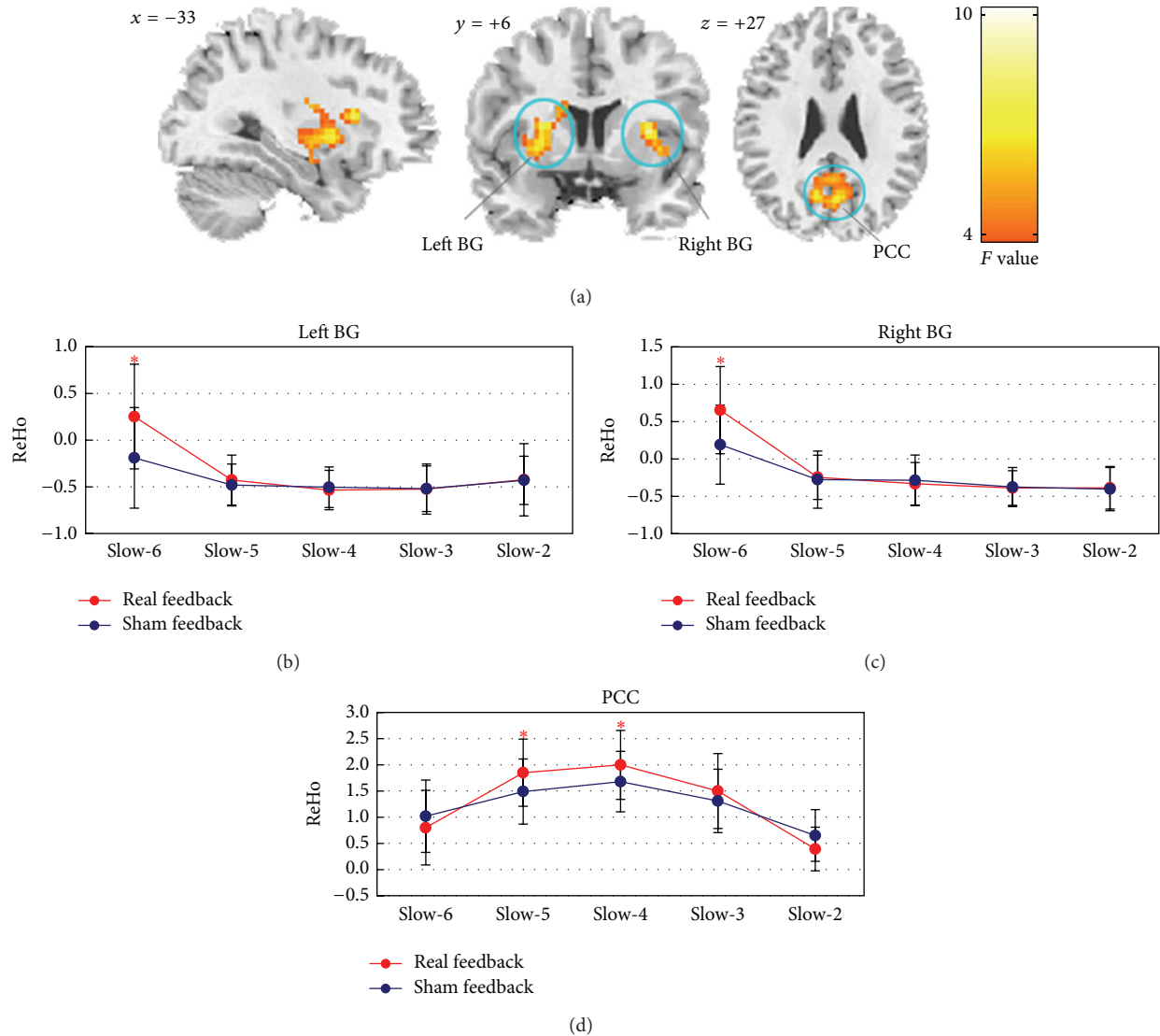
FIGURE 2: Clusters showing significant interaction effect between factors of the feedback condition and the frequency band and the relevant comparison results of ReHo in different frequency bands between real and sham feedback conditions. (a) Coronal, sagittal, and axial views of the spatial maps for the interaction effect between the feedback condition and the frequency band; (b) changes in ReHo of the left BG across the frequency bands during real and sham feedback; (c) changes in ReHo of the right BG across the frequency bands during real and sham feedback; (d) changes in ReHo of the PCC across the frequency bands during real and sham feedback. Red represents real feedback and blue represents sham feedback. ∗ indicates the significant difference of ReHo between real and sham feedback. The statistical threshold was set at $P < 0.05$, corrected for multiple comparisons.

4. Discussion

The present fMRI study investigated the neural substrate of motor feedback using a frequency-dependent analysis. The local synchronization of brain activity was assessed through a voxelwise measurement of ReHo in five separate subfrequency bands ranged from Slow-6 (0.0–0.01 Hz) to Slow-2 (0.198–0.25 Hz). Two intriguing results were observed: (1) as compared with sham feedback, real feedback recruited greater ReHo of the PCC, in Slow-5 and Slow-4; (2) ReHo differences in the left and right BG were mainly manifested in the ultraslow frequency band of Slow-6 which is less concerned in previous neuroimaging explorations.

Few previous investigations have performed fMRI investigations on the neural substrate of motor feedback in different subfrequency bands. This is probably because these investigations mostly employ the periodically blocked paradigm that is not suitable for the frequency-dependent analysis. The present study showed the benefits of the continuous paradigm and frequency-dependent ReHo analysis for examining the frequency-dependent fMRI signal characteristics in the process of task performing. The ReHo differences for the visual cortex and the mPFC were manifested in all but not some specific subfrequency bands. Real feedback recruited lower ReHo in visual cortex than sham feedback. The involvement of the visual cortex is mostly manifested in visually guided

motor feedback [13, 14]. It is thought that visual cortex mainly responds to update the visual information and further process the information for the adjustment of the force [13, 21, 31]. In our experiment, participants were requested to maintain their finger force according to real feedback, and, then, the visual processing may be more involved in this condition. Greater ReHo for the mPFC was observed while comparing real feedback with sham feedback. The mPFC is known to be highly sensitive to the sustained attention [32]. Thus, the greater ReHo in real feedback may be linked with the attentional processing of the visual stimuli [33].

The changes of ReHo in the PCC mainly came from Slow-5 and Slow-4 when comparing real feedback with sham feedback. The Slow-5 and Slow-4 cover the frequency range of 0.01–0.073 Hz which is roughly equivalent to the typical low frequency band (0.01–0.08 Hz) [34, 35]. Mostly recruited in the default mode network in the typical low frequency band, the PCC has been identified as the hubs of this network chiefly responsible for attentional lapses and mind wandering [36, 37]. In task state, these areas may play a role as a source of internal interference or noise and were suppressed as deactivation [37, 38], and the deactivation may further induce the elevation of ReHo. Thus, the greater ReHo in the PCC suggested that real feedback requires more suppression of internal interference than sham feedback, and, more importantly, our results indicated that the suppression was potentially associated with the local synchronization of the PCC in Slow-5 and Slow-4.

We observed that ReHo of the left and right BG in Slow-6 is greater for real feedback than it is for sham feedback. Slow-6, as an ultraslow frequency band, is less concerned in previous neuroimaging explorations. In resting state, it was thought that this ultraslow frequency band may reflect very low frequency drift [39]. However, a recent study provides new insights into this issue by showing that oscillations lower than 0.02 Hz contribute more to ReHo in putamen during resting state [40]. Our results support this finding and further indicate that, during motor feedback, the oscillation in the ultraslow frequency band of Slow-6 is critical for ReHo in BG (including bilateral putamen and caudate). The BG is an important brain area for motor feedback. It is suggested that the BG is involved in the planning and parameterizing of motor control [41]. Thus, the ultraslow frequency band of brain oscillation during motor feedback may be associated with these functional roles of BG. Remarkably, the BG disorders such as Parkinson's disease mostly result in the decreased ReHo in the BG [42], and the motor feedback has been employed in the treatment of these disorders exhibiting therapeutic effectiveness [43]. Thus, the ultraslow frequency band of local synchronization during motor feedback may possess the therapeutic value in these clinical practices.

Nevertheless, the current study has some limitations. The sampling rate in the present study (2 s) prevents us from performing the analysis in higher frequency band and we believed that fast sampling should provide more novel findings for motor feedback fMRI studies. Moreover, the results of the present study are restricted to the visual feedback, and the feedback presented in the auditory and sensory forms is commonly employed in practice. Further experimentation and investigation are still required to fully clarify these issues.

5. Conclusion

The present fMRI study shed light on the neural substrate of motor feedback by studying the local synchronization in the subfrequency bands ranged from Slow-6 to Slow-2. Using the measurement of ReHo, we found that the five subfrequency bands exhibit distinct contributions to the changes of ReHo between real and sham feedback, which provided novel insights into the neural substrate of motor feedback. The result that changes in left and right BG mainly depended on the ultraslow frequency band of Slow-6, which potentially helps to understand properties of the ultraslow frequency band of local synchronization.

Conflict of Interests

The authors declare that there is no conflict of interests regarding the publication of this paper.

Acknowledgments

References

[1] J. W. Noble, J. J. Eng, and L. A. Boyd, "Effect of visual feedback on brain activation during motor tasks: an fMRI study," *Motor Control*, vol. 17, no. 3, pp. 298–312, 2013.

[2] D. D. Damian, A. H. Arita, H. Martinez, and R. Pfeifer, "Slip speed feedback for grip force control," *IEEE Transactions on Biomedical Engineering*, vol. 59, no. 8, pp. 2200–2210, 2012.

[3] J. A. Barrios, K. M. Crossley, and I. S. Davis, "Gait retraining to reduce the knee adduction moment through real-time visual feedback of dynamic knee alignment," *Journal of Biomechanics*, vol. 43, no. 11, pp. 2208–2213, 2010.

[4] R. Barclay-Goddard, T. Stevenson, W. Poluha, M. E. Moffatt, and S. P. Taback, "Force platform feedback for standing balance training after stroke," *Cochrane Database of Systematic Reviews*, vol. 18, no. 4, Article ID CD004129, 2004.

[5] N. J. Seo, H. W. Fischer, R. A. Bogey, W. Z. Rymer, and D. G. Kamper, "Use of visual force feedback to improve digit force direction during pinch grip in persons with stroke: a Pilot Study," *Archives of Physical Medicine and Rehabilitation*, vol. 92, no. 1, pp. 24–30, 2011.

[6] N. Lodha, C. Patten, S. A. Coombes, and J. H. Cauraugh, "Bimanual force control strategies in chronic stroke: finger extension versus power grip," *Neuropsychologia*, vol. 50, no. 11, pp. 2536–2545, 2012.

[7] D. E. Vaillancourt, A. B. Slifkin, and K. M. Newell, "Intermittency in the visual control of force in Parkinson's disease," *Experimental Brain Research*, vol. 138, no. 1, pp. 118–127, 2001.

[8] G. Kriz, J. Hermsdörfer, C. Marquardt, and N. Mai, "Feedback-based training of grip force control in patients with brain damage," *Archives of Physical Medicine and Rehabilitation*, vol. 76, no. 7, pp. 653–659, 1995.

[9] S. K. Naik, C. Patten, N. Lodha, S. A. Coombes, and J. H. Cauraugh, "Force control deficits in chronic stroke: grip formation and release phases," *Experimental Brain Research*, vol. 211, no. 1, pp. 1–15, 2011.

[10] H. H. Ehrsson, A. Fagergren, T. Jonsson, G. Westling, R. S. Johansson, and H. Forssberg, "Cortical activity in precision-versus power-grip tasks: an fMRI study," *Journal of Neurophysiology*, vol. 83, no. 1, pp. 528–536, 2000.

[11] S. Haller, D. Chapuis, R. Gassert, E. Burdet, and M. Klarhöfer, "Supplementary motor area and anterior intraparietal area integrate fine-graded timing and force control during precision grip," *European Journal of Neuroscience*, vol. 30, no. 12, pp. 2401–2406, 2009.

[12] S. T. Grafton and E. Tunik, "Human basal ganglia and the dynamic control of force during on-line corrections," *The Journal of Neuroscience*, vol. 31, no. 5, pp. 1600–1605, 2011.

[13] J. P. Kuhtz-Buschbeck, R. Gilster, S. Wolff, S. Ulmer, H. Siebner, and O. Jansen, "Brain activity is similar during precision and power gripping with light force: an fMRI study," *NeuroImage*, vol. 40, no. 4, pp. 1469–1481, 2008.

[14] S. A. Coombes, D. M. Corcos, L. Sprute, and D. E. Vaillancourt, "Selective regions of the visuomotor system are related to gain-induced changes in force error," *Journal of Neurophysiology*, vol. 103, no. 4, pp. 2114–2123, 2010.

[15] H. H. Ehrsson, A. Fagergren, and H. Forssberg, "Differential fronto-parietal activation depending on force used in a precision grip task: an fMRI study," *Journal of Neurophysiology*, vol. 85, no. 6, pp. 2613–2623, 2001.

[16] B. Keisker, M.-C. Hepp-Reymond, A. Blickenstorfer, and S. S. Kollias, "Differential representation of dynamic and static power grip force in the sensorimotor network," *European Journal of Neuroscience*, vol. 31, no. 8, pp. 1483–1491, 2010.

[17] S. A. Coombes, D. M. Corcos, and D. E. Vaillancourt, "Spatiotemporal tuning of brain activity and force performance," *NeuroImage*, vol. 54, no. 3, pp. 2226–2236, 2011.

[18] P. Halder, S. Brem, K. Bucher et al., "Electrophysiological and hemodynamic evidence for late maturation of hand power grip and force control under visual feedback," *Human Brain Mapping*, vol. 28, no. 1, pp. 69–84, 2007.

[19] B. S. Oken, M. C. Salinsky, and S. M. Elsas, "Vigilance, alertness, or sustained attention: physiological basis and measurement," *Clinical Neurophysiology*, vol. 117, no. 9, pp. 1885–1901, 2006.

[20] W. S. Helton, "Impulsive responding and the sustained attention to response task," *Journal of Clinical and Experimental Neuropsychology*, vol. 31, no. 1, pp. 39–47, 2009.

[21] Z.-Y. Dong, D.-Q. Liu, J. Wang et al., "Low-frequency fluctuation in continuous real-time feedback of finger force: a new paradigm for sustained attention," *Neuroscience Bulletin*, vol. 28, no. 4, pp. 456–467, 2012.

[22] Y. T. Lv, D. S. Margulies, A. Villringer, and Y. F. Zang, "Effects of finger tapping frequency on regional homogeneity of sensorimotor cortex," *PLoS ONE*, vol. 8, no. 5, Article ID e64115, 2013.

[23] X.-N. Zuo, A. di Martino, C. Kelly et al., "The oscillating brain: complex and reliable," *NeuroImage*, vol. 49, no. 2, pp. 1432–1445, 2010.

[24] Y. Han, J. Wang, Z. Zhao et al., "Frequency-dependent changes in the amplitude of low-frequency fluctuations in amnestic mild cognitive impairment: a resting-state fMRI study," *NeuroImage*, vol. 55, no. 1, pp. 287–295, 2011.

[25] Y. Hou, X. Wu, M. Hallett, P. Chan, and T. Wu, "Frequency-dependent neural activity in Parkinson's disease," *Human Brain Mapping*, vol. 35, no. 12, pp. 5815–5833, 2014.

[26] H. van Duinen, R. Renken, N. Maurits, and I. Zijdewind, "Effects of motor fatigue on human brain activity, an fMRI study," *NeuroImage*, vol. 35, no. 4, pp. 1438–1449, 2007.

[27] C.-G. Yan and Y.-F. Zang, "DPARSF: a MATLAB toolbox for 'pipeline' data analysis of resting-state fMRI," *Frontiers in Systems Neuroscience*, vol. 4, article 13, 2010.

[28] X.-W. Song, Z.-Y. Dong, X.-Y. Long et al., "REST: a toolkit for resting-state functional magnetic resonance imaging data processing," *PLoS ONE*, vol. 6, no. 9, Article ID e25031, 2011.

[29] J. Ashburner and K. J. Friston, "Unified segmentation," *NeuroImage*, vol. 26, no. 3, pp. 839–851, 2005.

[30] Y. Zang, T. Jiang, Y. Lu, Y. He, and L. Tian, "Regional homogeneity approach to fMRI data analysis," *NeuroImage*, vol. 22, no. 1, pp. 394–400, 2004.

[31] D. E. Vaillancourt, K. R. Thulborn, and D. M. Corcos, "Neural basis for the processes that underlie visually guided and internally guided force control in humans," *Journal of Neurophysiology*, vol. 90, no. 5, pp. 3330–3340, 2003.

[32] M. Sarter, B. Givens, and J. P. Bruno, "The cognitive neuroscience of sustained attention: where top-down meets bottom-up," *Brain Research Reviews*, vol. 35, no. 2, pp. 146–160, 2001.

[33] T. M. Gill, M. Sarter, and B. Givens, "Sustained visual attention performance-associated prefrontal neuronal activity: evidence for cholinergic modulation," *The Journal of Neuroscience*, vol. 20, no. 12, pp. 4745–4757, 2000.

[34] B. Biswal, F. Z. Yetkin, V. M. Haughton, and J. S. Hyde, "Functional connectivity in the motor cortex of resting human brain using echo-planar mri," *Magnetic Resonance in Medicine*, vol. 34, no. 4, pp. 537–541, 1995.

[35] M. J. Lowe, B. J. Mock, and J. A. Sorenson, "Functional connectivity in single and multislice echoplanar imaging using resting-state fluctuations," *NeuroImage*, vol. 7, no. 2, pp. 119–132, 1998.

[36] M. F. Mason, M. I. Norton, J. D. van Horn, D. M. Wegner, S. T. Grafton, and C. N. Macrae, "Wandering minds: the default network and stimulus-independent thought," *Science*, vol. 315, no. 5810, pp. 393–395, 2007.

[37] A. Anticevic, M. W. Cole, J. D. Murray, P. R. Corlett, X.-J. Wang, and J. H. Krystal, "The role of default network deactivation in cognition and disease," *Trends in Cognitive Sciences*, vol. 16, no. 12, pp. 584–592, 2012.

[38] M. D. Greicius and V. Menon, "Default-mode activity during a passive sensory task: uncoupled from deactivation but impacting activation," *Journal of Cognitive Neuroscience*, vol. 16, no. 9, pp. 1484–1492, 2004.

[39] T. Starck, J. Nissilä, A. Aunio et al., "Stimulating brain tissue with light-resting state fMRI analysis," in *Proceedings of the International Society for Magnetic Resonance in Medicine*, p. 1594, 2011.

[40] X. Song, Y. Zhang, and Y. Liu, "Frequency specificity of regional homogeneity in the resting-state human brain," *PLoS ONE*, vol. 9, no. 1, Article ID e86818, 2014.

[41] J. Prodoehl, D. M. Corcos, and D. E. Vaillancourt, "Basal ganglia mechanisms underlying precision grip force control," *Neuroscience and Biobehavioral Reviews*, vol. 33, no. 6, pp. 900–908, 2009.

[42] T. Wu, X. Long, Y. Zang et al., "Regional homogeneity changes in patients with Parkinson's disease," *Human Brain Mapping*, vol. 30, no. 5, pp. 1502–1510, 2009.

[43] D. E. Vaillancourt, A. B. Slifkin, and K. M. Newell, "Intermittency in the visual control of force in Parkinson's disease," *Experimental Brain Research*, vol. 138, no. 1, pp. 118–127, 2001.

Research Article

Neural Correlates of Associative Memory in the Elderly: A Resting-State Functional MRI Study

Weicong Ren,[1,2] Rui Li,[1] Zhiwei Zheng,[1,2] and Juan Li[1,3,4]

[1]*Center on Aging Psychology, Key Laboratory of Mental Health, Institute of Psychology, Chinese Academy of Sciences, Beijing 100101, China*
[2]*University of Chinese Academy of Sciences, Beijing 100101, China*
[3]*Magnetic Resonance Imaging Research Center, Institute of Psychology, Chinese Academy of Sciences, Beijing 100101, China*
[4]*State Key Laboratory of Brain and Cognitive Science, Institute of Biophysics, Chinese Academy of Sciences, Beijing 100101, China*

Correspondence should be addressed to Juan Li; lijuan@psych.ac.cn

The neural correlates of associative memory in healthy older adults were investigated by examining the correlation of associative memory performance with spontaneous brain oscillations. Eighty healthy older adults underwent a resting-state functional MRI and took a paired-associative learning test (PALT). Correlations between the amplitude of low-frequency fluctuations (ALFF) as well as fractional ALFF (fALFF) in the whole brain and PALT scores were calculated. We found that spontaneous activity as indexed by both ALFF and fALFF in the parahippocampal gyrus (PHG) was significantly positively correlated with associative memory performance, suggesting that the PHG plays a critical role in associative memory in older people.

1. Introduction

Associative memory demonstrates a greater decline in older adults compared with item memory [1, 2]. It has been well evidenced that healthy aging is associated with cognitive decline in various domains, especially in episodic memory. A salient feature of age-related differences in episodic memory is the difficulty in creating and retrieving associations between single units of information (associative memory), while memory for individual items is less affected [3]. In other words, associative memory declines earlier than item memory as one gets older. It is important to figure out the neural correlates of associative memory in the older adults for comprehensively understanding the mechanism of cognitive decline with aging. Associative memory is typically assessed using paired-associative paradigms [4].

Many neuroimaging and lesion studies have explored the neuroanatomical underpinnings of associative memory and have suggested that the medial temporal lobe (MTL), lateral parietal cortex, and prefrontal cortex (PFC) play important roles in remembering associations. These regions are involved in binding and retrieving item-item or item-context associations or controlling and monitoring these processes [5–8].

Accumulating evidence suggests that, in older adults, several brain regions, particularly the MTL and PFC, show structural volumetric decreases and functional activation changes [9–11]. It has been demonstrated that aging differentially affects the brain substrates of memory, with the PFC being the most vulnerable, the hippocampus being moderately vulnerable, and the entorhinal cortex being relatively spared [12–14]. White matter connections of the frontal and temporal cortex as well as the frontal-subcortical white matter tracts also have been found to play critical roles in age-related differences in associative memory performance [15]. The structural morphology and functional changes in these regions may be the underlying reasons for the age-related decline in associative memory.

Resting-state functional magnetic resonance imaging (fMRI) is useful for exploring the spontaneous functional architecture of the brain [16–18]. In addition, it provides

a straightforward comparison of brain activity across different cognitive ability groups. Low-frequency fluctuations observed on resting-state fMRI are physiologically meaningful [16], which are thought to reflect spontaneous regional neuronal activity [19] and different physiological states of the brain [20]. The resting-state amplitude of low-frequency fluctuations (ALFF) can predict task-evoked brain activation [21, 22], as well as correlate with behavioral performance [23–25]. Therefore, the ALFF has been used to examine synchrony in healthy adults [26, 27] and disease-related changes in brain activity [28]. To improve the sensitivity and specificity in detecting spontaneous brain activities, fractional ALFF (fALFF) that is calculated as the ratio of power spectrum of low-frequency to that of the entire frequency range has also been introduced in resting-state fMRI studies [29].

In the present study, we focused on the relationship between the resting-state ALFF and associative memory in healthy older adults. In addition, fALFF was also employed to comprehensively investigate the relationship between oscillations and associative memory. The verbal paired-associative learning test (PALT) was used to assess associative memory [30]. To be specific, the objective of this study was to identify the neural correlates of associative memory in healthy older adults by examining correlations between the resting-state ALFF/fALFF and performance on PALT. Since the MTL and PFC play important roles in associative memory processes and are vulnerable to aging, we postulated that the oscillations in these two regions might be significantly correlated with PALT performance.

2. Materials and Methods

2.1. Participants. The participants were recruited via advertisements posted at communities near the Institute of Psychology, Chinese Academy of Sciences in Beijing. After baseline evaluation, we enrolled 80 healthy older volunteers who met the following criteria: (1) age $\geq$ 60 years; (2) education $\geq$ 6 years; (3) a score of $\geq$22 on the Beijing Version of the Montreal Cognitive Assessment (MoCA) [31]; and (4) no neurological and psychiatric disorders and traumatic brain injury. No participant was excluded and finally data from 80 participants (43 female, mean age = 70.29 years, range 60–80 years; mean years of education = 14.40 years, range 6–20 years) were analyzed.

This study was approved by the Institutional Review Board of the Institute of Psychology, Chinese Academy of Science. Written informed consent was supplied to all participants and they were paid for their participation. The study was registered in the Chinese Clinical Trial Registry (ChiCTR) (http://www.chictr.org/): ChiCTR-PNRC-13003813.

2.2. Memory Task. Associative memory performance was examined using the PALT. For this test, the participants first studied 12 word pairs of nouns, half of which consisted of six semantically related word pairs (e.g., sun-moon), and this was considered as easy condition. The other word pairs included six semantically unrelated word pairs (e.g., teacher-railway), which was considered as difficult condition. After the study

session, participants were asked to complete a cued recall task in which the first word of the pair was provided and they had to recall the other paired word. A correctly recalled word was scored 0.5 in the easy condition and 1 in the difficult condition, with the total score for the test equal to 9.

2.3. Data Acquisition. A 3.0-Tesla Siemens Trio scanner (Erlangen, Germany) was used for image acquisition at Beijing MRI Center for Brain Research. During the scan, the participants were placed in a supine position with their heads held snugly by a belt and foam pads. They were required to keep their eyes closed, relax, and keep their heads still but not to fall asleep during the scan. For each participant, functional images were collected using an echo-planar imaging sequence. The imaging parameters were repetition time (TR) = 2000 ms; echo time (TE) = 30 ms; flip angle = 90°; field of view (FOV) = 200 mm × 200 mm; slice thickness = 3.0 mm; gap = 0.6 mm; acquisition matrix = 64 × 64; in-plane resolution = 3.125 × 3.125; 33 axial slices; and 200 volumes.

Additionally, a high-resolution structural T1-weighted magnetization-prepared rapid gradient-echo image was also collected for each subject with the parameters as follows: 176 slices; acquisition matrix = 256 × 256; voxel size = 1 mm × 1 mm × 1 mm; TR = 1900 ms; TE = 2.2 ms; and flip angle = 9°.

2.4. Resting-State fMRI Data Processing and Statistics. Resting-state fMRI data analyses were performed using the Data Processing Assistant for Resting-State fMRI (DPARSF V2.2) Basic Edition, Statistical Parametric Mapping program (SPM8), and the Resting-State fMRI Data Analysis Toolkit (REST V1.8).

Preprocessing. The first ten volumes were discarded for signal equilibrium and participant's adaptation to scanning noise. The rest of the volumes were corrected for intravolume acquisition time delay between slices and intervolume geometrical displacement due to head movement. All functional data were normalized to the Montreal Neurological Institute (MNI) space with $3 \times 3 \times 3 \text{ mm}^3$ resampling. Spatial smoothing with a 4-mm Gaussian kernel and linear detrending were finally performed. No participant included in this study exhibited head motion of more than 2.0 mm in any direction or 2.0° rotation throughout the resting-state scans.

ALFF/fALFF Calculation. The ALFF value of each voxel was measured as the sum of amplitudes within the low-frequency range [32]. For each voxel, the time series was first converted to the frequency domain using a Fast Fourier Transform (FFT) analysis to obtain the power spectrum. The power spectrum was obtained by square-rooted FFT and averaged across 0.01–0.08 Hz at each voxel. The averaged square root was taken as the ALFF. To reduce global effects of variability across the participants, the ALFF value of each voxel was divided by the global mean ALFF value. For fALFF, the measure was calculated as the ratio of power of low-frequency fluctuations (0.01–0.08 Hz) to that of all available frequencies.

ALFF/fALFF-PALT Correlation. To find the neural correlates of associative memory indexed by resting-state ALFF/fALFF,

Table 1: Demographic characteristics and neuropsychological results of participants.

	Participants ($N = 80$)
Age	70.29 ± 5.64
Education (y)	14.40 ± 3.11
Female/male	43/37
MoCA	26.76 ± 2.34
PALT	2.94 ± 1.47

Note: MoCA: Montreal Cognitive Assessment; PALT: paired-associative learning test.

we performed correlation analyses between PALT scores and ALFF/fALFF in the whole brain. At each voxel, the Pearson correlation coefficient between ALFF/fALFF and PALT scores across participants was calculated, with age, gender, and years of education as covariates. Clusters were considered as significant at the combined voxel extent threshold of uncorrected $P < 0.01$ and cluster extent $> 486\,\text{mm}^3$, as determined based on AlphaSim correction by Monte Carlo simulation to $P < 0.05$ (single voxel $P < 0.01$, and spatial smoothness = 4 mm).

3. Results

3.1. Demographic and Neuropsychological Results. Demographic information and neuropsychological scores are shown in Table 1. MoCA scores ranged from 22 to 30, with an average of 26.76 ± 2.34. PALT scores ranged from 0 to 7 with an average of 2.94 ± 1.47.

3.2. Correlations between PALT Scores and the ALFF/fALFF in the Whole Brain. Voxelwise correlation analyses showed that resting-state ALFF values correlated with PALT scores in a number of brain regions (Figure 1(A), Table 2). Specifically, the ALFF values positively correlated with PALT scores in the bilateral parahippocampal gyri (PHG) and left insula, while negative correlations were found between them in the right inferior temporal gyrus (ITG) and right inferior frontal gyrus (IFG).

In the correlation analyses between fALFF values and PALT scores, fALFF in three regions showed significant positive correlation with PALT performance including the right PHG/superior temporal gyrus (STG), right inferior parietal lobule (IPL), and right supplementary motor area (SMA)/superior frontal gyrus (SFG) (Figure 1(B), Table 2).

As the results of the correlation analyses, spontaneous activity in the right PHG was demonstrated to be robustly correlated with associative memory performance assessed by PALT. Scatter plots of PALT scores versus ALFF/fALFF values were displayed to illustrate the relationship between spontaneous oscillations in the right PHG and PALT scores with age, education, and gender taken as covariates (Figure 2). ALFF/fALFF values under/over 3 standard deviations away from the mean value of the sample were identified as outliers and removed from the data set. Thus the ALFF value from one participant was removed during analyses. The results demonstrated that PALT scores were positively correlated

with ALFF ($r = 0.258$, $P = 0.023$) and fALFF ($r = 0.359$, $P = 0.001$) in the right PHG.

4. Discussion

The objective of this study was to investigate the neural correlates of associative memory in healthy older adults using resting-state fMRI. Results showed that spontaneous activity indexed by both ALFF and fALFF in the right PHG was significantly positively correlated with associative memory performance, suggesting a critical role of the right PHG in associative memory in older adults.

There is compelling evidence that the MTL, consisting of the hippocampal region and the adjacent perirhinal, entorhinal, and parahippocampal cortices, plays an important role in associative memory [33]. It has been shown that age-related shrinkage occurs in the MTL of healthy adults [13]. As the principal neocortical input pathway to the hippocampal region [34], the PHG is thought to function in memory formation [35]. Düzel et al. reported that the PHG was involved in the visual associative recognition memory for spatial and nonspatial stimulus configurations [36]. Recently, Bar and colleagues also found that the PHG was involved in contextual associations processing [37]. They found that PHG responds more strongly to the rich associations condition compared with the less associations condition. The present findings of significant correlations between ALFF/fALFF in the PHG and associative performance further provided the evidence that the PHG plays an important role in the memory of associations. It suggested that participants with higher regional spontaneous activity in the right PHG performed better in associative memory test, when age, years of education, and gender were controlled. Previous studies have found that both item-spatial context associations and item-nonspatial context associations activated the parahippocampal cortex more than noncontextual items, which indicated that the PHG functions importantly in processing of contextual associations [38]. The present finding further suggested that the PHG may be a pivotal region underlying association memory process.

The two measurements of ALFF and fALFF are highly related but not entirely the same [39]. In the correlation analyses between ALFF and PALT scores, positive correlations were found in the bilateral PHG and left insula, and negative correlations were found in the right ITG and right IFG. Using fALFF as a measurement, only significant positive correlations were found. In addition to a significant correlation between performance on PALT and fALFF in the right PHG, the significant correlations also appeared in the right IPL and right SMA/SFG, suggesting that these regions may also be involved in the network underlying memory process.

Insula was demonstrated to be involved in processing general cognition by the meta-analysis of neuroimaging literatures [40]. Activation in the insula has been shown to be associated with contextual binding of semantic relations and successful encoding for relation load [41, 42]. The parietal cortex also contributed importantly to episodic memory retrieval [43]. Wanger et al. showed that multiple parietal

TABLE 2: Peaks of regions showing significant ALFF/fALFF-PALT correlations.

Measurement	Regions	BA	Number of voxels	Peak MNI coordinates		
				x	y	z
ALFF	PHG (L)	35/36	24	−24	−27	−18
	PHG (R)	35/36	27	24	−27	−9
	Insula (L)	13	28	−33	−15	15
	ITG (R)	20	40	33	0	−42
	IFG (R)	47	35	15	9	−18
fALFF	PHG/STG (R)	38	33	30	12	−30
	IPL (R)	40	25	54	−54	48
	SFG/SMA (R)	6	21	6	−9	78

Note: MNI coordinates of the center of gravity of each cluster. PHG: parahippocampal gyrus; ITG: inferior temporal gyrus; IFG: inferior frontal gyrus; STG: superior temporal gyrus; IPL: inferior parietal lobule; SFG: superior frontal gyrus; SMA: supplementary motor area; L: left hemisphere; R: right hemisphere.

(A)

(B)
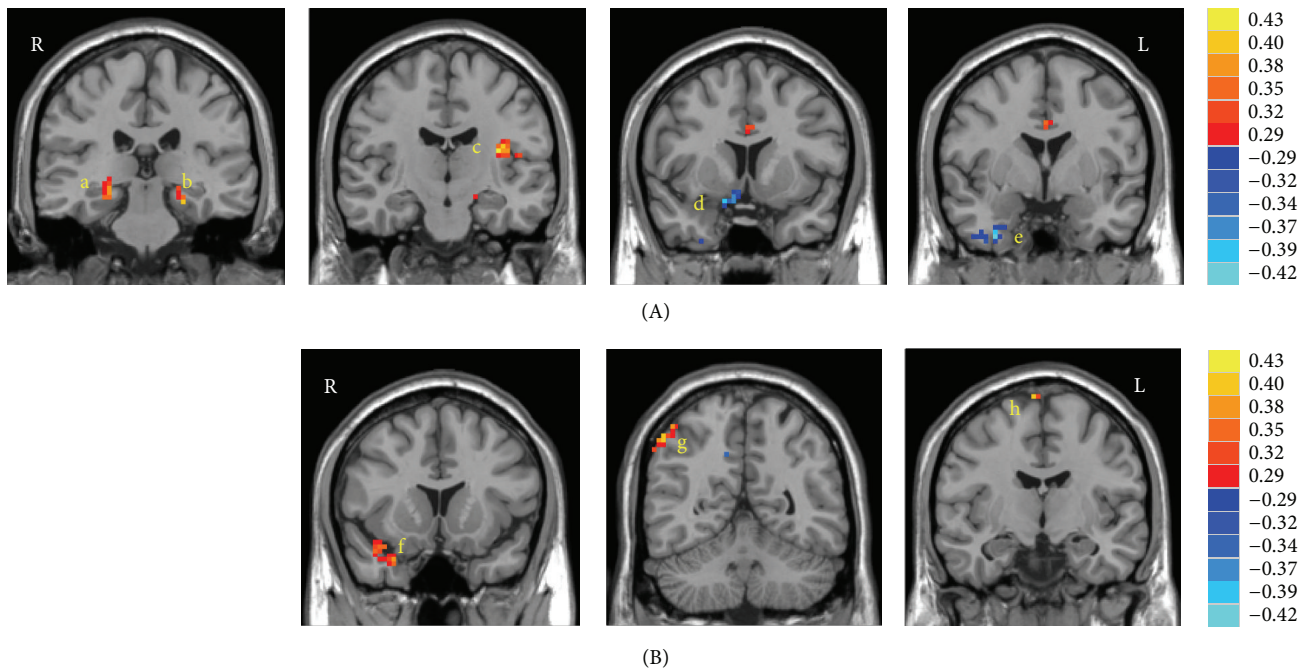
FIGURE 1: Regional oscillations and associative memory correlation analyses. (A) Statistical map for the correlations between performance on the PALT and ALFF in the bilateral PHG (a, b), left insula (c), right IFG (d), and right ITG (e). (B) Statistical map for the correlations between performance on the PALT and fractional ALFF in the right PHG/STG (f), right IPL (g), and right SMA/SFG (h). The correlation values are indicated using the color scales on the right.

regions were activated during episodic retrieval, including regions within the intraparietal sulcus extending laterally to the IPL. It is also interesting that ALFF in two regions located in ITG and IFC negatively correlated with individual PALT performance. Increased activity in the lateral temporal and superior frontal regions has been previously found in AD and MCI patients. Besides, AD patients also showed increased activity in the ITG as compared with MCI patients [28, 44]. Here the negative correlation between PALT scores and the ALFF in the right ITG and right IFG indicated that participants with lower performance in associative memory test may have higher ALFF value in these regions, similar to the results in the disease studies. Thus the result suggested

that, in addition to PHG playing a crucial role, the insula and some cortical regions especially the frontal and parietal regions may also be involved in associative memory in the elderly. It would be interesting in future studies to investigate how the PHG cooperates with other regions in the cortex to function in associative memory in older adults.

Finally it is methodologically important to note that as the ALFF is more prone to noise from physiological sources than fALFF, we could not rule out the potential effect of physiological noise on the ALFF results [32]. The ALFF-PALT results need to be examined in independent samples. In addition, the individual-level standardization in the ALFF/fALFF analysis used in the present study might
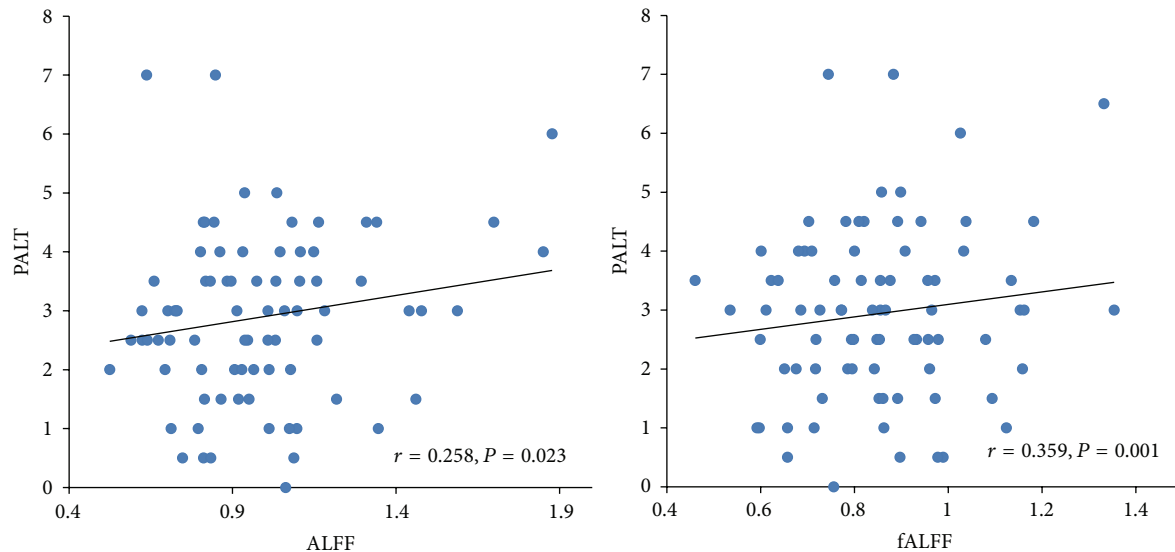
FIGURE 2: Scatter plots of the significant relationship between PALT scores and ALFF as well as fALFF values in the right PHG with age, gender, and education as covariates. Each dot represents data from one participant.

lose the individual differences in the group analysis, and a group-level standardized procedure is required to validate these results in future studies [45].

5. Conclusion

In the present study, we explored the neural correlates of associative memory by resting-state ALFF as well as fALFF. Our results showed that the PHG may be critically involved in associative memory in older adults, and participants with higher regional spontaneous activity in the right PHG performed better in associative memory test.

Conflict of Interests

The authors declare that there is no conflict of interests regarding the publication of this paper.

Authors' Contribution

Weicong Ren and Rui Li contributed equally to this work.

Acknowledgments

References

[1] S. R. Old and M. Naveh-Benjamin, "Differential effects of age on item and associative measures of memory: a meta-analysis," *Psychology and Aging*, vol. 23, no. 1, pp. 104–118, 2008.

[2] W. D. Spencer and N. Raz, "Differential effects of aging on memory for content and context: a meta-analysis," *Psychology and Aging*, vol. 10, no. 4, pp. 527–539, 1995.

[3] M. Naveh-Benjamin, "Adult age differences in memory performance: tests of an associative deficit hypothesis," *Journal of Experimental Psychology: Learning Memory and Cognition*, vol. 26, no. 5, pp. 1170–1187, 2000.

[4] B. Hanseeuw, L. Dricot, M. Kavec, C. Grandin, X. Seron, and A. Ivanoiu, "Associative encoding deficits in amnestic mild cognitive impairment: a volumetric and functional MRI study," *NeuroImage*, vol. 56, no. 3, pp. 1743–1748, 2011.

[5] R. A. Diana, A. P. Yonelinas, and C. Ranganath, "Imaging recollection and familiarity in the medial temporal lobe: a three-component model," *Trends in Cognitive Sciences*, vol. 11, no. 9, pp. 379–386, 2007.

[6] M. D. Rugg and K. L. Vilberg, "Brain networks underlying episodic memory retrieval," *Current Opinion in Neurobiology*, vol. 23, no. 2, pp. 255–260, 2013.

[7] J. S. Simons and H. J. Spiers, "Prefrontal and medial temporal lobe interactions in long-term memory," *Nature Reviews Neuroscience*, vol. 4, no. 8, pp. 637–648, 2003.

[8] K. J. Mitchell and M. K. Johnson, "Source monitoring 15 years later: what have we learned from fMRI about the neural mechanisms of source memory?" *Psychological Bulletin*, vol. 135, no. 4, pp. 638–677, 2009.

[9] R. Cabeza, N. D. Anderson, J. K. Locantore, and A. R. McIntosh, "Aging gracefully: compensatory brain activity in high-performing older adults," *NeuroImage*, vol. 17, no. 3, pp. 1394–1402, 2002.

[10] C. L. Grady, "Cognitive neuroscience of aging," *Annals of the New York Academy of Sciences*, vol. 1124, no. 1, pp. 127–144, 2008.

[11] N. Raz, U. Lindenberger, K. M. Rodrigue et al., "Regional brain changes in aging healthy adults: general trends, individual differences and modifiers," *Cerebral Cortex*, vol. 15, no. 11, pp. 1676–1689, 2005.

[12] N. Raz, "Aging of the brain and its impact on cognitive performance: integration of structural and functional findings," in *The Handbook of Aging and Cognition*, F. I. M. C. T. A. Salthouse, Ed., pp. 1–90, Lawrence Erlbaum Associates, Mahwah, NJ, USA, 2nd edition, 2000.

[13] N. Raz, K. M. Rodrigue, D. Head, K. M. Kennedy, and J. D. Acker, "Differential aging of the medial temporal lobe: a study of a five-year change," *Neurology*, vol. 62, no. 3, pp. 433–438, 2004.

[14] A. T. Du, N. Schuff, X. P. Zhu et al., "Atrophy rates of entorhinal cortex in AD and normal aging," *Neurology*, vol. 60, no. 3, pp. 481–486, 2003.

[15] S. N. Lockhart, A. B. V. Mayda, A. E. Roach et al., "Episodic memory function is associated with multiple measures of white matter integrity in cognitive aging," *Frontiers in Human Neuroscience*, vol. 6, article 56, 2012.

[16] B. Biswal, F. Z. Yetkin, V. M. Haughton, and J. S. Hyde, "Functional connectivity in the motor cortex of resting human brain using echo-planar MRI," *Magnetic Resonance in Medicine*, vol. 34, no. 4, pp. 537–541, 1995.

[17] M. D. Fox and M. E. Raichle, "Spontaneous fluctuations in brain activity observed with functional magnetic resonance imaging," *Nature Reviews Neuroscience*, vol. 8, no. 9, pp. 700–711, 2007.

[18] M. E. Raichle, "Two views of brain function," *Trends in Cognitive Sciences*, vol. 14, no. 4, pp. 180–190, 2010.

[19] N. K. Logothetis, J. Pauls, M. Augath, T. Trinath, and A. Oeltermann, "Neurophysiological investigation of the basis of the fMRI signal," *Nature*, vol. 412, no. 6843, pp. 150–157, 2001.

[20] H. Yang, X.-Y. Long, Y. Yang et al., "Amplitude of low frequency fluctuation within visual areas revealed by resting-state functional MRI," *NeuroImage*, vol. 36, no. 1, pp. 144–152, 2007.

[21] X. Liu, X.-H. Zhu, and W. Chen, "Baseline BOLD correlation predicts individuals' stimulus-evoked BOLD responses," *NeuroImage*, vol. 54, no. 3, pp. 2278–2286, 2011.

[22] M. Mennes, C. Kelly, X. N. Zuo et al., "Inter-individual differences in resting-state functional connectivity predict task-induced BOLD activity," *Neuroimage*, vol. 50, no. 4, pp. 1690–1701, 2010.

[23] M. Hampson, N. R. Driesen, P. Skudlarski, J. C. Gore, and R. T. Constable, "Brain connectivity related to working memory performance," *The Journal of Neuroscience*, vol. 26, no. 51, pp. 13338–13343, 2006.

[24] M. Hampson, N. Driesen, J. K. Roth, J. C. Gore, and R. T. Constable, "Functional connectivity between task-positive and task-negative brain areas and its relation to working memory performance," *Magnetic Resonance Imaging*, vol. 28, no. 8, pp. 1051–1057, 2010.

[25] M. Mennes, X.-N. Zuo, C. Kelly et al., "Linking inter-individual differences in neural activation and behavior to intrinsic brain dynamics," *NeuroImage*, vol. 54, no. 4, pp. 2950–2959, 2011.

[26] S. Lui, X. Huang, L. Chen et al., "High-field MRI reveals an acute impact on brain function in survivors of the magnitude 8.0 earthquake in China," *Proceedings of the National Academy of Sciences of the United States of America*, vol. 106, no. 36, pp. 15412–15417, 2009.

[27] C. Yan, D. Liu, Y. He et al., "Spontaneous brain activity in the default mode network is sensitive to different resting-state conditions with limited cognitive load," *PLoS ONE*, vol. 4, no. 5, Article ID e5743, 2009.

[28] Z. Wang, C. Yan, C. Zhao et al., "Spatial patterns of intrinsic brain activity in mild cognitive impairment and alzheimer's disease: a resting-state functional MRI study," *Human Brain Mapping*, vol. 32, no. 10, pp. 1720–1740, 2011.

[29] Q.-H. Zou, C.-Z. Zhu, Y. Yang et al., "An improved approach to detection of amplitude of low-frequency fluctuation (ALFF) for resting-state fMRI: fractional ALFF," *Journal of Neuroscience Methods*, vol. 172, no. 1, pp. 137–141, 2008.

[30] S. Xu and Z. Wu, "The construction of the clinical memory test," *Acta Psychologica Sinica*, vol. 18, no. 1, pp. 100–108, 1986.

[31] J. Yu, J. Li, and X. Huang, "The Beijing version of the montreal cognitive assessment as a brief screening tool for mild cognitive impairment: a community-based study," *BMC Psychiatry*, vol. 12, article 156, 2012.

[32] Y. Zang, Y. He, C. Zhu et al., "Altered baseline brain activity in children with ADHD revealed by resting-state functional MRI," *Brain and Development*, vol. 29, no. 2, pp. 83–91, 2007.

[33] L. R. Squire, C. E. L. Stark, and R. E. Clark, "The medial temporal lobe," *Annual Review of Neuroscience*, vol. 27, pp. 279–306, 2004.

[34] W. A. Suzuki and D. G. Amaral, "Perirhinal and parahippocampal cortices of the macaque monkey: cortical afferents," *The Journal of Comparative Neurology*, vol. 350, no. 4, pp. 497–533, 1994.

[35] A. D. Wagner, D. L. Schacter, M. Rotte et al., "Building memories: remembering and forgetting of verbal experiences as predicted by brain activity," *Science*, vol. 281, no. 5380, pp. 1188–1191, 1998.

[36] E. Düzel, R. Habib, M. Rotte, S. Guderian, E. Tulving, and H.-J. Heinze, "Human hippocampal and parahippocampal activity during visual associative recognition memory for spatial and nonspatial stimulus configurations," *The Journal of Neuroscience*, vol. 23, no. 28, pp. 9439–9444, 2003.

[37] M. Bar, E. Aminoff, and D. L. Schacter, "Scenes unseen: the parahippocampal cortex intrinsically subserves contextual associations, not scenes or places per se," *Journal of Neuroscience*, vol. 28, no. 34, pp. 8539–8544, 2008.

[38] E. Aminoff, N. Gronau, and M. Bar, "The parahippocampal cortex mediates spatial and nonspatial associations," *Cerebral Cortex*, vol. 17, no. 7, pp. 1493–1503, 2007.

[39] X. N. Zuo, A. di Martino, C. Kelly et al., "The oscillating brain: complex and reliable," *NeuroImage*, vol. 49, no. 2, pp. 1432–1445, 2010.

[40] L. J. Chang, T. Yarkoni, M. W. Khaw, and A. G. Sanfey, "Decoding the role of the insula in human cognition: functional parcellation and large-scale reverse inference," *Cerebral Cortex*, vol. 23, no. 3, pp. 739–749, 2013.

[41] S. M. Daselaar, S. E. Prince, and R. Cabeza, "When less means more: deactivations during encoding that predict subsequent memory," *NeuroImage*, vol. 23, no. 3, pp. 921–927, 2004.

[42] D. R. Addis and M. P. McAndrews, "Prefrontal and hippocampal contributions to the generation and binding of semantic associations during successful encoding," *NeuroImage*, vol. 33, no. 4, pp. 1194–1206, 2006.

[43] A. D. Wagner, B. J. Shannon, I. Kahn, and R. L. Buckner, "Parietal lobe contributions to episodic memory retrieval," *Trends in Cognitive Sciences*, vol. 9, no. 9, pp. 445–453, 2005.

[44] Y. Han, J. Wang, Z. Zhao et al., "Frequency-dependent changes in the amplitude of low-frequency fluctuations in amnestic mild cognitive impairment: a resting-state fMRI study," *NeuroImage*, vol. 55, no. 1, pp. 287–295, 2011.

[45] C.-G. Yan, R. C. Craddock, X.-N. Zuo, Y.-F. Zang, and M. P. Milham, "Standardizing the intrinsic brain: towards robust measurement of inter-individual variation in 1000 functional connectomes," *NeuroImage*, vol. 80, pp. 246–262, 2013.

Research Article

Altered Spontaneous Brain Activity in Schizophrenia: A Meta-Analysis and a Large-Sample Study

Yongjie Xu,[1] Chuanjun Zhuo,[2] Wen Qin,[1] Jiajia Zhu,[1] and Chunshui Yu[1]

[1]*Department of Radiology, Tianjin Key Laboratory of Functional Imaging, Tianjin Medical University General Hospital,*
 No. 154 Anshan Road, Heping District, Tianjin 300052, China
[2]*Tianjin Anning Hospital, Tianjin 300300, China*

Correspondence should be addressed to Chunshui Yu; chunshuiyu@vip.163.com

Altered spontaneous brain activity as measured by ALFF, fALFF, and ReHo has been reported in schizophrenia, but no consensus has been reached on alternations of these indexes in the disorder. We aimed to clarify the regional alterations in ALFF, fALFF, and ReHo in schizophrenia using a meta-analysis and a large-sample validation. A meta-analysis of activation likelihood estimation was conducted based on the abnormal foci of ten studies. A large sample of 86 schizophrenia patients and 89 healthy controls was compared to verify the results of the meta-analysis. Meta-analysis demonstrated that the alternations in ALFF and ReHo had similar distribution in schizophrenia patients. The foci with decreased ALFF/fALFF and ReHo in schizophrenia were mainly located in the somatosensory cortex, posterior parietal cortex, and occipital cortex; however, foci with increased ALFF/fALFF and ReHo were mainly located in the bilateral striatum, medial temporal cortex, and medial prefrontal cortex. The large-sample study showed consistent findings with the meta-analysis. These findings may expound the pathophysiological hypothesis and guide future research.

1. Introduction

Schizophrenia is a devastating and disabling neuropsychiatric disorder. The neural mechanisms of this disorder have been attributed to structural and functional abnormalities of the brain [1–5]. Schizophrenia patients have exhibited functional changes in both task-evoked activation and spontaneous brain activity [6, 7]. The spontaneous brain activity can be quantitatively measured by the amplitude of low frequency fluctuations (ALFF), fractional ALFF (fALFF), and regional homogeneity (ReHo) of the blood-oxygen-level-dependent (BOLD) signals derived from resting-state functional magnetic resonance imaging (rs-fMRI) [8, 9].

The ALFF measures the total power of the BOLD signal fluctuations within a specific low frequency range (0.01–0.08 Hz) at the single-voxel level [10]. The fALFF is a normalized index of ALFF, which measures the ratio of the amplitude in a low-frequency band relative to the amplitude in the total frequency bands [11]. The ReHo measures

the similarity of the time series of BOLD signals of a given voxel to those of its nearest neighbors in a voxel-wise way that provides important information about the regional temporal synchronization in the brain [12]. Synthetically, the ALFF/fALFF and ReHo provide complementary information about the regional spontaneous brain activity.

The ALFF/fALFF and ReHo have been used to identify functional abnormalities in schizophrenia patients. Nevertheless, studies of ALFF/fALFF and ReHo have yielded inconsistent results [13–22]. For instance, some studies reported that schizophrenia patients had increased ALFF [17, 18], fALFF [13, 18], and ReHo [21, 22] in medial prefrontal cortex (MPFC); however, some others revealed the opposite results [14, 16, 20].

In this study, we combined a meta-analysis and a large-sample study to clarify the two questions: first, regional alterations in ALFF/fALFF and ReHo in schizophrenia; second, the associations in alteration patterns between these measures.

2. Materials and Methods

2.1. Meta-Analysis

2.1.1. Data Sources and Inclusion Criteria. We reviewed all papers published in PubMed investigating ALFF, fALFF, or ReHo in patients with schizophrenia. The search strategy was carried out with keywords of "schizophrenia" and ("ALFF" or "fALFF" or "ReHo" or "amplitude of low-frequency oscillations" or "amplitude of low frequency fluctuations" or "regional homogeneity") and ("fMRI" or "functional magnetic resonance imaging"). In order to qualify for inclusion within the meta-analysis, papers were required (a) to report comparisons between schizophrenia patients and matched healthy controls; (b) to employ fMRI; (c) to report results based on voxel-wise analysis; and (d) to detail either the Talairach or Montreal Neurologic Institute (MNI) coordinates of altered brain regions. Studies not fulfilling these requirements were excluded.

Papers were searched independently by two investigators until they made a consensus. After applying the search strategy, we found 20 articles. After carefully reading these articles, we excluded ten of them for the following reasons: (1) three articles were not fMRI studies [23–25]; (2) one article was not focused on schizophrenia patients [26]; (3) three articles were lacking intergroup comparisons [27–29]; (4) one article was focused on imaging and genetic association [30]; and (5) two articles only focused on the ALFF or ReHo changes in the independent components or network nodes [31, 32]. In addition, none of the 10 qualified articles reported negative results. The detailed demographic and clinical data of the 10 qualified articles for meta-analysis are shown in Tables 1 and 2.

2.1.2. Meta-Analysis Procedures. Coordinate-based meta-analysis was performed using the revised version of Activation Likelihood Estimation (ALE) technique [33] implemented in GingerALE 2.3.1 (http://www.brainmap.org/). This algorithm identifies foci showing common activation across different experiments (or studies) if the merged activation is higher than that of the null-distribution reflecting a random spatial association between experiments. Coordinates of the foci reported in the original studies were transformed into the MNI space using the Lancaster transform (icbm2tal tool) in GingerALE. Activation coordinates extracted from each study were weighted to yield estimates of activation likelihood at each voxel, and then a modelled activation (MA) map was computed. The spatial uncertainty of each focus was considered as an independent Gaussian probability distribution. The Gaussian parameters (standard deviation and width) are empirically determined based on between-template and between-subject variances and weighted by the number of subjects. So each voxel has an activation probability value for a specific focus of a certain experiment. Then a MA map for each experiment is computed by summing the probability values for all the foci. After that, the ALE map was calculated by merging all the MA maps of included experiments, which represent the spatial probabilistic distribution about the convergent activation for each voxel. To enable spatial inference

on the ALE scores, a nonparametric permutation test was used to generate empirical null-distribution, which reflects the null-hypothesis of a random spatial association between experiments. Finally, each "true" ALE score is then compared to the null-distributed ALE scores to yield a nonparametric P value. Because only a few experiments (6 ALFF/fALFF studies and 4 ReHo studies) were enrolled in this meta-analysis, we used an uncorrected intensity threshold of $P < 0.05$ and an extent threshold of $540\,mm^3$. The same extent threshold was also applied in the following large-sample study.

2.2. Large-Sample Control Study

2.2.1. Participants. A total of 89 schizophrenia patients and 89 healthy controls were recruited in this study. Diagnoses for patients were confirmed using the Structured Clinical Interview for DSM-IV. Exclusion criteria were MRI contraindications, poor image quality, presence of a systemic medical illness or CNS disorder, history of head trauma, and substance abuse within the last 3 months or lifetime history of substance abuse or dependence. Additional exclusion criteria for healthy controls were history of any Axis I or II disorders and first-degree relative with a psychotic disorder. This study was approved by the Medical Research Ethics Committee at Tianjin Medical University General Hospital, and after complete description of the study to the participants, written informed consent was obtained.

2.2.2. Image Data Acquisition. MRI was performed using a 3.0-Tesla MR system (Discovery MR750, General Electric, Milwaukee, WI, USA). Tight but comfortable foam padding was used to minimize head motion, and earplugs were used to reduce scanner noise. Sagittal 3D T1-weighted images were acquired by a brain volume (BRAVO) sequence with the following parameters: repetition time (TR) = 8.2 ms; echo time (TE) = 3.2 ms; inversion time = 450 ms; flip angle (FA) = 12°; field of view (FOV) = 256 mm × 256 mm; matrix = 256 × 256; slice thickness = 1 mm, no gap; and 188 sagittal slices. Resting-state fMRI data were acquired using gradient-echo SENSE-SPIRAL (spiral in) sequence with the following parameters: TR/TE = 1400/30 ms; FOV = 220 mm × 220 mm; matrix = 64 × 64; FA = 60°; slice thickness = 4 mm; gap = 0.5 mm; 32 interleaved transverse slices; 250 volumes. During fMRI scans, all subjects were instructed to keep their eyes closed, to relax and keep motionless, to think of nothing in particular, and not to fall asleep.

2.2.3. ALFF/fALFF Calculation. The resting-state fMRI data were preprocessed as the following steps. The first 10 volumes from each subject were discarded to allow the signal to reach equilibrium and to allow the participant to adapt to the scanning noise. The remaining 240 volumes were corrected for the acquisition time delay between slices. Rigid realignment was then performed to estimate and correct the motion displacement. Three schizophrenia patients were excluded because of excessive head motion; the remaining subjects' fMRI data were within the defined head motion thresholds

TABLE 1: The demographic and clinical data of studies included in the meta-analysis.

References	Publication year	Scanners	Indices	Patients age (years)	Controls age (years)	Patients (cases/F)	Controls (cases/F)	Diagnosis	Duration of illness	PANSS total	PANSS positive	PANSS negative
Hoptman et al. [13]	2010	Siemens 1.5T	ALFF/fALFF	36.5 ± 11.0	41.9 ± 10.9	29/3	26/7	CS	13.0 ± 7.2 (years)	76.5 ± 16.6	18.4 ± 6.2	20.2 ± 6.2
Huang et al. [14]	2010	GE 3T	ALFF	24.2 ± 8.4	24.5 ± 8.6	66/36	66/36	FES	8.8 ± 14.1 (months)	107.2 ± 15.1	26.4 ± 5.2	20.7 ± 6.3
He et al. [15]	2013	GE 3T	fALFF	25.4 ± 8.3	26.6 ± 8.9	104/55	104/54	FES	39.5 ± 31.9 (weeks)	92.1 ± 17.5	—	—
Ren et al. [16]	2013	GE 3T	ALFF	24.3 ± 7.5	24.4 ± 7.6	100/59	100/59	FES	6.3 ± 11.0 (months)	97.9 ± 17.8	25.1 ± 6.0	18.8 ± 7.7
Turner et al. [17]*	2013	Siemens/GE 3T	ALFF/fALFF	34.4–44.8	34.4–42.5	146/35	160/46	CS	13.1–24.1 (years)	53.8–64.7	13.5–16.5	13.1–16.7
Yu et al. [18]	2014	Siemens 3T	ALFF/fALFF	31.7 ± 9.6	29.9 ± 8.6	69/35	62/27	CS	7.1 ± 6.5 (years)	52.9 ± 16.8	12.1 ± 4.7	13.4 ± 6.1
Liu et al. [19]	2006	GE 1.5T	ReHo	23.7 ± 4.4	24.4 ± 3.9	18/9	18/9	Mixed	26.8 ± 19.2 (months)	80.4 ± 18.7	—	—
Jiang et al. [20]	2010	GE 1.5T	ReHo	16.4 ± 0.8	16.3 ± 0.9	18/9	18/9	EOS	9.6 ± 5.9 (months)	91.8 ± 6.7	—	—
Chen et al. [21]	2013	Siemens 3T	ReHo	28.3 ± 1.43	35.7 ± 1.8	36/20	44/27	FES	—	25.2 ± 6.9	—	—
Yu et al. [22]	2013	Siemens 3T	ReHo	31.7 ± 9.6	29.9 ± 8.6	69/36	62/27	CS	7.1 ± 6.5 (years)	52.9 ± 16.8	12.1 ± 4.7	13.4 ± 6.1

*Turner et al. [17] present the demographic information in 7 sites, respectively. Thus we only show the ranges of mean values from the 7 sites.
All studies did not give the medication information except for the study of Hoptman et al. [13], so we did not list the information in the table.
F, female; PANSS, Positive and Negative Syndrome Scale; FES, first-episode schizophrenia; CS, chronic schizophrenia; Mixed, FES and CS; EOS, early onset schizophrenia.

Table 2: Detailed area of studies included in the meta-analysis.

Regions	ALFF		fALFF		ReHo	
	Increase	Decrease	Increase	Decrease	Increase	Decrease
L-MPFC		[14, 16]			[22]	[20]
R-MPFC	[17, 18]		[13, 18]		[21, 22]	[20]
OFC	[17]	[16]	[13]	[15]		[19]
R-PCL		[17]				[19]
L-post_CG						[19]
R-post_CG		[13, 17, 18]				[19, 22]
L-preCG		[18]		[18]		[22]
R-preCG		[13, 17, 18]		[18]		[22]
L-STG		[17]				[19, 21]
R-STG		[17]				[19]
L-MTG	[18]					[19]
R-MTG	[18]			[17]		
L-ITG	[17]					[19]
R-ITG						[19]
L-HG				[13]		[22]
L-PH	[13]					[19]
R-PH		[18]	[13]			
L-Fus	[17]			[18]		
L-HP	[17]			[13]		
L-aINS	[17]		[18]		[22]	
R-aINS		[16]	[18]		[22]	
L-pINS	[17]	[18]		[13]		[22]
L-MOG		[13, 18]		[13, 18]		[19, 22]
R-MOG	[16]	[13]		[13]		[19]
L-IOG	[16]					[19]
R-IOG				[18]		[19]
L-Cun		[13]		[13]		
R-Cun		[13, 17]		[13, 17, 18]		
L-LG		[13, 18]				
R-LG		[13, 18]		[13, 18]		
R-Cal	[16]					
L-Cau			[13]			
R-Cau				[13]		
L-Put	[14, 16]		[15]			
R-Put	[14, 16, 17]		[15]			
L-HTh	[17]					
L-Cla				[13]		
R-LN			[13]			
L-ACC						[19]
R-PCC		[17]		[13, 17]		
R-SPL						[19]
L-IPL		[16, 18]	[18]	[18]		
R-IPL		[16]				
L-Pcu		[13]				
R-Pcu		[13, 16–18]		[13]		[19, 22]

L, left; R, right; MPFC, medial prefrontal cortex; PCL, paracentral lobule; post_CG, postcentral gyrus; preCG, precentral gyrus; STG, superior temporal gyrus; MTG, middle temporal gyrus; ITG, inferior temporal gyrus; HG, Heschl gyrus; PH, parahippocampal; Fus, fusiform; HP, hippocampus; aINS, anterior insula; pINS, posterior insula; MOG, middle occipital gyrus; IOG, inferior occipital gyrus; Cun, cuneus; LG, lingual gyrus; Cal, calcarine; Cau, caudate; Put, putamen; HTh, hypothalamus; Cla, claustrum; LN, lentiform nucleus; ACC, anterior cingulate cortex; PCC, posterior cingulate cortex; SPL, superior parietal lobule; IPL, inferior parietal lobule; Pcu, precuneus.

(translational or rotational motion parameters lower than 2 mm or 2°). Then several nuisance covariates were regressed out from the motion corrected fMRI data, including the mean signals of white matter and cerebrospinal fluid, six rigid motion parameters and their first-level derivatives. We also regressed out spike volumes that had framewise displacement higher than 0.5 to further remove possible influence by head motion [34]. This was realized by generating a nuisance regressor for each time point with "1" for the bad time point and "0" for the remaining time points. A two-step coregistration method was used to transform the regressed fMRI data into the MNI space. First, the mean realigned fMRI images were affinely (12 parameters) coregistered with individual structural images; then the structural images were affinely (12 parameters) coregistered with the standard MNI T1-weighted template. The generated parameters for these two coregistration steps were concatenated and used to normalization of the regressed fMRI data. The normalized fMRI data were resampled into a voxel size of 3 mm × 3 mm × 3 mm. Finally, the normalized fMRI volumes were smoothed with a Gaussian kernel of 6 mm × 6 mm × 6 mm full-width at half maximum (FWHM).

The ALFF was calculated using REST software (http://www.restfmri.net/). The processing procedure was similar to that used in an earlier research [18]. The preprocessed time series were transformed to a frequency domain with a fast Fourier transform (FFT) and the power spectrum was then obtained. Because the power of a given frequency is proportional to the square of the amplitude of this frequency component of the original time series in the time domain, the square root was calculated at each frequency of the power spectrum, and the averaged square root was obtained across 0.01–0.08 Hz at each voxel. This averaged square root was taken as the ALFF. For standardization purposes, the ALFF of each voxel was divided by the global mean ALFF value of a certain subject. The fALFF was calculated based on the method described by Zou et al. [11], which provides a quantitative measure of spontaneous brain activity. In brief, the fALFF was calculated as the ratio of the power spectrum of low frequency (0.01–0.08 Hz) to that of the entire frequency range. For the purpose of standardization, the fALFF value of each voxel was divided by the global mean fALFF value for each subject.

2.2.4. ReHo Calculation.
The preprocessing steps for ReHo included slice timing, realignment, regression, band pass filtering (0.01–0.08), and normalization using the same parameters as the ALFF preprocessing. The ReHo was defined as the Kendall correlation coefficient (KCC) of the time series of a given voxel with those of its nearest neighbors (26 voxels) on a voxelwise basis [12]. The KCC can be computed by the following formula:

$$W = \frac{\sum \left(R_i\right)^2 - n\left(\overline{R}\right)^2}{(1/12) K^2 \left(n^3 - n\right)}, \tag{1}$$

where W is the KCC among given voxels, ranging from 0 to 1; R_i is the sum rank of the ith time point; $\overline{R} = [(n + 1)K]/2$

is the mean of the R_i; K is the number of time series within a measured cluster ($K = 27$; one given voxel plus its 26 neighbors); and n is the number of ranks ($n = 240$).

2.2.5. Group Statistical Analysis.
To explore the ALFF and ReHo differences between the two groups, a two-sample t-test was performed on the normalized ALFF/fALFF and ReHo maps in a voxelwise manner. False discovery rate (FDR) correction was applied with a corrected threshold of $P < 0.05$ (two-tailed) and a cluster size of >540 mm^3. All coordinates were reported in MNI space. Brain regions with significant intergroup differences in ALFF/fALFF/ReHo in the meta-analysis were defined as regions of interest (ROIs). We extracted the ALFF/fALFF/ReHo values of these ROIs from each subject of our own sample and compared them between schizophrenia patients and healthy controls ($P < 0.05$, uncorrected).

3. Results

3.1. Meta-Analysis

3.1.1. ALFF/fALFF.
A total of 6 experiments that involved 514 schizophrenia patients and 518 healthy subjects were recruited for this meta-analysis. All the 6 experiments showed both decreased and increased ALFF/fALFF in schizophrenia patients (Table 2). Compared to healthy controls, schizophrenia patients exhibited decreased ALFF/fALFF mainly in the bilateral occipital (OC), sensorimotor (SMC), and posterior parietal cortices (PPC). These patients also had decreased ALFF/fALFF in the bilateral superior temporal gyrus (STG), insula, and medial orbitofrontal cortex (MOFC) ($P < 0.05$, uncorrected). Schizophrenia patients had increased ALFF/fALFF in the bilateral medial (MPFC) and lateral prefrontal cortex (LPFC), medial temporal cortex (MTL), and striatum, and there were scattered foci in the bilateral OC, insula, and PPC (Figure 1 and Table S1 in Supplementary material available online at http://dx.doi.org/10.1155/2014/204628).

3.1.2. ReHo.
A total of 4 experiments with 141 schizophrenia patients and 142 healthy subjects were recruited for this meta-analysis. All the 4 experiments showed decreased ReHo and only 2 experiments showed increased ReHo in schizophrenia patients (Table 2). Compared to healthy controls, schizophrenia patients showed decreased ReHo mainly in the bilateral MOFC, STG, and OC, and there are scattered foci including bilateral SMC, PPC, and MTL. Schizophrenia patients had a higher ReHo in bilateral MPFC, LPFC, and right insula ($P < 0.05$, uncorrected) (Figure 2 and Table S2).

3.2. Validation Study.
A total of 86 schizophrenia patients and 89 healthy controls were included in this study. The demographic and clinical data of subjects are shown in Table 3.

3.2.1. ALFF.
In the voxel-based analysis, compared to healthy controls, schizophrenia patients showed decreased ALFF
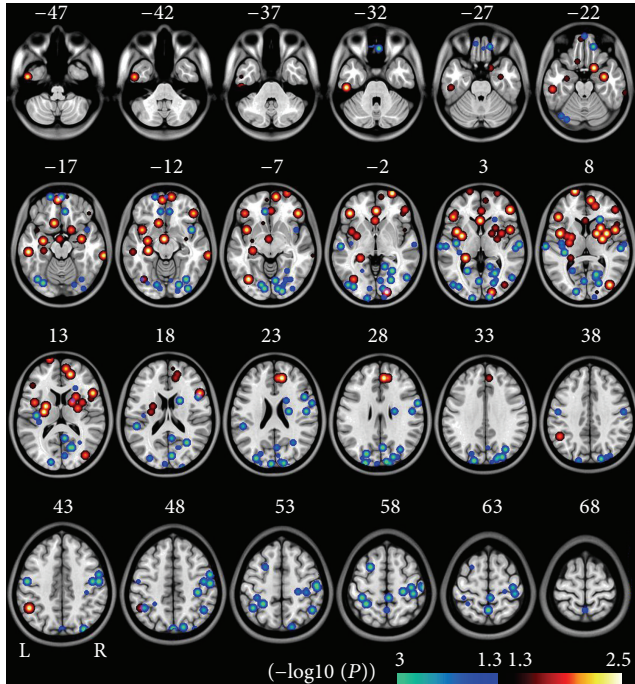
Figure 1: Brain regions with significant differences in ALFF/fALFF in meta-analysis between schizophrenia and healthy controls ($P <$ 0.05, uncorrected, cluster size >540 mm^3). The hot color represents the higher ALFF/fALFF in schizophrenia patients. The cold color represents the higher ALFF/fALFF in healthy controls. The overlapping area is marked in the pink color. Here, it represents the contradictory results between studies. The ($-\log10\ (P)$) value means the negative ten-logarithm transformation of P value. A larger value of ($-\log10\ (P)$) represents a smaller P value.

Figure 2: Brain regions with significant differences in ReHo in meta-analysis between schizophrenia and healthy controls ($P <$ 0.05, uncorrected, cluster size >540 mm^3). The hot color represents the higher ReHo in schizophrenia patients. The cold color represents the higher ReHo in healthy controls. The ($-\log10\ (P)$) value means the negative ten-logarithm transformation of P value. A larger value of ($-\log10\ (P)$) represents a smaller P value.

in the bilateral OC, PPC, and SMC and right STG and increased ALFF in bilateral striatum, MTL, MPFC, and lateral orbitofrontal cortex (LOFC) ($P < 0.05$, FDR corrected) (Figure 3).

3.2.2. fALFF. In the voxel-based analysis, compared to healthy controls, schizophrenia patients showed decreased fALFF mainly in bilateral OC and right postcentral gyrus and increased fALFF in bilateral striatum and MTL ($P < 0.05$, FDR corrected) (Figure 4).

3.2.3. ReHo. In the voxel-based analysis, compared to healthy controls, schizophrenia patients showed decreased ReHo in bilateral OC, SMC, thalamus, frontal pole, and right STG. Schizophrenia patients also showed increased ReHo in bilateral striatum, MTL, LOFC, MPFC, and SMA ($P < 0.05$, FDR corrected) (Figure 5).

3.2.4. ROI-Based Validation. The results of ROI-based intergroup comparisons in ALFF/fALFF/ReHo are shown in Tables S1 and S2. We found that more than a half of ROIs with significant intergroup differences in ALFF/fALFF/ReHo in the meta-analysis also had significant intergroup differences in our sample ($P < 0.05$, uncorrected).

Table 3: Demographic and clinical data of participants in the large-sample study.

Variables	Patients ($N = 86$)	Controls ($N = 89$)	P
Age (years)	33.4 ± 7.8	33.5 ± 10.6	0.957
Gender (males/females)	46/40	40/49	0.258
Illness duration (months)	16.3 ± 41.1	—	—
PANSS total	70.5 ± 23.4	—	—
PANSS positive	16.6 ± 8.1	—	—
PANSS negative	20.2 ± 8.9	—	—

Among the 86 schizophrenia patients, 6 patients were first-episode and 80 patients were chronic.

4. Discussion

After the first reports of ALFF [14] and ReHo [19] abnormalities in schizophrenia, several studies were conducted to investigate the altered ALFF and ReHo in this disorder, but the results were inconsistent. The reasons for these inconsistent results were complicated, and it was necessary to reconcile these conflicting results. Therefore, we combined a meta-analysis and a large-sample study to clarify the regional alterations of ALFF and ReHo in schizophrenia. We demonstrated that both ALFF/fALFF and ReHo were decreased in the bilateral OC, SMC, and PPC and increased
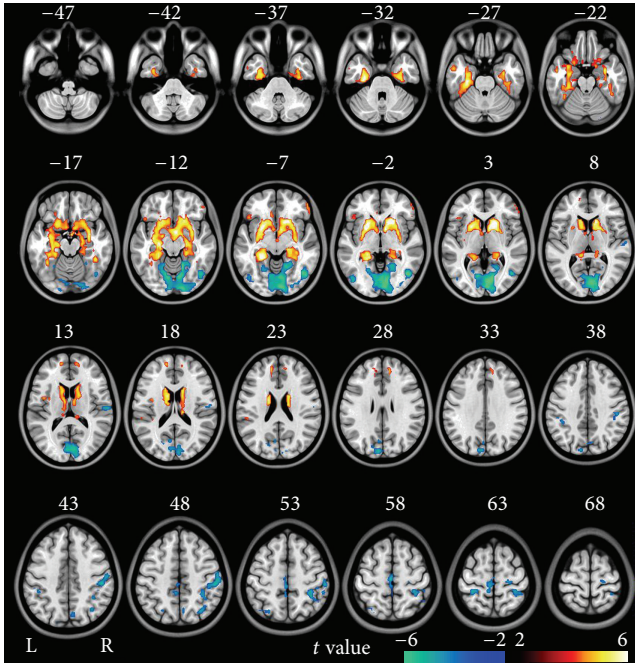
FIGURE 3: Brain regions with significant differences in ALFF in validation study between schizophrenia patients and healthy controls (FDR < 0.05, two-tailed, cluster size >540 mm^3). The hot color represents the higher ALFF in schizophrenia patients. The cold color represents the higher ALFF in healthy controls.

FIGURE 5: Brain regions with significant differences in ReHo in validation study between schizophrenia patients and healthy controls (FDR < 0.05, two-tailed, cluster size >540 mm^3). The hot color represents the higher ReHo in schizophrenia patients. The cold color represents the higher ReHo in healthy controls.

FIGURE 4: Brain regions with significant differences in fALFF in validation study between schizophrenia patients and healthy controls (FDR < 0.05, two-tailed, cluster size >540 mm^3). The hot color represents the higher fALFF in schizophrenia patients. The cold color represents the higher fALFF in healthy controls.

in the bilateral striatum, MTL, and MPFC in schizophrenia patients.

4.1. Foci with Consistently Decreased ALFF/ReHo in Schizophrenia. The reduced ALFF and ReHo of the occipital cortex in schizophrenia patients were observed in most of studies, which are consistent with deficits in low level visual processing in schizophrenia [35–38]. The functional abnormality of the occipital cortex has also been related to visual hallucinations and object-recognition deficits in schizophrenia [39, 40]. Moreover, Schechter et al. suggested that schizophrenia patients took 75% greater time in processing magnocellular-aimed stimuli and 20% longer duration in detecting parvocellular-aimed stimuli in the visual backwards masking experiment than healthy controls [41].

The PPC plays a key role in high-level cognitive processing and the precuneus is an important node of the default-mode network (DMN). The reduced ALFF/ReHo in the PPC may be consistent with the notion that the lower ALFF and ReHo of the PPC predict worse performance in working memory [42], whose function has been found to be impaired in schizophrenia [43]. The reduced ALFF/ReHo in the precuneus is also in agreement with the structural and functional deficits in this region in patients with schizophrenia [44–46].

We also observed decreased ALFF/fALFF and ReHo in the sensorimotor cortex (SMC) in schizophrenia, which is consistent with previous finding of the grey matter abnormalities in this region in schizophrenia [47, 48]. The structural

and functional impairment in the SMC in schizophrenia may be related to the increased involuntary movements in schizophrenia [49]. The SMC impairment may be also associated with neurological soft signs, describing the neurological abnormalities in sensory integration, motor regulation, sequencing complex motor acts, and primitive reflexes that occur in the majority of schizophrenia patients [50].

4.2. Foci with Consistently Increased ALFF/ReHo in Schizophrenia. We observed increased ALFF and ReHo in the striatum in schizophrenia, which are consistent with increased cerebral blood flow (CBF) and glucose metabolism in medicated patients with schizophrenia [51]. In drug-naïve schizophrenia patients, the striatum exhibited decreased volume and CBF compared to healthy controls [52, 53]. Thus, the increased spontaneous activity in the striatum may reflect the effects of antipsychotic drugs. The involvement of the striatum in schizophrenia is also supported by the dopamine hypothesis of schizophrenia, which postulates hyperdopaminergia in the striatum [54]. Indeed, increased striatal dopamine transmission has been reported in first-episode schizophrenia patients [55, 56].

We also found increased ALFF and ReHo in the hippocampus in schizophrenia, which are well consistent with increased cerebral blood flow (CBF) and glucose metabolism in this region in patients with schizophrenia [57]. The hippocampal disconnection has also been found in schizophrenia [58, 59], which may be associated with cognitive and emotional dysfunction.

4.3. Foci with Inconsistent Reports in the Schizophrenia. The OFC and MPFC are critical for social-emotional and insight processing. The impairment of these regions has been associated with emotionally instable, irritable, impulsive, and loss of insight in schizophrenia and other disorders [60–62]. Inconsistent alterations in ALFF and ReHo have been reported in the MPFC and OFC in schizophrenia patients, either decrease [14–16, 19, 20] or increase [13, 17, 18, 21, 22]. Our data only demonstrated increased ALFF and ReHo in the MPFC and OFC. Although the age, sex, illness duration, and medication may be related to the discrepancy, imaging sequence may also play a role. All previous studies on ALFF or ReHo used a single-shot echo planar imaging (EPI) sequence to collect the data. This sequence can inevitably induce image distortion and signal loss in the OFC due to phase error accumulation and susceptibility. In contrast, we applied a SENSE-SPIRAL sequence to reduce the above-mentioned artifacts, which may help us to obtain more plausible results.

The insula has demonstrated structural atrophy in schizophrenia [63–67]. Recent studies have revealed the functional disconnection of the insula in this disorder [65, 66, 68–72]. However, either increased [17, 18, 22] or decreased [13, 16, 18, 22] ALFF/ReHo has been reported in the insula in schizophrenia. Although our results did not show ALFF/ReHo changes in the insula in schizophrenia, the meta-analysis showed that the increased ALFF/ReHo was mainly located in the anterior insula, whereas the decreased ALFF/ReHo was mainly located in the posterior insula.

Recent studies have shown the different insula subregions demonstrated diverse connectivity patterns and functions: the anterior insula is closely connected with limbic system, middle and inferior temporal cortex, and anterior cingulate cortex, which plays a role in processing of emotion, attention, and salience; the posterior part is closely connected with the premotor, sensorimotor, supplementary motor, and middle-posterior cingulate cortices, which is related with sensorimotor integration [73, 74]. So the different change patterns in the anterior and posterior parts of the insula may reflect different aspect symptoms in the schizophrenia. Actually, the functional disconnection of the anterior insula has been associated with cognitive deficit in patients with schizophrenia [68].

Although the alternations of ALFF and ReHo showed similar distribution in schizophrenia patients, they also have some differences. On one hand, these two indices both reflect the spontaneous neural activity. Strong positive correlation has been shown between the two indices [75], and both ALFF and ReHo were found to correlate with cerebral blood flow [76]. The close association between ALFF and ReHo can interpret the consistent findings in schizophrenia. On the other hand, these two indices reflect different aspects of the spontaneous neural activity. The ALFF measures the low-frequency spontaneous fluctuation of neural activity for a certain voxel, while ReHo measures the regional homogeneity of spontaneous neural activity among neighboring voxels, which may interpret the differential findings in ALFF and ReHo. Brain regions with both ALFF and ReHo changes may enhance our confidence to conclude that these brain regions have altered spontaneous brain activity in schizophrenia. Some brain regions that only showed changes in ALFF or in ReHo indicate that the ALFF and ReHo can provide complementary information about the regional spontaneous brain activity.

Several limitations should be noted when one interpreting our findings. The reliability of an ALE analysis depends on the number of studies included. Too few studies may result in separate small foci (like in this study), which could be improved only when a large number of studies were included. A limitation of ALE is that the negative results cannot be included in the analysis; however, none of the qualified studies reported negative results which may lower the effect. The demographic characteristics are different across studies, particularly in symptoms, illness duration, and medication. Thus our results may reflect the generalized changes in spontaneous neural activity in a mixed sample of schizophrenia patients. It has been suggested that eyes-states (open or close) may affect the spontaneous brain activity [77]; however, at least 8/10 studies (the remaining 2 studies did not mention eyes-states) adopted an eye-closed scheme. Thus our results are more likely a reflection of eye-closed state. When normalization is done, it may also influence our results. However, all the 10 studies included in the meta-analysis performed normalization prior to obtaining derived connectivity metrics. In order to keep pace with the meta-analysis, we also performed normalization prior to obtaining derived connectivity metrics in the large-sample study. In our meta-analysis, a loose threshold ($P < 0.05$,

uncorrected) was used, which may prevent us from drawing a strong conclusion. However, we think our meta-analysis in combination with a large-sample study may provide a more comprehensive understanding of the change patterns of brain spontaneous activity in schizophrenia.

5. Conclusions

We performed a meta-analysis and a large-sample study on the alternations in ALFF and ReHo in schizophrenia. Our findings suggest that schizophrenia patients demonstrate an increased spontaneous brain activity in the striatum, medial temporal cortex, and medial prefrontal cortex and a decreased activity in the sensorimotor cortex, posterior parietal cortex, and occipital cortex. These findings may help to expound the pathophysiological hypothesis and to guide future researches.

Conflict of Interests

The authors declare that there is no conflict of interests regarding the publication of this paper.

Authors' Contribution

Yongjie Xu and Chuanjun Zhuo contributed equally to the paper.

Acknowledgments

References

[1] N. C. Andreasen, P. Nopoulos, V. Magnotta, R. Pierson, S. Ziebell, and B.-C. Ho, "Progressive brain change in schizophrenia: a prospective longitudinal study of first-episode schizophrenia," *Biological Psychiatry*, vol. 70, no. 7, pp. 672–679, 2011.

[2] T. Asami, S. Bouix, T. J. Whitford, M. E. Shenton, D. F. Salisbury, and R. W. McCarley, "Longitudinal loss of gray matter volume in patients with first-episode schizophrenia: DARTEL automated analysis and ROI validation," *NeuroImage*, vol. 59, no. 2, pp. 986–996, 2012.

[3] R. C. Chan, X. Di, G. M. McAlonan, and Q.-Y. Gong, "Brain anatomical abnormalities in high-risk individuals, first-episode, and chronic schizophrenia: an activation likelihood estimation meta-analysis of illness progression," *Schizophrenia Bulletin*, vol. 37, no. 1, pp. 177–188, 2011.

[4] I. Ellison-Wright, D. C. Glahn, A. R. Laird, S. M. Thelen, and E. Bullmore, "The anatomy of first-episode and chronic schizophrenia: an anatomical likelihood estimation meta-analysis," *The American Journal of Psychiatry*, vol. 165, no. 8, pp. 1015–1023, 2008.

[5] N. C. Andreasen, "The lifetime trajectory of schizophrenia and the concept of neurodevelopment," *Dialogues in Clinical Neuroscience*, vol. 12, no. 3, pp. 409–415, 2010.

[6] J. H. Yoon, M. J. Minzenberg, S. Raouf, M. D'Esposito, and C. S. Carter, "Impaired prefrontal-basal ganglia functional connectivity and substantia nigra hyperactivity in schizophrenia," *Biological Psychiatry*, vol. 74, no. 2, pp. 122–129, 2013.

[7] G. A. Light, J. L. Hsu, M. H. Hsieh et al., "Gamma band oscillations reveal neural network cortical coherence dysfunction in schizophrenia patients," *Biological Psychiatry*, vol. 60, no. 11, pp. 1231–1240, 2006.

[8] D. Cordes, V. M. Haughton, K. Arfanakis et al., "Frequencies contributing to functional connectivity in the cerebral cortex in "resting-state" data," *American Journal of Neuroradiology*, vol. 22, no. 7, pp. 1326–1333, 2001.

[9] D. S. Margulies, J. Böttger, X. Long et al., "Resting developments: a review of fMRI post-processing methodologies for spontaneous brain activity," *Magnetic Resonance Materials in Physics, Biology and Medicine*, vol. 23, no. 5-6, pp. 289–307, 2010.

[10] Y.-F. Zang, Y. He, C.-Z. Zhu et al., "Altered baseline brain activity in children with ADHD revealed by resting-state functional MRI," *Brain and Development*, vol. 29, no. 2, pp. 83–91, 2007.

[11] Q.-H. Zou, C.-Z. Zhu, Y. Yang et al., "An improved approach to detection of amplitude of low-frequency fluctuation (ALFF) for resting-state fMRI: fractional ALFF," *Journal of Neuroscience Methods*, vol. 172, no. 1, pp. 137–141, 2008.

[12] Y. Zang, T. Jiang, Y. Lu, Y. He, and L. Tian, "Regional homogeneity approach to fMRI data analysis," *NeuroImage*, vol. 22, no. 1, pp. 394–400, 2004.

[13] M. J. Hoptman, X.-N. Zuo, P. D. Butler et al., "Amplitude of low-frequency oscillations in schizophrenia: a resting state fMRI study," *Schizophrenia Research*, vol. 117, no. 1, pp. 13–20, 2010.

[14] X.-Q. Huang, S. Lui, W. Deng et al., "Localization of cerebral functional deficits in treatment-naive, first-episode schizophrenia using resting-state fMRI," *NeuroImage*, vol. 49, no. 4, pp. 2901–2906, 2010.

[15] Z. He, W. Deng, M. Li et al., "Aberrant intrinsic brain activity and cognitive deficit in first-episode treatment-naive patients with schizophrenia," *Psychological Medicine*, vol. 43, no. 4, pp. 769–780, 2013.

[16] W. Ren, S. Lui, W. Deng et al., "Anatomical and functional brain abnormalities in drug-naive first-episode schizophrenia," *The American Journal of Psychiatry*, vol. 170, no. 11, pp. 1308–1316, 2013.

[17] J. A. Turner, E. Damaraju, T. G. van Erp et al., "A multi-site resting state fMRI study on the amplitude of low frequency fluctuations in schizophrenia," *Frontiers in Neuroscience*, vol. 7, article 137, 2013.

[18] R. Yu, Y.-L. Chien, H.-L. S. Wang et al., "Frequency-specific alternations in the amplitude of low-frequency fluctuations in schizophrenia," *Human Brain Mapping*, vol. 35, no. 2, pp. 627–637, 2014.

[19] H. Liu, Z. Liu, M. Liang et al., "Decreased regional homogeneity in schizophrenia: a resting state functional magnetic resonance imaging study," *NeuroReport*, vol. 17, no. 1, pp. 19–22, 2006.

[20] S. Jiang, B. Zhou, Y. Liao et al., "Primary study of resting state functional magnetic resonance imaging in early onset schizophrenia using ReHo," *Zhong Nan Da Xue Xue Bao Yi Xue Ban*, vol. 35, no. 9, pp. 947–951, 2010.

[21] J. Chen, Y. Xu, K. Zhang et al., "Comparative study of regional homogeneity in schizophrenia and major depressive disorder,"

The American Journal of Medical Genetics Part B, vol. 162, no. 1, pp. 36–43, 2013.

[22] R. Yu, M. H. Hsieh, H.-L. S. Wang et al., "Frequency dependent alterations in regional homogeneity of baseline brain activity in schizophrenia," *PLoS ONE*, vol. 8, no. 3, Article ID e57516, 2013.

[23] A. T. Bates, K. A. Kiehl, K. R. Laurens, and P. F. Liddle, "Low-frequency EEG oscillations associated with information processing in schizophrenia," *Schizophrenia Research*, vol. 115, no. 2-3, pp. 222–230, 2009.

[24] L. Elliot Hong, L. V. Moran, X. Du, P. O'Donnell, and A. Summerfelt, "Mismatch negativity and low frequency oscillations in schizophrenia families," *Clinical Neurophysiology*, vol. 123, no. 10, pp. 1980–1988, 2012.

[25] L. V. Moran and L. E. Hong, "High vs low frequency neural oscillations in schizophrenia," *Schizophrenia Bulletin*, vol. 37, no. 4, pp. 659–663, 2011.

[26] H. Liao, L. Wang, B. Zhou et al., "A resting-state functional magnetic resonance imaging study on the first-degree relatives of persons with schizophrenia," *Brain Imaging and Behavior*, vol. 6, no. 3, pp. 397–403, 2012.

[27] F. Shi, Y. Liu, T. Jiang et al., "Regional homogeneity and anatomical parcellation for fMRI image classification: application to schizophrenia and normal controls," *Medical Image Computing and Computer-Assisted Intervention*, vol. 10, part 2, pp. 136–143, 2007.

[28] J. A. Turner, H. Chen, D. H. Mathalon et al., "Reliability of the amplitude of low-frequency fluctuations in resting state fMRI in chronic schizophrenia," *Psychiatry Research—Neuroimaging*, vol. 201, no. 3, pp. 253–255, 2012.

[29] Q. Yu, J. Sui, J. Liu et al., "Disrupted correlation between low frequency power and connectivity strength of resting state brain networks in schizophrenia," *Schizophrenia Research*, vol. 143, no. 1, pp. 165–171, 2013.

[30] J. Chen, Y. Xu, J. Zhang et al., "A combined study of genetic association and brain imaging on the DAOA gene in schizophrenia," *American Journal of Medical Genetics B*, vol. 162, no. 2, pp. 191–200, 2013.

[31] J. Sui, H. He, Q. Yu et al., "Combination of resting state fMRI, DTI, and sMRI data to discriminate schizophrenia by *N*-way MCCA + jICA," *Frontiers in Human Neuroscience*, vol. 7, p. 235, 2013.

[32] A. Zalesky, A. Fornito, G. F. Egan, C. Pantelis, and E. T. Bullmore, "The relationship between regional and inter-regional functional connectivity deficits in schizophrenia," *Human Brain Mapping*, vol. 33, no. 11, pp. 2535–2549, 2012.

[33] S. B. Eickhoff, A. R. Laird, C. Grefkes, L. E. Wang, K. Zilles, and P. T. Fox, "Coordinate-based activation likelihood estimation meta-analysis of neuroimaging data: a random-effects approach based on empirical estimates of spatial uncertainty," *Human Brain Mapping*, vol. 30, no. 9, pp. 2907–2926, 2009.

[34] J. D. Power, K. A. Barnes, A. Z. Snyder, B. L. Schlaggar, and S. E. Petersen, "Steps toward optimizing motion artifact removal in functional connectivity MRI; a reply to Carp," *NeuroImage*, vol. 76, pp. 439–441, 2013.

[35] D. C. Javitt, A.-M. Shelley, G. Silipo, and J. A. Lieberman, "Deficits in auditory and visual context-dependen processing in schizophrenia: defining the pattern," *Archives of General Psychiatry*, vol. 57, no. 12, pp. 1131–1137, 2000.

[36] E. F. Rabinowicz, G. Silipo, R. Goldman, and D. C. Javitt, "Auditory sensory dysfunction in schizophrenia: imprecision or distractibility?" *Archives of General Psychiatry*, vol. 57, no. 12, pp. 1149–1155, 2000.

[37] P. D. Butler, V. Zemon, I. Schechter et al., "Early-stage visual processing and cortical amplification deficits in schizophrenia," *Archives of General Psychiatry*, vol. 62, no. 5, pp. 495–504, 2005.

[38] P. D. Butler and D. C. Javitt, "Early-stage visual processing deficits in schizophrenia," *Current Opinion in Psychiatry*, vol. 18, no. 2, pp. 151–157, 2005.

[39] T. Onitsuka, R. W. McCarley, N. Kuroki et al., "Occipital lobe gray matter volume in male patients with chronic schizophrenia: a quantitative MRI study," *Schizophrenia Research*, vol. 92, no. 1–3, pp. 197–206, 2007.

[40] J. K. Wynn, M. F. Green, S. Engel et al., "Increased extent of object-selective cortex in schizophrenia," *Psychiatry Research—Neuroimaging*, vol. 164, no. 2, pp. 97–105, 2008.

[41] I. Schechter, P. D. Butler, G. Silipo, V. Zemon, and D. C. Javitt, "Magnocellular and parvocellular contributions to backward masking dysfunction in schizophrenia," *Schizophrenia Research*, vol. 64, no. 2-3, pp. 91–101, 2003.

[42] Q. Zou, T. J. Ross, H. Gu et al., "Intrinsic resting-state activity predicts working memory brain activation and behavioral performance," *Human Brain Mapping*, vol. 34, no. 12, pp. 3204–3215, 2013.

[43] S. S. Kang, S. R. Sponheim, M. V. Chafee, and A. W. MacDonald, "Disrupted functional connectivity for controlled visual processing as a basis for impaired spatial working memory in schizophrenia," *Neuropsychologia*, vol. 49, no. 10, pp. 2836–2847, 2011.

[44] C. C. Schultz, K. Koch, G. Wagner et al., "Complex pattern of cortical thinning in schizophrenia: results from an automated surface based analysis of cortical thickness," *Psychiatry Research*, vol. 182, no. 2, pp. 134–140, 2010.

[45] A. G. Garrity, G. D. Pearlson, K. McKiernan, D. Lloyd, K. A. Kiehl, and V. D. Calhoun, "Aberrant "default mode" functional connectivity in schizophrenia," *The American Journal of Psychiatry*, vol. 164, no. 3, pp. 450–457, 2007.

[46] V. D. Calhoun, J. Sui, K. Kiehl, J. Turner, E. Allen, and G. Pearlson, "Exploring the psychosis functional connectome: aberrant intrinsic networks in schizophrenia and bipolar disorder," *Frontiers in Psychiatry*, vol. 2, article 75, 2012.

[47] V. Molina, G. Galindo, B. Cortés et al., "Different gray matter patterns in chronic schizophrenia and chronic bipolar disorder patients identified using voxel-based morphometry," *European Archives of Psychiatry and Clinical Neuroscience*, vol. 261, no. 5, pp. 313–322, 2011.

[48] A. James, M. Hough, S. James et al., "Greater white and grey matter changes associated with early cannabis use in adolescent-onset schizophrenia (AOS)," *Schizophrenia Research*, vol. 128, no. 1–3, pp. 91–97, 2011.

[49] S. Pappa and P. Dazzan, "Spontaneous movement disorders in antipsychotic-naive patients with first-episode psychoses: a systematic review," *Psychological Medicine*, vol. 39, no. 7, pp. 1065–1076, 2009.

[50] I. Bombin, C. Arango, and R. W. Buchanan, "Significance and meaning of neurological signs in schizophrenia: two decades later," *Schizophrenia Bulletin*, vol. 31, no. 4, pp. 962–977, 2005.

[51] J. Liu, M. Qiu, R. T. Constable, and B. E. Wexler, "Does baseline cerebral blood flow affect task-related blood oxygenation level dependent response in schizophrenia?" *Schizophrenia Research*, vol. 140, no. 1–3, pp. 143–148, 2012.

[52] A. Glenthoj, B. Y. Glenthoj, T. Mackeprang et al., "Basal ganglia volumes in drug-naive first-episode schizophrenia patients before and after short-term treatment with either a typical or

an atypical antipsychotic drug," *Psychiatry Research—Neuroimaging*, vol. 154, no. 3, pp. 199–208, 2007.

[53] M. G. Livingston, "Regional cerebral blood flow in first-episode schizophrenia patients before and after antipsychotic drug treatment. Scottish Schizophrenia Research Group," *Acta Psychiatrica Scandinavica*, vol. 97, no. 6, pp. 440–449, 1998.

[54] O. D. Howes and S. Kapur, "The dopamine hypothesis of schizophrenia: version III—the final common pathway," *Schizophrenia Bulletin*, vol. 35, no. 3, pp. 549–562, 2009.

[55] G. J. E. Schmitt, E. M. Meisenzahl, T. Frodl et al., "Increase of striatal dopamine transmission in first episode drug-naive schizophrenic patients as demonstrated by [^{123}I]IBZM SPECT," *Psychiatry Research—Neuroimaging*, vol. 173, no. 3, pp. 183–189, 2009.

[56] L. S. Kegeles, A. Abi-Dargham, W. G. Frankle et al., "Increased synaptic dopamine function in associative regions of the striatum in schizophrenia," *Archives of General Psychiatry*, vol. 67, no. 3, pp. 231–239, 2010.

[57] S. A. Small, S. A. Schobel, R. B. Buxton, M. P. Witter, and C. A. Barnes, "A pathophysiological framework of hippocampal dysfunction in ageing and disease," *Nature Reviews Neuroscience*, vol. 12, no. 10, pp. 585–601, 2011.

[58] B. P. Godsil, J. P. Kiss, M. Spedding, and T. M. Jay, "The hippocampal-prefrontal pathway: the weak link in psychiatric disorders?" *European Neuropsychopharmacology*, vol. 23, no. 10, pp. 1165–1181, 2013.

[59] Y. Zhou, N. Shu, Y. Liu et al., "Altered resting-state functional connectivity and anatomical connectivity of hippocampus in schizophrenia," *Schizophrenia Research*, vol. 100, no. 1–3, pp. 120–132, 2008.

[60] J. Bramham, R. G. Morris, J. Hornak, P. Bullock, and C. E. Polkey, "Social and emotional functioning following bilateral and unilateral neurosurgical prefrontal cortex lesions," *Journal of Neuropsychology*, vol. 3, part 1, pp. 125–143, 2009.

[61] P. Fransson, "Spontaneous low-frequency BOLD signal fluctuations: an fMRI investigation of the resting-state default mode of brain function hypothesis," *Human Brain Mapping*, vol. 26, no. 1, pp. 15–29, 2005.

[62] K.-H. Lee, W. H. Brown, P. N. Egleston et al., "A functional magnetic resonance imaging study of social cognition in schizophrenia during an acute episode and after recovery," *The American Journal of Psychiatry*, vol. 163, no. 11, pp. 1926–1933, 2006.

[63] G. Spalletta, F. Piras, I. Alex Rubino, C. Caltagirone, and S. Fagioli, "Fronto-thalamic volumetry markers of somatic delusions and hallucinations in schizophrenia," *Psychiatry Research*, vol. 212, no. 1, pp. 54–64, 2013.

[64] T. Takahashi, S. J. Wood, B. Soulsby et al., "Follow-up MRI study of the insular cortex in first-episode psychosis and chronic schizophrenia," *Schizophrenia Research*, vol. 108, no. 1–3, pp. 49–56, 2009.

[65] L. Palaniyappan and P. F. Liddle, "Does the salience network play a cardinal role in psychosis? An emerging hypothesis of insular dysfunction," *Journal of Psychiatry and Neuroscience*, vol. 37, no. 1, pp. 17–27, 2012.

[66] L. Palaniyappan, T. P. White, and P. F. Liddle, "The concept of salience network dysfunction in schizophrenia: from neuroimaging observations to therapeutic opportunities," *Current Topics in Medicinal Chemistry*, vol. 12, no. 21, pp. 2324–2338, 2012.

[67] N. Makris, J. M. Goldstein, D. Kennedy et al., "Decreased volume of left and total anterior insular lobule in schizophrenia," *Schizophrenia Research*, vol. 83, no. 2-3, pp. 155–171, 2006.

[68] L. V. Moran, M. A. Tagamets, H. Sampath et al., "Disruption of anterior insula modulation of large-scale brain networks in schizophrenia," *Biological Psychiatry*, vol. 74, no. 6, pp. 467–474, 2013.

[69] T. P. White, V. Joseph, S. T. Francis, and P. F. Liddle, "Aberrant salience network (bilateral insula and anterior cingulate cortex) connectivity during information processing in schizophrenia," *Schizophrenia Research*, vol. 123, no. 2-3, pp. 105–115, 2010.

[70] A. Manoliu, V. Riedl, A. Zherdin et al., "Aberrant dependence of default mode/central executive network interactions on anterior insular salience network activity in schizophrenia," *Schizophrenia Bulletin*, vol. 40, no. 2, pp. 428–437, 2014.

[71] L. Palaniyappan, M. Simmonite, T. White, E. Liddle, and P. Liddle, "Neural primacy of the salience processing system in schizophrenia," *Neuron*, vol. 79, no. 4, pp. 814–828, 2013.

[72] S. J. Iwabuchi, P. F. Liddle, and L. Palaniyappan, "Structural connectivity of the salience-executive loop in schizophrenia," *European Archives of Psychiatry and Clinical Neuroscience*, 2014.

[73] V. Menon and L. Q. Uddin, "Saliency, switching, attention and control: a network model of insula function," *Brain Structure and Function*, vol. 214, no. 5-6, pp. 655–667, 2010.

[74] F. Cauda, F. D'Agata, K. Sacco, S. Duca, G. Geminiani, and A. Vercelli, "Functional connectivity of the insula in the resting brain," *NeuroImage*, vol. 55, no. 1, pp. 8–23, 2011.

[75] R. Yuan, X. Di, E. H. Kim, S. Barik, B. Rypma, and B. B. Biswal, "Regional homogeneity of resting-state fMRI contributes to both neurovascular and task activation variations," *Magnetic Resonance Imaging*, vol. 31, no. 9, pp. 1492–1500, 2013.

[76] Z. Li, Y. Zhu, A. R. Childress, J. A. Detre, and Z. Wang, "Relations between BOLD fMRI-derived resting brain activity and cerebral blood flow," *PLoS ONE*, vol. 7, no. 9, Article ID e44556, 2012.

[77] H. Yang, X.-Y. Long, Y. Yang et al., "Amplitude of low frequency fluctuation within visual areas revealed by resting-state functional MRI," *NeuroImage*, vol. 36, no. 1, pp. 144–152, 2007.

Research Article

Assessment of Functional Characteristics of Amnestic Mild Cognitive Impairment and Alzheimer's Disease Using Various Methods of Resting-State FMRI Analysis

Jungho Cha,[1] Jung-Min Hwang,[1] Hang Joon Jo,[2] Sang Won Seo,[3] Duk L. Na,[3] and Jong-Min Lee[1]

[1]*Department of Biomedical Engineering, Hanyang University, Seoul 133-791, Republic of Korea*
[2]*Section on Functional Imaging Methods, Laboratory of Brain and Cognition,*
 National Institute of Mental Health, National Institutes of Health, Bethesda, MD 20892, USA
[3]*Department of Neurology, Samsung Medical Center, Sungkyunkwan University School of Medicine, Seoul 135-710, Republic of Korea*

Correspondence should be addressed to Jong-Min Lee; jmlee@bme.hanyang.ac.kr

Resting-state functional magnetic resonance imaging (RS FMRI) has been widely used to analyze functional alterations in amnestic mild cognitive impairment (aMCI) and Alzheimer's disease (AD) patients. Although many clinical studies of aMCI and AD patients using RS FMRI have been undertaken, conducting a meta-analysis has not been easy because of seed selection bias by the investigators. The purpose of our study was to investigate the functional differences in aMCI and AD patients compared with healthy subjects in a meta-analysis. Thus, a multimethod approach using regional homogeneity, amplitude of low-frequency fluctuation (ALFF), fractional ALFF (fALFF), and global brain connectivity was used to investigate differences between three groups based on previously published data. According to the choice of RS FMRI approach used, the patterns of functional alteration were slightly different. Nevertheless, patients with aMCI and AD displayed consistently decreased functional characteristics with all approaches. All approaches showed that the functional characteristics in the left parahippocampal gyrus were decreased in AD patients compared with healthy subjects. Although some regions were slightly different according to the different RS FMRI approaches, patients with aMCI and AD showed a consistent pattern of decreased functional characteristics with all approaches.

1. Introduction

Resting-state functional magnetic resonance imaging (RS FMRI) does not require subjects to perform a specific task or stimuli to be applied; it simply requires the participants to keep their mind clear. Not having to perform a task provides a significant benefit, especially for patients who may have difficulties performing such a task. As a result, RS FMRI has been widely used to analyze the functional differences in Alzheimer's disease (AD) and amnestic mild cognitive impairment (aMCI) patients compared with healthy subjects. Although many clinical studies of aMCI and AD patients using RS FMRI have been undertaken, conducting a meta-analysis has not been easy. One limitation has been

the use of a seed-based approach. Typically, seeds are based on an anatomical atlas, using either the location of activity during the task or the standardized coordinates. The choice of seed may include selection bias by the investigator, and the patterns of functional connections may be quite different depending on the seed location [1]. Therefore, studies that used a seed-based approach are not suitable for inclusion in a meta-analysis. Apart from the seed-based approach, other approaches have been used to analyze the findings from RS FMRI. To avoid selection bias, several methods such as regional homogeneity (ReHo), amplitude of low-frequency fluctuation (ALFF), fractional ALFF (fALFF), and global brain connectivity (GBC) can be considered for meta-analysis.

ReHo is based on the similarity of a given voxel to its neighbor voxels over a time series [2]. The similarity over a number of time series can be measured using Kendall's coefficient concordance (KCC) [3]. This method is based on the hypothesis that significant brain activities are more likely to occur in clusters rather than in a single voxel [4]. The patterns identified using ReHo were found to be similar to those in regions deactivated during demanding cognitive tasks in previous positron emission tomography studies [5, 6]. This indicates that the ReHo method can be used to investigate the complexity of human brain function. In addition, previous studies have shown that the ReHo index patterns in the resting state can be used as a potential clinical marker for aMCI and AD [7, 8].

The ALFF and fALFF methods measure regional spontaneous brain activity. The ALFF technique measures the amplitude of resting-state spontaneous brain activity by calculating the square root of the power spectrum in the low-frequency range [9]. However, the ALFF is weak because of physiological noise near the large ventricles [10, 11]. To overcome these problems, previous studies have suggested use of the fALFF method [10]. The fALFF method measures the ratio of the low-frequency power spectrum to that of the entire frequency range and has been shown to have improved sensitivity and specificity in the detection of spontaneous brain activity compared with the ALFF approach [10, 11]. Previous studies have shown that the specific patterns of ALFF and fALFF in aMCI and AD patients provide insights into the biological mechanisms of the disease [12–15].

The technique of GBC identifies the brain's most globally connected regions. GBC uses the seed-based correlations of each voxel with all other brain voxels [16]. These values are then averaged together. The high-GBC regions occur mainly in the cognitive control network (CCN) and the default mode network (DMN) [17]. Therefore, the GBC patterns represent the complex brain functions. A previous study showed that the GBC patterns could explain the patterns of vulnerability seen in AD patients [18]. However, the GBC patterns of aMCI patients were clearly understood.

The purpose of our study was to investigate the regions of functional differences in aMCI and AD patients compared with healthy aging subjects using a meta-analysis. Thus, a multimethod approach using ReHo, ALFF/fALFF, and GBC was used to investigate differences between three groups. To aid this meta-analysis, we analyzed existing data published on resting-state FMRI [19]. In previous study using spatial independent component analysis (sICA), we showed that there were significant differences between healthy subjects and patients with aMCI and AD. The results of several approaches using the same data can considerably encourage the further meta-analysis.

2. Materials and Methods

2.1. Subjects. This study reanalyzed previously published RS FMRI data [19]. Sixty-two healthy subjects (male/female ratio, 17/45; age, 68.5 ± 8.0), 34 patients with aMCI (18/16, 68.4 ± 7.9 years old), and 37 patients with AD (10/27, 72.8 ± 8.2 years old) participated in this study. We obtained

TABLE 1: Demographic and clinical findings of healthy subjects and patients with amnestic mild cognitive impairment (aMCI) or Alzheimer's disease (AD).

	Healthy subjects	aMCI	AD	P value
Number of subjects	62	34	37	
MMSE score	28.6 ± 1.9	27.1 ± 2.1	16.8 ± 6.9	$P < 0.0001$
Age	68.5 ± 8.0	68.4 ± 7.9	72.8 ± 8.2	$P < 0.03$
Sex (M/F)	17/45	18/16	10/27	$P < 0.03$
Education	10.9 ± 5.2	11.5 ± 5.2	10.9 ± 5.3	$P > 0.25$

Data for age, education, and MMSE (mini-mental state examination) score: mean ± SD; M, male; F, female. The P value was obtained by one-way ANOVA and chi-square test.

written informed consent, according to the Declaration of Helsinki, from all subjects and the study was approved by the Institutional Review Board of the Samsung Medical Center, Seoul, South Korea. The demographic and clinical data of the participants are presented in Table 1.

2.2. Data Acquisition. All imaging was carried out at the Samsung Medical Center. The scanner was a Philips Intera Achieva 3.0 Tesla scanner equipped with an 8-channel SENSE head coil (Philips Healthcare, The Netherlands). A high-resolution T1-weighted anatomical image was acquired using a magnetization-prepared gradient echo (MPRAGE) sequence (TR = 9.9 ms; TE = 4.6 ms; flip angle = 8°; $0.5 \times 0.5 \times 0.5\,\text{mm}^3$ voxel resolution). And whole-brain echo-planar imaging (EPI) time-series scans (TR = 3 s; TE = 35 ms; flip angle = 90°; $1.7 \times 1.7 \times 4\,\text{mm}^3$ voxel resolution) were acquired. RS FMRI data consisted of 100 volumes. During each scan, participants were instructed to rest with their eyes open.

2.3. Preprocessing of RS FMRI Data. Preprocessing of the RS FMRI data was performed using Analysis of Functional NeuroImage (AFNI) software (http://afni.nimh.nih.gov/) [20]. To correct for physiological noise, we first identified cardiac and respiratory noises of the RS FMRI data [21] using PESTICA software (Physiologic EStimation by Temporal ICA, http://www.nitrc.org/projects/pestica/). PESTICA includes IRF-RETROICOR, an improved correction method [22] that calculates the impulse response function (IRF) of each heartbeat or breath. For stabilization of the magnetic field and signal equilibrium, the initial three volumes from each functional image were removed. Slice timing and head motion corrections at the RS echo-planer imaging (EPI) time courses were then applied. Then, data were corrected using the anatomy-based correlation corrections (ANATICOR) method [23]. The data that were regressed included (1) six parameters obtained from the correction of head motion, (2) the signal from the eroded large ventricle mask, and (3) the signal from a region of the local white matter erosion mask ($r = 15\,\text{mm}$). To obtain the large ventricle masks and white matter mask, T1 images registered and corrected for intensity non-uniformities resulting from inhomogeneity in the magnetic field were divided into white matter, gray

matter (GM), cerebrospinal fluid, and background using an advanced neural-net classifier [24]. Although there has been debate about global signal, we did not perform the regression analysis with global signal. Previous studies showed that global signal regression may induce artificial negative correlations and influence the long- and short-range functional connections [25–27]. The anatomical T1 image was registered to the functional images using the local Pearson correlation cost function [28], and all masks were converted to EPI space. The large ventricle mask and the white matter mask were eroded by one voxel to minimize partial volume effects.

2.4. Postprocessing for Several Methods

2.4.1. ALFF/fALFF Analysis. We used the AFNI software to process the ALFF data, which have been depicted in previous studies [9, 29]. The time series were first converted to the frequency domain using a fast Fourier transform (FFT), and the power spectrum was then acquired. As the transformed frequency within the power spectrum is proportional to the square of the amplitude of this frequency component in the original time series, the power spectrum obtained by FFT was calculated and averaged across the frequency range 0.009–0.08 Hz at each voxel over the time courses. This averaged square root was taken as the ALFF [9]. To improve the ALFF approach, we also used the fALFF, the ratio of the power of the low-frequency fluctuations to that of the entire frequency range (0.009–0.25 Hz), which has been reported to be more sensitive than the original ALFF in detecting spontaneous brain activity [10]. After the calculation of the ALFF and fALFF maps, the GM mask was applied to reduce the inclusion of unwanted blood oxygen level-dependent signals or other physiological signals that occur because of large draining vessels. The ALFF and fALFF maps then underwent spatial smoothing with a 6 mm full-width-at-half-maximum (FWHM) Gaussian kernel and were normalized to the MNI152 template.

2.4.2. Regional Homogeneity Analysis. Regional homogeneity was calculated by the KCC values using the AFNI software. This method has been described as measuring the similarity of the time series within a cluster defined by the nearest neighbor voxels (27, 19, or 7, including a given voxel) in the whole brain [2]. Before the calculation of regional homogeneity, band-pass filtering (0.009 Hz < f < 0.08 Hz) was performed and the GM mask was applied. And the images underwent spatial smoothing with a 6 mm FWHM Gaussian kernel and were normalized to the MNI152 template. Then, the KCC was computed using

$$W = \frac{\sum (R_i)^2 - n (\overline{R})^2}{(1/12) K^2 (n^3 - n)},$$ (1)

where $W [0 \; 1]$ is the value of KCC for a given set of voxels, R_i is the sum rank of the i_{th} time point, $\overline{R} = ((n + 1) \times K)/2$ is the mean of R_i, K is the number of time courses within a measured cluster, and n is the number of ranks. We set the number of neighboring voxels to 27. The individual ReHo maps were obtained by computing KCC for each voxel.

2.4.3. Global Brain Connectivity (GBC) Analysis. GBC analysis [17] was calculated by globally connected regions. Before the calculation of the GBC maps, preprocessed functional images were performed band-pass filtered (0.009 Hz < f < 0.08 Hz), GM masked, spatial smoothed with 6 mm FWHM Gaussian kernel and normalized to the MNI152 template. The GBC maps, which calculated the correlation coefficients with all the other voxels within brain for each voxel, were computed with AFNI software (3dTcorrMap). The correlation values were converted to z values using Fisher's z transformation. The transformed values were averaged and the value was assigned to that voxel. The individual GBC map was then obtained.

2.5. Group Comparisons.
All the results from the different RS FMRI techniques were masked out, with the group mask obtained by selecting a threshold of 0.3 on the mean GM map of all subjects. To explore differences in the functional characteristics between the three groups, an analysis of covariance (ANCOVA) was performed using sex, age, and education as covariates. The correction of Type I errors (parameters: individual voxel P value = 0.01, simulated 10,000 times iteratively, 6 mm FWHM Gaussian filter width with the group mask) was reckoned using Monte Carlo simulations with AFNI's AlphaSim software program. The AlphaSim program provides an overall significance level achieved for various combinations of cluster size thresholds and probability thresholds for each voxel [30]. This is performed by Monte Carlo simulation of the process of image generation, masking, spatial correlation of voxels, voxel intensity thresholding, and cluster identification. The probability of the false positive detection per image is determined from the frequency count of cluster size [31].

The significance level was set at $P_\alpha < 0.05$ (uncorrected individual voxel height threshold of $P < 0.01$, $F > 4.776$) and a cluster size of 864 mm^3. *Post hoc* two-sample t-tests were employed between pairs of groups for voxelwise statistics at a corrected significance level of $P_\alpha < 0.05$.

3. Results

To allow visual inspection of the different approaches, mean images were generated for each group. The majority of the clusters were consistent across all groups and the patterns were quite similar to the previous results for each approach (Figure 1). These regions included the PCC/precuneus, middle frontal gyrus, anterior cingulate cortex (ACC), inferior parietal lobule, and middle temporal gyrus.

The results of the ANCOVA using age, sex, and education as covariates showed significant differences between the patients with aMCI and AD and healthy subjects (see Figures 2(a), 3(a), 4(a), and 5(a) and Tables 2–5 for details). Then, as shown in Figures 2(b)–2(d), 3(b)–3(d), 4(b)–4(d), and 5(b)–5(d) and Tables 6, 7, 8, and 9, we performed *post hoc* two-sample t-tests between pairs of groups. The ReHo, ALFF, fALFF, and GBC approaches showed that regions of the brain had decreased indices in patients with aMCI and AD compared with the healthy subjects. In particular, all RS FMRI approaches showed that the functional characteristics
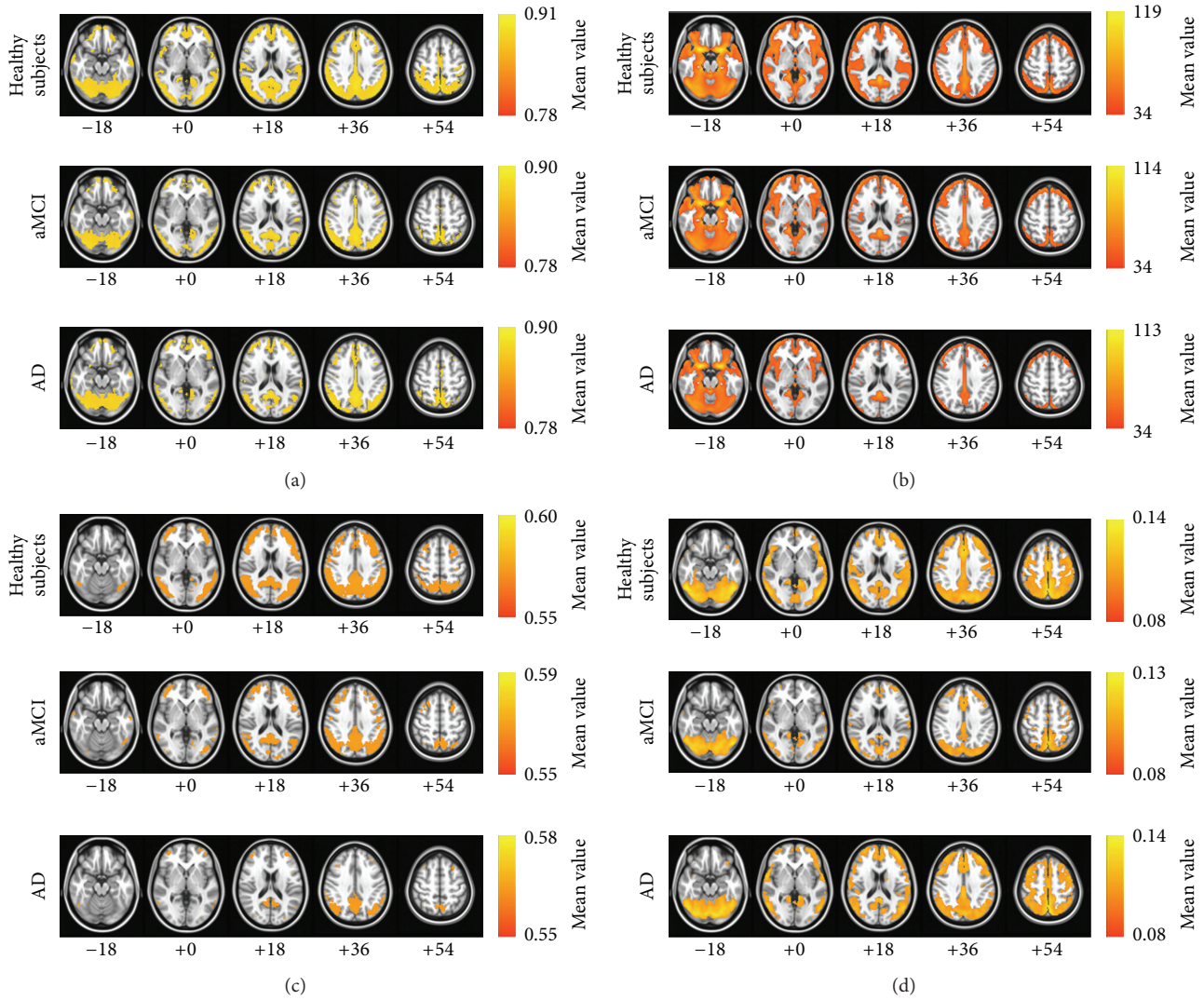
FIGURE 1: The mean images of each resting-state FMRI analysis approach: (a) regional homogeneity (ReHo), (b) amplitude of low-frequency fluctuation (ALFF), (c) fractional ALFF, and (d) global brain connectivity (GBC). The first row of each approach is the map for the healthy subjects, the second row of each approach is the map for the patients with aMCI, and the third row of each approach is the map for the patients with AD. The images are oriented with the anterior side placed at the top and the left side placed to the right. The red and blue colors represent positive and negative functional connectivity, respectively.

in the left parahippocampal gyrus were decreased in AD patients compared with healthy subjects. Therewith, significant group differences of the ReHo index were found in the middle temporal gyrus, ACC, postcentral gyrus, insula, precuneus, middle occipital gyrus, inferior parietal lobule, PCC, cingulate gyrus, and inferior frontal gyrus ($P_\alpha < 0.05$; AlphaSim corrected, uncorrected $P < 0.01$ at a cluster size of at least 108 voxels; see Figure 2(a) and Table 2 for a detailed list of the regions). And significant group differences in the ALFF were found in superior temporal gyrus, medial frontal gyrus, parahippocampal gyrus, insula, superior frontal gyrus, caudate, and superior temporal gyrus (see Figure 3(a) and Table 3 for a detailed list of the regions). On the other hand, significant group differences in the fALFF were found in inferior parietal lobule, PCC, fusiform gyrus, middle frontal gyrus, precuneus, precentral gyrus, inferior frontal gyrus,

middle temporal gyrus, parahippocampal gyrus, and cuneus (see Figure 4(a) and Table 4 for a detailed list of the regions). Significant group differences in the GBC index were found in the ACC, superior temporal gyrus, postcentral gyrus, parahippocampal gyrus, and cingulate gyrus (see Figure 5(a) and Table 5 for a detailed list of the regions).

4. Discussion

Here, we showed the functional alterations of the patients with aMCI and AD by applying several different RS FMRI techniques (ReHo, ALFF, fALFF, and GBC) to the data for healthy subjects and the data for patients with aMCI and patients with AD. In addition, these data also showed significant differences between healthy subjects and patients with aMCI and AD using the sICA reported in previous

FIGURE 2: Brain regions exhibiting significant differences in the regional homogeneity (ReHo) index. (a) Brain regions showed significant differences in ReHo between healthy subjects and patients with aMCI and patients with AD ($P_\alpha < 0.05$ (uncorrected $P < 0.01$, $F > 4.78$, 864 mm^3, and AlphaSim corrected)). The results of the *post hoc* two-sample t-tests between pairs of the healthy subjects and patients with AD and patients with aMCI were as follows: significant differences in brain regions were found (b) in patients with aMCI compared with healthy subjects, (c) in patients with AD compared with patients with aMCI, and (d) in patients with AD compared with healthy subjects ($P_\alpha < 0.05$). The images are oriented with the anterior side placed at the top and the left side placed to the right.

studies [19]. Although previous study showed differences between normal control and patients with MCI and AD with some similar method [32], this study was the first study of the whole brain voxel-based analysis. In conclusion, we showed that the results of using multiple approaches, excluding seed-based approaches, in RS FMRI analysis were useful for meta-analysis using the same data.

According to the various RS FMRI approaches, the patterns of functional alteration in patients with aMCI and AD were slightly different. Nevertheless, patients with aMCI and AD had significantly decreased functional characteristics compared with normal aging subjects for all approaches. Our major findings were as follows: (1) patients with aMCI and AD had decreased functional patterns compared with healthy subjects for all approaches. The ReHo, ALFF, fALFF, and GBC approaches showed that regions of the brain had decreased indices in patients with aMCI and AD compared with the healthy subjects. In particular, all RS FMRI approaches showed that the functional characteristics in the left parahippocampal gyrus were decreased in AD patients compared with healthy subjects, and (2) the ALFF and fALFF approaches showed that the indices in the posterior cingulate cortex (PCC), parahippocampal gyrus, middle temporal gyrus, and left inferior parietal lobule decreased significantly in the patients with AD compared with the patients with aMCI. The other methods did not show any differences between the patients with AD and aMCI. Taken together with the findings of our previous study, ALFF, fALFF, and sICA
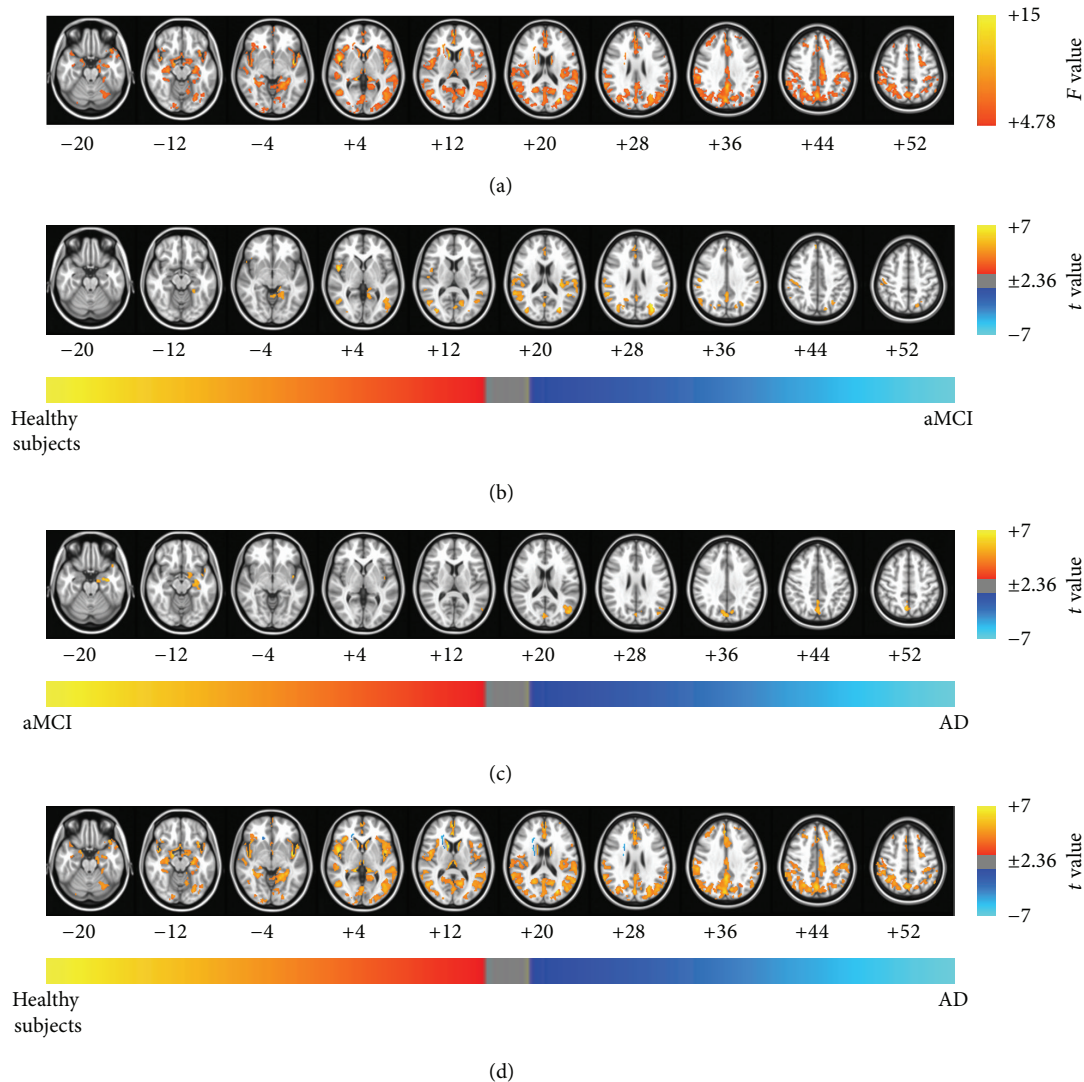
FIGURE 3: Brain regions exhibiting significant differences in the amplitude of low-frequency fluctuation (ALFF) index. (a) Brain regions showed significant differences in ALFF between healthy subjects and patients with aMCI and patients with AD ($P_\alpha < 0.05$ (uncorrected $P < 0.01$, $F > 4.78$, 864 mm^3, and AlphaSim corrected)). The results of the *post hoc* two-sample t-tests between pairs of the healthy subjects and patients with AD and patients with aMCI were as follows: significant differences in brain regions were found (b) in patients with aMCI compared with healthy subjects, (c) in patients with AD compared with patients with aMCI, and (d) in patients with AD compared with healthy subjects ($P_\alpha < 0.05$). The images are oriented with the anterior side placed at the top and the left side placed to the right.

were found to be more sensitive methods than the other RS FMRI approaches in patients with aMCI and AD. These major findings strongly encourage meta-analysis in patients with aMCI and AD with RS FMRI.

The mean images of ReHo, ALFF, fALFF, and GBC for the three groups were very similar to those of the human DMN reported in previous studies [6, 33]. A previous study demonstrated that the ReHo maps showed the existence of the DMN prominently and consistently during the resting and conscious states [34]. The DMN also had significantly higher ALFF and fALFF during the resting state than the other brain areas [9–11, 29]. In addition, the GBC values mainly occurred in the DMN and CCN. A previous study showed that high GBC was found in both the CCN and DMN

[17]. Therefore, the results of all four approaches were highly related to the DMN.

The regions of significant group differences from some of the different approaches were consistent with previous studies in patients with aMCI and AD [4, 7, 8, 12, 13, 18]. Interestingly, the *post hoc* two-sample t-tests between pairs of groups showed that the functional characteristics of all RS FMRI approaches in the left parahippocampal gyrus were decreased in AD patients compared with the healthy subjects. A previous study showed that there were structural changes in the left parahippocampal gyrus [35, 36] and reduced functional connectivity in the left parahippocampal gyrus [19]. The ReHo approach provides information about the intraregional functional characteristics, and the ALFF/fALFF
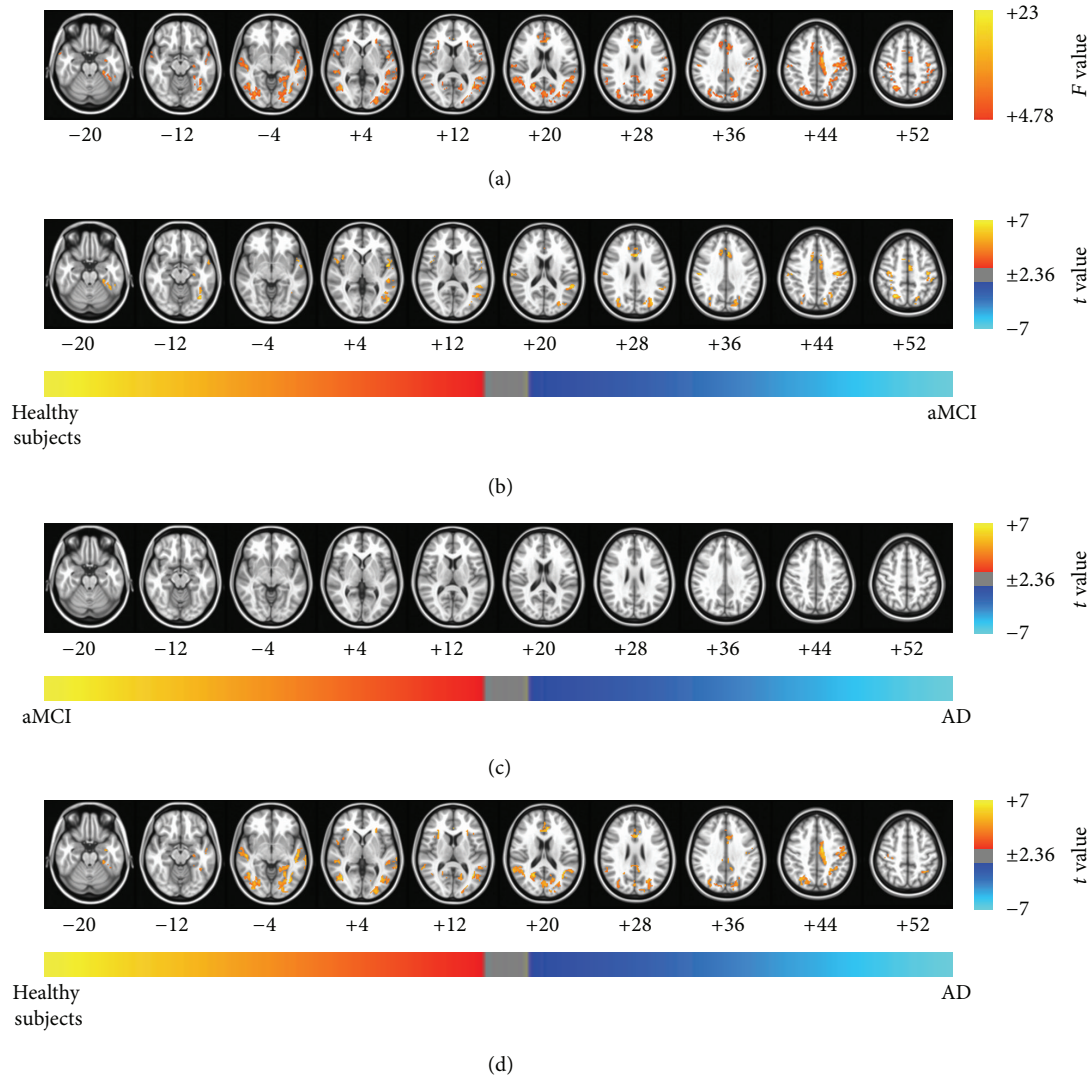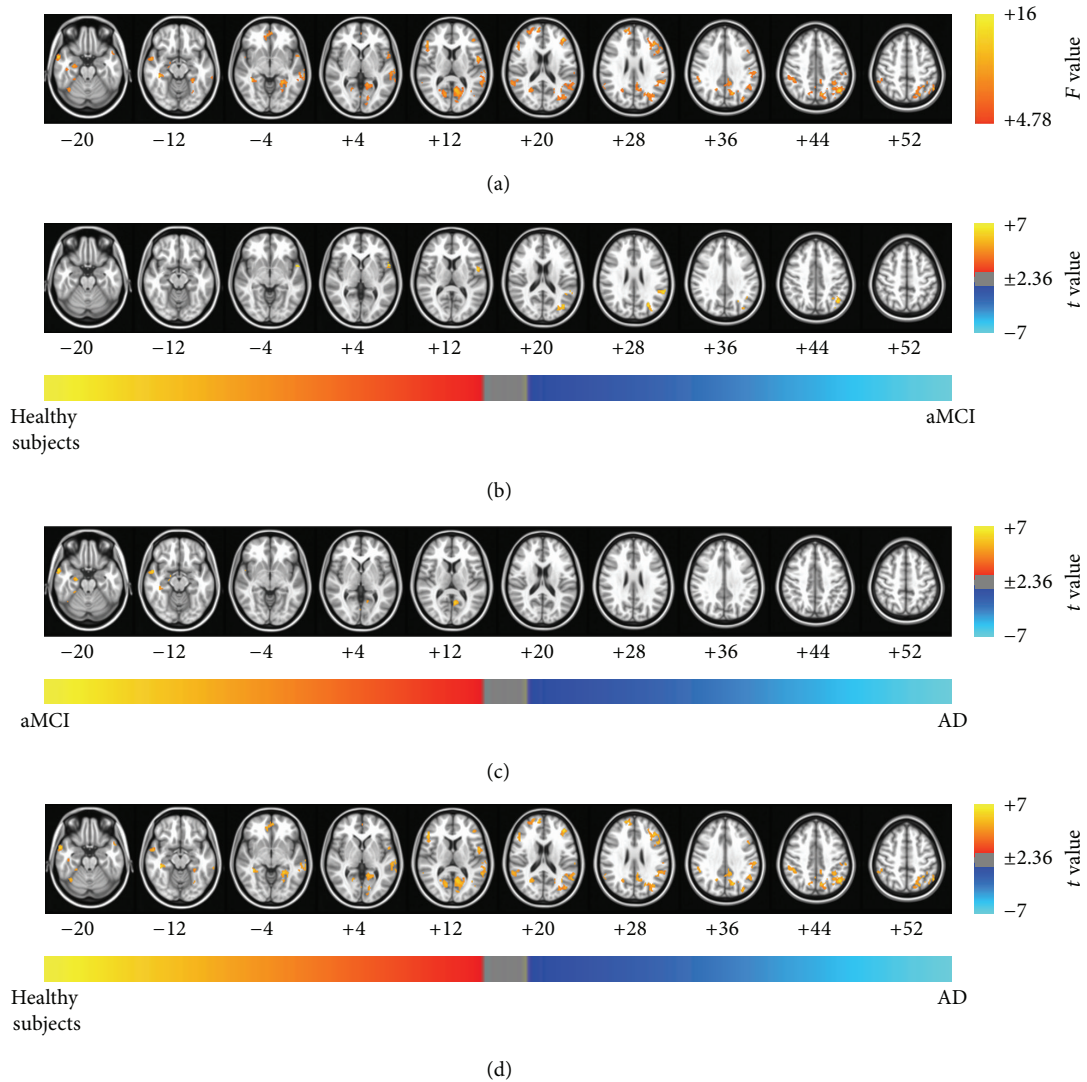
FIGURE 4: Brain regions exhibiting significant differences in the fractional ALFF (fALFF) index. (a) Brain regions showed significant differences in fALFF between healthy subjects and patients with aMCI and patients with AD ($P_\alpha < 0.05$ (uncorrected $P < 0.01$, $F > 4.78$, 864 mm³, and AlphaSim corrected)). The results of the *post hoc* two-sample t-tests between pairs of the healthy subjects and patients with AD and aMCI were as follows: significant differences in brain regions was found (b) in patients with aMCI compared with healthy subjects, (c) in patients with AD compared with patients with aMCI, and (d) in patients with AD compared with healthy subjects ($P_\alpha < 0.05$). The images are oriented with the anterior side placed at the top and the left side placed to the right.

approaches provide information about the oscillating brain activity. In addition, the GBC index provides information about the synchronization among remote areas. Therefore, from the perspective of both the intra- and interregional functional features, the functional characteristics in the left parahippocampal gyrus were decreased in patients with AD. In conclusion, the changes identified in the functional characteristics of the left parahippocampal gyrus provide a potential diagnosis of AD, regardless of the approach used to perform RS FMRI analysis.

Despite the consistency in the differences found between three groups by the four different methods, some inconsistency was exhibited because of the differences between these methods. The group differences observed using the ALFF approach were larger than those of the other approaches. Previous studies have shown that the ALFF method is more prone to noise from physiological sources, particularly near the ventricles and large blood vessels [10, 11]. Therefore, although we performed physiological noise removal with PESTICA, the results of the ALFF approach might still have been affected by noise. The fALFF approach was used to overcome this disadvantage and suppressed the group differences. The patterns of group differences observed using the fALFF approach were similar to those seen using the ReHo method. However, the fALFF approach showed differences between patients with AD and aMCI in the parahippocampal gyrus, cuneus, and middle temporal gyrus, whereas the ReHo approach did not show any difference between patients with
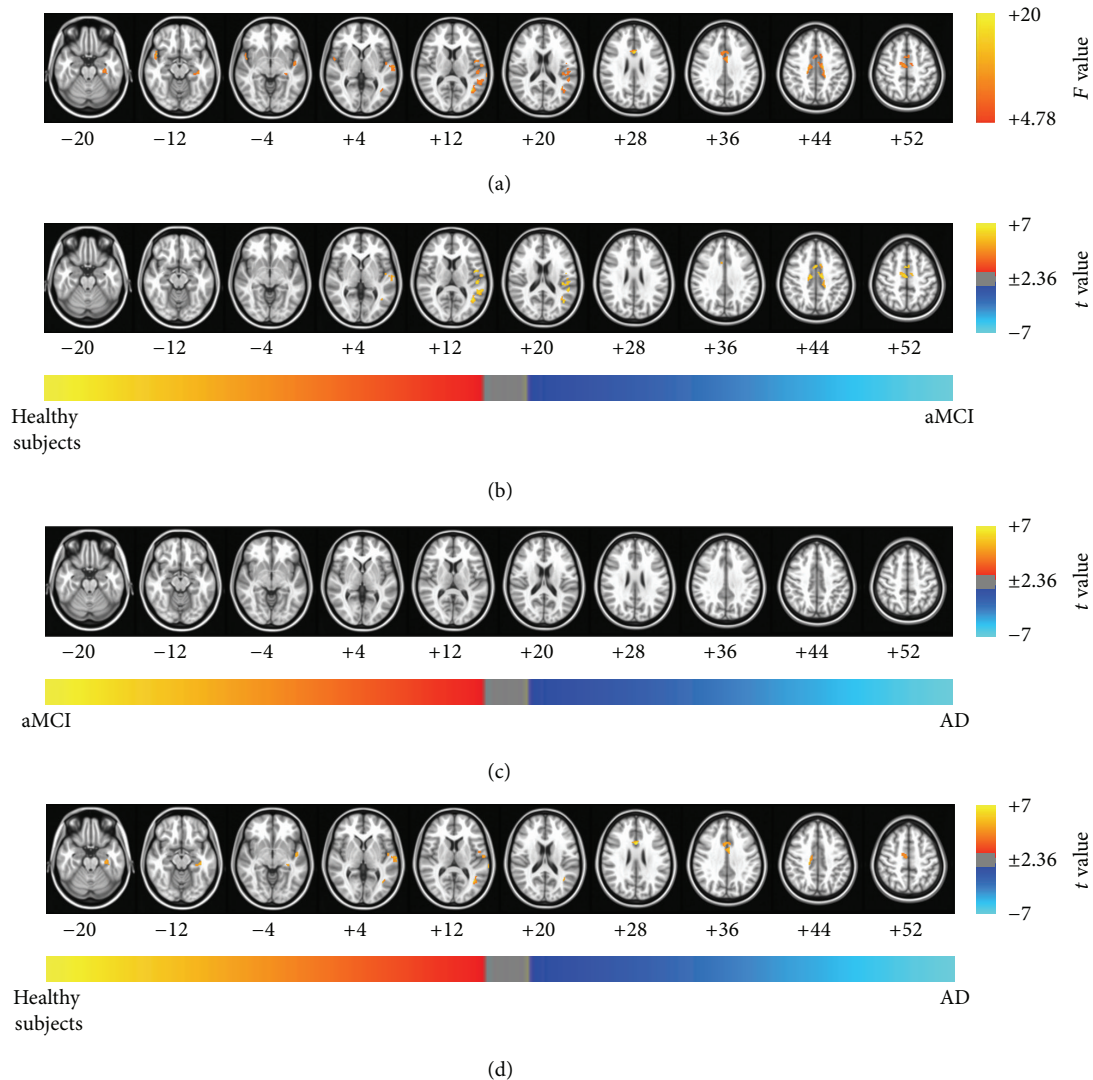
FIGURE 5: Brain regions exhibiting significant differences in the global brain connectivity (GBC) index. (a) Brain regions showed significant differences in the GBC index between healthy subjects and patients with aMCI and patients with AD ($P_\alpha < 0.05$ (uncorrected $P < 0.01$, $F > 4.78$, $864\,mm^3$, and AlphaSim corrected)). The results of the *post hoc* two-sample t-tests between pairs of the healthy subjects and patients with AD and aMCI were as follows: significant differences in the brain regions were found (b) in patients with aMCI compared with healthy subjects, (c) in patients with AD compared with patients with aMCI, and (d) in patients with AD compared with healthy subjects ($P_\alpha < 0.05$). The images are oriented with the anterior side placed at the top and the left side placed to the right.

AD and aMCI. The ALFF and fALFF approaches showed that the index in the PCC, parahippocampal gyrus, MTG, and left IPL was significantly decreased in the patients with AD compared with the patients with aMCI. The other methods did not show these differences between the patients with AD and aMCI.

Several additional issues need to be addressed. First, the number of subjects in this study ($n = 133$) was greater than those in previous studies. Therefore, this study might have greater statistical power than previous studies, and this might have caused different results to be obtained. However, patients with aMCI and AD displayed significantly decreased functional characteristics with every analysis approach, in agreement with previous studies. Second, when we performed analysis using the ALFF and fALFF approaches,

we restricted the frequency band (0.009–0.08 Hz) to enable comparison with the other methods. A previous study suggested the patterns of ALFF and fALFF obtained patients with aMCI were sensitive to the choice of frequency band [15]. The ALFF and fALFF abnormalities were greater in the slow-5 band (0.01–0.027 Hz) than in the slow-4 band (0.027–0.073 Hz). Therefore, a study using various frequency bands is required for further analysis of alterations to the functional characteristics in patients with aMCI and AD. Third, our results might relate to the possible confounding interference of gray matter loss. Although the analyses of functional differences with controlling gray matter losses are important, there is a need to overcome some issues about notable resolution differences between EPI and T1 image. With the improved technical method, a further study is needed to

TABLE 2: Brain regions with significant differences in regional homogeneity index between healthy subjects and patients with aMCI or AD.

Brain regions	R/L	Coordinates (mm)			Peak F values	Voxels
		x	y	z		
Healthy subjects versus aMCI versus AD						
Middle temporal gyrus	L	−40	−60	8	19.59	3286
Middle temporal gyrus	R	44	−58	4	16.07	848
ACC	L	−2	16	28	23.40	736
Middle temporal gyrus	R	32	−68	30	15.98	690
Postcentral gyrus	L	−36	−30	42	16.36	469
Postcentral gyrus	R	38	−32	56	15.62	301
Insula	R	38	16	6	15.86	272
ACC	R	14	28	28	16.29	224
Precuneus	R	2	−78	28	11.92	212
Middle occipital gyrus	R	34	−76	−6	12.02	186
IPL	L	−58	−26	28	14.60	171
Postcentral gyrus	R	52	−18	32	12.40	167
PCC	R	22	−58	18	16.72	162
Precuneus	L	−18	−68	16	13.20	160
Cingulate gyrus	L	−4	−34	30	11.61	160
Inferior frontal gyrus	L	−26	6	6	15.43	144

ACC: anterior cingulate cortex, IPL: inferior parietal gyrus, and PCC: posterior cingulate cortex. Threshold: corrected $P_\alpha < 0.05$ (uncorrected individual voxel height threshold of $P < 0.01$, $F > 4.776$ with a minimum cluster size of 864 mm^3).

TABLE 3: Brain regions with significant differences in amplitude of low-frequency fluctuations (ALFF) index between healthy subjects and patients with aMCI or AD.

Brain regions	R/L	Coordinates (mm)			Peak F values	Voxels
		x	y	z		
Healthy subjects versus aMCI versus AD						
Superior temporal gyrus	R	48	4	2	24.71	20320
Medial frontal gyrus	L	0	54	8	21.73	1412
Cerebellum	L	−24	−76	−50	20.83	1019
Parahippocampal gyrus	R	14	−6	−16	19.93	586
Cerebellum	R	20	−86	−40	13.57	573
Parahippocampal gyrus	R	16	−36	0	19.95	491
Middle frontal gyrus	R	20	30	42	9.51	279
Parahippocampal gyrus	R	36	−40	−4	14.35	270
Insula	R	24	28	10	17.84	258
Superior frontal gyrus	L	−18	34	44	9.96	230
Caudate	R	10	12	10	24.43	184
Superior frontal gyrus	L	−50	16	−32	12.75	166
Middle frontal gyrus	L	−24	−4	48	10.47	154

Threshold: corrected $P_\alpha < 0.05$ (uncorrected individual voxel height threshold of $P < 0.01$, $F > 4.776$ with a minimum cluster size of 864 mm^3).

TABLE 4: Brain regions with significant differences in fractional ALFF (fALFF) index between healthy subjects and patients with aMCI or AD.

Brain regions	R/L	Coordinates (mm)			Peak F values	Voxels
		x	y	z		
Healthy subjects versus aMCI versus AD						
Inferior parietal lobule	L	−54	−56	48	15.82	1654
PCC	L	−8	−60	12	13.17	743
Fusiform gyrus	R	38	−40	−8	16.58	461
Cerebellum	L	−24	−12	−36	12.98	422
Middle frontal gyrus	L	−40	38	18	13.38	416
Inferior parietal lobule	R	50	−40	46	9.66	246
Precuneus	R	14	−68	40	9.14	205
Middle frontal gyrus	R	10	58	22	12.49	201
Precentral gyrus	L	−52	2	8	13.33	200
Postcentral gyrus	L	−48	−30	36	12.26	195
Inferior frontal gyrus	R	48	22	16	12.23	167
Middle temporal gyrus	R	58	6	−22	13.34	164
Superior temporal gyrus	R	50	−42	16	8.70	163
Parahippocampal gyrus	R	34	−12	−28	10.76	146
Cuneus	R	14	−68	6	12.11	140
Medial frontal gyrus	L	−2	52	−4	9.09	134

PCC: posterior cingulate cortex. Threshold: corrected $P_\alpha < 0.05$ (uncorrected individual voxel height threshold of $P < 0.01$, $F > 4.776$ with a minimum cluster size of 864 mm^3).

TABLE 5: Brain regions with significant differences in global brain connectivity (GBC) index between healthy subjects and patients with aMCI or AD.

Brain regions	R/L	Coordinates (mm)			Peak F values	Voxels
		x	y	z		
Healthy subjects versus aMCI versus AD						
ACC	L	−2	12	28	15.36	763
Superior temporal gyrus	L	−68	−24	6	11.24	282
Cerebellum	L	−28	−46	−48	10.10	253
Postcentral gyrus	L	−20	−52	66	8.41	208
Superior temporal gyrus	L	−38	−58	12	16.27	170
Superior temporal gyrus	L	−50	−42	14	9.37	159
Parahippocampal gyrus	L	−38	−26	−12	8.74	153
Cingulate gyrus	L	−12	−14	40	14.49	145
Transverse temporal gyrus	L	−50	−24	12	7.29	143
Superior temporal gyrus	R	46	8	−16	12.21	127

ACC: anterior cingulate cortex. Threshold: corrected $P_\alpha < 0.05$ (uncorrected individual voxel height threshold of $P < 0.01$, $F > 4.776$ with a minimum cluster size of 864 mm^3).

TABLE 6: Results of *post hoc* two-sample *t*-tests between every pair of the healthy subjects and patients with AD and aMCI groups in ReHo approach.

Brain regions	R/L	Coordinates (mm)			Peak *t* value	Voxels
		x	*y*	*z*		
Healthy subject versus aMCI						
Superior parietal lobule	L	−18	−76	56	4.27	531
Cingulate gyrus	L	−4	−4	48	5.12	381
Precuneus	R	26	−62	50	5.59	284
Middle occipital gyrus	L	−38	−66	−12	5.39	279
Precentral gyrus	L	−40	−18	42	4.88	270
Superior temporal gyrus	L	−50	−2	2	5.25	266
Superior temporal gyrus	L	−54	−42	16	4.83	250
Precentral gyrus	R	40	−24	60	4.98	235
Middle occipital gyrus	L	−52	−72	2	5.07	220
Cingulate gyrus	R	8	24	38	5.19	184
Middle temporal gyrus	R	34	−70	26	4.27	177
Postcentral gyrus	R	52	−18	32	4.94	149
Insula	R	38	16	6	4.63	146
aMCI versus AD						
No result						
Healthy subject versus AD						
Middle temporal gyrus	L	−40	−60	8	6.22	1460
Middle temporal gyrus	R	44	−58	4	5.44	735
ACC	L	−2	16	28	6.49	551
Middle temporal gyrus	L	−50	−20	−8	5.31	399
Middle temporal gyrus	R	32	−68	30	5.21	329
Precentral gyrus	R	36	−24	54	4.97	197
Superior parietal lobule	L	−34	−56	54	4.58	184
Insula	R	30	22	12	4.49	178
Postcentral gyrus	L	−50	−20	40	4.89	175
Precuneus	R	2	−78	28	4.76	165
Parahippocampal gyrus	L	−32	−10	−20	5.01	164
Cingulate gyrus	L	−4	−34	30	4.80	160
Precuneus	L	−18	−68	16	5.06	159
PCC	R	22	−58	18	5.78	155
Middle occipital gyrus	R	36	−86	−6	4.74	149
Cerebellum	L	−26	28	4	5.28	125

ACC: anterior cingulate cortex, PCC: posterior cingulate gyrus. Positive values: healthy subjects > aMCI, aMCI > AD, and healthy subjects > AD. Negative values: aMCI > healthy subjects, AD > aMCI, and AD > healthy subjects. Threshold: corrected $P_\alpha < 0.05$.

TABLE 7: Results of *post hoc* two-sample *t*-tests between each pair of the healthy subjects and patients with AD and aMCI groups in ALFF approach.

Brain regions	R/L	Coordinates (mm)			Peak *t* value	Voxels
		x	*y*	*z*		
Healthy subject versus aMCI						
Inferior parietal lobule	R	56	−46	24	3.87	729
Supramarginal gyrus	L	−52	−50	24	3.98	585
Middle temporal gyrus	L	−30	−68	26	4.94	428
Middle occipital gyrus	R	34	−80	8	4.15	413
Postcentral gyrus	R	52	−8	16	3.46	353
Parahippocampal gyrus	L	−24	−40	−12	3.44	335
Superior temporal gyrus	R	50	6	0	4.59	222
Precuneus	R	2	−68	18	3.49	221
Middle temporal gyrus	L	−44	−62	4	3.78	217
Postcentral gyrus	R	52	−18	32	3.73	217
Medial frontal gyrus	R	4	46	42	3.60	202
Precuneus	L	0	−50	32	3.69	188
Precuneus	L	−16	−76	42	3.43	128
aMCI versus AD						
Precuneus	L	0	−70	46	4.19	654
Cerebellum	L	−22	−84	−44	4.75	594
Cerebellum	R	16	−84	−38	3.73	350
Parahippocampal gyrus	L	−26	−8	−18	4.34	345
Middle temporal gyrus	L	−48	−66	22	4.08	306
Superior temporal gyrus	L	−40	18	−28	4.30	185
Healthy subject versus AD						
Superior temporal gyrus	R	48	4	2	3.13	20151
Medial frontal gyrus	L	0	54	8	6.54	1411
Cerebellum	L	−24	−76	−50	6.22	957
Parahippocampal gyrus	R	14	−6	−16	6.30	575
Cerebellum	R	20	−86	−40	5.12	564
Parahippocampal gyrus	R	14	−36	2	6.15	490
Medial frontal gyrus	R	20	30	42	4.17	278
Parahippocampal gyrus	R	36	−40	−4	5.11	270
Lentiform Nucleus	R	24	6	20	−5.82	258
Superior frontal gyrus	L	−18	3	44	4.36	230
Caudate	R	10	12	10	6.78	184
Superior temporal gyrus	L	−50	16	−32	4.73	164
Medial frontal gyrus	L	−26	−6	48	4.41	153

Positive values: healthy subjects > aMCI, aMCI > AD, and healthy subjects > AD; Negative values: aMCI > healthy subjects, AD > aMCI, and AD > healthy subjects; Threshold: corrected $P_\alpha < 0.05$.

TABLE 8: Results of *post hoc* two-sample *t*-tests between every pair of the healthy subjects and patients with AD and aMCI groups in fALFF approach.

Brain regions	R/L	Coordinates (mm)			Peak *t* value	Voxels
		x	*y*	*z*		
Healthy subject versus aMCI						
Middle temporal gyrus	L	−30	−72	24	3.89	256
Superior temporal gyrus	L	−56	8	0	4.32	143
Inferior parietal lobule	L	−42	−58	38	4.14	136
Inferior parietal lobule	L	−50	−46	22	4.14	131
aMCI versus AD						
Parahippocampal gyrus	R	42	−30	−16	4.61	249
Cuneus	R	0	−72	6	4.23	173
Cerebellum	L	−26	−12	−36	4.48	163
Parahippocampal gyrus	R	34	−12	−28	4.60	135
Middle temporal gyrus	R	60	4	−22	4.04	131
Healthy subject versus AD						
Inferior parietal lobule	R	−48	−62	42	5.37	2324
PCC	L	−8	−62	12	4.92	832
Fusiform gyrus	R	38	−40	−8	5.75	504
Middle frontal gyrus	L	−40	38	18	5.10	409
Middle temporal gyrus	L	−48	10	−32	4.79	399
Inferior parietal lobule	R	50	−40	46	4.33	242
Precuneus	R	26	−60	22	4.17	205
Medial frontal gyrus	R	10	58	22	4.95	198
Postcentral gyrus	L	−58	−26	38	4.75	191
Inferior frontal gyrus	R	48	22	16	4.85	167
Superior temporal gyrus	R	60	−46	14	3.92	163
Middle frontal gyrus	R	58	6	−22	4.97	147
Cuneus	R	14	−68	6	4.84	140
Postcentral gyrus	L	−52	2	10	4.65	136
Medial frontal gyrus	L	−2	52	−5	4.04	125

PCC: posterior cingulated cortex. Positive values: healthy subjects > aMCI, aMCI > AD, and healthy subjects > AD. Negative values: aMCI > healthy subjects, AD > aMCI, and AD > healthy subjects. Threshold: corrected $P_\alpha <$ 0.05.

examine relationship between functional connectivity and gray matter density.

5. Conclusions

Our study demonstrated differences in the functional characteristics of patients with aMCI and AD compared with healthy subjects using multimethod analysis. The patterns of functional alteration in patients with aMCI and AD were slightly different depending on the RS FMRI approach used. Nevertheless, patients with aMCI and AD had consistently decreased functional characteristics compared with healthy subjects, regardless of the approach used. All RS FMRI approaches showed that the functional characteristics in the left parahippocampal gyrus were decreased in AD

TABLE 9: Results of *post hoc* two-sample *t*-tests between every pair of the healthy subjects and patients with AD and aMCI groups in GBC approach.

Brain regions	R/L	Coordinates (mm)			Peak *t* value	Voxels
		x	*y*	*z*		
Healthy subject versus aMCI						
Superior frontal gyrus	R	2	2	58	4.26	525
Postcentral gyrus	L	−20	−52	66	4.04	207
Precentral gyrus	L	−48	−4	12	3.59	162
Middle temporal gyrus	L	−40	−58	10	5.88	158
Superior temporal gyrus	L	−50	−42	14	4.19	154
Transverse temporal gyrus	L	−50	−24	12	3.77	143
Cingulate gyrus	L	−12	−14	40	4.06	136
aMCI versus AD						
Cerebellum	L	−28	−48	−52	3.65	141
Healthy subject versus AD						
Superior temporal gyrus	L	−68	−24	6	4.36	258
Cerebellum	L	−28	−46	−48	4.48	246
ACC	L	−2	12	28	5.53	241
Cingulate gyrus	R	16	−20	40	5.09	165
Parahippocampal gyrus,	L	−36	−28	−12	4.07	153
Superior temporal gyrus	L	−38	−58	12	130	130

ACC: anterior cingulate gyrus. Positive values: healthy subjects > aMCI, aMCI > AD, and healthy subjects > AD. Negative values: aMCI > healthy subjects, AD > aMCI, and AD > healthy subjects. Threshold: corrected $P_\alpha <$ 0.05.

patients compared with healthy subjects. The ALFF and fALFF approaches both showed that the index decreased significantly in the patients with AD compared with the patients with aMCI, whereas the other methods did not show such differences. Therefore, the ALFF, fALFF, and sICA techniques provided more sensitive measurements than the other RS FMRI approaches in patients with aMCI and AD. These major findings strongly encourage meta-analysis in patients with aMCI and AD with RS FMRI.

Conflict of Interests

The authors declare that there is no conflict of interests regarding the publication of this paper.

Acknowledgment

References

[1] D. S. Margulies, J. Böttger, X. Long et al., "Resting developments: a review of fMRI post-processing methodologies for spontaneous brain activity," *Magnetic Resonance Materials in Physics, Biology and Medicine*, vol. 23, no. 5-6, pp. 289–307, 2010.

[2] Y. Zang, T. Jiang, Y. Lu, Y. He, and L. Tian, "Regional homogeneity approach to fMRI data analysis," *NeuroImage*, vol. 22, no. 1, pp. 394–400, 2004.

[3] M. G. Kendall and J. D. Gibbons, *Rank Correlation Methods*, Edward Arnold, London, UK, 5th edition, 1990.

[4] Y. Liu, K. Wang, C. YU et al., "Regional homogeneity, functional connectivity and imaging markers of Alzheimer's disease: a review of resting-state fMRI studies," *Neuropsychologia*, vol. 46, no. 6, pp. 1648–1656, 2008.

[5] D. A. Gusnard and M. E. Raichle, "Searching for a baseline: Functional imaging and the resting human brain," *Nature Reviews Neuroscience*, vol. 2, no. 10, pp. 685–694, 2001.

[6] M. E. Raichle, A. M. MacLeod, A. Z. Snyder, W. J. Powers, D. A. Gusnard, and G. L. Shulman, "A default mode of brain function," *Proceedings of the National Academy of Sciences of the United States of America*, vol. 98, no. 2, pp. 676–682, 2001.

[7] Y. He, L. Wang, Y. Zang et al., "Regional coherence changes in the early stages of Alzheimer's disease: a combined structural and resting-state functional MRI study," *NeuroImage*, vol. 35, no. 2, pp. 488–500, 2007.

[8] Z. Zhang, Y. Liu, T. Jiang et al., "Altered spontaneous activity in Alzheimer's disease and mild cognitive impairment revealed by Regional Homogeneity," *NeuroImage*, vol. 59, no. 2, pp. 1429–1440, 2012.

[9] Y. F. Zang, Y. He, C. Z. Zhu et al., "Altered baseline brain activity in children with ADHD revealed by resting-state functional MRI," *Brain and Development*, vol. 29, no. 2, pp. 83–91, 2007.

[10] Q.-H. Zou, C.-Z. Zhu, Y. Yang et al., "An improved approach to detection of amplitude of low-frequency fluctuation (ALFF) for resting-state fMRI: fractional ALFF," *Journal of Neuroscience Methods*, vol. 172, no. 1, pp. 137–141, 2008.

[11] X. N. Zuo, A. di Martino, C. Kelly et al., "The oscillating brain: complex and reliable," *NeuroImage*, vol. 49, no. 2, pp. 1432–1445, 2010.

[12] Z. Wang, C. Yan, C. Zhao et al., "Spatial patterns of intrinsic brain activity in mild cognitive impairment and alzheimer's disease: a resting-state functional MRI study," *Human Brain Mapping*, vol. 32, no. 10, pp. 1720–1740, 2011.

[13] Y. Zhou, F. Yu, and T. Q. Duong, "White matter lesion load is associated with resting state functional MRI activity and amyloid pet but not FDG in mild cognitive impairment and early alzheimer's disease patients," *Journal of Magnetic Resonance Imaging*, 2013.

[14] Z. Zhao, J. Lu, X. Jia et al., "Selective changes of resting-state brain oscillations in aMCI: an fMRI study using ALFF," *BioMed Research International*, vol. 2014, Article ID 920902, 7 pages, 2014.

[15] Y. Han, J. Wang, Z. Zhao et al., "Frequency-dependent changes in the amplitude of low-frequency fluctuations in amnestic mild cognitive impairment: a resting-state fMRI study," *NeuroImage*, vol. 55, no. 1, pp. 287–295, 2011.

[16] M. W. Cole and W. Schneider, "The cognitive control network: integrated cortical regions with dissociable functions," *NeuroImage*, vol. 37, no. 1, pp. 343–360, 2007.

[17] M. W. Cole, S. Pathak, and W. Schneider, "Identifying the brain's most globally connected regions," *NeuroImage*, vol. 49, no. 4, pp. 3132–3148, 2010.

[18] R. L. Buckner, J. Sepulcre, T. Talukdar et al., "Cortical hubs revealed by intrinsic functional connectivity: mapping, assessment of stability, and relation to Alzheimer's disease," *Journal of Neuroscience*, vol. 29, no. 6, pp. 1860–1873, 2009.

[19] J. Cha, H. J. Jo, H. J. Kim et al., "Functional alteration patterns of default mode networks: comparisons of normal aging, amnestic mild cognitive impairment and Alzheimer's disease," *European Journal of Neuroscience*, vol. 37, no. 12, pp. 1916–1924, 2013.

[20] R. W. Cox, "AFNI: software for analysis and visualization of functional magnetic resonance neuroimages," *Computers and Biomedical Research*, vol. 29, no. 3, pp. 162–173, 1996.

[21] E. B. Beall and M. J. Lowe, "Isolating physiologic noise sources with independently determined spatial measures," *NeuroImage*, vol. 37, no. 4, pp. 1286–1300, 2007.

[22] E. B. Beall, "Adaptive cyclic physiologic noise modeling and correction in functional MRI," *Journal of Neuroscience Methods*, vol. 187, no. 2, pp. 216–228, 2010.

[23] H. J. Jo, Z. S. Saad, W. K. Simmons, L. A. Milbury, and R. W. Cox, "Mapping sources of correlation in resting state FMRI, with artifact detection and removal," *NeuroImage*, vol. 52, no. 2, pp. 571–582, 2010.

[24] A. Zijdenbos, A. Evans, F. Riahi, J. Sled, J. Chui, and V. Kollokian, "Automatic quantification of multiple sclerosis lesion volume using stereotaxic space," in *Visualization in Biomedical Computing*, vol. 1131 of *Lecture Notes in Computer Science*, pp. 439–448, 1996.

[25] K. Murphy, R. M. Birn, D. A. Handwerker, T. B. Jones, and P. A. Bandettini, "The impact of global signal regression on resting state correlations: are anti-correlated networks introduced?" *NeuroImage*, vol. 44, no. 3, pp. 893–905, 2009.

[26] A. Weissenbacher, C. Kasess, F. Gerstl, R. Lanzenberger, E. Moser, and C. Windischberger, "Correlations and anticorrelations in resting-state functional connectivity MRI: a quantitative comparison of preprocessing strategies," *NeuroImage*, vol. 47, no. 4, pp. 1408–1416, 2009.

[27] Z. S. Saad, S. J. Gotts, K. Murphy et al., "Trouble at rest: how correlation patterns and group differences become distorted after global signal regression," *Brain Connectivity*, vol. 2, no. 1, pp. 25–32, 2012.

[28] Z. S. Saad, D. R. Glen, G. Chen, M. S. Beauchamp, R. Desai, and R. W. Cox, "A new method for improving functional-to-structural MRI alignment using local Pearson correlation," *NeuroImage*, vol. 44, no. 3, pp. 839–848, 2009.

[29] H. Yang, X.-Y. Long, Y. Yang et al., "Amplitude of low frequency fluctuation within visual areas revealed by resting-state functional MRI," *NeuroImage*, vol. 36, no. 1, pp. 144–152, 2007.

[30] J.-B. Poline, K. J. Worsley, A. C. Evans, and K. J. Friston, "Combining spatial extent and peak intensity to test for activations in functional imaging," *NeuroImage*, vol. 5, no. 2, pp. 83–96, 1997.

[31] B. D. Ward, "Simultaneous inference for fMRI data," AFNI 3d Deconvolve Documentation, Medical College of Wisconsin, 2000.

[32] Y. Liu, C. Yu, X. Zhang et al., "Impaired long distance functional connectivity and weighted network architecture in alzheimer's disease," *Cerebral Cortex*, vol. 24, no. 6, pp. 1422–1435, 2014.

[33] M. D. Greicius, B. Krasnow, A. L. Reiss, and V. Menon, "Functional connectivity in the resting brain: a network analysis of the default mode hypothesis," *Proceedings of the National Academy of Sciences of the United States of America*, vol. 100, no. 1, pp. 253–258, 2003.

[34] X.-Y. Long, X.-N. Zuo, V. Kiviniemi et al., "Default mode network as revealed with multiple methods for resting-state functional MRI analysis," *Journal of Neuroscience Methods*, vol. 171, no. 2, pp. 349–355, 2008.

[35] C. Pennanen, M. Kivipelto, S. Tuomainen et al., "Hippocampus and entorhinal cortex in mild cognitive impairment and early AD," *Neurobiology of Aging*, vol. 25, no. 3, pp. 303–310, 2004.

[36] C. Echávarri, P. Aalten, H. B. Uylings et al., "Atrophy in the parahippocampal gyrus as an early biomarker of Alzheimer's disease," *Brain Structure and Function*, vol. 215, no. 3-4, pp. 265–271, 2011.

Research Article

Diagnostic Prediction for Social Anxiety Disorder via Multivariate Pattern Analysis of the Regional Homogeneity

Wenjing Zhang,[1] Xun Yang,[1,2] Su Lui,[1,3] Yajing Meng,[4] Li Yao,[1] Yuan Xiao,[1] Wei Deng,[4] Wei Zhang,[4] and Qiyong Gong[1]

[1] *Huaxi MR Research Center (HMRRC), Department of Radiology, West China Hospital, Sichuan University, Chengdu 610041, China*
[2] *School of Sociality and Psychology, Southwest University for Nationalities, Chengdu 610041, China*
[3] *Radiology Department of the Second Affiliated Hospital, Wenzhou Medical University, Wenzhou, Zhejiang 325027, China*
[4] *Department of Psychiatry, West China Hospital, Sichuan University, Chengdu 610041, China*

Correspondence should be addressed to Su Lui; lusuwcums@tom.com

Although decades of efforts have been spent studying the pathogenesis of social anxiety disorder (SAD), there are still no objective biological markers that could be reliably used to identify individuals with SAD. Studies using multivariate pattern analysis have shown the potential value in clinically diagnosing psychiatric disorders with neuroimaging data. We therefore examined the diagnostic potential of regional homogeneity (ReHo) underlying neural correlates of SAD using support vector machine (SVM), which has never been studied. Forty SAD patients and pairwise matched healthy controls were recruited and scanned by resting-state fMRI. The ReHo was calculated as synchronization of fMRI signals of nearest neighboring 27 voxels. A linear SVM was then adopted and allowed the classification of the two groups with diagnostic accuracy of ReHo that was 76.25% (sensitivity = 70%, and specificity = 82.5%, $P \leq 0.001$). Regions showing different discriminating values between diagnostic groups were mainly located in default mode network, dorsal attention network, self-referential network, and sensory networks, while the left medial prefrontal cortex was identified with the highest weight. These results implicate that ReHo has good diagnostic potential in SAD, and thus may provide an initial step towards the possible use of whole brain local connectivity to inform the clinical evaluation.

1. Introduction

Previously termed social phobia, social anxiety disorder (SAD) was characterized by persistent fear of social or performance situations in which there is judgment or scrutiny by others [1]. As the most common anxiety disorder, SAD shows a high lifetime prevalence of 12% and a 12-month prevalence of 7.1% [2]. Early onset, delay, or avoidance in seeking treatment leads to significant social and occupational disability for individuals with SAD. Currently, according to the diagnostic criteria in DSM-IV (Diagnostic and Statistical Manual of Mental Disorders, Fourth Edition), the diagnosis of SAD is based on observed behaviors and examinations of psychiatric signs and symptoms. However, the use of such a symptom-based approach would sometimes cause uncorrected diagnosis due to high rates of comorbidity with depressive conditions and substance abuse [3]. Therefore, it is necessary to

establish other objective and reliable approaches or biological markers, which could be used to assist the diagnosis of SAD and improve the accuracy.

As a more objective approach, neuroimaging holds great promise for detecting abnormalities crucial to the pathophysiologic models of SAD. Resting-state functional magnetic resonance imaging (fMRI) studies have revealed that, relative to the healthy controls, SAD is associated with abnormal activation within amygdala and default model network (DMN) mainly involved [4–6]. The amygdala is thought to be important in the acquisition and expression of conditioned fear and also performs a protective role, allowing the organism to detect and avoid danger [4], whilst role of DMN may be relevant to social perception and self-referential processing which are underlying psychological symptoms and pathophysiological mechanisms in SAD [6, 7]. These findings are valuable in helping us understand the functional changes

TABLE 1: Demographic and clinical characteristics of SAD patients and healthy comparison subjects.

Demographic and clinical characteristics	SAD (n = 40)		HC (n = 40)		P
	Mean	SD	Mean	SD	
Age (years)	25.95	6.48	24.80	3.35	0.323
Duration of illness (years)	7.76	4.61			
Age of onset (years)	18.15	6.70			
LSAS					
Total	65.42	21.23	33.80	22.01	0.000
Fear factor	32.45	10.39	15.70	11.90	0.000
Avoidance factor	32.47	11.91	17.85	11.34	0.000
	N	%	N	%	P
Gender					
Female	14	35	14	35	1.000
Male	26	65	26	65	

SAD, social anxiety disorder; HC, healthy controls; SD, standard deviation; LSAS, Liebowitz Social Anxiety Scale; n/N, number.
Significance levels were set at $P < 0.05$.

which underlie clinical symptoms associated with SAD; however, the extrapolation of any potential biomarkers and the clinical translation of the results have been hindered by the group level inference of the data. For the imaging findings to be clinically useful, one must be able to make inferences at the individual rather than the group level.

Relative to traditional univariate methods, multivariate pattern analysis (MVPA) allows predictions individually and it takes the patterns of information that might be presented across multiple variables into account, therefore providing results that have higher translational applicability in clinical practice [8]. For fMRI data, MVPA involves whole brain pattern classification aimed at decoding information in the pattern of activation across all voxels that may distinguish between two classes at the individual level. The most commonly used MVPA for pattern recognition in neuroimaging literature is support vector machine (SVM) [9]: an algorithm uses a well-defined dataset to create decision function or "hyperplane" which can best distinguish between categories (in current study, patients and controls), and then the produced decision function or "hyperplane" will be used to predict which predefined group a new observation belongs to. These two phases are systematically known as training and testing [9]. The overall accuracy of the SVM depends on its sensitivity (i.e., the proportion of patients identified as having the disease) and specificity (i.e., the proportion of controls identified as not having the disease). In recent years, SVM algorithm has been successfully applied to classify various neuropsychiatric disorders and achieved good diagnostic accuracy [10].

To date, there have been only two studies using MVPA in SAD but concentrating on task-based fMRI and regional grey matter volume [11], or functional connectivity [7]. As reflected by resting-state fMRI, functional connectivity can reveal the synchronization of remote brain regions, while, by contrast, regional homogeneity (ReHo) has been developed to measure the local synchronization of spontaneous fMRI signals by calculating similarity of dynamic fluctuations of

voxels within a given cluster, revealing important information about local connectivity, and reflects the temporal synchrony of the regional fMRI BOLD signals [12, 13]. Abnormal ReHo is assumed to be associated with aberrant changes in the temporal aspects of the spontaneous neural activity in the regional brain [14] and may be a sign of disrupted local functionality [15]. More importantly, ReHo can indicate some unexpected hemodynamic responses that model-driven methods may fail to discover in resting-state fMRI [13]. Although being successfully applied to various neuropsychiatric disorders [14, 16–20], the ReHo approach has been little investigated in SAD.

Thus, we particularly used SVM to examine ReHo maps in differentiating SAD patients from healthy controls, which has never been investigated. The purposes were to find out whether SVM would allow accurate discrimination between diagnostic groups and, if so, which brain regions or intrinsic brain networks would principally contribute to the discrimination.

2. Materials and Methods

2.1. Participants. Forty Structured Interview for the DSM-IV (SCID) Patient Edition confirmed SAD patients and an equal number of healthy controls were recruited at the Mental Health Centre of West China Hospital (Table 1). The Ethics Committee of West China Hospital, Sichuan University, has offered approval to our study and all participants gave written informed consent to their participation. Diagnosis of SAD was determined by consensus of two experienced psychiatrists. Psychological ratings and clinical symptoms associated with SAD were evaluated with the Liebowitz Social Anxiety Scale (LSAS). Of the 40 patients, 12 had the antianxiety medication but they underwent at least two-week washing-out prior to the MR examination.

Healthy controls were recruited from the local area via poster advertisements and were screened using the SCID-Non-Patient Version to ascertain the lifetime absence of

psychiatric and neurological illness. It was confirmed that they had no history of psychiatric illness among their first-degree relatives. All subjects' demographic characteristics and clinical variables were obtained by 2 experienced clinical psychiatrists before MR examinations. Patients with SAD and control subjects were pairwise matched in age, gender, and handedness (Table 1). The following exclusion criteria applied to both groups: (1) the existence of a neurological disorder or other psychiatric disorders, (2) substance abuse, (3) pregnancy, or (4) major physical illness such as cardiovascular disease or hepatitis, as assessed by clinical evaluations and medical records. T1-weighted and T2-weighted images of brain were inspected by an experienced neuroradiologist, and no scanning artifacts and gross abnormalities were observed in any participants.

2.2. MRI Acquisition. The MRI examinations were performed on a whole-body 3.0 T MR scanner (Siemens Trio, Erlangen, Germany) with a 12-channel head coil. Earplugs were employed to protect the hearing while foam pads upon them were used to restrict head motion during the scanning. The resting-state fMRI sensitized to changes in BOLD signal levels was obtained with a gradient-echo planar imaging sequence (TR/TE = 2000/30 ms; flip angle = 90°). A field of view (FOV) of 240×240 mm^2 was used with an acquisition matrix = 64×64, producing 30 continuous axial slices with thickness = 5.0 mm with no gap and voxel size = $3.75 \times 3.75 \times 5$ mm^3 in-plane resolution in each brain volume. Each functional run contained 205 volumes of which the first 5 were discarded to ensure steady-state longitudinal magnetization and subjects' adaptation to the environment. All participants were simply instructed to keep still with their eyes closed and remain awake but not to think of anything in particular. After the scanning, the volumes of all subjects were corrected for the temporal difference and head motion by setting the translational or rotational parameters at the threshold of ± 1.5 mm or $\pm 1.5°$.

2.3. Imaging Preprocessing. The fMRI data was preprocessed using Data Processing Assistant for Resting-State fMRI (DPARSF, http://www.restfmri.net, version 2.1), implemented within the MATLAB toolbox, to calculate the ReHo maps. This software involves an integrated image process mainly including slice timing, realignment, and normalization to the Montreal Neurological Institute echo planar imaging template (each voxel was resampled to $3 \times 3 \times 3$ mm^3), removing linear trend and the ReHo calculation. Given the fact that ReHo shows the similarity or synchronization of fMRI signals of nearest neighboring voxels and Kendall's coefficient of concordance (KCC) is used for the measurement based on the regional homogeneity hypothesis [13], we defined 27 nearest neighboring voxels as a cluster and a KCC value was given to the voxel at the center of this cluster. The individual ReHo map was generated in a voxel-wise fashion, and all ReHo maps were smoothed with a Gaussian filter of 4 mm full-width half maximum (FWHM) kernel to manage the anatomical variability that was not compensated for by spatial normalization.

2.4. Comparison of Demographic Characteristics and Variables. The Statistical Package for the Social Sciences (SPSS, version 18.0) will be used for the comparison of demographic variables. Differences in age and LSAS scores between groups were analyzed using the two-sample t-tests, whereas gender ratio was compared with Chi-square test, with significance levels setting at $P < 0.05$.

2.5. Multivariate Pattern Analysis and Support Vector Machine. SVM as implemented in the PROBID software package (http://www.brainmap.co.uk/probid.htm, version 1.04) was employed and a linear kernel SVM was adopted to classify the diagnostic groups based on their ReHo maps. The detailed description of the application of SVM in MRI data has been given [8, 21]. In the context of supervised multivariate classification method as SVM [22], individual brain scans were treated as points located at high-dimensional space defined by the ReHo map in the preprocessed images. In this high-dimensional space, a linear decision boundary was defined by a "hyperplane" that separated the individual brain scans according to a class label (i.e., patients versus controls). The optimal hyperplane was computed based on the whole multivariate pattern of ReHo map across each image and could most accurately capture the relationship between each example and its respective label. The algorithm is initially trained on a subset of the data $\langle x, c \rangle$ to find a hyperplane that best separates the input space according to the class labels c (patients versus controls), where x represents the input data (i.e., ReHo map). The linear kernel SVM adopted could reduce the risk of overfitting the data and allow direct extraction of the weight vector as an image (i.e., the SVM discrimination map). Furthermore, the linear kernel matrix implicated in PROBID could be precomputed and supplied to the classifier, an approach which affords a substantial increase in computational efficiency and permits whole brain classification without requiring explicit dimensionality reduction [23]. A parameter C, which controls the tradeoff between having zero training errors and allowing misclassifications in the linear model, was fixed at $C = 1$ for all cases (default value). A grey matter mask of $3 \times 3 \times 3$ mm was used to constrain the search of significant group differences in voxels/features within grey matter in the comparison of ReHo maps.

Consistent with previous studies using SVM on SAD [7, 11], a "leave-one-out" cross validation was used, which means a single subject of each group would be excluded from the training and was later used to test the capability of the classifier learned from the remaining subjects, to reliably distinguish between categories (in our study, SAD or controls). Each subject pair would undergo this procedure to make the accuracy of the SVM fully estimated [8]. Statistical significance of the overall classification accuracy was determined by permutation testing [24, 25], a nonparametric test that involved repeating the classification procedure 1000 times with a different random permutation of the training group labels and counting the number of permutations achieving higher sensitivity and specificity than the true labels. Finally, to show the multivariate discriminating pattern of ReHo
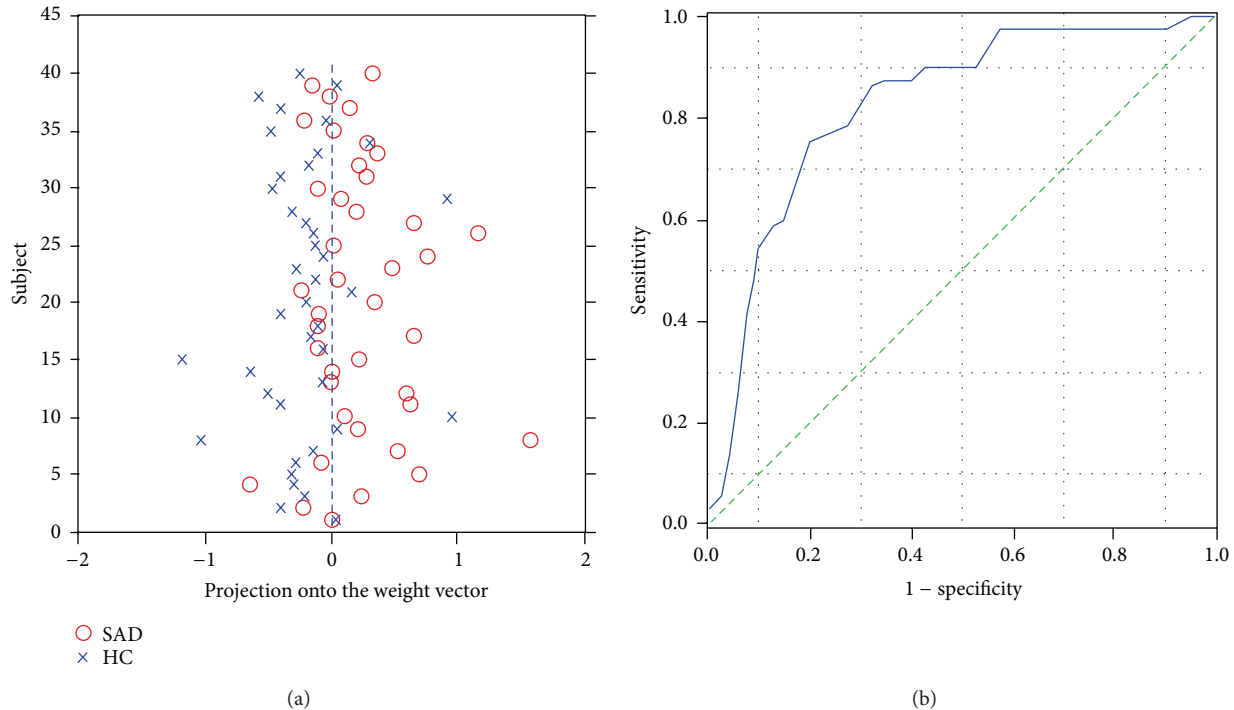
(a)

(b)

FIGURE 1: Classification plot (a) obtained from PROBID and receiver operating characteristic (ROC) curve and (b) obtained from SPSS for the discrimination between SAD patients and healthy controls using ReHo maps, yielding an accuracy of 76.25% (sensitivity = 70.0% and specificity = 82.5%, $P \leq 0.001$).

maps, a threshold would be set at 30% of the maximum weight vector value of the discrimination and voxels with greater value would be exhibited.

The test margin (the shortest distance from the optimal hyperplane), which could show the capability of the SVM with ReHo in classification of each subject, was calculated for all participants. Based on the label and test margin of each subject, the receiver operating characteristic (ROC) curve of the classification with ReHo maps was obtained with SPSS. To further explore whether the classification is driven by anxious symptoms and the extent if so, correlation analysis has been performed between the test margin and the level of symptom severity as determined by LSAS scores for all participants.

3. Result

3.1. Demographic and Clinical Characteristics. Demographic and clinical characteristics for all of participants are presented in Table 1. No significant differences were found in gender ratio and age between patients and healthy controls ($P > 0.05$). Compared to healthy control, SAD patients had significantly higher scores on the anxiety symptoms measured with LSAS total score and subscales ($P < 0.05$). All participants were right-handed. Twenty-eight patients were drug-naïve while the remaining 12 had taken different medication (5 paroxetine, 3 paroxetine with intermittent risperidone, alprazolam, and buspirone, resp., 3 sertraline, and 1 amitriptyline and doxepin) for 1 week to 5 years. The medicated patients had been drug-free for at least 2 weeks.

3.2. Multivariate Pattern Recognition. The classification of the two groups with overall diagnostic accuracy of ReHo maps was 76.25% (sensitivity = 70% and specificity = 82.5%, $P \leq 0.001$) achieved by SVM (Figure 1). The set of regions showed different value between the diagnostic groups mainly located in frontal, temporal, and occipital regions (Figure 2, Table 2). In the discrimination map, a positive value means a relative higher weight in SAD (red scale) and helps in the identification of individuals with SAD, with regions mainly located at right orbitofrontal gyrus (OFG), right middle frontal gyrus, right pars triangularis, right superior temporal gyrus (STG), left middle temporal gyrus (MTG), right postcentral gyrus (PCG), left inferior parietal lobe (IPL), and right precuneus, while a negative value means a relative higher weight in healthy controls and contributes to the identification of healthy subjects, locating in left medial prefrontal cortex (mPFC), bilateral middle frontal gyrus (MFG), right inferior occipital gyrus (IOG), and right cuneus (Figure 2).

3.3. Relationship between Test Margin and Severity of Symptom. Across all of the patients, the test margin was found not correlated to total LSAS scores, scores for fear factor, or scores for avoidance factor ($P > 0.05$).

4. Discussion

To the best of our knowledge, the current study is the first to examine the capability of SVM with ReHo in distinguishing patients with SAD from healthy subjects and involves
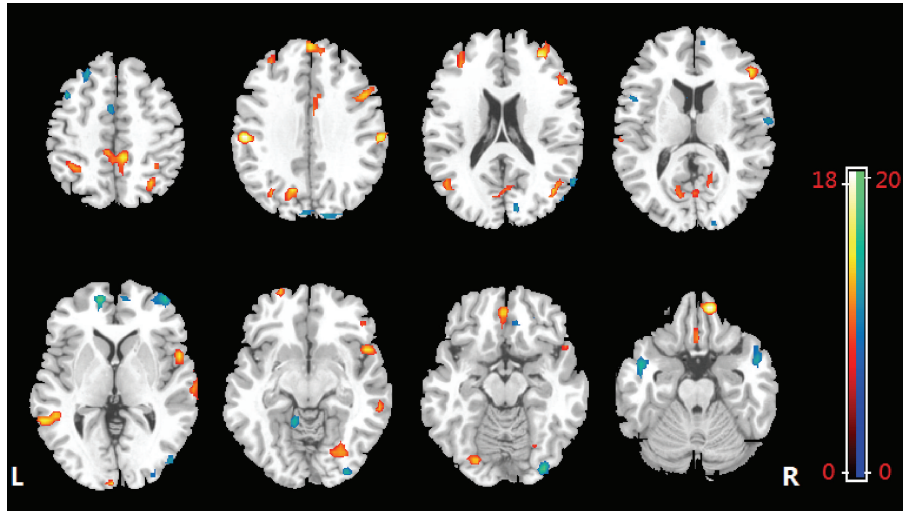
FIGURE 2: The discrimination maps for ReHo. Regions displayed were identified by setting the threshold to ≥30% of the weight vector scores. Warm color (positive value) indicated higher discriminated values in SAD than in healthy controls; cool color (negative weights) indicates higher values in healthy controls than in SAD.

the largest sample of SAD patients in employing MVPA approach. By identifying the intergroup differences in whole brain ReHo pattern with an overall classification accuracy of 76.25%, the present study suggests local connectivity and synchronization extracted from fMRI BOLD signal could be a potential biomarker to identify SAD patients and demonstrates that multivariate analysis allows discrimination between individuals with SAD and healthy controls at relatively high level of accuracy. This pattern of results provides preliminary support to the development of SVM as a promising diagnostic tool in SAD to improve the diagnostic accuracy and minimize errors in detecting malingering where possible [26].

The discriminating pattern in the present study was attributable to widespread ReHo alterations, mainly involving DMN, dorsal attention network (DAN), self-referential network (SRN), and sensory networks. By contrast, the only one study using ReHo in SAD before found significantly decreased ReHo mainly in the DMN and central executive network (CEN) while it found increased ReHo in occipital regions and the right putamen in a relative small sample of SAD patients via mass-univariate analysis [27]. Relatively, our findings consistently revealed abnormalities within DMN but identified more regions, and other distributed regions across brain have also been showed with different local connectivity between SAD and control subjects. One explicable fact is that MVPA implicated in SVM takes the interregional correlation into account [8]. This multivariate nature of SVM rendered a high discriminative power for a given cluster deriving not only from differences in ReHo in that region between groups, but also from any intergroup differences in its functional correlations with other regions. Thus, the findings of the altered ReHo across brain should not be deemed as individual regions but as a spatially distributed pattern. Taken collectively, ReHo investigation gives insight into coherent local connectivity of a functional cluster and is necessary for further interpreting functional changes in SAD patients, whilst

the combination with SVM identifies more distributed and subtle ReHo changes helpful in characterization at individual level therefore yielding results with great potential in clinical translation.

The consistent finding of altered local connectivity in relation to DMN emphasizes its critical role underlying the pathogenesis of SAD. The DMN is deemed as a higher-level cognitive network and consists of brain regions that typically activate during resting-state but deactivate during performance of goal-directed tasks [28], within which a set of regions connectively contributes to the social cognitive aspects. The precuneus, along with posterior cingulate cortex (PCC), is featured as the pivotal hub of DMN and related to perception of social cognition and self-related mental representations [28, 29]. Patients with SAD showed a lower deactivation in regions comprising precuneus during task conditions [30] and abnormal functional connectivity in precuneus has also been suggested to be associated with the pathophysiological mechanism underlying SAD [31]. The mPFC is another hub in DMN and is identified with the highest weight. Activity in mPFC may reflect an interaction between cognitive processing and emotional state [32], especially for the anxiety-related emotion processing, in which mPFC has been considered of ongoing importance [33]. These data, along with our findings, supported the notion that DMN accounts for prominence in cognitive behavioral models of SAD.

DAN [34, 35] and SRN [36] are another two important networks with many regions found with alteration with ReHo in SAD patients. DAN is considered to mediate goal-directed (top-down) processing for stimuli selection and responses and involved in many higher-order cognitive tasks [34]. Particularly emotion regulation, the regulating of anxious feelings, has been emphasized in the cognitive models underlying SAD [37], and failure in emotion regulation has been considered another key feature of SAD [38]. In this term of view, we speculate that there is an important

TABLE 2: Regions of ReHo map discriminating between individuals with SAD and control subjects. These regions were exhibited by setting the threshold to ≥30% of the maximum weight vector value.

Regions (SAD > HC)	x	y	z	w_i	Regions (SAD < HC)	x	y	z	w_i
Frontal lobe					**Frontal lobe**				
Left superior frontal gyrus	−23	64	−8	11.29	Left medial superior frontal gyrus	−11	56	5	−19.03
Right medial superior frontal gyrus	9	51	35	9.55	Right medial superior frontal gyrus	10	58	5	−11.89
Left medial superior frontal gyrus	1	53	35	12.16	Left superior frontal gyrus	−3	3	53	−13.96
Right middle frontal gyrus	33	47	23	16.54	Right middle frontal gyrus	45	57	2	−16.49
	50	14	32	13.19	Left middle frontal gyrus	−39	14	48	−13.32
Left middle frontal gyrus	−31	42	35	10.85		−25	33	51	−13.64
Right inferior frontal gyrus	48	37	−9	8.65	Left inferior frontal gyrus	−48	10	13	−8.1
Right pars triangularis	51	33	13	12.6					
Left medial orbitofrontal gyrus	−2	46	−14	13.04					
Right orbitofrontal gyrus	12	49	−22	17.88					
Right precuneus	7	−40	54	17.73					
	17	−58	13	9.07					
Temporal lobe					**Temporal lobe**				
Right superior temporal gyrus	56	9	−1	14.13	Right middle temporal gyrus	52	8	−24	−13.16
	68	−21	3	11.14	Left temporal pole	−45	3	−19	−14.59
Right middle temporal gyrus	63	−37	−10	8.38	Right postcentral gyrus	66	−9	14	−12.53
	48	−64	0	8.63					
Left superior temporal gyrus	−60	−26	11	10.26					
Left middle temporal gyrus	−44	−63	17	8.79					
	−58	−47	2	13.92					
Occipital lobe					**Occipital lobe**				
Left middle occipital gyrus	−33	−71	33	10.99	Right inferior occipital gyrus	35	−88	−15	−17.29
Right fusiform gyrus	24	−74	−10	9.96	Right cuneus	49	−80	−1	−14.91
Left cuneus	−2	−101	5	12.31		15	−82	23	−14.57
Left cuneus	−11	−71	13	10.05	Left cuneus	−2	−87	35	−11.1
Left lingual gyrus	−24	−81	−16	13.19					
Parietal lobe					**Cerebellum**				
Right superior parietal gyrus	32	−62	50	10.75	Left cerebellum	−9	−47	−9	−14.75
Left inferior parietal gyrus	−53	−22	35	17.59					
	−33	−47	50	9.3					
Left precuneus	−13	−67	32	12.02					
Right postcentral gyrus	63	−23	32	16.56					

SAD, social anxiety disorder; HC, healthy controls.

w_i: weight of each cluster centroid, the value which indicates the relative contribution to the classification.

role of brain regions within DAN in emotion regulation, and abnormalities in these regions usually result in a high level of self-awareness, typically in SAD patients. While the SRN has exhibited peculiar physiological characteristics with increased neural activity during resting [28], OFC is a primary region observed with local coherence alteration. As involved in the engagement of interpersonal relationships, moral behavior, and social aggression [39–41], OFC with inappropriate function might strengthen the response to stressors or stimuli of fear conditions, resulting in severe impairments in social behavior [5]. Reduced orbitofrontal activation was observed in patients with SAD during public speaking [42] and anxiety-provoking tasks [43], implying a hypoactive OFC was associated with a failure of fear and anxiety inhibition.

There are still main regions implicated in visual network (VN), auditory network (AN), and somatomotor network (SMN). However, sensory networks could be regarded as the lower-order system of cognition. Within VN, abnormalities in IOG may be associated with the hypervigilance and hyperprosexia characteristic of social interaction in SAD [44]. Additionally, together with SMN, VN has been suggested to show significantly greater BOLD responses in SAD for social threat in previous emotional fMRI study [45]. As for AN, regions within which have been found to related to dysfunction of cognitive reappraisal in SAD patients [46]. Consistent with these findings, our results imply a role for sensory networks in the perceptual and some other psychological impairments in SAD to variable extents.

Although the discriminating pattern above successfully allowed the identification of patients with SAD, the accuracy was not that high to achieve the goal of MVPA of automated MR image analysis in finding better sensitivity and specificity of antemortem diagnosis than what is currently possible [47]. While the performance, generalizability, and significance of the SVM findings would benefit from a large sample size and better feature selection methods [48], future studies incorporating large sample are needed to improve characterization of underlying features, as to establishment of a model which could most accurately predict new subjects for better classification. Furthermore, expanding feature selection to include other imaging properties, behavioral data, and genomic information may offer better discriminative information for predicting SAD.

In the exploratory analysis, no significant association was found between the test margin and clinical symptoms. In other words, the distance away from the hyperplane may not be driven or affected by the severity of symptoms as assessed by LSAS scores for a given subject, suggesting the discriminating pattern of ReHo obtained is relatively stable. This may be because the discrimination pattern produced derived mostly from the intergroup ReHo differences free from clinical ratings, which is of great significance since the identification of SAD will not be confounded by the psychological situations, reducing the rate of false negative findings resulting from individuals with mild symptoms.

It is noteworthy that there are some limitations implicated in the present study. First, although most of patients were drug-naïve, a small proportion of the SAD sample had taken medication before. However, we have prepared two weeks for the washing-out before scanning to reduce the confounding effect resulting from medication. Besides, given the effect of antianxiety medication in attenuating abnormally activated neural activity in social anxiety [49], we thus speculated that the medication effect would probably not exaggerate but instead tend to underestimate the capability of SVM in identifying patients. That might also be the reason why the present study did not find the abnormal alterations in amygdala due to attenuated amygdala responsiveness [50]. Second, as we have added whole voxels in the grey matter in the pattern analysis, the intrinsic structural differences may act as confounding factors in the pattern recognition analysis. However, ReHo and structural properties are different features in the SVM analysis; since we used the functional features implicated in ReHo, the confounding influence of structural differences was assumed marginal, if there were any. While we did not have sufficient structural images to conduct the same analysis to rule out confounding factors, future studies with different imaging modalities will be needed as a synthesized biomarker to strengthen the classification and achieve more reliable clinical diagnosis of this complex disorder. Finally, as a common psychiatric disorder, social anxiety has a potential correlation but differs from a personality trait known as shyness. While in current study, we only compare the cohort of SAD patients with healthy subjects, leaving an issue unresolved whether the application of SVM to ReHo would also discriminate SAD patients from mentally healthy people with shyness. The future studies may help to address this question by including a third group of subjects who have a level of shyness but without SAD.

5. Conclusion

This study used a MVPA method which is based on whole brain ReHo pattern, to distinguish individuals with SAD from healthy subjects. By presenting widespread differential map of coherence abnormalities which could be used to identify patients with SAD at the individual level, this study provides evidence that the ReHo of brain has the diagnostic potential and can possibly act as a supplementary approach to identify SAD, especially regions with high weight. Future studies with the integration of ReHo with other different imaging modality measurements may give a better insight into the imaging biomarkers of the condition.

Conflict of Interests

The authors declare that there is no conflict of interests regarding the publication of this paper.

Authors' Contribution

Wenjing Zhang and Xun Yang made equal contribution to this paper.

Acknowledgments

References

[1] M. B. Stein and D. J. Stein, "Social anxiety disorder," *The Lancet*, vol. 371, no. 9618, pp. 1115–1125, 2008.

[2] R. C. Kessler, T. C. Wai, O. Demler, and E. E. Walters, "Prevalence, severity, and comorbidity of 12-month DSM-IV disorders in the National Comorbidity Survey Replication," *Archives of General Psychiatry*, vol. 62, no. 6, pp. 617–627, 2005.

[3] A. A. Mather, M. B. Stein, and J. Sareen, "Social anxiety disorder and social fears in the Canadian military: prevalence, comorbidity, impairment, and treatment-seeking," *Journal of Psychiatric Research*, vol. 44, no. 14, pp. 887–893, 2010.

[4] M. C. Freitas-Ferrari, J. E. C. Hallak, C. Trzesniak et al., "Neuroimaging in social anxiety disorder: a systematic review of the literature," *Progress in Neuro-Psychopharmacology and Biological Psychiatry*, vol. 34, no. 4, pp. 565–580, 2010.

[5] A. Hahn, P. Stein, C. Windischberger et al., "Reduced resting-state functional connectivity between amygdala and orbitofrontal cortex in social anxiety disorder," *NeuroImage*, vol. 56, no. 3, pp. 881–889, 2011.

[6] W. Liao, H. Chen, Y. Feng et al., "Selective aberrant functional connectivity of resting state networks in social anxiety disorder," *NeuroImage*, vol. 52, no. 4, pp. 1549–1558, 2010.

[7] F. Liu, W. Guo, J.-P. Fouche et al., "Multivariate classification of social anxiety disorder using whole brain functional connectivity," *Brain Structure and Function*, pp. 1–15, 2013.

[8] F. Pereira, T. Mitchell, and M. Botvinick, "Machine learning classifiers and fMRI: a tutorial overview," *NeuroImage*, vol. 45, no. 1, pp. S199–S209, 2009.

[9] V. N. Vapnik, *The Nature of Statistical Learning Theory*, Statistics for Engineering and Information Science, Springer, New York, NY, USA, 2nd edition, 2000.

[10] G. Orrù, W. Pettersson-Yeo, A. F. Marquand, G. Sartori, and A. Mechelli, "Using Support Vector Machine to identify imaging biomarkers of neurological and psychiatric disease: a critical review," *Neuroscience and Biobehavioral Reviews*, vol. 36, no. 4, pp. 1140–1152, 2012.

[11] A. Frick, M. Gingnell, A. F. Marquand et al., "Classifying social anxiety disorder using multivoxel pattern analyses of brain function and structure," *Behavioural Brain Research*, vol. 259, pp. 330–335, 2014.

[12] X. Y. Long, X. N. Zuo, V. Kiviniemi et al., "Default mode network as revealed with multiple methods for resting-state functional MRI analysis," *Journal of Neuroscience Methods*, vol. 171, no. 2, pp. 349–355, 2008.

[13] Y. Zang, T. Jiang, Y. Lu, Y. He, and L. Tian, "Regional homogeneity approach to fMRI data analysis," *NeuroImage*, vol. 22, no. 1, pp. 394–400, 2004.

[14] T. Wu, X. Long, Y. Zang et al., "Regional homogeneity changes in patients with parkinson's disease," *Human Brain Mapping*, vol. 30, no. 5, pp. 1502–1510, 2009.

[15] Y. He, L. Wang, Y. Zang et al., "Regional coherence changes in the early stages of Alzheimer's disease: a combined structural and resting-state functional MRI study," *NeuroImage*, vol. 35, no. 2, pp. 488–500, 2007.

[16] J. Chen, Y. Xu, K. Zhang et al., "Comparative study of regional homogeneity in schizophrenia and major depressive disorder," *American Journal of Medical Genetics B: Neuropsychiatric Genetics*, vol. 162, no. 1, pp. 36–43, 2013.

[17] Y. Liu, K. Wang, C. YU et al., "Regional homogeneity, functional connectivity and imaging markers of Alzheimer's disease: a review of resting-state fMRI studies," *Neuropsychologia*, vol. 46, no. 6, pp. 1648–1656, 2008.

[18] J. J. Paakki, J. Rahko, X. Long et al., "Alterations in regional homogeneity of resting-state brain activity in autism spectrum disorders," *Brain Research*, vol. 1321, pp. 169–179, 2010.

[19] Q.-Z. Wu, D.-M. Li, W.-H. Kuang et al., "Abnormal regional spontaneous neural activity in treatment-refractory depression revealed by resting-state fMRI," *Human Brain Mapping*, vol. 32, no. 8, pp. 1290–1299, 2011.

[20] C.-Z. Zhu, Y.-F. Zang, Q.-J. Cao et al., "Fisher discriminative analysis of resting-state brain function for attention-deficit/hyperactivity disorder," *NeuroImage*, vol. 40, no. 1, pp. 110–120, 2008.

[21] B. Schölkopf and A. J. Smola, *Support Vector Machines and Kernel Algorithms*, The Handbook of Brain Theory and Neural Networks, MIT Press, Cambridge, UK, 2002.

[22] T. Hastie, R. Tibshirani, J. Friedman, and J. Franklin, "The elements of statistical learning: data mining, inference and prediction," *The Mathematical Intelligencer*, vol. 27, no. 2, pp. 83–85, 2005.

[23] S. Maji, A. C. Berg, and J. Maliks, "Classification using intersection kernel support vector machines is efficient," in *Proceedings of the IEEE Conference on Computer Vision and Pattern Recognition (CVPR '08)*, pp. 1–8, Anchorage, Alaska, USA, June 2008.

[24] T. E. Nichols and A. P. Holmes, "Nonparametric permutation tests for functional neuroimaging: a primer with examples," *Human Brain Mapping*, vol. 15, no. 1, pp. 1–25, 2002.

[25] P. Golland and B. Fischl, "Permutation tests for classification: towards statistical significance in image-based studies," *Information Processing in Medical Imaging*, vol. 18, pp. 330–341, 2003.

[26] G. Sartori, S. Pellegrini, and A. Mechelli, "Forensic neurosciences: from basic research to applications and pitfalls," *Current Opinion in Neurology*, vol. 24, no. 4, pp. 371–377, 2011.

[27] C. Qiu, W. Liao, J. Ding et al., "Regional homogeneity changes in social anxiety disorder: a resting-state fMRI study," *Psychiatry Research: Neuroimaging*, vol. 194, no. 1, pp. 47–53, 2011.

[28] M. E. Raichle, A. M. MacLeod, A. Z. Snyder, W. J. Powers, D. A. Gusnard, and G. L. Shulman, "A default mode of brain function," *Proceedings of the National Academy of Sciences of the United States of America*, vol. 98, no. 2, pp. 676–682, 2001.

[29] R. L. Buckner, J. R. Andrews-Hanna, and D. L. Schacter, "The brain's default network," *Annals of the New York Academy of Sciences*, vol. 1124, no. 1, pp. 1–38, 2008.

[30] C. Gentili, E. Ricciardi, M. I. Gobbini et al., "Beyond amygdala: default Mode Network activity differs between patients with

Social Phobia and healthy controls," *Brain Research Bulletin*, vol. 79, no. 6, pp. 409–413, 2009.

[31] J. M. Warwick, P. Carey, G. P. Jordaan, P. Dupont, and D. J. Stein, "Resting brain perfusion in social anxiety disorder: a voxel-wise whole brain comparison with healthy control subjects," *Progress in Neuro-Psychopharmacology and Biological Psychiatry*, vol. 32, no. 5, pp. 1251–1256, 2008.

[32] J. R. Simpson Jr., A. Z. Snyder, D. A. Gusnard, and M. E. Raichle, "Emotion-induced changes in human medial prefrontal cortex: I. During cognitive task performance," *Proceedings of the National Academy of Sciences of the United States of America*, vol. 98, no. 2, pp. 683–687, 2001.

[33] W. M. Kelley, C. N. Macrae, C. L. Wyland, S. Caglar, S. Inati, and T. F. Heatherton, "Finding the self? An event-related fMRI study," *Journal of Cognitive Neuroscience*, vol. 14, no. 5, pp. 785–794, 2002.

[34] M. Corbetta and G. L. Shulman, "Control of goal-directed and stimulus-driven attention in the brain," *Nature Reviews Neuroscience*, vol. 3, no. 3, pp. 201–215, 2002.

[35] D. Mantini, M. G. Perrucci, C. del Gratta, G. L. Romani, and M. Corbetta, "Electrophysiological signatures of resting state networks in the human brain," *Proceedings of the National Academy of Sciences of the United States of America*, vol. 104, no. 32, pp. 13170–13175, 2007.

[36] A. D'Argembeau, F. Collette, M. Van Der Linden et al., "Self-referential reflective activity and its relationship with rest: a PET study," *NeuroImage*, vol. 25, no. 2, pp. 616–624, 2005.

[37] D. M. Clark and F. McManus, "Information processing in social phobia," *Biological Psychiatry*, vol. 51, no. 1, pp. 92–100, 2002.

[38] S. G. Hofmann, "Cognitive mediation of treatment change in social phobia," *Journal of Consulting and Clinical Psychology*, vol. 72, no. 3, pp. 392–399, 2004.

[39] R. J. R. Blair, J. S. Morris, C. D. Frith, D. I. Perrett, and R. J. Dolan, "Dissociable neural responses to facial expressions of sadness and anger," *Brain*, vol. 122, no. 5, pp. 883–893, 1999.

[40] J. D. Greene, R. B. Sommerville, L. E. Nystrom, J. M. Darley, and J. D. Cohen, "An fMRI investigation of emotional engagement in moral judgment," *Science*, vol. 293, no. 5537, pp. 2105–2108, 2001.

[41] M. R. Milad and S. L. Rauch, "The role of the orbitofrontal cortex in anxiety disorders," *Annals of the New York Academy of Sciences*, vol. 1121, pp. 546–561, 2007.

[42] M. Tillfors, T. Furmark, I. Marteinsdottir et al., "Cerebral blood flow in subjects with social phobia during stressful speaking tasks: a PET study," *The American Journal of Psychiatry*, vol. 158, no. 8, pp. 1220–1226, 2001.

[43] J. R. Simpson Jr., W. C. Drevets, A. Z. Snyder, D. A. Gusnard, and M. E. Raichle, "Emotion-induced changes in human medial prefrontal cortex: II. During anticipatory anxiety," *Proceedings of the National Academy of Sciences of the United States of America*, vol. 98, no. 2, pp. 688–693, 2001.

[44] S. M. Bögels and W. Mansell, "Attention processes in the maintenance and treatment of social phobia: hypervigilance, avoidance and self-focused attention," *Clinical Psychology Review*, vol. 24, no. 7, pp. 827–856, 2004.

[45] P. R. Goldin, T. Manber, S. Hakimi, T. Canli, and J. J. Gross, "Neural bases of social anxiety disorder: emotional reactivity and cognitive regulation during social and physical threat," *Archives of General Psychiatry*, vol. 66, no. 2, pp. 170–180, 2009.

[46] M. Ziv, P. R. Goldin, H. Jazaieri, K. S. Hahn, and J. J. Gross, "Emotion regulation in social anxiety disorder: behavioral and neural responses to three socio-emotional tasks," *Biology of Mood & Anxiety Disorders*, vol. 3, article 20, 2013.

[47] S. Klöppel, C. M. Stonnington, C. Chu et al., "Automatic classification of MR scans in Alzheimer's disease," *Brain*, vol. 131, no. 3, pp. 681–689, 2008.

[48] H. Ung, J. E. Brown, K. A. Johnson, J. Younger, J. Hush, and S. Mackey, "Multivariate classification of structural MRI data detects chronic low back pain," *Cerebral Cortex*, vol. 24, no. 4, pp. 1037–1044, 2014.

[49] T. Furmark, L. Appel, Å. Michelgård et al., "Cerebral blood flow changes after treatment of social phobia with the neurokinin-1 antagonist GR205171, citalopram, or placebo," *Biological Psychiatry*, vol. 58, no. 2, pp. 132–142, 2005.

[50] V. Faria, L. Appel, F. Åhs et al., "Amygdala subregions tied to SSRI and placebo response in patients with social anxiety disorder," *Neuropsychopharmacology*, vol. 37, no. 10, pp. 2222–2232, 2012.

Research Article

Connectome-Scale Assessments of Functional Connectivity in Children with Primary Monosymptomatic Nocturnal Enuresis

Du Lei,[1,2] Jun Ma,[3] Jilei Zhang,[1] Mengxing Wang,[1] Kaihua Zhang,[1] Fuqin Chen,[2] Xueling Suo,[2] Qiyong Gong,[2] and Xiaoxia Du[1]

[1] *Shanghai Key Laboratory of Magnetic Resonance, Department of Physics, East China Normal University,*
 3663 North Zhongshan Road, Shanghai 200062, China
[2] *MR Research Center, Department of Radiology, West China Hospital of Sichuan University, Chengdu, Sichuan 610044, China*
[3] *Department of Developmental and Behavioral Pediatrics of Shanghai Children's Medical Center,*
 XinHua Hospital Affiliated to Shanghai Jiao Tong University School of Medicine,
 Shanghai Key Laboratory of Children's Environmental Health, Shanghai 200127, China

Correspondence should be addressed to Xiaoxia Du; xxdu@phy.ecnu.edu.cn

Primary monosymptomatic nocturnal enuresis (PMNE) is a common developmental disorder in children. Previous literature has suggested that PMNE not only is a micturition disorder but also is characterized by cerebral structure abnormalities and dysfunction. However, the biological mechanisms underlying the disease are not thoroughly understood. Graph theoretical analysis has provided a unique tool to reveal the intrinsic attributes of the connectivity patterns of a complex network from a global perspective. Resting-state fMRI was performed in 20 children with PMNE and 20 healthy controls. Brain networks were constructed by computing Pearson's correlations for blood oxygenation level-dependent temporal fluctuations among the 2 groups, followed by graph-based network analyses. The functional brain networks in the PMNE patients were characterized by a significantly lower clustering coefficient, global and local efficiency, and higher characteristic path length compared with controls. PMNE patients also showed a reduced nodal efficiency in the bilateral calcarine sulcus, bilateral cuneus, bilateral lingual gyri, and right superior temporal gyrus. Our findings suggest that PMNE includes brain network alterations that may affect global communication and integration.

1. Introduction

Nocturnal enuresis is a common developmental disorder that affects 15–20% of 5-year-old children [1]. This disorder can persist in adolescence and has important negative effects on the self-image and performance of these children [2]. The condition is defined as primary monosymptomatic nocturnal enuresis (PMNE) when a child has enuresis without additional lower urinary tract symptoms (excluding nocturia) or a history of bladder dysfunction and has never had a period of established urinary continence for more than six months [3].

Several factors are associated with and contribute to nocturnal enuresis, including heredity, polyuria, detrusor overactivity, sleep, and central nervous system mechanisms [4]. Recently, maturational delays of the central nervous system have been indicators of PMNE pathogenesis. Toros et al. reported an increased frequency of a high-level hyperventilation response in recordings of a resting-state electroencephalogram, suggesting the existence of delayed cortical maturity in PMNE [5]. Event-related brain potentials have also been used to study enuresis; results have shown longer P300 latency in primary enuretics compared with nonenuretics [6], and P300 amplitude is decreased in the parietal recordings of enuretics when compared with the controls [7], which is evidence of a maturational delay in the central nervous system function [6, 7]. Freitag et al. also reported the existence of increased I-III and I-V interpeak

latencies of the brainstem auditory evoked potential, suggesting maturational deficits in the brain stems of nocturnal enuretic children [8]. Desamino-arginine vasopressin and alarm therapy for nocturnal enuresis were shown to increase the prepulse inhibition of startle reflexes, thus supporting the hypothesis of a maturational delay of reflex inhibition in nocturnal enuresis [9, 10].

In recent years, magnetic resonance imaging (MRI) techniques, such as structural MRI, functional MRI, and diffusion MRI, have provided an efficient, feasible, and noninvasive method to investigate the biological mechanisms of incontinence. Using functional MRI, a number of studies have reported alterations in several brain functions in patients with urgency and urge incontinence [11, 12]. One study utilized event-related fMRI in PMNE subjects and revealed that children with PMNE had deficits in working memory [13]. Abnormal functional connectivity has also been found in children with PMNE, including the cerebellum, frontal lobe, and thalamus in the cerebello-thalamo-frontal circuit [14]. We have performed a series of MRI experiments to investigate the functional and structural abnormalities that are associated with PMNE. We previously reported that forebrain activation was altered during a response inhibition task [15] and that the nature of the local intrinsic activity (i.e., amplitude low frequency fluctuation and regional homogeneity) changed in the prefrontal cortex during the resting state in children with PMNE [16]. We also identified microstructural abnormalities in the thalamus, the medial frontal gyrus, the anterior cingulated cortex, and the insular cortex of children with PMNE using diffusion tensor imaging [17] and neurochemical abnormalities in the prefrontal cortex and the pons of children with PMNE using proton magnetic resonance spectroscopy [18]. These studies showed that children with PMNE have structural, functional, and neurochemical abnormalities in the brain.

Prior studies mostly focused on several regions which involved cerebral micturition control network. In fact, children with PMNE probably have more serious problems beyond the micturition control; they probably have potential cognitive problems, such as working memory [14] and response inhibition [15]. Actually, the whole brain can be modeled as a large-scale complex network; its function can be fulfilled through both segregated and integrated specific functional connections patterns with optimized efficiency [19, 20]. The investigation of PMNE-related alterations in whole brain functional networks, instead of specific brain regions or local networks, may give further network-level information about the children with PMNE. Up to now, little is known about the PMNE-related alterations in topological properties, especially the topological efficiency of the whole brain functional networks during resting state. The advantage of a graph theory-based network analysis is that it provides measures for both global and local connectivity.

The topological organization of brain networks has recently been studied with graph theory [19, 21, 22]. Graph theory-based approaches model the brain as a complex network, representing it graphically using a collection of nodes and edges. Generally speaking, a network consists of N nodes that are linked by K edges. Networks can be described by an adjacent matrix $A(n, n)$ in which n is the number of nodes and the value of A_{ij} refers to the edge linking node i and node j. There are many graph metrics that can be used to describe the topological properties of a network, including the clustering coefficient (C_p), characteristic path length (L_p), normalized clustering coefficient (γ), normalized characteristic path length (λ), small-worldness (σ), global efficiency (E_{glob}), local efficiency (E_{loc}), nodal betweenness, nodal degree, and nodal efficiency. After the network modeling procedure, various graph theoretical metrics can be used to investigate the organizational mechanism underlying the relevant networks. The graph-based network analyses enable us not only to visualize the overall connectivity pattern among all brain regions but also to quantitatively characterize the global organization. Graph-based techniques used to study brain networks, including normal development, aging, and various brain disorders, have increased [21–25]. Previous studies showed that the brain's intrinsic activity is organized as a small-world, highly efficient network, with significant modularity and highly connected hub regions [19], which have also been found to change throughout normal development and aging and in various pathological conditions [21–25]. In the present paper, we propose a connectome-scale assessment of functional connectivity for children with PMNE via resting-state fMRI data.

2. Methods

2.1. Subjects. We studied 24 children with PMNE and 29 healthy children with the consent of the children and their guardians. All children were right-handed with an IQ greater than 75, and the presence of neurological and psychiatric diseases was excluded based on both a clinical examination (the DSM-IV criteria) and a structured interview. All children with PMNE were outpatients of the Shanghai Children's Medical Center. This study was approved by the IRB of the Shanghai Children's Medical Center in affiliation with the Shanghai Jiao Tong University School of Medicine (number SCMC-201014).

The inclusion criteria for all participants were listed as follows: (1) a physical, psychiatric, and neurological evaluation conducted by at least 3 members of a team of certified and experienced developmental and behavioral pediatricians; (2) age 7–15 years; (3) right-handedness; (4) children diagnosed with PMNE based on the criteria: a child has enuresis without additional lower urinary tract symptoms (excluding nocturia) or history of bladder dysfunction and has never had a period of established urinary continence for more than six months; (5) the Wechsler Intelligence Scale for Children-Revised (WISC-R) test employed to determine the intelligence quotient (IQ) of all subjects; and (6) the number and gender of each subgroup being matched.

The exclusion criteria for this study were listed as follows: (1) attention deficit/hyperactivity disorder, autism, or any psychiatric comorbid disorders; (2) previous head trauma, neurologic disorders, psychosurgery, or substantial physical illness; (3) fMRI data with obvious artifacts and distortions; (4) left-handedness, as assessed with the Annett Hand

Preference Questionnaire; and (5) a full-scale IQ less than 80 according to an age appropriate WISC-Chinese Revision.

Due to excessive head motion in some cases, functional images of 20 PMNE patients and 20 healthy children were available for further analysis. There were 2 groups of children: the average age was 10.8 ± 2.0 years for the PMNE group (14 males, 6 females) and 9.9 ± 2.0 years for the normal control group (14 males, 6 females). Additional clinical data regarding the patient groups are shown in Supplementary Material 1 in Supplementary Material available online at http://dx.doi.org/10.1155/2015/463708.

2.2. Data Acquisition. All subjects underwent a resting-state functional MRI scan using a 3T magnetic resonance system (Siemens, Magnetom Trio Tim) with a 12-channel phased array head coil. The sequence parameters were as follows: repetition time/echo time $(T_R/T_E) = 2,000/30$ ms; flip angle = 90°; 32 axial slices per volume; 3 mm slice thickness (33% dist. factor); matrix = 64×64; and FOV = 220×220 mm^2. Each functional run contained 210 image volumes, resulting in a total scanning time of 420 s for each participant. The first ten scans were discarded before the preprocessing of the data to remove the impact of magnetization stabilization. All participants were instructed not to focus their thoughts on anything in particular and to keep their eyes closed during the acquisition.

2.3. Data Preprocessing. Image preprocessing was performed using the SPM8 package (http://www.fil.ion.ucl.ac.uk/spm/; Wellcome Trust Centre for Neuroimaging, University College London, United Kingdom) and Graph Theoretical Network Analysis (GRETNA, http://www.nitrc.org/projects/gretna/). First, for each participant, the first 10 time points were discarded to avoid the instability of the initial MRI signal and to familiarize the subjects with the fMRI scanning noise. Next, the remaining fMRI data were corrected for the intravolume acquisition time delay and head motion. The head motion parameters of all participants were determined, and the extendable inclusion criteria for translational movement were <3.0 mm and <3.0° rotation. After these corrections, the images were spatially normalized to the standard space of the standard Montreal Neurological Institute (MNI) template by applying the EPI template at a $3 \times 3 \times 3$ mm^3 resolution. Finally, the resulting data were further filtered through a temporal band pass (0.0–0.08 Hz) to reduce the effects of low-frequency drift and high-frequency physiological noises.

2.4. Network Construction and Analysis. We used GRETNA to construct the network. To define the brain nodes, an atlas of Automated Anatomical Labeling [26] was employed to divide the entire brain into 90 cortical and subcortical regions of interest, each representing a node of the network. To define the network edges, first, the representative mean time series of each region was acquired by averaging the time series of all voxels within that region, followed by a correction of head motion effects by regressing out the head motion profiles estimated in the image realignment from the mean time-course. Then, the residuals of the regression analyses were

used to compute the partial correlation in this study, resulting in a 90×90 partial correlation matrix for each subject. Finally, individual partial correlation matrices were converted into weighted matrices; this method has been used in previous brain network studies [27–31].

We applied a wide range sparsity threshold S to all correlation matrices, which is determined in this procedure to guarantee that the threshold networks were estimable for small-worldness (scalar σ was larger than 1.1) and had sparse properties with as few spurious edges as possible and the average degree over all nodes of each threshold network was larger than $2 \times \log(90)$ [29, 32]. Our generated threshold range was $0.10 < S < 0.34$ with an interval of 0.01. For brain networks at each sparsity threshold, we calculated both global and node network metrics.

The global metrics included (1) small-world parameters [32] (i.e., clustering coefficient C_p, characteristic path length L_p, normalized clustering coefficient γ, normalized characteristic path length λ, and small-worldness σ) and (2) network efficiency [33] (i.e., local efficiency E_{loc} and global efficiency E_{glob}). The node metrics induced three nodal centrality metrics: the degree, efficiency, and betweenness. Furthermore, we calculated the area under the curve (AUC) for each network metric, which provides a summarized scalar for the topological characterization of brain networks independent of a single threshold selection. The AUC for a network metric Y, which was calculated over the sparsity threshold range of S_1 to S_n with interval of ΔS, was computed as $Y^{AUC} = \sum_{k=1}^{n-1} [Y(S_k) + Y(S_{k+1})] \times \Delta S/2$. In the current study, $S_1 = 0.10$, $S_n = 0.34$, and $\Delta S = 0.01$ (supplementary materials 2). The AUC metric has been used in previous brain network studies and is sensitive in detecting topological alterations of brain disorders [29, 34–36].

Moreover, to further localize the specific pairs of brain regions in which functional connectivity was altered in the PMNE patients, we identified region pairs that exhibited between-group differences in nodal characteristics and utilized the network based statistics (NBS) method (http://www.nitrc.org/projects/nbs/) [37] to localize the connected networks that exhibited significant changes in the PMNE patients.

Specially, we firstly choose the nodes which exhibited between-group differences in at least one of the three nodal centralities (the node degree, efficiency, and betweenness). Then a subset of connections matrix for each participant was conducted according to these altered nodes. Subsequently, the NBS approach was applied to define a set of suprathreshold links that included any connected components (threshold, $T = 1.6$, $P < 0.05$). To estimate the significance for each component, the nonparametric permutation approach (10000 permutations) was also conducted. For a detailed description, see [37].

2.5. Statistical Analysis. We used nonparametric permutation tests [29] for each network metric's AUC. We compared the overall topologies (i.e., small-world properties, weight clustering coefficient, and weight characteristic shortest path length) and the nodal characteristics (i.e., nodal degree, nodal
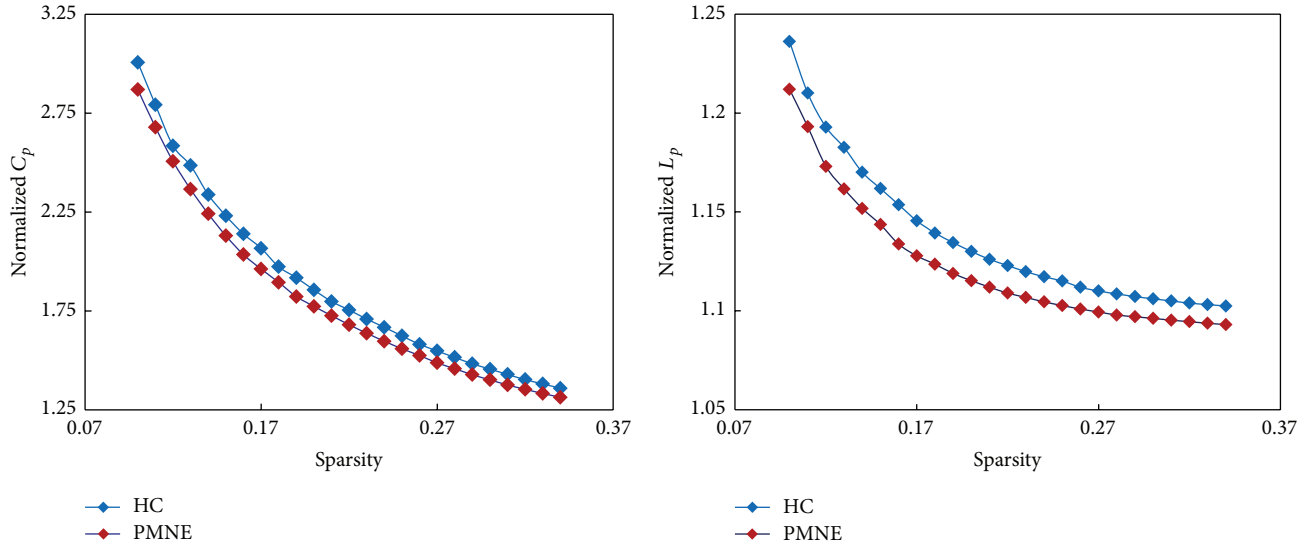
FIGURE 1: The key small-world parameters of functional network as a function of sparsity threshold. Both PMNE group and non-PMNE group showed normalized C_p larger than 1 and normalized L_p approximately equal to 1, indicating both groups exhibited a small-world topology. PMNE: children with primary monosymptomatic nocturnal enuresis; HC: healthy children; C_p: clustering coefficient; L_p: characteristic path length.

efficiency, and betweenness centrality) of the functional connectivity network between the patients and controls. Briefly, we first calculated the between-group difference in the mean value of each network metric. To test the null hypothesis that the observed group differences could occur by chance, for each network metric we then randomly reallocated all the values into two groups and recomputed the mean differences between the two randomized groups. This randomization procedure was repeated 10,000 times, and the 95th percentile points of each distribution were used as the critical values for a two-tailed test of the null hypothesis with a probability of type I error of 0.05. Additionally, to address the problem of multiple comparisons, the nodal centralities were tested on whether they survived a false discovery rate (FDR) threshold of $q = 0.05$.

3. Results

3.1. Global Topological Organization of the Functional Connectome. The whole-brain connectome of both the PMNE and control groups exhibited typical features of small-world topology; that is, compared with matched random networks, the functional brain networks had higher clustering coefficients (C_p) but similar characteristic path length (L_p) (Figure 1).

The patient group showed significantly lower values for C_p ($P = 0.007$) and higher values for L_p ($P = 0.0008$). No significant ($P > 0.05$) differences were found in the λ, γ, or σ. In terms of network efficiency, the comparisons revealed significant decreases in both E_{glob} ($P = 0.001$) and E_{loc} ($P = 0.001$) in the functional brain networks of the patients compared with the healthy controls (Figure 2).
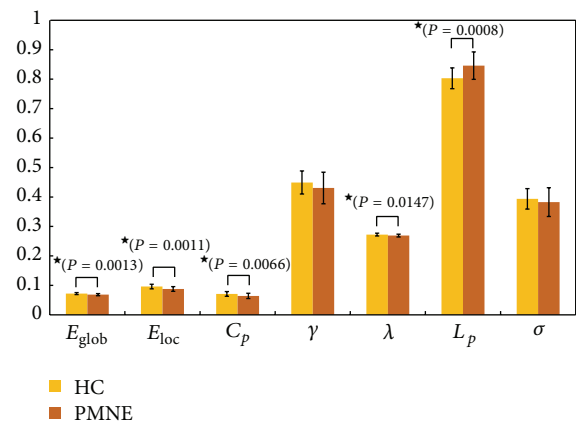

FIGURE 2: Differences in topological properties of functional brain networks between pediatric PMNE patients and trauma exposed non-PMNE controls. Significant differences were found in C_p ($P = 0.0066$), λ ($P = 0.0147$), E_{glob} ($P = 0.0013$), and E_{loc} ($P = 0.0011$) between pediatric PMNE patients and non-PMNE controls. $\star$: the black stars indicate the significantly statistical difference between the two groups ($P < 0.05$, uncorrected). Error bars denote standard deviations. PMNE: children with primary monosymptomatic nocturnal enuresis; HC: healthy children; E_{glob}: global efficiency; E_{loc}: local efficiency; C_p: clustering coefficient; γ: normalized clustering coefficient; λ: normalized characteristic path length; L_p: characteristic path length; σ: small-worldness.

3.2. Regional Topological Organization of the Functional Connectome. We identified the brain regions showing significant between-group differences in at least one nodal metric ($P < 0.05$, FDR corrected). Compared with normal control subjects, the patients showed decreased nodal centralities in

TABLE 1: Regions showing decreased nodal centralities in PMNE patients as compared with control subjects.

Brain regions	P values		
	Nodal betweenness	Nodal degree	Nodal efficiency
Left calcarine sulcus	0.460	0.016	**0.001**
Right calcarine sulcus	0.383	0.023	**0.002**
Left cuneus	0.124	0.022	**0.001**
Right cuneus	0.502	0.017	**0.002**
Left lingual gyrus	0.351	0.008	**0.000**
Right lingual gyrus	0.128	**0.000**	**0.000**
Right superior temporal gyrus	0.020	0.017	**0.003**

Regions were considered abnormal in PMNE patients if they exhibited significant between-group differences (FDR corrected $P < 0.05$ shown in bold font) in at least one of the three nodal centralities.
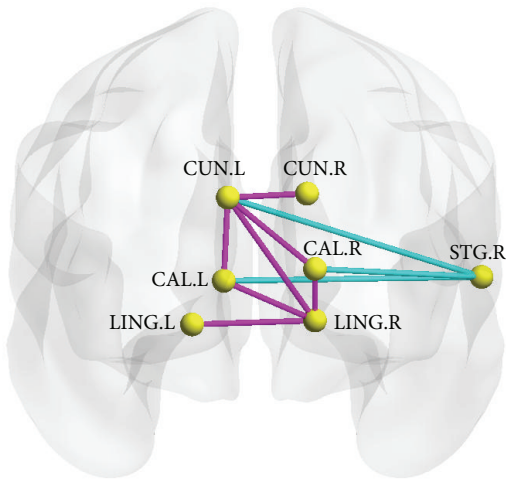

FIGURE 3: The region pairs showing altered nodal centralities brain regions and functional connections in the PMNE patients. These connections formed a single connected network with 7 nodes and 10 connections, which was significantly ($P < 0.05$, corrected) abnormal in the patients. Edge in cyan: increased functional connections in the PMNE patients; edge in magenta: decreased functional connections in the PMNE patients. CUN, cuneus; LING, lingual gyrus; CAL, calcarine sulcus; STG, superior temporal gyrus; R, right hemisphere; P, posterior. The nodes and connections were mapped onto the cortical surfaces using the BrainNet Viewer package (http://www.nitrc.org/projects/bnv).

several brain regions, including the bilateral calcarine sulcus, the bilateral cuneus, the bilateral lingual gyri, and the right superior temporal gyrus (Figure 3, Table 1). There were no significantly increased nodal centralities.

3.3. Disrupted Functional Network Connectivity in the Patients. Using NBS [37], we identified a connected network with 7 nodes and 10 connections; this network was significantly altered in the PMNE group ($P < 0.05$, corrected) (Figure 3, Table 2). Within this network, both decreased and increased connections were detected in the patients compared with the control subjects. The connections of the left cuneus in the bilateral calcarine sulcus, the left cuneus in the right cuneus, and the left cuneus in the right lingual gyrus

were decreased. Furthermore, the connections of the right lingual gyrus in the left lingual gyrus and the right lingual gyrus in bilateral calcarine sulcus were also decreased. On the other side, the increased connections included the right superior temporal gyrus in the bilateral calcarine sulcus and the right superior temporal gyrus in the left cuneus.

4. Discussion

4.1. Global Topological Organization of the Functional Connectome. In our study, we computed small-word metrics of 90 node networks based on the ALL template and found that λ, γ, and σ of the functional networks were not significantly changed in the PMNE group; however, the patient group showed significantly lower values for C_p and higher values for L_p, and the network efficiency parameters E_{glob} and E_{loc} were significantly decreased in the functional brain networks of the patients.

According to graph theory, a high C_p indicates that the nodes tend to form dense regional cliques, implying that the efficiency in local information transfer and processing is high [38]; a low L_p indicates a high transfer speed through the overall network, implying that the network has a high global efficiency [38]. Thus, the C_p and E_{loc} were reduced in PMNE group, which demonstrated that the efficiency in local information transfer and processing is low in children with PMNE. The higher L_p and lower E_{glob} in the PMNE group suggested that the brain network has a low global efficiency and a low ability of integrating information. Our present results are correlated with the previous findings that the efficiency of regional information processing and the efficiency of overall information transfer across the entire network were reduced in children with PMNE [38]. Therefore, our results suggest that intrinsic brain functional organization was disrupted in PMNE and that there was reduced efficiency in information exchange and integration in both local and global regions.

4.2. Regional Topological Organization of the Functional Connectome. Children with PMNE showed significant decreased nodal efficiency in the bilateral calcarine sulcus, bilateral cuneus, bilateral lingual gyri, and right superior temporal gyrus. The calcarine sulcus, cuneus, and lingual gyrus are in the occipital lobe, which is part of visual network. The right

TABLE 2: Altered functional connections in the PMNE patients group as compared to the control group.

Region 1	Region 2	t-score	Increase/decrease
Right superior temporal gyrus	Left cuneus	3.95	Increase
Right superior temporal gyrus	Left calcarine sulcus	2.29	Increase
Right superior temporal gyrus	Right calcarine sulcus	2.21	Increase
Left cuneus	Left calcarine sulcus	2.25	Decrease
Left cuneus	Right cuneus	1.75	Decrease
Left cuneus	Right calcarine sulcus	1.70	Decrease
Left cuneus	Right lingual gyrus	1.65	Decrease
Right lingual gyrus	Left lingual gyrus	3.36	Decrease
Right lingual gyrus	Left calcarine sulcus	2.06	Decrease
Right lingual gyrus	Right calcarine sulcus	1.72	Decrease

Connections are listed in descending order of statistical significance ($P < 0.05$). These connections formed a connected network that was identified using a network-based statistical approach. See Figure 2 for a graphical representation of these connections.

superior temporal gyrus is an essential structure involved in auditory processing and part of the auditory network.

Tomasi and Volkow reported that the cuneus is one of 4 major cortical hubs, and the cuneus hub network is both correlated with the somatosensory network and anticorrelated with the default mode network activity of other networks [39]. The calcarine cortex, lingual gyri, fusiform, occipital gyri, and paracentral lobule were the secondary hubs identified in this network, which suggests that the visual processing performed by the secondary hubs is integrated in the cuneus [39]. A previous study suggests that the cuneus and lingual gyrus take part in stop-down processes of visuospatial attention [40]. The cuneus is an important node of the default mode network and is also affected by attention-deficit/hyperactivity disorder [41, 42]. Decreased connectivity in the left cuneus has also been found in individuals with borderline personality disorder [43]. Additionally, gray matter volume in the cuneus has been suggested to be associated with better inhibitory control in bipolar depression patients [44], and dysfunction has been reported in the response inhibition in children with PMNE [15]. Thus, reduced nodal efficiency in the cuneus may point to insufficiencies in communications between executive control regions and visual processing regions.

In our results, the nodal efficiency was reduced in the bilateral lingual gyri, and the degree was reduced in the right lingual gyrus. Interestingly, the lingual gyrus has been associated with psychopathology, such as major depression [45], posttraumatic stress disorder [46, 47], and childhood maltreatment [48]. A previous task related neuroimaging study reported that the lingual gyrus was associated with the identification of facial expressions of emotion [49]. Equit et al. reported that children with nocturnal enuresis processed emotions differently from children with attention-deficit/hyperactivity disorder and controls [50]. Thus, we speculated that the abnormality in the lingual gyri would be related to the burden of disease and negative psychological factors.

4.3. Disrupted Functional Network Connectivity in the Patients.

The NBS method analysis showed increased connections between auditory system (right superior temporal gyrus) and visual system and decreased connections within the visual network, including the bilateral calcarine sulcus, the bilateral cuneus, and the bilateral lingual gyri. These findings suggest that connectivity of the auditory and visual networks is unbalanced in children with PMNE.

Visual information is the main source of information, and the visual network is closely linked to other brain networks. When the visual network functions abnormally, a great potential for harm is induced, possibly resulting in damage to cognitive function. Abnormal visual network functionality can also result in reduced efficiency of the global network and can affect global communication and integration. The network efficiency of both E_{glob} and E_{loc} in the functional brain networks of the patients was significantly decreased. This observation suggests that the disruption of brain communication and integration may also be an important factor in PMNE disorders.

Several issues must be addressed further. First, the brain networks were constructed by parcellating the entire brain into 90 brain regions at a coarsely regional level. Future studies should use a more precise parcellation strategy or spatial scale to overcome this challenge. Second, the functional brain networks constructed from the r-fMRI data were largely constrained by anatomical pathways [51, 52]. Thus, combining multimodal neuroimaging data could facilitate the uncovering of the structure-function relationships in PMNE patients. Finally, the results in this paper are different from those of our previous resting-state fMRI study [16], which focused on local intrinsic activity. We did not identify a direct relationship between the results in this study and the pathology of PMNE. However, this study sheds light on the functional connectivity of children with PMNE and suggests that there may be potential cognition dysfunction in children with PMNE.

It is important to note some limitations in this study. First, functional brain networks were constructed at a regional level

by parcellating the whole brain into 90 regions based on a previously published atlas. Brain networks derived using different parcellation schemes or at different spatial scales exhibit distinct topological architectures [53, 54]. Further studies are needed to determine which brain parcellation strategy or spatial scale is more appropriate for the characterization of network topology in PMNE. Second, we have not found the direct relationship between our results and the pathology of PMNE. The regions showing abnormality nodal centralities in PMNE patients were not involved in the micturition neural control network. However, our results give direct evidence that the PMNE probably has cognitive problem.

5. Conclusion

This is the first study to investigate the characteristics of PMNE patients with network-based graph theory using resting-state fMRI. In the PMNE group, there were reduced local and global efficiency in the brain, as well as disturbances in connectivity. The alterations in network topologies primarily occurred in the right superior temporal gyrus (auditory network), and decreased connectivity was observed in the visual network, including the bilateral calcarine sulcus, the bilateral cuneus, and the bilateral lingual gyri. Our findings suggest that PMNE includes brain network alterations, which may affect both local and global communication and integration.

Conflict of Interests

The authors declare that there is no conflict of interests regarding the publication of this paper.

Acknowledgments

References

[1] M. Riccabona, "Evaluation und management of enuresis: an update," *Urologe—Ausgabe A*, vol. 49, no. 7, pp. 861–870, 2010.

[2] M. Theunis, E. van Hoecke, S. Paesbrugge, P. Hoebeke, and J. Vande Walle, "Self-image and performance in children with nocturnal enuresis," *European Urology*, vol. 41, no. 6, pp. 660–667, 2002.

[3] T. Nevéus, A. von Gontard, P. Hoebeke et al., "The standardization of terminology of lower urinary tract function in children and adolescents: report from the Standardisation Committee of the International Children's Continence Society," *Journal of Urology*, vol. 176, no. 1, pp. 314–324, 2006.

[4] T. Nevéus, "Diagnosis and management of nocturnal enuresis," *Current Opinion in Pediatrics*, vol. 21, no. 2, pp. 199–202, 2009.

[5] F. Toros, A. Özge, M. Bozlu, and S. Çayan, "Hyperventilation response in the electroencephalogram and psychiatric problems in children with primary monosymptomatic nocturnal enuresis," *Scandinavian Journal of Urology and Nephrology*, vol. 37, no. 6, pp. 471–476, 2003.

[6] A. Iscan, Y. Ozkul, D. Unal et al., "Abnormalities in event-related potential and brainstem auditory evoked response in children with nocturnal enuresis," *Brain and Development*, vol. 24, no. 7, pp. 681–687, 2002.

[7] R. Karlidag, H. I. Ozisik, A. Soylu et al., "Topographic abnormalities in event-related potentials in children with monosymptomatic nocturnal enuresis," *Neurourology and Urodynamics*, vol. 23, no. 3, pp. 237–240, 2004.

[8] C. M. Freitag, D. Röhling, S. Seifen, R. Pukrop, and A. von Gontard, "Neurophysiology of nocturnal enuresis: evoked potentials and prepulse inhibition of the startle reflex," *Developmental Medicine & Child Neurology*, vol. 48, no. 4, pp. 278–284, 2006.

[9] S. Schulz-Juergensen, A. Langguth, and P. Eggert, "Effect of alarm therapy on conditioning of central reflex control in nocturnal enuresis: pilot study on changes in prepulse inhibition (PPI)," *Pediatric Nephrology*, vol. 29, no. 7, pp. 1209–1213, 2014.

[10] S. Schulz-Juergensen, M. Rieger, J. Schaefer, A. Neusuess, and P. Eggert, "Effect of 1-desamino-8-D-arginine vasopressin on prepulse inhibition of startle supports a central etiology of primary monosymptomatic enuresis," *Journal of Pediatrics*, vol. 151, no. 6, pp. 571–574, 2007.

[11] C. J. Fowler and D. J. Griffiths, "A decade of functional brain imaging applied to bladder control," *Neurourology and Urodynamics*, vol. 29, no. 1, pp. 49–55, 2010.

[12] D. J. Griffiths and S. D. Tadic, "Bladder control, urgency, and urge incontinence: evidence from functional brain imaging," *Neurourology and Urodynamics*, vol. 27, no. 6, pp. 466–474, 2008.

[13] B. Yu, Q. Guo, G. Fan, H. Ma, L. Wang, and N. Liu, "Evaluation of working memory impairment in children with primary nocturnal enuresis: evidence from event-related functional magnetic resonance imaging," *Journal of Paediatrics and Child Health*, vol. 47, no. 7, pp. 429–435, 2011.

[14] B. Yu, H. Sun, H. Ma et al., "Aberrant whole-brain functional connectivity and intelligence structure in children with primary nocturnal enuresis," *PLoS ONE*, vol. 8, no. 1, Article ID e51924, 2013.

[15] D. Lei, J. Ma, X. Du, G. Shen, M. Tian, and G. Li, "Altered brain activation during response inhibition in children with primary nocturnal enuresis: an fMRI study," *Human Brain Mapping*, vol. 33, no. 12, pp. 2913–2919, 2012.

[16] D. Lei, J. Ma, X. Du, G. Shen, M. Tian, and G. Li, "Spontaneous brain activity changes in children with primary monosymptomatic nocturnal enuresis: a resting-state fMRI study," *Neurourology and Urodynamics*, vol. 31, no. 1, pp. 99–104, 2012.

[17] D. Lei, J. Ma, X. Shen et al., "Changes in the brain microstructure of children with primary monosymptomatic nocturnal enuresis: a diffusion tensor imaging study," *PLoS ONE*, vol. 7, no. 2, Article ID e31023, 2012.

[18] J. Zhang, D. Lei, J. Ma et al., "Brain metabolite alterations in children with primary nocturnal enuresis using proton magnetic resonance spectroscopy," *Neurochemical Research*, vol. 39, no. 7, pp. 1355–1362, 2014.

[19] Y. He and A. Evans, "Graph theoretical modeling of brain connectivity," *Current Opinion in Neurology*, vol. 23, pp. 341–350, 2010.

[20] D. S. Bassett and E. Bullmore, "Small-world brain networks," *Neuroscientist*, vol. 12, no. 6, pp. 512–523, 2006.

[21] J. Wang, X. Zuo, and Y. He, "Graph-based network analysis of resting-state functional MRI," *Frontiers in Systems Neuroscience*, vol. 4, article 16, 2010.

[22] Y. Iturria-Medina, "Anatomical brain networks on the prediction of abnormal brain states," *Brain Connectivity*, vol. 3, no. 1, pp. 1–21, 2013.

[23] K. Wu, Y. Taki, K. Sato et al., "Topological organization of functional brain networks in healthy children: differences in relation to age, sex, and intelligence," *PLoS ONE*, vol. 8, no. 2, Article ID e55347, 2013.

[24] M. Cao, J.-H. Wang, Z.-J. Dai et al., "Topological organization of the human brain functional connectome across the lifespan," *Developmental Cognitive Neuroscience*, vol. 7, pp. 76–93, 2014.

[25] B. M. Tijms, A. M. Wink, W. de Haan et al., "Alzheimer's disease: connecting findings from graph theoretical studies of brain networks," *Neurobiology of Aging*, vol. 34, no. 8, pp. 2023–2036, 2013.

[26] N. Tzourio-Mazoyer, B. Landeau, D. Papathanassiou et al., "Automated anatomical labeling of activations in SPM using a macroscopic anatomical parcellation of the MNI MRI single-subject brain," *NeuroImage*, vol. 15, no. 1, pp. 273–289, 2002.

[27] Y. Liu, M. Liang, Y. Zhou et al., "Disrupted small-world networks in schizophrenia," *Brain*, vol. 131, no. 4, pp. 945–961, 2008.

[28] L. Ferrarini, I. M. Veer, E. Baerends et al., "Hierarchical functional modularity in the resting-state human brain," *Human Brain Mapping*, vol. 30, no. 7, pp. 2220–2231, 2009.

[29] J. Zhang, J. Wang, Q. Wu et al., "Disrupted brain connectivity networks in drug-naive, first-episode major depressive disorder," *Biological Psychiatry*, vol. 70, no. 4, pp. 334–342, 2011.

[30] R. Salvador, J. Suckling, M. R. Coleman, J. D. Pickard, D. Menon, and E. Bullmore, "Neurophysiological architecture of functional magnetic resonance images of human brain," *Cerebral Cortex*, vol. 15, no. 9, pp. 1332–2342, 2005.

[31] Y. He, Z. Chen, and A. Evans, "Structural insights into aberrant topological patterns of large-scale cortical networks in Alzheimer's disease," *The Journal of Neuroscience*, vol. 28, no. 18, pp. 4756–4766, 2008.

[32] D. J. Watts and S. H. Strogatz, "Collective dynamics of "small-world" networks," *Nature*, vol. 393, no. 6684, pp. 440–442, 1998.

[33] V. Latora and M. Marchiori, "Efficient behavior of small-world networks," *Physical Review Letters*, vol. 87, no. 19, Article ID 198701, 2001.

[34] S. Achard and E. Bullmore, "Efficiency and cost of economical brain functional networks," *PLoS Computational Biology*, vol. 3, no. 2, article e17, 2007.

[35] Y. He, A. Dagher, Z. Chen et al., "Impaired small-world efficiency in structural cortical networks in multiple sclerosis associated with white matter lesion load," *Brain*, vol. 132, no. 12, pp. 3366–3379, 2009.

[36] J. Wang, L. Wang, Y. Zang et al., "Parcellation-dependent small-world brain functional networks: a resting-state fmri study," *Human Brain Mapping*, vol. 30, no. 5, pp. 1511–1523, 2009.

[37] A. Zalesky, A. Fornito, and E. T. Bullmore, "Network-based statistic: identifying differences in brain networks," *NeuroImage*, vol. 53, no. 4, pp. 1197–1207, 2010.

[38] T. Xie and Y. He, "Mapping the alzheimer's brain with connectomics," *Frontiers in Psychiatry*, vol. 2, article 77, 2012.

[39] D. Tomasi and N. D. Volkow, "Association between functional connectivity hubs and brain networks," *Cerebral Cortex*, vol. 21, no. 9, pp. 2003–2013, 2011.

[40] B. Hahn, T. J. Ross, and E. A. Stein, "Neuroanatomical dissociation between bottom-up and top-down processes of visuospatial selective attention," *NeuroImage*, vol. 32, no. 2, pp. 842–853, 2006.

[41] B. de Celis Alonso, S. H. Tobón, P. D. Suarez et al., "A multi-methodological MR resting state network analysis to assess the changes in brain physiology of children with ADHD," *PLoS ONE*, vol. 9, no. 6, Article ID e99119, 2014.

[42] X. Wang, Y. Jiao, T. Tang, H. Wang, and Z. Lu, "Altered regional homogeneity patterns in adults with attention-deficit hyperactivity disorder," *European Journal of Radiology*, vol. 82, no. 9, pp. 1552–1557, 2013.

[43] R. C. Wolf, F. Sambataro, N. Vasic et al., "Aberrant connectivity of resting-state networks in borderline personality disorder," *Journal of Psychiatry and Neuroscience*, vol. 36, no. 6, pp. 402–411, 2011.

[44] M. Haldane, G. Cunningham, C. Androutsos, and S. Frangou, "Structural brain correlates of response inhibition in Bipolar Disorder I," *Journal of Psychopharmacology*, vol. 22, no. 2, pp. 138–143, 2008.

[45] I. M. Veer, C. F. Beckmann, M.-J. van Tol et al., "Whole brain resting-state analysis reveals decreased functional connectivity in major depression," *Frontiers in Systems Neuroscience*, vol. 4, article 41, 2010.

[46] L.-D. Qin, Z. Wang, Y.-W. Sun et al., "A preliminary study of alterations in default network connectivity in post-traumatic stress disorder patients following recent trauma," *Brain Research*, vol. 1484, pp. 50–56, 2012.

[47] Y. Yin, C. Jin, L. T. Eyler, H. Jin, X. Hu, and L. Duan, "Altered regional homogeneity in post-traumatic stress disorder: a resting-state functional magnetic resonance imaging study," *Neuroscience Bulletin*, vol. 28, no. 5, pp. 541–549, 2012.

[48] S. J. A. van der Werff, J. N. Pannekoek, I. M. Veer et al., "Resilience to childhood maltreatment is associated with increased resting-state functional connectivity of the salience network with the lingual gyrus," *Child Abuse and Neglect*, vol. 37, no. 11, pp. 1021–1029, 2013.

[49] R. Kitada, I. S. Johnsrude, T. Kochiyama, and S. J. Lederman, "Brain networks involved in haptic and visual identification of facial expressions of emotion: an fMRI study," *NeuroImage*, vol. 49, no. 2, pp. 1677–1689, 2010.

[50] M. Equit, A. Becker, D. El Khatib, M. Rubly, N. Becker, and A. von Gontard, "Central nervous system processing of emotions in children with nocturnal enuresis and attention-deficit/hyperactivity disorder," *Acta Paediatrica*, vol. 103, no. 8, pp. 868–878, 2014.

[51] J. S. Damoiseaux and M. D. Greicius, "Greater than the sum of its parts: a review of studies combining structural connectivity and resting-state functional connectivity," *Brain Structure and Function*, vol. 213, no. 6, pp. 525–533, 2009.

[52] C. J. Honey, O. Sporns, L. Cammoun et al., "Predicting human resting-state functional connectivity from structural connectivity," *Proceedings of the National Academy of Sciences of the United States of America*, vol. 106, no. 6, pp. 2035–2040, 2009.

[53] A. Fornito, A. Zalesky, and E. T. Bullmore, "Network scaling effects in graph analytic studies of human resting-state fMRI data," *Frontiers in Systems Neuroscience*, vol. 4, article 22, 2010.

[54] A. Zalesky, A. Fornito, I. H. Harding et al., "Whole-brain anatomical networks: does the choice of nodes matter?" *NeuroImage*, vol. 50, no. 3, pp. 970–983, 2010.

Research Article
Examination of Local Functional Homogeneity in Autism

Lili Jiang,[1,2] Xiao-Hui Hou,[1,2,3] Ning Yang,[1,2,3] Zhi Yang,[1,2] and Xi-Nian Zuo[1,2,4]

[1]Key Laboratory of Behavioral Science, Institute of Psychology, Chinese Academy of Sciences, No. 16 Lincui Road,
 Chaoyang District, Beijing 100101, China
[2]Magnetic Resonance Imaging Research Center, Institute of Psychology, Chinese Academy of Sciences, No. 16 Lincui Road,
 Chaoyang District, Beijing 100101, China
[3]University of Chinese Academy of Sciences, Shijingshan, Beijing 100049, China
[4]Laboratory for Functional Connectome and Development, Institute of Psychology, Chinese Academy of Sciences,
 No. 16 Lincui Road, Chaoyang District, Beijing 100101, China

Correspondence should be addressed to Xi-Nian Zuo; zuoxn@psych.ac.cn

Increasing neuroimaging evidence suggests that autism patients exhibit abnormal brain structure and function. We used the Autism Brain Imaging Data Exchange (ABIDE) sample to analyze locally focal (~8 mm) functional connectivity of 223 autism patients and 285 normal controls from 15 international sites using a recently developed surface-based approach. We observed enhanced local connectivity in the middle frontal cortex, left precuneus, and right superior temporal sulcus, and reduced local connectivity in the right insular cortex. The local connectivity in the right middle frontal gyrus was positively correlated with the total score of the autism diagnostic observation schedule whereas the local connectivity within the right superior temporal sulcus was positively correlated with total subscores of both the communication and the stereotyped behaviors and restricted interests of the schedule. Finally, significant interactions between age and clinical diagnosis were detected in the left precuneus. These findings replicated previous observations that used a volume-based approach and suggested possible neuropathological impairments of local information processing in the frontal, temporal, parietal, and insular cortices. Novel site-variability analysis demonstrated high reproducibility of our findings across the 15 international sites. The age-disease interaction provides a potential target region for future studies to further elucidate the neurodevelopmental mechanisms of autism.

1. Introduction

Autism spectrum disorder (ASD) is an increasingly recognized group of neurodevelopmental disorders with early onset and lifelong persistence. ASD is reported to occur in ~1% of children [1] and is characterized by abnormalities in language, social interaction, and a range of stereotyped and repetitive behaviors.

Neuroimaging studies of ASD have accumulated a wealth of empirical data on the abnormal brain connectomics associated with ASD [2–4]. Reduced long distance but increased local connectivity in ASD has been proposed [5], and a number of FMRI studies have consistently found underconnectivity in ASD [2, 6–8]. However, a significant number of other studies report mixed or increased functional connectivity in ASD [9–11]. Regarding these inconsistencies,

Muller and colleagues systematically illustrated that different methodological choices could produce different results in functional connectivity studies [4]. Although methodological choices may affect the statistical results of ASD studies, a consistent and reliable demonstration of brain function using a large sample would be a good step towards elucidating the brain mechanisms of ASD.

Using a local connectivity index of functional homogeneity, ReHo, both increases and decreases of ReHo were observed in resting-state FMRI studies of ASD [12, 13]. ReHo is a promising index of human brain function that has been applied to multiple neuropsychiatric disorders [2, 12–14]. It employs Kendall's coefficient of concordance (KCC) to measure the functional coherence between a given area (e.g., a voxel) and its adjacent areas (e.g., neighboring voxels) [15]. Previous studies on spontaneous brain activity

in ASD used volume-based ReHo (3dReHo), ignoring the two-dimensional nature of the laminar cerebral cortex [2, 14]. In volume space, voxel's neighbors may not be close to the voxel across the cortical mantle. Recently, our lab developed a surface-based ReHo method (2dReHo) that demonstrated moderate to high test-retest reliability and correlated with neurobiological information processing hierarchies [16, 17]. The present study began by testing the consistency between the previous 3dReHo and our new 2dReHo results across a large-scale autism sample. Furthermore, as revealed by our recent work [17], 2dReHo is a neurobiologically meaningful metric of the functional organization of the human brain. We thus aimed to examine the effects of ASD on brain functional organization.

Abnormal cortical development and organization in children with ASD has been characterized in terms of brain cortical volume, surface area, and cortical thickness [18, 19]. Previous genetic findings, coupled with brain imaging studies, suggested a potential unifying model of ASD in which higher-order association areas of the brain that normally connect to the frontal lobe are partially disconnected during development [20, 21]. In general, autism is conceived as a heterogeneous childhood neurodevelopmental disorder because of its early onset and lifelong persistence. Using 223 ASD and 285 healthy controls (HC) from the autism brain imaging data exchange (ABIDE) lifetime sample [2, 22], we examined both group differences and diagnosis-age interactions in local functional homogeneity measured by 2dReHo, as well as behavioral correlations in ASD.

2. Materials and Methods

2.1. Participants and MR Imaging. The ABIDE sample was part of the 1000 Functional Connectomes Project (FCP: http://fcon_1000.projects.nitrc.org/fcpClassic/FcpTable.html) and the International Neuroimaging Data-Sharing Initiative (INDI: http://fcon_1000.projects.nitrc.org/indi/pro/nki.html) and included RFMRI images of 539 ASD (aged 17.01 ± 8.37) and 573 healthy controls (aged 17.08 ± 7.72) from 18 international sites [2]. Detailed phenotypic and scanning information can be found at the ABIDE website: http://fcon_1000.projects.nitrc.org/indi/abide/. The overlap of phenotypic protocol across sites consisted of age at scan, sex, IQ, and diagnostic information. All contributions were based on studies approved by the local institutional review boards, and written informed consent was obtained from the parents of all the early onset patients and corresponding healthy controls, as well as all the adult participants.

Similar to the ABIDE consortium paper [2], 794 subjects from the original participant pool were selected for subsequent imaging analyses. The criteria were (1) individuals without other comorbidities; (2) male subjects, as they represent 90% of the ABIDE sample; (3) sites with fIQ estimated for >75% and subjects with fIQ scores; (4) individuals with fIQ within 2 s.d. of the overall ABIDE sample mean (i.e., 108 ± 15); (5) sites with at least 9 participants per group after the above exclusions.

2.2. Image Preprocessing. For each participant, all MRI images were preprocessed with the Connectome Computation System (CCS: http://lfcd.psych.ac.cn/ccs.html) [16]. This system was developed based on FCP scripts for providing a computational platform for multimodal brain connectome analysis by integrating AFNI [23, 24], FSL [25], and FreeSurfer [26] and has been used in our previous studies [16, 17].

All structural MRI images were processed with the CCS structural pipeline. Briefly, the structural images were processed for cortical surface reconstruction [27–31], including (1) noise removal with a spatially adaptive nonlocal means filter [32, 33] operation and correction for intensity inhomogeneity; (2) brain extraction with a hybrid watershed/surface deformation; (3) tissue segmentation of the cerebrospinal fluid (CSF), white matter (WM), and deep gray matter (GM); (4) cutting plane generation to disconnect the two hemispheres and subcortical structures; (5) fixation of the interior holes of the segmentation; (6) a triangular mesh tessellation over the GM-WM boundary and mesh deformation to produce a smooth GM-WM interface (white surface) and GM-CSF interface (pial surface); (7) topological defect correction on the surface; (8) individual surface mesh inflated into a sphere; and (9) estimation of the deformation between the resulting spherical mesh and a common spherical coordinate system that aligned the cortical folding patterns across subjects.

All functional images were preprocessed with the CCS functional pipeline, involving the following steps: (1) eliminating the first 5 EPI volumes from each scan to allow for signal equilibration; (2) despiking time series to detect and reduce outliers (spikes) using an hyperbolic tangent function; (3) slice timing using Fourier interpolation to temporally correct the interleaved slice acquisition; (4) aligning each volume to a "base" image (the mean EPI image) using Fourier interpolation to correct between-head movements; (5) normalizing the 4D global mean intensity to 10,000 to allow intersubject comparisons; (6) regressing out the WM/CSF mean time series and the Friston-24 motion time series to reduce the effects of these confounding factors [16, 34]; (7) filtering the residual time series with a passband filter (0.01–0.1 Hz) to extract low-frequency fluctuations; (8) removing both linear and quadratic trends; and (9) aligning individual motion corrected functional images to the individual anatomical image using a GM-WM boundary-based registration (BBR) algorithm [35]. Individual preprocessed 4D RFMRI time series were projected onto the *fsaverage5* standard cortical surface with 10,242 vertices per hemisphere and gaps of 4 mm on average [36].

2.3. Quality Control Procedure. The CCS quality control procedure provides an interactive environment for users (http://lfcd.psych.ac.cn/ccs/QC.html) to examine the quality of (1) brain extraction or skull stripping, (2) brain tissue segmentation, (3) pial and white surface reconstruction, (4) functional-structural image realignment with BBR registration, and (5) head motion during RFMRI, calculated using several quantities: (1) the maximum distance of translational head movement (maxTran), (2) the maximum degree of

TABLE 1: ABIDE sample composition in the current study.

Site name	ASD number	HC number	Age (years)
Caltech	4	6	29.5 ± 11.8
CMU	7	2	27.8 ± 6.0
KKI	3	11	10.0 ± 1.5
Leuven	14	12	22.8 ± 3.6
MaxMum	15	24	26.3 ± 11.0
NYU	30	69	15.7 ± 6.6
OHSU	9	13	10.5 ± 1.6
Olin	7	11	17.2 ± 3.0
Pitt	22	21	19.0 ± 6.9
Stanford	7	9	10.1 ± 1.7
Trinity	17	24	16.9 ± 3.4
UCLA	35	29	13.1 ± 2.4
UM	9	16	16.3 ± 3.8
USM	35	22	23.8 ± 8.2
Yale	9	16	12.1 ± 2.6

rotational head movement (maxRot), (3) the mean framewise displacement (meanFD) [37, 38], and (4) the minimal cost of the BBR coregistration (mcBBR). All subjects with bad brain extraction, tissue segmentation, and surface reconstruction were excluded from the subsequent computation. All datasets filled the following criteria: (1) maxTran ≤ 2 mm, (2) maxRot ≤ 2°, (3) meanFD ≤ 0.4 mm, and (4) mcBBR< 0.75. We were left with a total of 508 subjects (223 ASD, 285 HC) from 15 different sites passing the above quality control procedure for the final statistical analysis (see Table 1 for the composition of the final sample).

2.4. 2dReHo and Statistics. We applied surface-based 2dReHo to characterize local functional homogeneity in both ASD and HC subjects due to its high test-retest reliability [16] neurobiological significance [17]. Specifically, for a given vertex v_0 on the surface grid *fsaverage5*, we identified its K nearest neighbors $v_{i=1,2,...,K}$ and denoted by $v_i(t)$ their RFMRI time series. The 2dReHo measure of this vertex was computed as Kendall's coefficient of concordance (KCC) using these time series. The mathematical formula is shown as (1), where $R_{i=1,...,n}$ represents the ranks of $v_i(t)$, n is the number of time points, R_i is the mean rank across its neighbors at the ith time point, and R is the overall mean rank across all neighbors and across all the time points. A vertexwise 2dReHo surface map was produced by repeating this computation procedure for every vertex on the surface of both hemispheres. Both length-one (6 neighbors) and length-two (19 neighbors) 2dReHo maps, denoted by 2dReHo1 and 2dReHo2, respectively, were generated for subsequent analyses:

$$\text{KCC} = \frac{\sum_{i=1}^n R_i^2 - n\left(\overline{R}\right)^2}{(1/12)\, K^2\left(n^3 - n\right)} = 12\frac{\sum_{i=1}^n \left(\overline{R}_i\right)^2}{\left(n^3 - n\right)} - 3\frac{(n+1)}{(n-1)}. \quad (1)$$

A general linear model was constructed by modeling diagnosis (ASD versus HC), site, age, and fIQ as covariates of interests (see details in (2)). Notably, before the group level

analysis of 2dReHo, we first removed the effects of meanFD, mcBBR, Jacobian values of white surface, and global mean (gm) 2dReHo (see details in (3)). We have found that this computation is equivalent to directly including all these factors in the final group analysis for the purpose of examining the effects of the variables of interest. Here, the mean FD indicates the mean framewise displacement [37] and mcBBR indicates the warp distortion for BBR-based function-to-structure realignment. The vertexwise significance values for group difference and age by group interactions were corrected for multiple comparisons with a clusterwise method based on random field theory (cluster-defining $P = 0.01$, cluster-level corrected $P = 0.05$):

$$Y = \beta_1 \times \text{age} + \beta_2 \times \text{site} + \beta_3 \times \text{fIQ}$$
$$+ \beta_4 \times \text{Group} + \beta_5 \times \text{Group} \times \text{age} + e, \quad (2)$$

$$Y^{\text{adj}} = Y - \left(\beta_{\text{gm}} \times \text{gm} + \beta_{\text{fd}} \times \text{meanFD}\right.$$
$$\left. + \beta_{\text{bbr}} \times \text{mcBBR} + \beta_{\text{jac}} \times \text{JAC}\right). \quad (3)$$

2.5. Behavioral Correlations. Autism diagnostic observation schedule (ADOS) [39], autism diagnostic interview (ADI), and the Gotham algorithm of the ADOS (ADOS_GOTHAM) were selected for the final behavioral correlation analyses, as each of these subscale scores represented >40% of the whole patient group. Within each cluster showing a significant group difference in 2dReHo, we calculated the Pearson correlation coefficient between the average 2dReHo values of the cluster and the behavioral measurements. ADOS includes the total score (ADOS_TOTAL), the communication total subscore (ADOS_COMM), the social total subscore (ADOS_SOCIAL), and the stereotyped behaviors and restricted interests total subscore (ADOS_STEREO_BEHAV). ADI includes the reciprocal social interaction subscore (A) total for the autism diagnostic interview-revised (ADI_R_SOCIAL_TOTAL_A), the abnormality in communication subscore (B) total for the autism diagnostic interview-revised (ADI_R_VERBAL_TOTAL_BV), the restricted, repetitive, and stereotyped patterns of behavior subscore (C) total for the autism diagnostic interview-revised (ADI_R_RRB_TOTAL_C), and the abnormality of development evidence at or before 36-month subscore (D) total for the autism diagnostic interview-revised (ADI_R_ONSET_TOTAL_D). ADOS_GOTHAM includes the social affect total subscore for the Gotham algorithm of the ADOS (ADOS_GOTHAM_SOC_AFFECT), restricted and repetitive behaviors total subscore for the Gotham algorithm of the ADOS (ADOS_GOTHAM_RRB), the sum of the social affect total and restricted and repetitive behaviors total (ADOS_GOTHAM_TOTAL), and the individual calibrated severity score for the Gotham algorithm of the ADOS (ADOS_GOTHAM_SEVERITY).

3. Results

3.1. Sample Composition. The final analysis was conducted on 508 participants from 15 sites. The details of the sample

TABLE 2: Cortical clusters demonstrating significant differences in 2dReHo between ASD and HC.

Cluster	Vertex number	MNI coordination	$-\text{sign}(t)\log_{10}(P)$
Middle frontal sulcus	52	30, −41, −18	2.86
Superior frontal sulcus	39	20, −7, −60	3.35
Precuneus gyrus	34	6, 71, −47	2.95
Middle frontal gyrus	32	33, −32, −32	3.05
Middle frontal sulcus	78	−24, −41, −32	3.27
Superior temporal sulcus	38	−45, 37, 3	4.96
Middle frontal gyrus	35	−39, −46, −20	3.28
Insular cortex	39	−38, 10, −19	−3.45
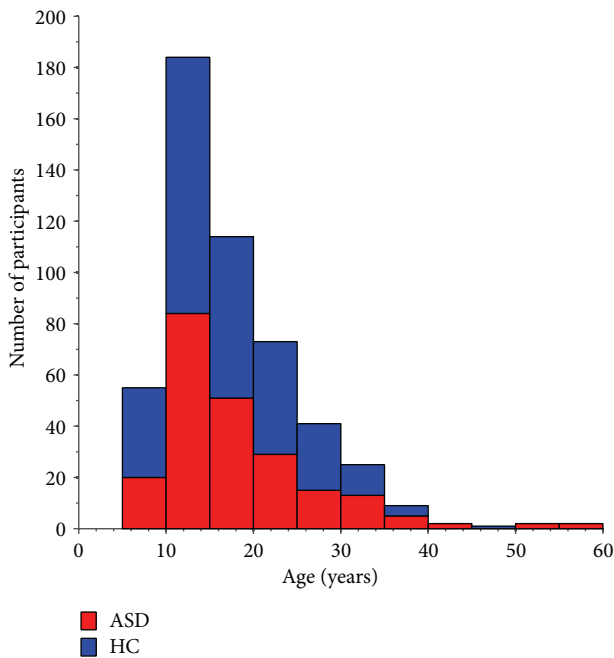
FIGURE 1: Sample characteristics of the ABIDE sites included in the final analyses.

composition are presented in Table 1. The number of participants per site ranged from 3 to 35 ASD patients and from 2 to 69 HC subjects. The age distribution is shown in Figure 1. The red and blue bars represent the ASD and HC numbers for a particular age bin, respectively. There is no significant difference in age between the ASD and HC subjects ($t = 1.40$; $P = 0.16$). Results derived with 2dReHo1 and 2dReHo2 were almost identical and we thus presented the findings based upon 2dReHo1, which were detailed in below.

3.2. Group Differences in 2dReHo. There was no difference in the global 2dReHo between ASD and HC subjects ($t = −0.33$, $P = 0.75$). Figure 2 depicts the brain areas that significantly differed between ASD and HC subjects. The anatomical labels and locations are summarized in Table 2. The middle frontal cortex, the left precuneus gyrus, and right superior temporal sulcus exhibited increased local functional homogeneity (warm colors) in ASD compared with HC. The right insular cortex had decreased local functional homogeneity (cool colors) in ASD compared to HC subjects.

3.3. Age by Diagnosis Interactions. The age-diagnosis interaction was examined for differences in correlations between age and local functional homogeneity (i.e., the developmental effect) between ASD and HC subjects. Significant group by age interaction effects were detected in the left precuneus gyrus (Figure 3(a)), where ASD patients demonstrated lower 2dReHo than HC subjects (Figure 2). To look into the details of 2dReHo changes across this large age span, we also visualized the age dependence of 2dReHo as scatter plots for ASD and HC subjects (Figure 3(b)). Clearly, the scatter plot shows that ASD subjects had increased 2dReHo with age, whereas HC subjects had decreased 2dReHo, the opposite pattern, with age.

3.4. Site Effects and Reproducibility. Because this was a multisite study, we included site as one covariate of interest. Site effects revealed by the statistical model are illustrated in Figure 4. Multiple regions showed significant site effects, implying a remarkable variability of 2dReHo across the 15 international sites. Specifically, the left pre/postcentral gyrus, the middle/inferior frontal gyrus, the left medial prefrontal cortex, the left superior parietal gyrus, and cingulate gyrus exhibited significant site variability in 2dReHo. In contrast, the superior temporal gyrus, the right postcentral gyrus, the inferior part of the precentral sulcus, the inferior frontal sulcus, the right insular cortex, the right precuneus, the left calcarine sulcus, the occipital-temporal gyrus, and right medial prefrontal cortex exhibited an inverse pattern of site variability.

To further investigate the impacts of site variability on the findings presented, we applied a leave-one-site-out validation (LOSOV) approach. Specifically, we left one of the 15 sites out from the ASD-HC comparisons and repeated the group level analyses using the datasets from the other 14 sites. The site reproducibility of the current findings was measured as the number of replications of the voxelwise ASD-HC significance maps. Figure 5 illustrates the reproducibility of the findings, which were highly replicated for the middle frontal cortex, the right superior temporal sulcus, and left precuneus.

3.5. Behavioral Correlations. The mean 2dReHo values within the right middle frontal gyrus were positively correlated with the ADOS_TOTAL scores ($r = 0.1728$; $P = 0.0171$), whereas the mean 2dReHo values within the right superior temporal sulcus were positively correlated with both the ADOS_COMM ($r = 0.1542$; $P = 0.0428$) and ADOS_STEREO_BEHAV ($r = 0.1620$; $P = 0.0477$) scores.
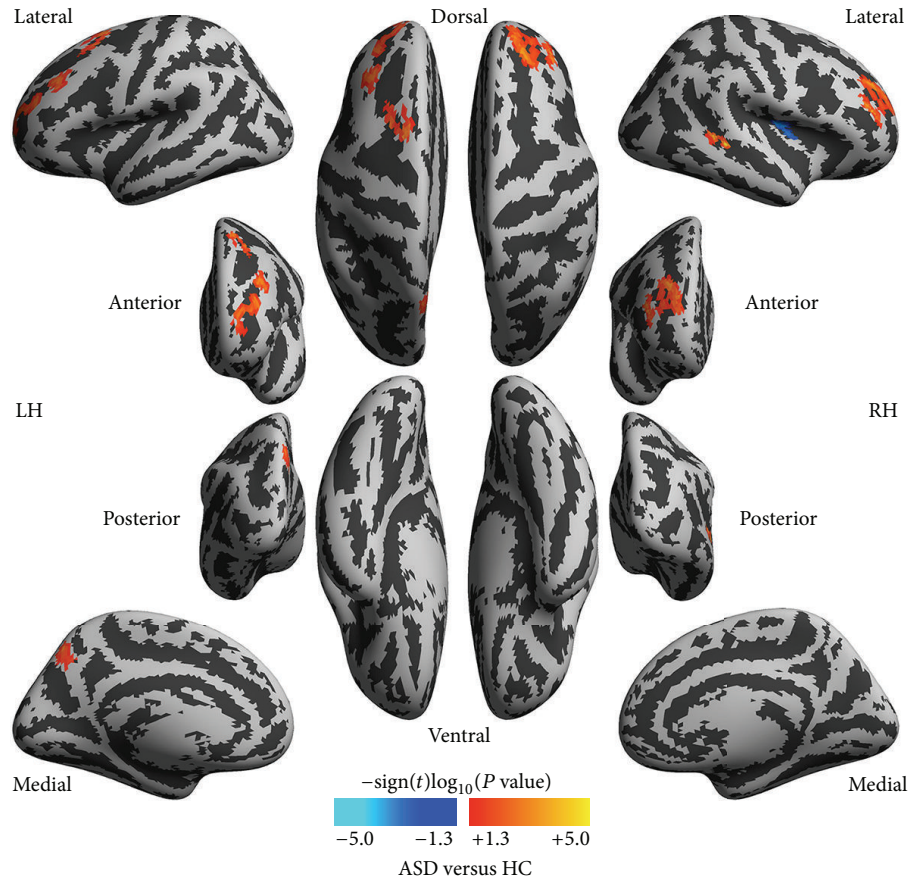
FIGURE 2: Group differences in local functional homogeneity between autism spectrum disorder (ASD) patients and healthy controls (HC). The vertexwise significance of group comparisons is measured with signed $\log_{10}$ transformed P values and is rendered onto the cortical surfaces of the left hemisphere (LH) and right hemisphere (RH). These inflated surfaces are defined by FreeSurfer as the *fsaverage5* surface model and visualized from six different (lateral, medial, posterior, anterior, dorsal, and ventral) views. Light gray colors indicate a cortical gyrus whereas dark gray colors show a cortical sulcus.

4. Discussion

Based upon an aggregated large sample with a wide age range, the ABIDE consortium paper [2] examined different aspects of the functional architecture of autism brains using various derivatives but did not explore age or site effects. The current study quantitatively examined the local functional homogeneity of ASD and age/site effects. Using the ABIDE resting-state FMRI samples of 223 ASD patients and 285 normal controls from 15 different sites, we observed increased local functional homogeneity measured by 2dReHo in the middle frontal cortex, the left precuneus, and the right superior temporal sulcus and decreased 2dReHo in the right insular cortex. Within the left precuneus, ASD patients exhibited decreased 2dReHo with age, but normal controls showed increased 2dReHo with age. Notably, 2dReHo demonstrated a widely distributed spatial pattern of variability across sites. Across-site reproducibility of the observation was thus conducted to show the dependency of our findings, which revealed a novel contribution to assessment to both the variability and reproducibility of the findings across sites in a multicenter design. These findings indicate alterations in the complexity of functional information processing across the

associative cortex and further correlate with multiple behavioral outcomes in ASD. The age-disease interaction offers a target region, the left precuneus, for future developmental studies on ASD.

Consistent with the volume-based 3dReHo method used by Di Martino et al. [2], the middle frontal cortex exhibited increased ReHo in ASD patients. The reduction of ReHo in the right insular cortex in ASD is consistent with a previous study of adults with autism [13]. A study on children with autism [12] reported that the right temporal region exhibited greater ReHo in autism compared with typical developing controls. These consistencies and replications validate our computation and analyses and suggest a possible neuropathology in the frontal, temporal, precuneus (parietal), and insular cortices. A widely distributed spatial pattern of local functional organization across the association cortex is disrupted in ASD. There were also some inconsistencies in the group differences in local functional connectivity between ASD patients and healthy controls across the previous studies. The reason may lie in the heterogeneity of the disorder and the different age distribution of the participants, as well as different methodological choices [4]. More importantly, if ASD was indeed characterized by an atypical neurodevelopmental
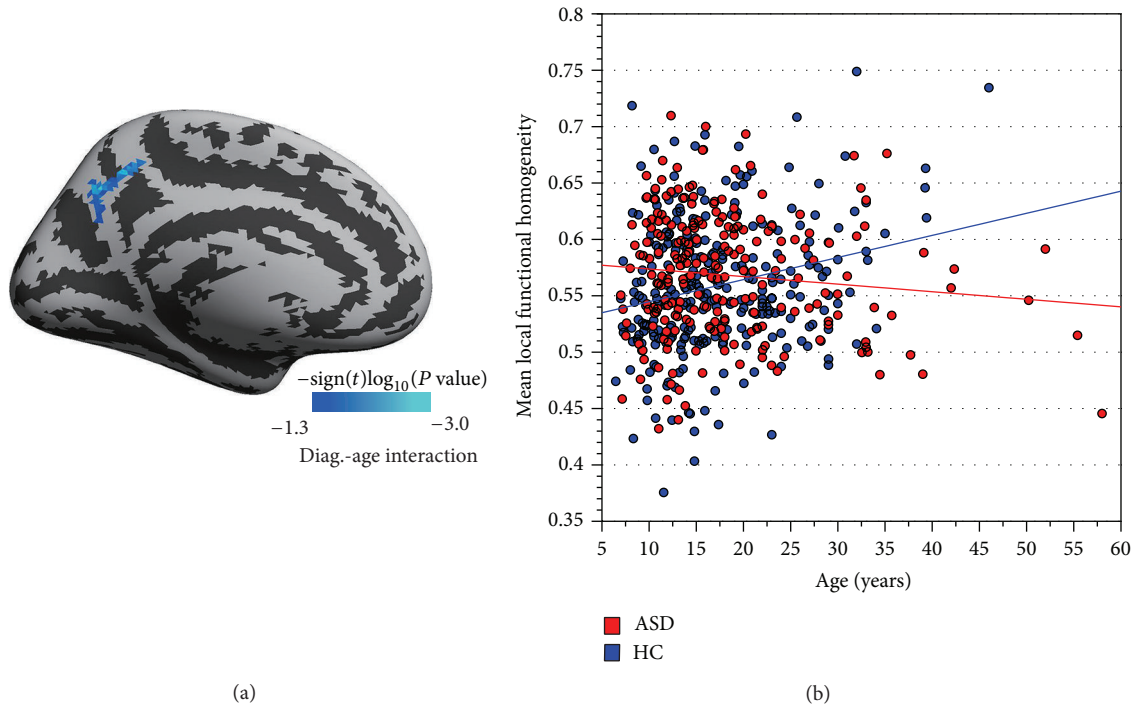
(a)   (b)

FIGURE 3: The vertexwise significance (the signed $\log_{10}$ transformed P values) of interactions between clinical diagnosis (diag.: ASD versus HC) and age is visualized on the left medial cortical surface (a). The details of the diag.-age interaction are further plotted as scatters in (b), where each dot represents the individual mean local functional homogeneity in the left precuneus cluster indicated in (a).
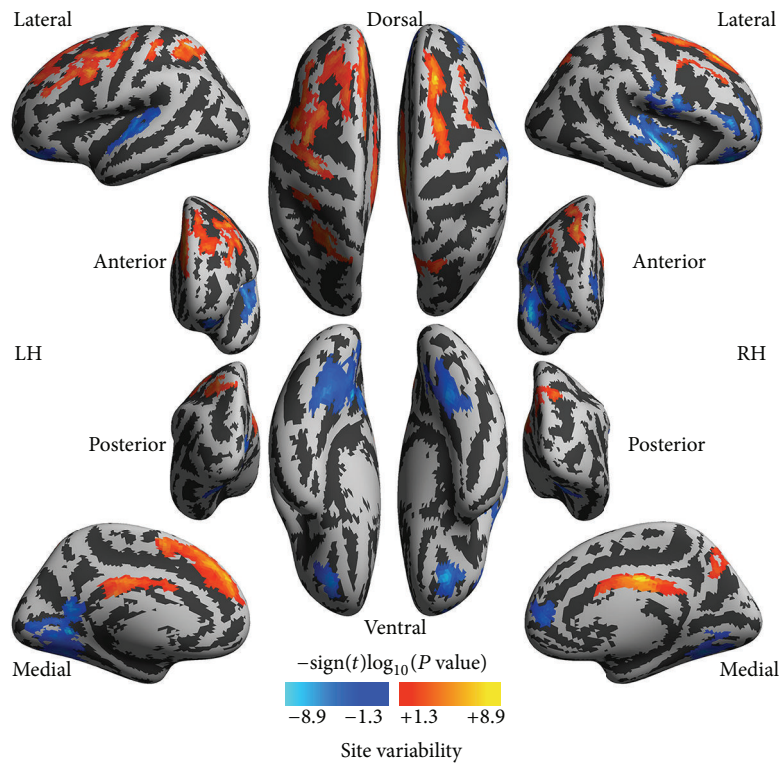

FIGURE 4: Site variability in local functional homogeneity. The vertexwise significance of site variability is measured with signed $\log_{10}$ transformed P values and rendered onto the cortical surfaces of the left hemisphere (LH) and right hemisphere (RH). These inflated surfaces are defined by FreeSurfer as the *fsaverage5* surface model and visualized in six different (lateral, medial, posterior, anterior, dorsal, and ventral) views. Light gray colors indicate a cortical gyrus whereas dark gray colors indicate a cortical sulcus.
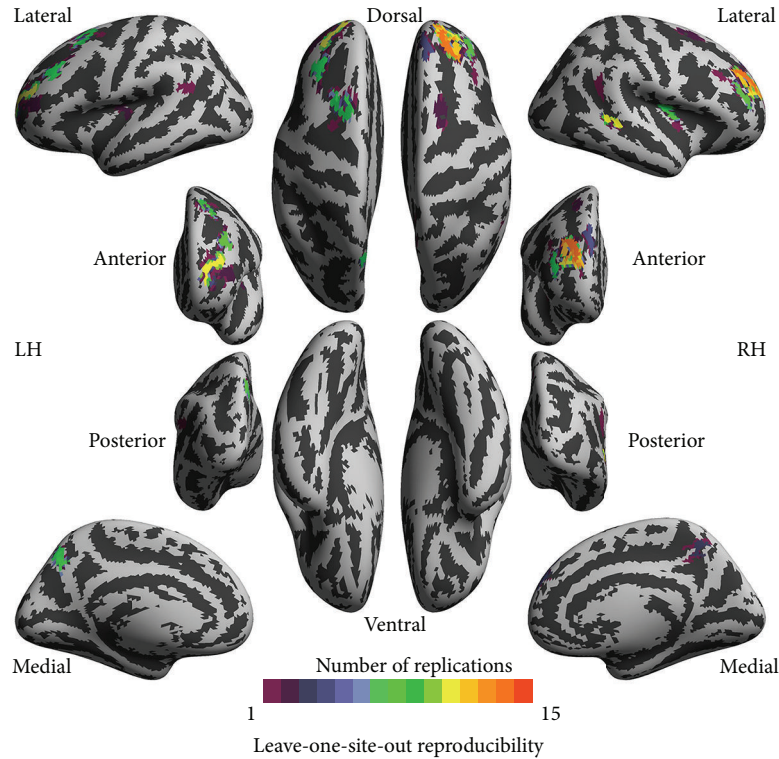
FIGURE 5: Leave-one-site-out reproducibility of group differences in local functional homogeneity between autism spectrum disorders (ASD) patients and healthy controls (HC). The vertexwise numbers of replications of group comparisons are rendered onto the cortical surfaces of the left hemisphere (LH) and right hemisphere (RH). These inflated surfaces are defined by FreeSurfer as the *fsaverage5* surface model and visualized in six different (lateral, medial, posterior, anterior, dorsal, and ventral) views. Light gray colors indicate a cortical gyrus whereas dark gray colors show a cortical sulcus.

pattern, even a moderate difference in the age range could have a substantial influence on the results [40]. Beyond these inconsistencies, the implication of the spatial patterns of local functional organization will be discussed in the following sections.

We observed increased local functional homogeneity in ASD patients compared to normal controls in the middle frontal cortex, part of the prefrontal cortex. In addition to the above evidence for frontal alterations in ASD with 2dReHo, both the fractional amplitude of low-frequency fluctuations and the degree centrality of human brain function exhibited impaired patterns in the frontal cortex in ASD [2]. During brain development, in ASD, higher-order association areas that normally connect to the frontal lobe are partially disconnected [20], and local connectivity is strengthened while long-distance connectivity is impaired in the frontal cortex [5]. Structural abnormalities, such as a thicker left frontal cortex, have also been reported [19]. Based upon our recent study on the neurobiological significance of ReHo in [17], increased ReHo in the middle frontal cortex may indicate reduced functional segregation or a reduced complexity of local information processing. The frontal cortex is responsible for executive function, which may involve coordination of multiple human brain networks [17]. ASD may involve disrupted functional segregation in this area, which may induce abnormal behaviors in patients.

The superior temporal sulcus showed increased ReHo in ASD compared to normal controls. Similar abnormalities in the superior temporal sulcus have been characterized using cerebral blood flow (CBF), brain morphology, and functional metrics in previous studies. In greater detail, metabolism was reduced, as indicated by decreased rCBF, in autistic patients at the superior temporal regions [41]. A decreased concentration of grey matter in the superior temporal sulcus was observed in autistic children [42]. Directly related to the current report, Shukla and colleagues observed that the right temporal regions exhibited greater ReHo in autism compared with typically developing controls [12]. Using the ABIDE datasets, Anderson and colleagues recently reported the best accuracy of whole brain classification between ASD and HC using intrinsic functional connectivity of Wernicke's area, which is located in the temporal lobe [22]. Increases of 2dReHo in the superior temporal sulcus implied decreases of local functional separation or differentiation [17] and a decreased complexity of information processing [17, 43]. Taking this explanation a step further because this area is a part of the language network [44] and ASD patients exhibit abnormal functional architecture of the superior temporal sulcus, these results may explain impaired language function and social interactions in ASD.

The right insula was the only region with decreased ReHo in ASD patients. Abnormality of the insula is one of the most

consistent findings of fMRI studies on ASD. In addition to abnormal ReHo in the insular areas of ASD [13], alterations of VMHC (voxel-mirrored homotopic connectivity) and DC in the insular were observed in ASD [2]. The classification accuracy between ASD and HC using functional connectivity was best in the insular cortex using the same ABIDE data as the current study [22]. Meanwhile, decreased left posterior insular activity during auditory language in autism was reported previously [45]. A longitudinal study on children aged 5–11 years showed decreases in left posterior insular activity with age [46]. Given the neurobiological significance of ReHo [17], decreased ReHo in the insular cortex may indicate decreased functional integration. Considering the roles of the insular region in emotion and decision-making [47] and as a hub in supporting the brain connectome [48, 49], alterations of local functional homogeneity in the insular area may correlate with impaired emotion processing and other high-level cognitive processings in autism.

ASD patients and normal controls displayed different trends of age dependencies. This finding may help to explain the neurodevelopmental mechanisms of ASD. Other studies reported abnormalities in the left precuneus in ASD compared with normal controls. Functional alterations of VMHC [22] and a thicker cortex in the left precuneus gyrus [19] were found in two separate studies. Mak-Fan and colleagues confirmed a similar age by group interaction pattern of overall brain volume, overall grey matter volume, overall surface area, and mean thickness of the brain in ASD and HC [19]. Another study also explored the age by group interaction in ASD focusing on brain morphology [18]. Importantly, the current study found consistent group differences and age by group interactions in the left precuneus gyrus. The left precuneus may therefore be a target region for future developmental studies of ASD.

The increases of local functional homogeneity in the right middle frontal gyrus and right superior temporal sulcus in ASD are associated with the severity of ASD symptoms. Considering both the high test-retest reliability [16] and the emerging neurobiological significance of 2dReHo, we propose that 2dReHo may serve as a neuroimaging marker for the diagnosis, treatment, and prevention of ASD in the future [50]. As illustrated in the group difference subsection of the Discussion, the frontal cortex and superior temporal sulcus are two major areas of autism studies for both brain structure and function [20, 51]. The current findings were also mostly reproducible across different sites for these two regions (Figure 5). The correlations of average ReHo with ADOS symptoms indicate that these regions may be targets for further explorations of the neuropathology of ASD [51].

4.1. Limitations and Future Directions. The ABIDE consortium paper [2] reported less commonly explored regions such as the thalamus. In the current study, the subcortical regions and cerebellum were excluded due to the limitation of the surface-based ReHo method. These regions may be a direction of future studies by developing surface-based ReHo approaches for these noncerebral structures. The second limitation of ReHo is its nature of local short-range connectivity and being not suitable for characterizing global long-range

connectivity. A sample limitation is that the sample was composed of mainly males with ASD (>90%). Therefore, sex differences may be crucial in ASD progression during brain development, and future studies with a comparable number of male and female ASD patients could improve our understanding of the neuropathology of the disorder. Thirdly, the subgroup of ASD generally included autism, Asperger's syndrome, or PDD-NOS. There is an ongoing debate about clinical standards for the classification of the four subgroups. However, enough samples for each subgroup would give more insight into the classification in terms of neuroimaging-based data mining approaches (see a pilot demonstration in early onset schizophrenia in [52]). Finally, all age-related findings observed in the present study are derived from a cross-sectional dataset and should be interpreted with caution that these age-related changes can be interpreted as developmental effects only with a longitudinal sample in future.

5. Conclusions

In the current study, using the ABIDE sample with 223 ASD and 285 healthy controls with wide age span, we observed increased local functional homogeneity ReHo in the middle frontal sulcus and gyrus, the left precuneus gyrus, and right superior temporal sulcus, together with decreased local functional homogeneity ReHo in the right insular. Significant group by age interactions in the left precuneus gyrus were also found, and the group difference (increased 2dReHo in ASD) decreased with age. At the same time, the average 2dReHo values within the right middle frontal gyrus were significantly positively correlated with ADOS_TOTAL scores, and the average 2dReHo values within the right superior temporal sulcus were significantly positively correlated with ADOS_COMM and ADOS_STEREO_BEHAV scores. All of these findings, especially the consistent group differences, the interaction effects in the precuneus gyrus, and the behavioral correlations, contribute to our understanding of the neurodevelopmental pathological mechanisms of ASD.

Conflict of Interests

The authors declare that there is no conflict of interests regarding the publication of this paper.

Acknowledgments

References

[1] Y. S. Kim, B. L. Leventhal, Y. J. Koh et al., "Prevalence of autism spectrum disorders in a total population sample," *The American Journal of Psychiatry*, vol. 168, no. 9, pp. 904–912, 2011.

[2] A. Di Martino, C.-G. Yan, Q. Li et al., "The autism brain imaging data exchange: towards a large-scale evaluation of the intrinsic brain architecture in autism," *Molecular Psychiatry*, vol. 19, no. 6, pp. 659–667, 2014.

[3] R. C. M. Philip, M. R. Dauvermann, H. C. Whalley, K. Baynham, S. M. Lawrie, and A. C. Stanfield, "A systematic review and meta-analysis of the fMRI investigation of autism spectrum disorders," *Neuroscience and Biobehavioral Reviews*, vol. 36, no. 2, pp. 901–942, 2012.

[4] R. A. Müller, P. Shih, B. Keehn, J. R. Deyoe, K. M. Leyden, and D. K. Shukla, "Underconnected, but how? A survey of functional connectivity MRI studies in autism spectrum disorders," *Cerebral Cortex*, vol. 21, no. 10, pp. 2233–2243, 2011.

[5] M. K. Belmonte, G. Allen, A. Beckel-Mitchener, L. M. Boulanger, R. A. Carper, and S. J. Webb, "Autism and abnormal development of brain connectivity," *Journal of Neuroscience*, vol. 24, no. 42, pp. 9228–9231, 2004.

[6] J. R. Hughes, "Autism: the first firm finding = underconnectivity?" *Epilepsy & Behavior*, vol. 11, no. 1, pp. 20–24, 2007.

[7] M. A. Just, V. L. Cherkassky, T. A. Keller, and N. J. Minshew, "Cortical activation and synchronization during sentence comprehension in high-functioning autism: evidence of underconnectivity," *Brain*, vol. 127, no. 8, pp. 1811–1821, 2004.

[8] M. A. Just, V. L. Cherkassky, T. A. Keller, R. K. Kana, and N. J. Minshew, "Functional and anatomical cortical underconnectivity in autism: evidence from an fmri study of an executive function task and corpus callosum morphometry," *Cerebral Cortex*, vol. 17, no. 4, pp. 951–961, 2007.

[9] H. Koshino, P. A. Carpenter, N. J. Minshew, V. L. Cherkassky, T. A. Keller, and M. A. Just, "Functional connectivity in an fMRI working memory task in high-functioning autism," *NeuroImage*, vol. 24, no. 3, pp. 810–821, 2005.

[10] C. S. Monk, S. J. Peltier, J. L. Wiggins et al., "Abnormalities of intrinsic functional connectivity in autism spectrum disorders," *NeuroImage*, vol. 47, no. 2, pp. 764–772, 2009.

[11] P. Shih, M. Shen, B. Öttl, B. Keehn, M. S. Gaffrey, and R.-A. Müller, "Atypical network connectivity for imitation in autism spectrum disorder," *Neuropsychologia*, vol. 48, no. 10, pp. 2931–2939, 2010.

[12] D. K. Shukla, B. Keehn, and R. A. Müller, "Regional homogeneity of fMRI time series in autism spectrum disorders," *Neuroscience Letters*, vol. 476, no. 1, pp. 46–51, 2010.

[13] J.-J. Paakki, J. Rahko, X. Long et al., "Alterations in regional homogeneity of resting-state brain activity in autism spectrum disorders," *Brain Research*, vol. 1321, pp. 169–179, 2010.

[14] D. H. Peng, K. D. Jiang, Y. R. Fang et al., "Decreased regional homogeneity in major depression as revealed by resting-state functional magnetic resonance imaging," *Chinese Medical Journal*, vol. 124, no. 3, pp. 369–373, 2011.

[15] Y. Zang, T. Jiang, Y. Lu, Y. He, and L. Tian, "Regional homogeneity approach to fMRI data analysis," *NeuroImage*, vol. 22, no. 1, pp. 394–400, 2004.

[16] X.-N. Zuo, T. Xu, L. Jiang et al., "Toward reliable characterization of functional homogeneity in the human brain: preprocessing, scan duration, imaging resolution and computational space," *NeuroImage*, vol. 65, pp. 374–386, 2013.

[17] L. Jiang, T. Xu, Y. He et al., "Toward neurobiological characterization of functional homogeneity in the human cortex: regional variation, morphological association and functional covariance network organization," *Brain Structure and Function*, 2014.

[18] A. Raznahan, R. Toro, E. Daly et al., "Cortical anatomy in autism spectrum disorder: an in vivo MRI study on the effect of age," *Cerebral Cortex*, vol. 20, no. 6, pp. 1332–1340, 2010.

[19] K. M. Mak-Fan, M. J. Taylor, W. Roberts, and J. P. Lerch, "Measures of cortical grey matter structure and development in children with autism spectrum disorder," *Journal of Autism and Developmental Disorders*, vol. 42, no. 3, pp. 419–427, 2012.

[20] D. H. Geschwind and P. Levitt, "Autism spectrum disorders: developmental disconnection syndromes," *Current Opinion in Neurobiology*, vol. 17, no. 1, pp. 103–111, 2007.

[21] E. Courchesne and K. Pierce, "Why the frontal cortex in autism might be talking only to itself: local over-connectivity but long-distance disconnection," *Current Opinion in Neurobiology*, vol. 15, no. 2, pp. 225–230, 2005.

[22] J. A. Nielsen, B. A. Zielinski, P. T. Fletcher et al., "Multisite functional connectivity MRI classification of autism: ABIDE results," *Frontiers in Human Neuroscience*, vol. 7, article 599, 2013.

[23] R. W. Cox, "AFNI: software for analysis and visualization of functional magnetic resonance neuroimages," *Computers and Biomedical Research*, vol. 29, no. 3, pp. 162–173, 1996.

[24] R. W. Cox, "AFNI: what a long strange trip it's been," *NeuroImage*, vol. 62, no. 2, pp. 743–747, 2012.

[25] M. Jenkinson, C. F. Beckmann, T. E. J. Behrens, M. W. Woolrich, and S. M. Smith, "FSL," *NeuroImage*, vol. 62, no. 2, pp. 782–790, 2012.

[26] B. Fischl, "FreeSurfer," *NeuroImage*, vol. 62, no. 2, pp. 774–781, 2012.

[27] A. M. Dale, B. Fischl, and M. I. Sereno, "Cortical surface-based analysis: I. Segmentation and surface reconstruction," *NeuroImage*, vol. 9, no. 2, pp. 179–194, 1999.

[28] B. Fischl, M. I. Sereno, and A. M. Dale, "Cortical surface-based analysis: II. Inflation, flattening, and a surface-based coordinate system," *NeuroImage*, vol. 9, no. 2, pp. 195–207, 1999.

[29] B. Fischl, A. Liu, and A. M. Dale, "Automated manifold surgery: constructing geometrically accurate and topologically correct models of the human cerebral cortex," *IEEE Transactions on Medical Imaging*, vol. 20, no. 1, pp. 70–80, 2001.

[30] F. Segonne, A. M. Dale, E. Busa et al., "A hybrid approach to the skull stripping problem in MRI," *NeuroImage*, vol. 22, no. 3, pp. 1060–1075, 2004.

[31] F. Ségonne, J. Pacheco, and B. Fischl, "Geometrically accurate topology-correction of cortical surfaces using nonseparating loops," *IEEE Transactions on Medical Imaging*, vol. 26, no. 4, pp. 518–529, 2007.

[32] X.-X. Xing, Y.-L. Zhou, J. S. Adelstein, and X.-N. Zuo, "PDE-based spatial smoothing: a practical demonstration of impacts on MRI brain extraction, tissue segmentation and registration," *Magnetic Resonance Imaging*, vol. 29, no. 5, pp. 731–738, 2011.

[33] X.-N. Zuo and X.-X. Xing, "Effects of non-local diffusion on structural MRI preprocessing and default network mapping: statistical comparisons with isotropic/anisotropic diffusion," *PLoS ONE*, vol. 6, no. 10, Article ID e26703, 2011.

[34] C.-G. Yan, B. Cheung, C. Kelly et al., "A comprehensive assessment of regional variation in the impact of head micro-movements on functional connectomics," *NeuroImage*, vol. 76, pp. 183–201, 2013.

[35] D. N. Greve and B. Fischl, "Accurate and robust brain image alignment using boundary-based registration," *NeuroImage*, vol. 48, no. 1, pp. 63–72, 2009.

[36] B. T. T. Yeo, F. M. Krienen, J. Sepulcre et al., "The organization of the human cerebral cortex estimated by intrinsic functional connectivity," *Journal of Neurophysiology*, vol. 106, no. 3, pp. 1125–1165, 2011.

[37] J. D. Power, K. A. Barnes, A. Z. Snyder, B. L. Schlaggar, and S. E. Petersen, "Spurious but systematic correlations in functional connectivity MRI networks arise from subject motion," *NeuroImage*, vol. 59, no. 3, pp. 2142–2154, 2012.

[38] R. Patriat, E. K. Molloy, T. B. Meier et al., "The effect of resting condition on resting-state fMRI reliability and consistency: a comparison between resting with eyes open, closed, and fixated," *NeuroImage*, vol. 78, pp. 463–473, 2013.

[39] C. Lord, S. Risi, L. Lambrecht et al., "The Autism Diagnostic Observation Schedule-Generic: a standard measure of social and communication deficits associated with the spectrum of autism," *Journal of Autism and Developmental Disorders*, vol. 30, no. 3, pp. 205–223, 2000.

[40] K. Mevel, P. Fransson, and S. Bolte, "Multimodal brain imaging in autism spectrum disorder and the promise of twin research," *Autism*, vol. 18, no. 5, pp. 1–15, 2014.

[41] T. Ohnishi, H. Matsuda, T. Hashimoto et al., "Abnormal regional cerebral blood flow in childhood autism," *Brain*, vol. 123, no. 9, pp. 1838–1844, 2000.

[42] N. Boddaert, N. Chabane, H. Gervais et al., "Superior temporal sulcus anatomical abnormalities in childhood autism: a voxel-based morphometry MRI study," *NeuroImage*, vol. 23, no. 1, pp. 364–369, 2004.

[43] J. S. Anderson, B. A. Zielinski, J. A. Nielsen, and M. A. Ferguson, "Complexity of low-frequency blood oxygen level-dependent fluctuations covaries with local connectivity," *Human Brain Mapping*, vol. 35, no. 4, pp. 1273–1283, 2014.

[44] A. D. Friederici and S. M. Gierhan, "The language network," *Current Opinion in Neurobiology*, vol. 23, no. 2, pp. 250–254, 2013.

[45] J. S. Anderson, N. Lange, A. Froehlich et al., "Decreased left posterior insular activity during auditory language in autism," *American Journal of Neuroradiology*, vol. 31, no. 1, pp. 131–139, 2010.

[46] J. P. Szaflarski, V. J. Schmithorst, M. Altaye et al., "A longitudinal functional magnetic resonance imaging study of language development in children 5 to 11 years old," *Annals of Neurology*, vol. 59, no. 5, pp. 796–807, 2006.

[47] T. R. Scott, "Insular cortex as a mediator of emotion: commentary on emotion and decision-making explained, by Edmund T. Rolls," *Cortex*, 2014.

[48] X.-N. Zuo, R. Ehmke, M. Mennes et al., "Network centrality in the human functional connectome," *Cerebral Cortex*, vol. 22, no. 8, pp. 1862–1875, 2012.

[49] M. P. van den Heuvel and O. Sporns, "Rich-club organization of the human connectome," *The Journal of Neuroscience*, vol. 31, no. 44, pp. 15775–15786, 2011.

[50] M. Zilbovicius, I. Meresse, N. Chabane, F. Brunelle, Y. Samson, and N. Boddaert, "Autism, the superior temporal sulcus and social perception," *Trends in Neurosciences*, vol. 29, no. 7, pp. 359–366, 2006.

[51] X. N. Zuo and X. X. Xing, "Test-retest reliabilities of resting-state FMRI measurements in human brain functional connecomics: a systems neuroscience perspective," *Neuroscience & Biobehavioral Reviews*, vol. 45, pp. 100–118, 2014.

[52] Z. Yang, Y. Xu, T. Xu et al., "Brain network informed subject community detection in early-onset schizophrenia," *Scientific Reports*, vol. 4, article 5549, 2014.

Research Article

Aberrant Functional Connectivity Architecture in Alzheimer's Disease and Mild Cognitive Impairment: A Whole-Brain, Data-Driven Analysis

Bo Zhou,[1] Hongxiang Yao,[2] Pan Wang,[1] Zengqiang Zhang,[1,3] Yafeng Zhan,[4,5] Jianhua Ma,[5] Kaibin Xu,[4,6] Luning Wang,[1] Ningyu An,[2] Yong Liu,[4,6] and Xi Zhang[1]

[1]*Department of Neurology, Institute of Geriatrics and Gerontology, Chinese PLA General Hospital, Beijing 100853, China*

[2]*Department of Radiology, Chinese PLA General Hospital, Beijing 100853, China*

[3]*Hainan Branch of Chinese PLA General Hospital, Sanya 572014, China*

[4]*Brainnetome Center, Institute of Automation, Chinese Academy of Sciences, Beijing 100190, China*

[5]*School of Biomedical Engineering, Southern Medical University, Guangzhou, Guangdong 510515, China*

[6]*National Laboratory of Pattern Recognition, Institute of Automation, Chinese Academy of Sciences, Beijing 100190, China*

Correspondence should be addressed to Yong Liu; yliu@nlpr.ia.ac.cn and Xi Zhang; zhangxi@301hospital.com.cn

The purpose of our study was to investigate whether the whole-brain functional connectivity pattern exhibits disease severity-related alterations in patients with Alzheimer's disease (AD) and mild cognitive impairment (MCI). Resting-state functional magnetic resonance imaging data were acquired in 27 MCI subjects, 35 AD patients, and 27 age- and gender-matched subjects with normal cognition (NC). Interregional functional connectivity was assessed based on a predefined template which parcellated the brain into 90 regions. Altered whole-brain functional connectivity patterns were identified via connectivity comparisons between the AD and NC subjects. Finally, the relationship between functional connectivity strength and cognitive ability according to the mini-mental state examination (MMSE) was evaluated in the MCI and AD groups. Compared with the NC group, the AD group exhibited decreased functional connectivities throughout the brain. The most significantly affected regions included several important nodes of the default mode network and the temporal lobe. Moreover, changes in functional connectivity strength exhibited significant associations with disease severity-related alterations in the AD and MCI groups. The present study provides novel evidence and will facilitate meta-analysis of whole-brain analyses in AD and MCI, which will be critical to better understand the neural basis of AD.

1. Introduction

It has been estimated that more than 81.1 million individuals will suffer from dementia by 2040, and Alzheimer's disease (AD) will account for the underlying pathology in the majority of these cases [1]. Mild cognitive impairment (MCI) is a stage involving greater cognitive decline than expected based on an individual's age and educational level. MCI is thought to be the prodromal stage of dementia; in particular, the amnestic subtype of MCI carries a very high risk of progression to AD [2]. Nevertheless, the definitive relationship between AD and MCI requires further investigation.

The past decade has witnessed great progress in resting-state functional magnetic resonance imaging (rs-fMRI), which is based on the measurement of spontaneous low-frequency fluctuations of blood oxygen level-dependent (BOLD) signals [3]. The correlations/similarities of these types of fluctuations among various brain regions have been thought to represent the interregional functional connectivity [4]. Convergent evidence identified via rs-fMRI has suggested that alterations in functional connectivity/networks are prevalent in AD and MCI [5–14]. Thus, the previous literature has suggested that AD/MCI is a disconnection syndrome [15–17].
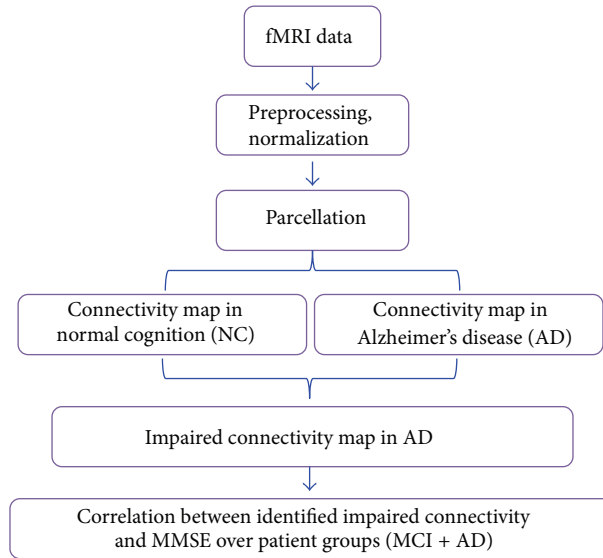
Figure 1: Schematic map of the experimental design of the present study.

Despite previous elegant studies that identified alterations in the connections between specific brain regions or networks [8, 10, 18–23], the patterns of whole-brain resting-state functional connectivity in AD and MCI have not been well studied, which may limit our understanding of the pathophysiological substrate of the disease from an integrative perspective. In the first whole-brain connectivity study in AD, Wang and colleagues demonstrated that AD patients exhibited an anterior-posterior disconnection phenomenon, especially between the prefrontal and parietal lobes, as well as compensatory increases in intralobe connections [11]. In MCI subjects, Bai and colleagues also found diffuse abnormalities in functional connections, especially between the subcortical regions and the frontal cortices. These disturbances were related to cognitive variables and became more evident over time [5]. Almost at the same time, Chen and colleagues demonstrated that impairments in the functional connectivity strength were significantly correlated with cognitive abilities in AD/MCI subjects, and the large-scale interconnectivity patterns among brain regions can be used to differentiate cognitively normal subjects from patients with AD or MCI [7]; these findings are consistent with other independent classification studies [24–26]. Using detailed parcellated brain regions, Liu and colleagues demonstrated that the disease severity was related to the loss of long-distance connectivity in AD and MCI [9]. Despite the diversity of the results, these studies support the hypothesis that AD is a disconnection syndrome [16, 17]. Moreover, an additional independent whole-brain functional connectivity study based on a larger sample will further strengthen our understanding of the impaired functional connectivity patterns and provide novel evidence for a future meta-analysis of AD/MCI.

Based on the previous literature, we hypothesized that the changes in functional connectivity would represent the distribution of decreased long-distance interregions in AD.

We also expected that the altered brain functional connectivity in AD patients would be decreased in subjects with MCI. Furthermore, the abnormal brain functional connectivity would be correlated with variations between patients in the severity of cognitive impairment according to the mini-mental state examination (MMSE). To test these hypotheses in the current study, we explored functional connectivity throughout the brain to investigate whether alterations exist in 35 patients with severe AD and 27 age-matched volunteers with normal cognition (NC). First, we investigated interregional functional connectivity by dividing each individual's brain into 90 regions using an automated anatomical labeling (AAL) template [27]. Second, we identified significant differences in functional connectivities via comparisons of the correlation coefficients of each pair of brain regions between the AD and NC samples. To determine whether the identified altered functional connectivity varied with disease progression, Pearson's correlation analyses were performed between the functional connectivity strengths and the clinical variables (MMSE) in the MCI and AD patients (Figure 1).

2. Materials and Methods

The samples used in the present study have been examined in our previous studies of regional homogeneity [13], amygdalar connectivity [12, 28], thalamic connectivity [14], and marginal division connectivity [29] during resting states. All subjects met identical methodological stringency criteria, and the comprehensive clinical details have been described in our previous work [12–14, 29]. This study is orthogonal to any previously published studies, which ensures the independence of the reported effects. However, we have provided a brief introduction regarding the data inclusion/exclusion criteria, acquisition, and processing to maintain the scientific integrity of the present study.

2.1. Standard Protocol Approvals, Registration, and Patient Consent. This study was approved by the Medical Ethics Committee of PLA General Hospital. Written informed consent was obtained from each enrolled subject or his/her authorized guardian. The participants underwent general physical, psychological, and laboratory examinations prior to enrollment in the formal study. The participants did not take medications that might have influenced cognition during the scans, and all patients received professional suggestions for further treatment.

2.2. Subjects. The participants were recruited from two sources: outpatients from the Chinese PLA General Hospital or recruitment through a website advertisement (http://www.301ad.com.cn/, Chinese version). Each subject was right-handed and underwent a battery of neuropsychological tests, including the MMSE, Montreal Cognitive Assessment, Trail Making Test, Clock Drawing Test, Similarities Test, Complex Figure Replication, Verbal Fluency Test, Auditory Verbal Learning Test (AVLT), Geriatric Depression Scale, Clinical Dementia Rating (CDR), and Activities of Daily Living (ADL) scale. The detailed diagnostic criteria for AD, amnestic MCI, and normal healthy aging can be found in our previous studies [12–14]. Briefly, following the exclusion of subjects with substantial head motion (see the criteria for data preprocessing), 89 subjects, including 27 MCI subjects, 35 AD patients, and 27 age- and gender-matched normal cognitive (NC) subjects, were included in the subsequent analyses. The demographic and neuropsychological details regarding the subjects are shown in Table S1 (see Table S1 in Supplementary Material available online at http://dx.doi.org/10.1155/2015/495375).

2.3. Data Acquisition. A 3.0 T GE MR system (GE Healthcare, USA) with a standard head coil was used to acquire the MR images. Resting-state fMRI scans were performed using an echo planar imaging (EPI) sequence with the following parameters: repetition time = 2,000 ms, echo time = 30 ms, flip angle = 90°, matrix = 64 × 64, field of view = 220 × 220 mm^2, slice thickness = 3 mm, and slice gap = 1 mm. Each volume comprised 30 axial slices, and each functional run lasted for 6 minutes and 40 seconds. During the scanning, the subjects were instructed to keep their eyes closed and to relax; comfortable foam padding was used to minimize head motion, and ear plugs were used to reduce the scanner noise. For each subject, T2-weighted images were collected and evaluated by two senior radiologists during the scan.

2.4. Connectivity Analysis Pipeline. The analysis consisted of the following steps: (1) data preprocessing; (2) defining brain nodes with whole-brain parcellation; (3) calculating connectivity matrices for each subject; (4) comparing matrices to identify significant differences between groups in terms of correlation strength; and (5) investigating the relationships between altered functional connectivity and cognitive variables (see Figure 1 for a schematic of this analysis).

2.5. Data Preprocessing. The data were preprocessed in steps consistent with the protocols of our previously published studies using in-house Brainnetome fMRI toolkit (Brat, http://www.brainnetome.org/en/brat) based on statistical parametric mapping (SPM8, http://www.fil.ion.ucl.ac.uk/spm/). These steps included (1) slice-timing for time correction, (2) realignment to reduce head motion, (3) normalization to a standard EPI template and reslicing to 2 × 2 × 2 mm cubic voxels, (4) denoising by regressing out several effects, for example, six motion parameters, linear drift, and the mean time series of all voxels within the white matter and cerebrospinal fluid, and (5) temporal filtering (0.01–0.08 Hz) to reduce noise [9, 12–14].

2.6. Defining the Connectivity Nodes. The registered normalized fMRI time series were segmented into 90 regions (45 regions per hemisphere, Table S2) using an automated anatomical labeling template [27] that has been used in several previous studies [30–36]. For each sample, a representative time series of each brain region was obtained by averaging the fMRI time series over all voxels in the region.

2.7. Estimation of Interregional Functional Connectivity. The regional mean time series were estimated by averaging the time series of all voxels in the region [31, 37, 38]. Pearson's correlation coefficients were computed between each pair of brain regions for each subject. For subsequent statistical analysis, Fisher's r-to-z transformation was applied to improve the normality of the correlation coefficients [32, 33]. To determine whether disease severity-related alterations existed, we also evaluated altered whole-brain connectivity patterns between the NC and MCI, MCI and AD, and NC and AD groups.

Individual z-scores were compared using a one-sample two-tailed t-test to determine whether the two brain regions exhibited significant functional connectivity within each group. They were also analyzed by a two-sample two-tailed t-test to determine whether the functional connectivities were significantly different between the AD and NC groups. A two-sample two-tailed t-test was performed for all 4005 (90 × 89/2) functional connectivities; thus, a correction for multiple comparisons was strictly necessary. The false discovery rate (FDR) approach was applied to identify a threshold that would restrict the expected proportion of type I errors [38, 39]. In this study, we identified significant differences in the functional connectivities between the normal healthy and AD subjects according to the following two criteria: (a) the z values were significantly different from zero in at least one group at $P < 0.05$ (one-sample two-tailed t-test; Bonferroni corrected) and (b) the z-scores were significantly different between the two groups at $P < 0.05$ (two-sample two-tailed t-test; FDR-corrected).

2.8. Relationship between Altered Functional Connectivity and Cognitive Ability. To investigate the relationship between functional connectivity strength and cognitive ability, we also evaluated Pearson's correlation between the MMSE scores (as a measure of cognitive function) and functional connectivity
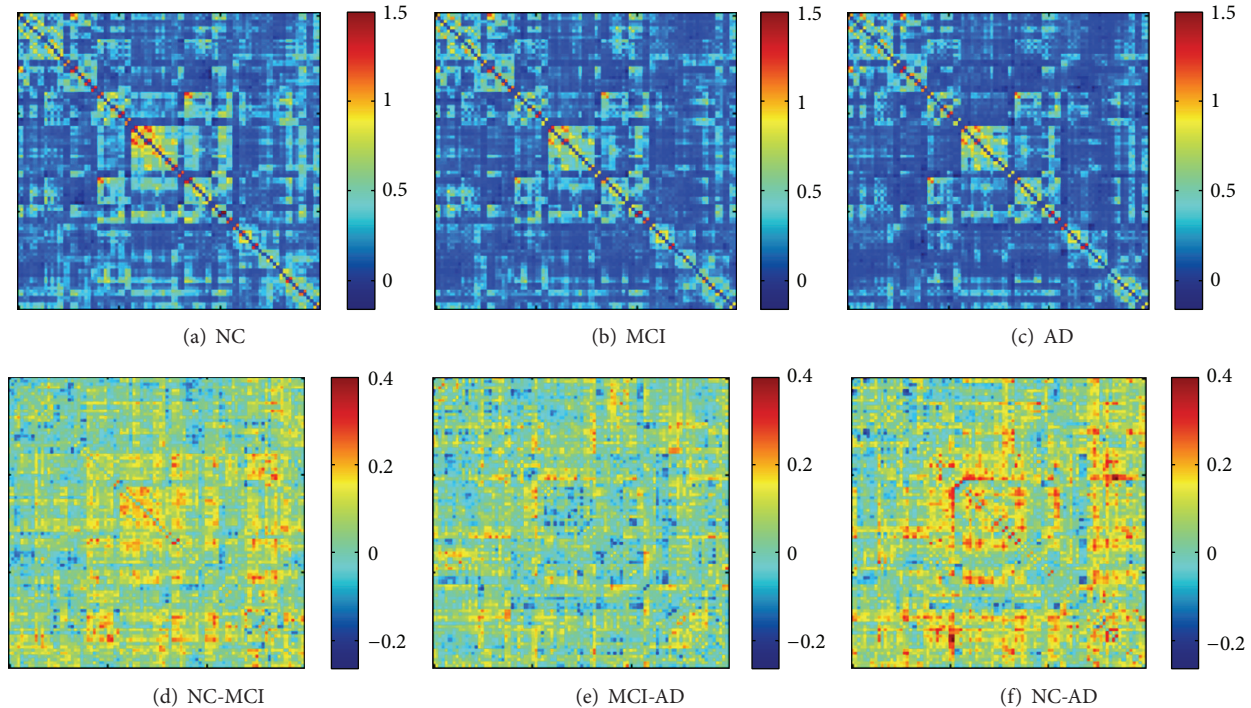
(a) NC

(b) MCI

(c) AD

(d) NC-MCI

(e) MCI-AD

(f) NC-AD

FIGURE 2: Mean absolute z-score matrices for normal control (a), MCI (b), and AD (c). Each figure shows a 90×90 square matrix, in which each entry indicates the mean functional connectivity strength between the corresponding pair of brain regions. The diagonal running from the lower right to the upper left is intentionally set in black. The z-score of the functional connectivity is indicated with a colored bar. The lower row indicates the regions that exhibit visual differences between the normal control and MCI (d), MCI and AD (e), and normal control and AD groups (f), which were calculated using the functional connectivity strengths of the former minus the latter.

strength among the identified functional connectivities in the MCI, AD, and MCI plus AD groups. Because these relationships were exploratory in nature, we used a statistical significance level of $P < 0.05$ (uncorrected).

3. Results

3.1. Direct Comparisons between Groups. For each group, the mean functional connectivity matrix was calculated by averaging the $N \times N$ ($N = 90$ in the present study) connection matrix of all subjects. In the NC group, most of the strong functional connectivities (large z-scores) were between interhemispheric homogeneous regions, within a lobe, and between anatomically adjacent brain areas (Figure 2(a)), which is consistent with many previous studies of whole-brain functional connectivity during the resting state [9, 11, 30–32, 36, 40]. The AD and MCI groups exhibited similar functional connectivity patterns compared with that of the NC group (main effect of group, $F_{2,86} = 2.55$, $P = 0.084$) (Figures 2(b) and 2(c)). Post hoc analysis demonstrated that the mean correlation strength was slightly lower in the AD group compared with the normal cognitive subjects (main effect of group, $F_{1,52} = 3.4$, $P = 0.070$). The mean correlation strength in the MCI group was located between those of the normal cognitive and AD groups (Figures 2(d)–2(f)).

Specifically, compared with the normal cognitive subjects, the AD group exhibited decreased functional connectivities

at the threshold of $P < 0.05$ (FDR-corrected) (Figure 3(a)). The most significantly affected regions included several important nodes of the default mode network (DMN), such as the posterior cingulate gyrus (PCC), the medial superior frontal gyrus (SFGmed), the precuneus (PCUN), and the parahippocampal gyrus (PHIP), as well as the median- and paracingulate gyrus (MCC), the superior occipital gyrus (SOG), and the paracentral lobule (PCL) (Figure 3(a), for details, please refer to Table S3 and Figure S1). We also noted that the most affected type of functional connectivity was the interlobe connections, such as the temporal lobe to the frontal and parietal lobes, and that the most affected brain lobe was the temporal lobe (Figure 3(b), for details, please refer to Table S3 and Figure S1).

3.2. Clinical Cognitive Variables and Functional Connectivity Strength. The results showed that approximately half (35 of 76 altered connectivities) of the decreased functional connectivities exhibited significantly positive correlations with the MMSE scores in the MCI and AD patients ($P < 0.05$). Namely, increased illness severity was correlated with reduced functional connectivity strength (Figure 4(c), Table S3). For the identified altered brain regions, we determined that only a subset of functional connectivities between the various regions were significantly correlated with the MMSE scores in the AD or MCI groups (Figures 4(a) and 4(b) and Table S3). For example, the functional connectivity between
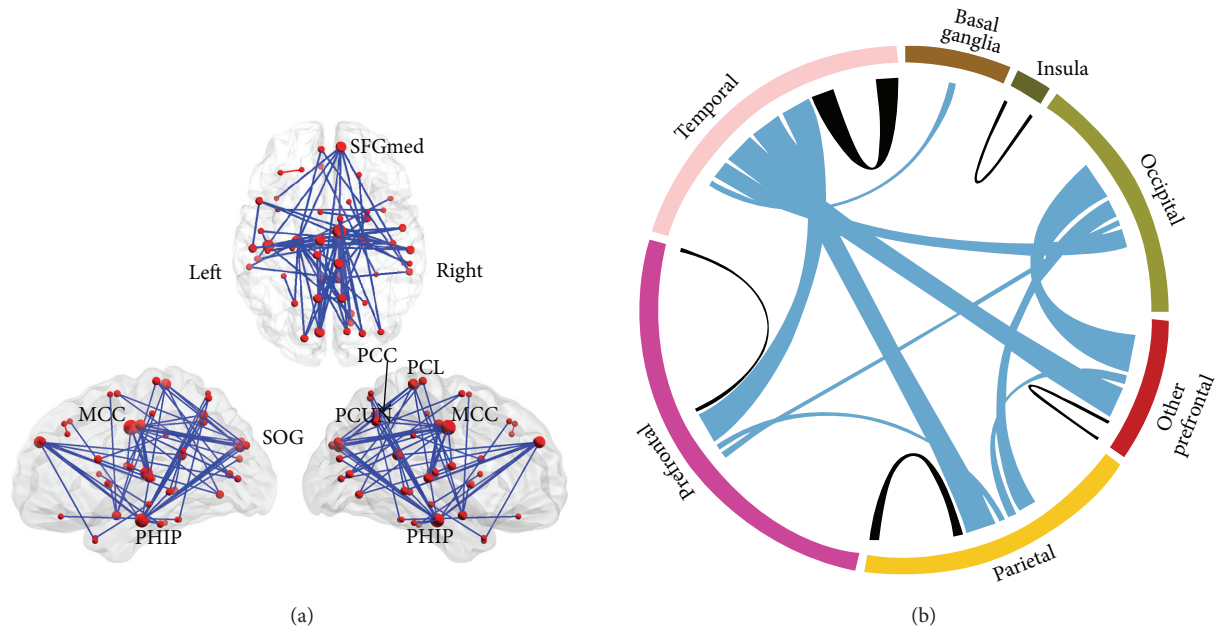
FIGURE 3: Altered whole-brain connectivity patterns in the AD group compared with the normal control group. (a) Three-dimensional representation of the connectivities and most of the affected nodes ($P < 0.05$, FDR-corrected) in AD. The blue and red lines denote decreased and increased functional connectivities, respectively. (b) Distribution of the altered functional connectivities. The colored ring represents the various brain lobes. The blue and black colors represent the interlobe and intralobe functional connectivities, respectively. For details, please see Tables S2-S3 and Figure S1.

the right medial superior frontal gyrus (SFGmed) and the posterior cingulate gyrus (PCC) exhibited the strongest correlation in the patients (Figure 4(f) and Table S3); there was also a strong correlation in the AD group (Figure 4(e)) and a tendency toward correlation in the MCI group (Figure 4(d)).

4. Discussion

Consistent with previous studies, the present study identified widespread impaired functional connectivity patterns in AD patients, including anterior-posterior and interlobe disconnections [5, 7, 9, 11, 25]. These findings indicate that the pattern of decreased long-distance connection is a consistent functional manifestation in AD patients and supports the notion that AD is a disconnection syndrome [16, 17]. More importantly, the present results demonstrated that the identified impaired connectivity strengths in the MCI patients were located between those of the normal cognitive subjects and AD patients (Figures 2(d)–2(f)) and that most of the identified functional connectivity strengths were significantly correlated with cognitive variables in the patient groups (Figure 4). Thus, these findings provide additional evidence that MCI is a prodromal stage of AD [41].

Consistent with the findings of previous whole-brain studies [11, 26], the present study demonstrated that the connectivities of several important nodes of the default mode network, such as the PCC, the precuneus, the parahippocampal gyrus, and the medial superior frontal gyrus, are affected in AD/MCI subjects (Figures 4 and S1 and Table S2). The default mode network plays a key role in various cognitive

processes, such as remembering past events, envisioning the future [3, 42–44], and episodic memory [6, 43]. These cognitive functions are particularly vulnerable in AD/MCI [45, 46] and have been thoroughly studied using multiple imaging techniques, including positron emission tomography, diffusion MRI, structural MRI, and functional MRI. Imaging findings have consistently identified abnormal changes in the default mode network and its relationship to the cognitive degradation observed in AD/MCI patients (for a review, see [6, 8, 47–49]). It should be highlighted that the present study demonstrated that decreased functional connectivity is positively correlated with impaired cognitive ability according to MMSE scores (Figure 4 and Table S3). This finding illustrates that the default mode network is the most affected network, and an abnormal change in this network may represent a potential biomarker for the early identification of MCI and AD.

The temporal lobe, especially the parahippocampal gyrus, exhibited most changes in interlobe functional connectivity (Figures 3 and S1). The temporal lobe is associated with complex functions that range from primary auditory sensation to advanced cognitive roles, such as social cognition and memory [50–52], and most of these functions are impaired in AD/MCI. The anterior parahippocampal region was identified as the first site of neurofibrillary tangles in AD via neuropathological studies [53, 54]. Previous studies have also indicated that volume loss of parahippocampal white matter contributes to the memory impairments observed in mild AD and can be considered a predictor of MCI and AD [55, 56]. Studies have also indicated that certain regions

(a) MCI   (b) AD   (c) MCI and AD

(d) MCI   (e) AD   (f) MCI and AD
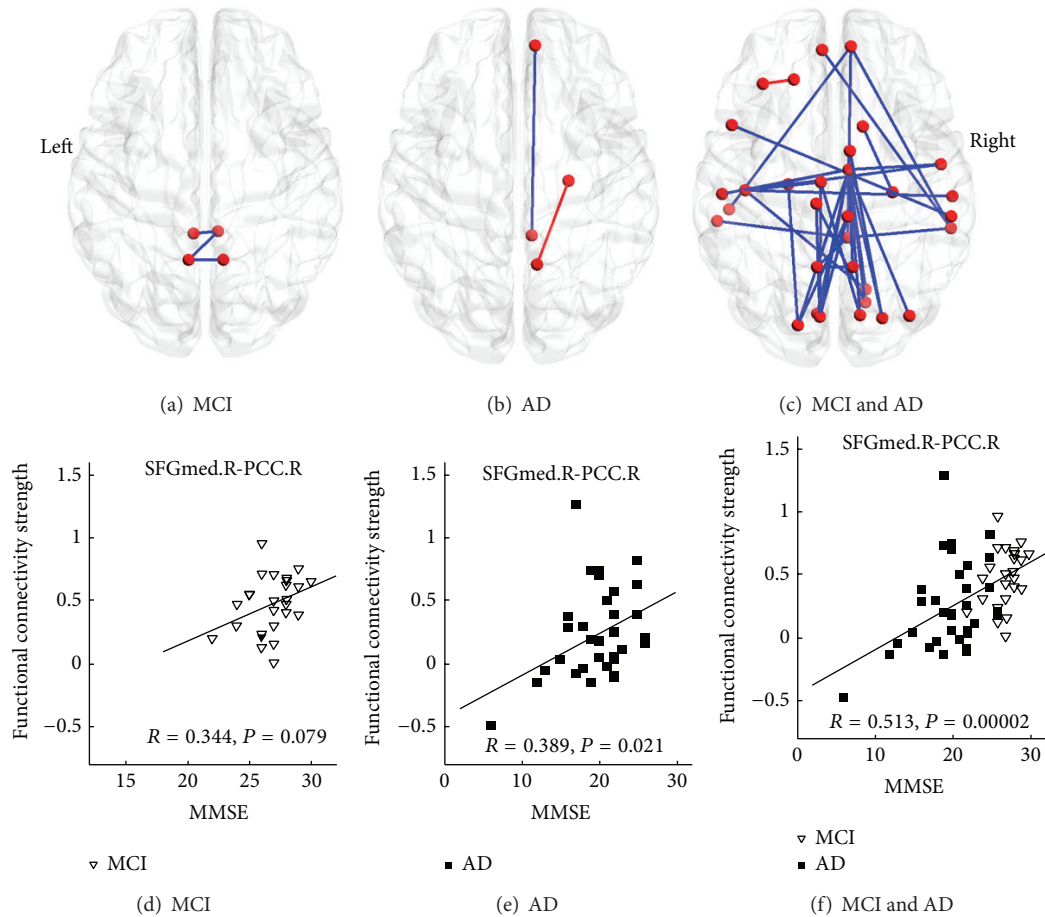
FIGURE 4: The correlation between the MMSE scores and the functional connectivity strengths. The upper line denotes the functional connectivities significantly correlated with the MMSE scores in the MCI (a), AD (b), and combined MCI and AD (c) groups. The blue color represents the functional connectivity that is positively correlated with the MMSE scores, and the red color represents the functional connectivity that is negatively correlated with the MMSE scores. The lower line denotes the correlation between the MMSE scores and the functional connectivity strength (e.g., between the right medial superior frontal gyrus (SFGmed) and the posterior cingulate gyrus (PCC)) in the MCI (d), AD (e), and combined AD and MCI (f) groups. For details, please refer to Table S3.

in the temporal lobe, especially the parahippocampus and hippocampus, are key regions of the episodic memory network [57–59]. Episodic memory impairment is typically the earliest symptom and a core clinical symptom of AD and MCI [45, 46]. Therefore, the impaired interlobe functional connectivity of the temporal lobe and its correlation with reduced cognitive ability may be indirectly associated with broad cognitive functional degradation, such as the episodic memory impairment in AD/MCI subjects.

We also found abnormal functional connectivities to the MCC in the AD subjects in the present study (Figures 3 and S1 and Table S3), in agreement with the results of previous studies [5, 11]. The MCC is involved in rather complex cognitive and emotional functions (e.g., cognitive control and negative affect) [60–63] and has been identified as one of the most affected regions by the impaired glucose metabolism that occurs in AD/MCI [64]. Interestingly, the connectivity strengths between the MCC and several regions, including the precuneus and superior temporal lobe, were significantly correlated with the MMSE scores in the AD and MCI groups

(Figure 4(c), Table S3). Considering this phenotype and the fact that emotional dysfunction is also a key component of clinical manifestations of AD/MCI [65], we speculate that the altered functional connections between the MCC and other regions may be related to cognitive and emotional impairments in AD/MCI.

It should be noted that we assessed whole-brain functional connectivity to evaluate disease severity-related altered functional connectivity patterns in AD subjects. We then investigated the patterns of the identified connectivities in MCI, which may have missed some information, such as the connectivities that exhibited a compensatory increase in the AD/MCI subjects. The identified altered functional connectivities in AD did not exhibit strong correlations with those of the MCI group regarding the relationship between functional connectivity strength and cognitive ability; only the combined patient groups exhibited significant disease severity-related correlations. One potential reason may be because of the limited sample size of each subgroup; thus, these findings should be carefully interpreted because not all

MCI subjects will convert to AD. We should also note that the atlas used in the present study is still not a well-defined parcellated template for regions with inhomogeneous functions; for example, the thalamus can be further parcellated into finely defined subregions [66, 67]. Thus, the development of a new, well-defined connectivity atlas combined with the assessment of neuropsychiatric symptoms is needed to better elucidate the precise neural mechanism of AD/MCI.

5. Conclusion

The present data-driven whole-brain functional connectivity study demonstrated that brain functional connectivity patterns are significantly impaired in AD/MCI patients. Distributions of abnormal functional connectivity were identified in several important nodes of the default mode network, but they were not confined to this network. More importantly, decreased functional connectivity strength was significantly and positively correlated with the MMSE scores in the MCI and AD patients, suggesting that altered connectivities are related to disease severity and clinical manifestations. These results increase the current understanding of the specific alterations in whole-brain functional connectivity patterns in these patients and contribute novel data for future meta-analysis to examine the impaired connectivity patterns in AD/MCI.

Conflict of Interests

The authors declare that there is no conflict of interests regarding the publication of this paper.

Acknowledgments

References

[1] C. Ballard, S. Gauthier, A. Corbett, C. Brayne, D. Aarsland, and E. Jones, "Alzheimer's disease," *The Lancet*, vol. 377, no. 9770, pp. 1019–1031, 2011.

[2] R. C. Petersen, R. O. Roberts, D. S. Knopman et al., "Mild cognitive impairment: ten years later," *Archives of Neurology*, vol. 66, no. 12, pp. 1447–1455, 2009.

[3] M. D. Fox and M. E. Raichle, "Spontaneous fluctuations in brain activity observed with functional magnetic resonance imaging," *Nature Reviews Neuroscience*, vol. 8, no. 9, pp. 700–711, 2007.

[4] B. Biswal, F. Z. Yetkin, V. M. Haughton, and J. S. Hyde, "Functional connectivity in the motor cortex of resting human brain using echo-planar MRI," *Magnetic Resonance in Medicine*, vol. 34, no. 4, pp. 537–541, 1995.

[5] F. Bai, W. Liao, D. R. Watson et al., "Abnormal whole-brain functional connection in amnestic mild cognitive impairment patients," *Behavioural Brain Research*, vol. 216, no. 2, pp. 666–672, 2011.

[6] R. L. Buckner, J. R. Andrews-Hanna, and D. L. Schacter, "The brain's default network: anatomy, function, and relevance to disease," *Annals of the New York Academy of Sciences*, vol. 1124, pp. 1–38, 2008.

[7] G. Chen, B. D. Ward, C. Xie et al., "Classification of Alzheimer disease, mild cognitive impairment, and normal cognitive status with large-scale network analysis based on resting-state functional MR imaging," *Radiology*, vol. 259, no. 1, pp. 213–221, 2011.

[8] M. D. Greicius, G. Srivastava, A. L. Reiss, and V. Menon, "Default-mode network activity distinguishes Alzheimer's disease from healthy aging: evidence from functional MRI," *Proceedings of the National Academy of Sciences of the United States of America*, vol. 101, no. 13, pp. 4637–4642, 2004.

[9] Y. Liu, C. Yu, X. Zhang et al., "Impaired long distance functional connectivity and weighted network architecture in alzheimer's disease," *Cerebral Cortex*, vol. 24, no. 6, pp. 1422–1435, 2014.

[10] C. Sorg, V. Riedl, M. Mühlau et al., "Selective changes of resting-state networks in individuals at risk for Alzheimer's disease," *Proceedings of the National Academy of Sciences of the United States of America*, vol. 104, no. 47, pp. 18760–18765, 2007.

[11] K. Wang, M. Liang, L. Wang et al., "Altered functional connectivity in early Alzheimer's disease: a resting-state fMRI study," *Human Brain Mapping*, vol. 28, no. 10, pp. 967–978, 2007.

[12] H. Yao, Y. Liu, B. Zhou et al., "Decreased functional connectivity of the amygdala in Alzheimer's disease revealed by resting-state fMRI," *European Journal of Radiology*, vol. 82, no. 9, pp. 1531–1538, 2013.

[13] Z. Zhang, Y. Liu, T. Jiang et al., "Altered spontaneous activity in Alzheimer's disease and mild cognitive impairment revealed by Regional Homogeneity," *NeuroImage*, vol. 59, no. 2, pp. 1429–1440, 2012.

[14] B. Zhou, Y. Liu, Z. Zhang et al., "Impaired functional connectivity of the thalamus in Alzheimer's disease and mild cognitive impairment: a resting-state fMRI study," *Current Alzheimer Research*, vol. 10, no. 7, pp. 754–766, 2013.

[15] R. Bajo, F. Maestú, A. Nevado et al., "Functional connectivity in mild cognitive impairment during a memory task: implications for the disconnection hypothesis," *Journal of Alzheimer's Disease*, vol. 22, no. 1, pp. 183–193, 2010.

[16] X. Delbeuck, F. Collette, and M. Van der Linden, "Is Alzheimer's disease a disconnection syndrome? Evidence from a crossmodal audio-visual illusory experiment," *Neuropsychologia*, vol. 45, no. 14, pp. 3315–3323, 2007.

[17] X. Delbeuck, M. Van Der Linden, and F. Collette, "Alzheimer's disease as a disconnection syndrome?" *Neuropsychology Review*, vol. 13, no. 2, pp. 79–92, 2003.

[18] F. Agosta, M. Pievani, C. Geroldi, M. Copetti, G. B. Frisoni, and M. Filippi, "Resting state fMRI in Alzheimer's disease: beyond the default mode network," *Neurobiology of Aging*, vol. 33, no. 8, pp. 1564–1578, 2012.

[19] G. Allen, H. Barnard, R. McColl et al., "Reduced hippocampal functional connectivity in Alzheimer disease," *Archives of Neurology*, vol. 64, no. 10, pp. 1482–1487, 2007.

[20] M. R. Brier, J. B. Thomas, and B. M. Ances, "Network dysfunction in Alzheimer's disease: refining the disconnection hypothesis," *Brain Connectivity*, vol. 4, no. 5, pp. 299–311, 2014.

[21] M. R. Brier, J. B. Thomas, A. Z. Snyder et al., "Loss of intranetwork and internetwork resting state functional connections with Alzheimer's disease progression," *Journal of Neuroscience*, vol. 32, no. 26, pp. 8890–8899, 2012.

[22] L. Wang, C. M. Roe, A. Z. Snyder et al., "Alzheimer disease family history impacts resting state functional connectivity," *Annals of Neurology*, vol. 72, no. 4, pp. 571–577, 2012.

[23] L. Wang, Y. Zang, Y. He et al., "Changes in hippocampal connectivity in the early stages of Alzheimer's disease: evidence from resting state fMRI," *NeuroImage*, vol. 31, no. 2, pp. 496–504, 2006.

[24] Z. Dai, C. Yan, Z. Wang et al., "Discriminative analysis of early Alzheimer's disease using multi-modal imaging and multi-level characterization with multi-classifier (M3)," *NeuroImage*, vol. 59, no. 3, pp. 2187–2195, 2012.

[25] C.-Y. Wee, P.-T. Yap, D. Zhang et al., "Identification of MCI individuals using structural and functional connectivity networks," *NeuroImage*, vol. 59, no. 3, pp. 2045–2056, 2012.

[26] D. Zhu, K. Li, D. P. Terry et al., "Connectome-scale assessments of structural and functional connectivity in MCI," *Human Brain Mapping*, vol. 35, no. 7, pp. 2911–2923, 2014.

[27] N. Tzourio-Mazoyer, B. Landeau, D. Papathanassiou et al., "Automated anatomical labeling of activations in SPM using a macroscopic anatomical parcellation of the MNI MRI single-subject brain," *NeuroImage*, vol. 15, no. 1, pp. 273–289, 2002.

[28] H. Yao, B. Zhou, Z. Zhang et al., "Longitudinal alteration of amygdalar functional connectivity in mild cognitive impairment subjects revealed by resting-state FMRI," *Brain Connectivity*, vol. 4, no. 5, pp. 361–370, 2014.

[29] Z. Zhang, Y. Liu, B. Zhou et al., "Altered functional connectivity of the marginal division in Alzheimer's disease," *Current Alzheimer Research*, vol. 11, no. 2, pp. 145–155, 2014.

[30] S. Achard and E. Bullmore, "Efficiency and cost of economical brain functional networks," *PLoS Computational Biology*, vol. 3, no. 2, article e17, 2007.

[31] S. Achard, R. Salvador, B. Whitcher, J. Suckling, and E. Bullmore, "A resilient, low-frequency, small-world human brain functional network with highly connected association cortical hubs," *Journal of Neuroscience*, vol. 26, no. 1, pp. 63–72, 2006.

[32] Y. Liu, M. Liang, Y. Zhou et al., "Disrupted small-world networks in schizophrenia," *Brain*, vol. 131, no. 4, pp. 945–961, 2008.

[33] Y. Liu, C. Yu, M. Liang et al., "Whole brain functional connectivity in the early blind," *Brain*, vol. 130, no. 8, pp. 2085–2096, 2007.

[34] R. Salvador, A. Martínez, E. Pomarol-Clotet, S. Sarró, J. Suckling, and E. Bullmore, "Frequency based mutual information measures between clusters of brain regions in functional magnetic resonance imaging," *NeuroImage*, vol. 35, no. 1, pp. 83–88, 2007.

[35] K. Supekar, V. Menon, D. Rubin, M. Musen, and M. D. Greicius, "Network analysis of intrinsic functional brain connectivity in Alzheimer's disease," *PLoS Computational Biology*, vol. 4, no. 6, Article ID e1000100, 2008.

[36] X. Zhao, Y. Liu, X. Wang et al., "Disrupted small-world brain networks in moderate Alzheimer's disease: a resting-state fMRI study," *PLoS ONE*, vol. 7, no. 3, Article ID e33540, 2012.

[37] R. Salvador, J. Suckling, M. R. Coleman, J. D. Pickard, D. Menon, and E. Bullmore, "Neurophysiological architecture of functional magnetic resonance images of human brain," *Cerebral Cortex*, vol. 15, no. 9, pp. 1332–1342, 2005.

[38] R. Salvador, J. Suckling, C. Schwarzbauer, and E. Bullmore, "Undirected graphs of frequency-dependent functional connectivity in whole brain networks," *Philosophical Transactions of the Royal Society B: Biological Sciences*, vol. 360, no. 1457, pp. 937–946, 2005.

[39] Y. Benjamini and D. Yekutieli, "The control of the false discovery rate in multiple testing under dependency," *The Annals of Statistics*, vol. 29, no. 4, pp. 1165–1188, 2001.

[40] Y. Li, Y. Liu, J. Li et al., "Brain anatomical network and intelligence," *PLoS Computational Biology*, vol. 5, no. 5, Article ID e1000395, 2009.

[41] S. Gauthier, B. Reisberg, M. Zaudig et al., "Mild cognitive impairment," *The Lancet*, vol. 367, no. 9518, pp. 1262–1270, 2006.

[42] R. L. Buckner and D. C. Carroll, "Self-projection and the brain," *Trends in Cognitive Sciences*, vol. 11, no. 2, pp. 49–57, 2007.

[43] M. E. Raichle, A. M. MacLeod, A. Z. Snyder, W. J. Powers, D. A. Gusnard, and G. L. Shulman, "A default mode of brain function," *Proceedings of the National Academy of Sciences of the United States of America*, vol. 98, no. 2, pp. 676–682, 2001.

[44] D. Zhang and M. E. Raichle, "Disease and the brain's dark energy," *Nature Reviews Neurology*, vol. 6, no. 1, pp. 15–28, 2010.

[45] B. Dubois, H. H. Feldman, C. Jacova et al., "Research criteria for the diagnosis of Alzheimer's disease: revising the NINCDS-ADRDA criteria," *The Lancet Neurology*, vol. 6, no. 8, pp. 734–746, 2007.

[46] B. Dubois, H. H. Feldman, C. Jacova et al., "Advancing research diagnostic criteria for Alzheimer's disease: the IWG-2 criteria," *The Lancet Neurology*, vol. 13, no. 6, pp. 614–629, 2014.

[47] R. L. Buckner, J. Sepulcre, T. Talukdar et al., "Cortical hubs revealed by intrinsic functional connectivity: mapping, assessment of stability, and relation to Alzheimer's disease," *Journal of Neuroscience*, vol. 29, no. 6, pp. 1860–1873, 2009.

[48] B. C. Dickerson, A. Bakkour, D. H. Salat et al., "The cortical signature of Alzheimer's disease: regionally specific cortical thinning relates to symptom severity in very mild to mild AD dementia and is detectable in asymptomatic amyloid-positive individuals," *Cerebral Cortex*, vol. 19, no. 3, pp. 497–510, 2009.

[49] J. Zhou and W. W. Seeley, "Network dysfunction in Alzheimer's disease and frontotemporal dementia: implications for psychiatry," *Biological Psychiatry*, vol. 75, no. 7, pp. 565–573, 2014.

[50] R. Adolphs, "Cognitive neuroscience of human social behaviour," *Nature Reviews Neuroscience*, vol. 4, no. 3, pp. 165–178, 2003.

[51] H. Eichenbaum, A. P. Yonelinas, and C. Ranganath, "The medial temporal lobe and recognition memory," *Annual Review of Neuroscience*, vol. 30, pp. 123–152, 2007.

[52] L. R. Squire, C. E. L. Stark, and R. E. Clark, "The medial temporal lobe," *Annual Review of Neuroscience*, vol. 27, pp. 279–306, 2004.

[53] E. Braak and H. Braak, "Alzheimer's disease: transiently developing dendritic changes in pyramidal cells of sector CA1 of the Ammon's horn," *Acta Neuropathologica*, vol. 93, no. 4, pp. 323–325, 1997.

[54] H. Braak and E. Braak, "Neuropathological stageing of Alzheimer-related changes," *Acta Neuropathologica*, vol. 82, no. 4, pp. 239–259, 1991.

[55] T. R. Stoub, L. DeToledo-Morrell, and B. C. Dickerson, "Parahippocampal white matter volume predicts Alzheimer's disease risk in cognitively normal old adults," *Neurobiology of Aging*, vol. 35, no. 8, pp. 1855–1861, 2014.

[56] C. Wang, G. T. Stebbins, D. A. Medina et al., "Atrophy and dysfunction of parahippocampal white matter in mild Alzheimer's disease," *Neurobiology of Aging*, vol. 33, no. 1, pp. 43–52, 2012.

[57] B. C. Dickerson and H. Eichenbaum, "The episodic memory system: neurocircuitry and disorders," *Neuropsychopharmacology*, vol. 35, no. 1, pp. 86–104, 2010.

[58] S. Kühn and J. Gallinat, "Segregating cognitive functions within hippocampal formation: a quantitative meta-analysis on spatial navigation and episodic memory," *Human Brain Mapping*, vol. 35, no. 4, pp. 1129–1142, 2014.

[59] N. Nellessen, C. Rottschy, S. B. Eickhoff et al., "Specific and disease stage-dependent episodic memory-related brain activation patterns in Alzheimer's disease: a coordinate-based meta-analysis," *Brain Structure and Function*, 2014.

[60] M. A. Parvaz, T. Maloney, S. J. Moeller et al., "Multimodal evidence of regional midcingulate gray matter volume underlying conflict monitoring," *NeuroImage: Clinical*, vol. 5, pp. 10–18, 2014.

[61] A. J. Shackman, T. V. Salomons, H. A. Slagter, A. S. Fox, J. J. Winter, and R. J. Davidson, "The integration of negative affect, pain and cognitive control in the cingulate cortex," *Nature Reviews Neuroscience*, vol. 12, no. 3, pp. 154–167, 2011.

[62] B. A. Vogt, "Pain and emotion interactions in subregions of the cingulate gyrus," *Nature Reviews Neuroscience*, vol. 6, no. 7, pp. 533–544, 2005.

[63] C. Yu, Y. Zhou, Y. Liu et al., "Functional segregation of the human cingulate cortex is confirmed by functional connectivity based neuroanatomical parcellation," *NeuroImage*, vol. 54, no. 4, pp. 2571–2581, 2011.

[64] G. Sanabria-Diaz, E. Martínez-Montes, and L. Melie-Garcia, "Glucose metabolism during resting state reveals abnormal brain networks organization in the Alzheimer's disease and mild cognitive impairment," *PLoS ONE*, vol. 8, no. 7, Article ID e68860, 2013.

[65] Y. E. Geda, L. S. Schneider, L. N. Gitlin et al., "Neuropsychiatric symptoms in Alzheimer's disease: past progress and anticipation of the future," *Alzheimer's and Dementia*, vol. 9, no. 5, pp. 602–608, 2013.

[66] H. Johansen-Berg, T. E. J. Behrens, E. Sillery et al., "Functional-anatomical validation and individual variation of diffusion tractography-based segmentation of the human thalamus," *Cerebral Cortex*, vol. 15, no. 1, pp. 31–39, 2005.

[67] D. Zhang, A. Z. Snyder, M. D. Fox, M. W. Sansbury, J. S. Shimony, and M. E. Raichle, "Intrinsic functional relations between human cerebral cortex and thalamus," *Journal of Neurophysiology*, vol. 100, no. 4, pp. 1740–1748, 2008.

Research Article

Altered Regional Homogeneity in Rolandic Epilepsy: A Resting-State fMRI Study

Ye-Lei Tang,[1] Gong-Jun Ji,[2,3] Yang Yu,[1,2,3] Jue Wang,[2,3] Zhong-Jin Wang,[1] Yu-Feng Zang,[2,3] Wei Liao,[2,3] and Mei-Ping Ding[1]

[1] *Department of Neurology, the Second Affiliated Hospital of Medial College, Zhejiang University, No. 88 Jiefang Road, Hangzhou 310009, China*

[2] *Center for Cognition and Brain Disorders and the Affiliated Hospital, Hangzhou Normal University, Hangzhou 310015, China*

[3] *Zhejiang Key Laboratory for Research in Assessment of Cognitive Impairments, Hangzhou 310015, China*

Correspondence should be addressed to Wei Liao; weiliao.wl@gmail.com and Mei-Ping Ding; meipingd@163.com

Children with rolandic epilepsy (RE) are often associated with cognitive deficits and behavioral problems. Findings from neurophysiological and neuroimaging studies in RE have now demonstrated dysfunction not only in rolandic focus, but also in distant neuronal circuits. Little is known, however, about whether there is distributed abnormal spontaneous brain activity in RE. Using resting-state functional magnetic resonance imaging (RS-fMRI), the present study aimed to determine whether children with RE show abnormal local synchronization during resting state and, if so, whether these changes could be associated with the behavioral/clinical characteristics of RE. Regional homogeneity (ReHo) in children with RE ($n = 30$) and healthy children ($n = 20$) was computed on resting-state functional MRI data. In comparison with healthy children, children with RE showed increased ReHo in the central, premotor, and prefrontal regions, while they showed decreased ReHo in bilateral orbitofrontal cortex and temporal pole. In addition, the ReHo value in the left orbitofrontal cortex negatively was corrected with performance intelligence quotient in the children with RE. The aberrant local synchronization, not strictly related to primary site of the typical rolandic focus, indicates the neuropathophysiological mechanism of RE. The study findings may shed new light on the understanding of neural correlation of neuropsychological deficiencies in the children with RE.

1. Introduction

Rolandic epilepsy (RE) is an idiopathic focal epilepsy syndrome, which occurs in childhood [1], and results in clinical manifestations of biphasic sharp wave discharges around the rolandic fissure [2, 3]. Since nearly 90% of these children with or without an antiepileptic drug spontaneously remits from seizures before puberty [4], RE is also known as a benign childhood epilepsy. However, children with RE are usually associated with a variety of cognitive disturbances [5, 6], and the underlying pathophysiological mechanisms remain largely unknown.

Although it is a focal epilepsy, findings from neuroimaging studies demonstrate dysfunction not only in rolandic focus but also in distant neuronal circuits. Recent studies using quantitative structural magnetic resonance imaging have shown widespread morphological changes in RE [7–11]. In addition, diffusion tensor imaging examinations have revealed alterations of white matter tracts' integrity [12–15]. Taken together, these structural aberrances associated with their cognitive abnormalities may reflect the progress of long-term impairment. Functional magnetic resonance imaging (fMRI) studies with simultaneously recorded electroencephalogram (EEG), on the other hand, have found concordant focal spike-associated blood-oxygen-level-dependent (BOLD) activation in perisylvian, central, premotor, and prefrontal regions, and all these findings are well corresponding to a typical seizure semiology [16–20]. However, a few studies

found the findings of spike-related BOLD deactivation [21, 22], while others did not.

Recently, resting-state fMRI (rs-fMRI) techniques have been applied to demonstrate intrinsic abnormalities in various types of epilepsy [23–31]. Regional homogeneity (ReHo), as one of the rs-fMRI methods, could measure the functional coherence or synchronization of a given voxel with its nearest voxels, reflecting the local synchronization of the spontaneous BOLD fluctuations [32]. This local synchronization has neurobiological relevance that is likely determined by anatomical, developmental, and neurocognitive factors [33]. Thus, ReHo would serve as a neuroimaging marker to investigate the intact and/or abnormal brain function [34]. It may be speculated that an abnormal ReHo may be a clue to disrupted local functionality and may provide insight into the pathophysiology of brain disorder [35]. Thus, this method has been suggested to investigate the functional modulations and to characterize the neuropsychological changes in the resting state in patients with various clinical populations [36–42]. In particular, abnormal ReHo has mostly been used to depict aberrant spontaneous brain temporal synchrony in epilepsy [43–47]. Little is known, however, about the changes of local synchronization of spontaneous BOLD fluctuations in RE.

Based on previous EEG-fMRI findings regarding spike-related brain functional alterations in RE, we expect to find disrupted local synchronization of spontaneous BOLD fluctuations. We hypothesized that abnormal local synchronization persisted in RE during the interictal period and might be associated with neuropsychological deficiencies. Thus, the aim of the current study was to determine whether children with RE show abnormal local synchronization during resting state and, if so, whether these changes were correlated with the behavioral/clinical characteristics of RE. The purpose of this work was to delineate the neurophysiologically significant abnormal synchronous neuronal activity and neural correlation with neuropsychological deficiencies in the children with RE.

2. Materials and Methods

2.1. Participants. Thirty children whose conditions were diagnosed as RE (18 girls and 12 boys; all right-handed;, age [mean ± SD]: 9.60±2.11 years) at the Second Affiliated Hospital of Zhejiang University School of Medicine were included prospectively in this study. Written informed consent was obtained from all parents. The study protocol was reviewed and approved by the Local Medical Ethics Committee of Center for Cognition and Brain Disorders, Hangzhou Normal University. The inclusion criteria for patients were as follows: (i) clinical and EEG findings evident of RE; (ii) aged between 6 and 13 years; (iii) attending regular schools; (iv) without developmental disabilities; (v) full-scale intelligence quotient (IQ) more than 70; and (vi) without history of addictions or neurologic diseases other than epilepsy. The patients' conditions were diagnosed on the basis of all available clinical and EEG data with the following criteria: (i) recommendations set by the International League against Epilepsy classification [48] and recent literature [2]; (ii) having simple partial,

often facial, motor, or tonic-clonic seizures during sleep; and (iii) having spike-wave in centrotemporal regions, especially nocturnal interictal epileptiform discharges (IEDs) on EEG. Exclusion criteria were (i) focal abnormality in routine structural MRI examinations, (ii) falling asleep during rs-fMRI, and (iii) head motion parameters exceeding 3 mm in translation or 3 degrees in rotation.

Twenty sex- and age-matched healthy children controls (10 girls and 10 boys; all right-handed; age [mean ± SD]: 9.55 ± 2.14 years) were also included in the study. They had no history of neurologic disorders or psychiatric illnesses and no gross abnormalities on brain MR examinations. No significant difference in age ($T = 0.08$, $P = 0.94$) or gender ($\chi^2 = 0.70$, $P = 0.49$) was found between groups. Demographic and clinical information is detailed in Table 1.

2.2. Simultaneous EEG-fMRI Acquisition. All patients underwent one or two simultaneous EEG-fMRI sessions to archive more IED as far as possible. Simultaneous EEG was not recorded in healthy controls. During fMRI acquisition, EEG data was continuously recorded with an MR-compatible EEG recording system (Brain Products, Germany). The 32 Ag/AgCl electrodes (through a 10/20 system) were attached to the scalp with conductive cream. Three electrooculogram/electrocardiogram channels were simultaneously recorded. Twenty-nine EEG electrodes were connected to a BrainAmp amplifier, with a sampling rate of 5 kHz. The amplifier was connected to the recording computer outside the scanner room through a fiber optic cable.

The EEG data was processed offline to filter out MR artifacts and to remove ballistocardiogram artifacts (Brain Vision Analyzer 2.0, Germany). IEDs were marked independently by two experienced electroencephalographers, according to both spatial distribution and morphology. Disagreements about the markers were resolved and consensuses were reached after discussion.

2.3. Neuropsychological Assessment. To test cognitive performance, a neuropsychological evaluation was administered. General intelligence was assessed using the Chinese version of Wechsler Intelligence Scale for Children (WISC-III), which included verbal IQ, performance IQ, and full-scale IQ. In addition, three factorial subscales of WISC-III were used to assess language comprehension, perceptual organization, and memory/attention. All scores were standardized for age and gender.

2.4. fMRI Data Acquisition. Functional and structural imaging data were acquired on a 3.0-Tesla MRI scanner (GE Discovery 750 MRI, General Electric, Milwaukee, WI, USA) at the Center for Cognition and Brain Disorders, Hangzhou Normal University. Foam padding was used to minimize head motion for all subjects. Functional images were acquired using an echoplanar imaging sequence (repetition time = 2000 ms, echo time = 30 ms, and flip angle = 90°). Thirty transverse slices (field of view = 220 × 220 mm^2, in-plane matrix = 64 × 64, slice thickness = 3.2 mm, no interslice gap, and voxel size = 3.44 × 3.44 × 3.2 mm^3) aligned along

TABLE 1: Demographic and clinical characteristics of participants.

Characteristic	Patients ($n = 30$)	Controls ($n = 20$)	P value
Age (years)	9.60 ± 2.11	9.55 ± 2.14	0.935[a]
Sex (female/male)	18/12	10/10	0.485[b]
IQ			
Full-scale IQ	110.0 ± 14.95	116.2 ± 16.51	0.210[a]
Verbal IQ	103.5 ± 14.75	118.9 ± 16.94	**0.003**[a]
Performance IQ	115.2 ± 16.45	110.8 ± 15.75	0.378[a]
Education (years)	3.4 ± 1.96	4.2 ± 2.22	0.186[a]
Onset age (years)	7.53 ± 2.11	N.A.	—
Duration (months)	26.43 ± 35.66	N.A.	—
FD (mm)	0.18 ± 0.11	0.14 ± 0.08	0.210[c]

The intelligence quotient (IQ) scores in patients and controls were based on the results of 29 and 16 participants, respectively. FD denotes mean framewise displacement. The other values are illustrated as mean ± SD.
[a]Two-sample t-test.
[b]Chi-square test.
[c]Mann Whitney U-test.

the anterior commissure-posterior commissure line were acquired. In each session, a total of 240 volumes were collected, resulting in a total scan time of 480 s. For each patient, one or two sessions were acquired. Subjects were instructed simply to rest with their eyes closed, not to think of anything in particular, and not to fall asleep. Subsequently, 3D T1-weighted anatomical images were acquired in the sagittal orientation using a magnetization prepared rapid acquisition gradient-echo sequence (repetition time = 8.06 ms, echo time = 3.136 ms, flip angle = 8°, field of view = 256×256 mm^2, matrix size = 256×256, slice thickness = 1 mm, no interslice gap, voxel size = $1 \times 1 \times 1$ mm^3, and 176 slices) on each subject.

2.5. fMRI Data Preprocessing. Considering that the healthy controls underwent one session, the first session of RE was selected for further comparison. Preprocessing of functional images was carried out using DPARSF (http://www.restfmri.net) [49] and SPM8 (http://www.fil.ion.ucl.ac.uk/spm) toolkits. Functional images, after exclusion of the first 10 images, were initially corrected by slice-timing and realignment. No translation or rotation parameters in any given data set exceeded ±3 mm or ±3°. Moreover, the mean framewise displacement (FD) was computed by averaging FDi from every time point for each subject [50]. There were no differences for the mean FD between groups ($P = 0.21$) (Table 1). Individual 3D T1-weighted anatomical image was coregistered to functional images. The 3D T1-weighted anatomical images were segmented (grey matter, white matter, and cerebrospinal fluid). A nonlinear spatial deformation was then calculated from the grey matter images to a grey matter template in Montreal Neurological Institute space using 12 parameters affine linear transformation. This transformation was then applied to the functional images, which were resliced at a resolution of $3 \times 3 \times 3$ mm^3. Several sources of spurious variances (six head motion parameters, mean FD, global brain signal, and averaged signal from white matter signal and cerebrospinal fluid) were regressed out using a

multiple linear regression analysis. Finally, data with linear trend were removed, and temporal band-pass was filtered (0.01–0.08 Hz).

2.6. ReHo Analysis. The similarity of the time series within a cluster was measured based on the regional homogeneity method [32]. The ReHo of the voxel at the center of the 27 nearest neighboring voxels cluster was calculated by Kendall's coefficient of concordance algorithm by REST software (http://www.restfmri.net) [51]. For standardization purposes, the individual ReHo map was divided by its whole brain mean ReHo value. Finally, the standardized ReHo maps were spatially smoothed with 4 mm of full width at half maximum isotropic Gaussian kernel.

2.7. Statistical Analysis. Differences in demographic and clinical data between RE children and healthy children were analyzed using a two-sample t-test and χ^2-test.

To investigate the differences in local synchronization between two groups, a two-sample t-test was performed on the individual standardized ReHo maps. Significant threshold was set at a corrected $P < 0.05$ (combined height threshold $P < 0.01$ and a minimum cluster size of 20 voxels) using the AlphaSim program in the REST software, which applied Monte Carlo simulation to calculate the probability of false positive detection by taking into consideration both the individual voxel probability thresholding and cluster size.

To explore the relationship between local synchronization and clinical behavior in children with RE, the averaged ReHo value of each sphere region of interests (centered at the peak voxel of each abnormal area, radius = 3 mm) was correlated with the clinical factor (epilepsy duration) and neuropsychological variables (including full-scale IQ, verbal IQ, and performance IQ) using Pearson correlation analysis on the patients group. The statistical threshold was set at $P < 0.05$.

3. Results

3.1. Neuropsychological Results. Demographic characteristics and neuropsychological scores are shown in Table 1. Children with RE had a significantly lower score of verbal IQ ($T = 3.179$, $P = 0.003$). There was no significant difference in full-scale IQ and performance IQ between the two groups (Table 1). There was also no significant correlation between IQ (full-scale IQ, verbal IQ, and performance IQ) and clinical characteristics (age of onset and duration of disease).

3.2. Between-Group ReHo Differences. The results obtained from the two-sample t-test showed significant differences in ReHo between two groups ($P < 0.05$, AlphaSim corrected; Figure 1, Table 2). Compared with healthy children, children with RE showed significantly increased ReHo in the bilateral precentral gyrus, right postcentral gyrus, right supramarginal gyrus, left inferior and superior frontal gyrus, and superior parietal lobule, while decreased ReHo was observed mainly in the bilateral temporal pole, bilateral orbitofrontal area, and putamen.

TABLE 2: Brain regions showing abnormal regional homogeneity in patients with rolandic epilepsy.

Brain region	MNI coordinates (X Y Z)	BA	t value	Voxel number
Patients > controls				
Precentral gyrus R.	48 3 30	4	4.73	44
Precentral gyrus L.	−51 3 24	4	3.96	31
Postcentral gyrus R.	58 −12 24	4/3	4.56	97
Inferior frontal gyrus L.	−51 18 24	45/46	3.35	31
Superior frontal gyrus L.	−18 12 72	6	3.70	22
Superior parietal lobule L.	12 −78 51	7	4.41	316
Superior parietal lobule R.	30 −63 63	7	5.59	87
Supramarginal gyrus R.	69 −39 33	40	4.47	44
Angular gyrus R.	45 −78 36	39	3.91	93
Patients < controls				
Temporal pole L.	−51 12 −33	38	−3.76	64
Temporal pole R.	54 0 −33	38/21	−4.10	162
Obitofrontal area L.	30 45 −12	11	−4.28	308
Obitofrontal area R.	−15 33 −18	11	−4.96	340
Angular gyrus L.	−42 −51 24	39	−4.26	20
Cerebellum	−12 −69 −33	—	−3.82	39
Cerebellum	−15 −63 −51	—	−5.17	430
Putamen R.	30 6 −6	—	−3.69	44

MNI: Montreal Neurological Institute; BA: Brodmann area; L: left; R: right.

3.3. Correlation between ReHo of Affected Areas with Clinical Features. Significant positive correlations were observed between the epilepsy duration and local synchronization in the left superior frontal gyrus ($r = 0.42$, $P = 0.020$). The performance IQ was negatively corrected with local synchronization in the left orbitofrontal area ($r = 0.4569$, $P = 0.010$) (Figure 1). Note that these two ROI's correlations have not survived multiple comparisons. There were no significant correlations between ReHo in the other abnormal areas and clinical and/or neuropsychological variables.

4. Discussion

To the best of our knowledge, this is the first study to examine local BOLD coherence in children with RE during resting state. Compared with healthy children, children with RE showed increased ReHo at the lower part of sensorimotor cortex and cortices around rolandic fissure, and they showed decreased ReHo in the limbic system. In addition, aberrant ReHo of several brain regions was associated with clinical or neuropsychological variables. The current findings extend understanding to the neuropathophysiological mechanisms of RE.

Epilepsy documents the altered neural substrates with hyperexcitable seizure networks [52]. Electrophysiological findings from both animal models and human brains have suggested an increased synchronization in the epileptogenic zone during ictal and interictal states [53, 54]. Therefore, it is worthwhile to investigate local synchronization

of spontaneous fMRI BOLD signals in children with RE. Recently, ReHo was developed to characterize the coherence of spontaneous neuronal activity and was utilized to detect spontaneous brain dysfunction in various epileptic brains [43, 45, 46]. This study, using this method, aimed to test a hypothesis that the abnormal regional synchronization persists in children with RE in the interictal period.

Previous simultaneous EEG and fMRI studies found that interictal discharge could result in facial sensorimotor area involvement in RE seizures [17–22]. As expected, it was found that children with RE showed increased ReHo in the lower part of sensorimotor area and cortices around rolandic fissure. This is in line with the typical seizure semiology of RE that manifests paresthesia and jerking of the mouth, face, and hand [55]. Moreover, the study finding suggests that the abnormal function not only occurs during interictal discharges, but also exists throughout the interical period.

In children with RE, increased local BOLD synchronization was also observed in the left premotor cortex (Brodmann area 6) (Figure 1 and Table 2). The premotor cortex not only was involved in the planning of complex and coordinated movements, but also was associated with spatial attention and executive control [56]. Functionally, premotor cortex was connected with attention- and control-related networks in healthy juveniles and young adults. A previous study found that IEDs could cause hemodynamic changes in premotor regions in children with RE, indicating the motor and cognitive dysfunctions [21]. In the current study, deficits of BOLD coherence along with a positive
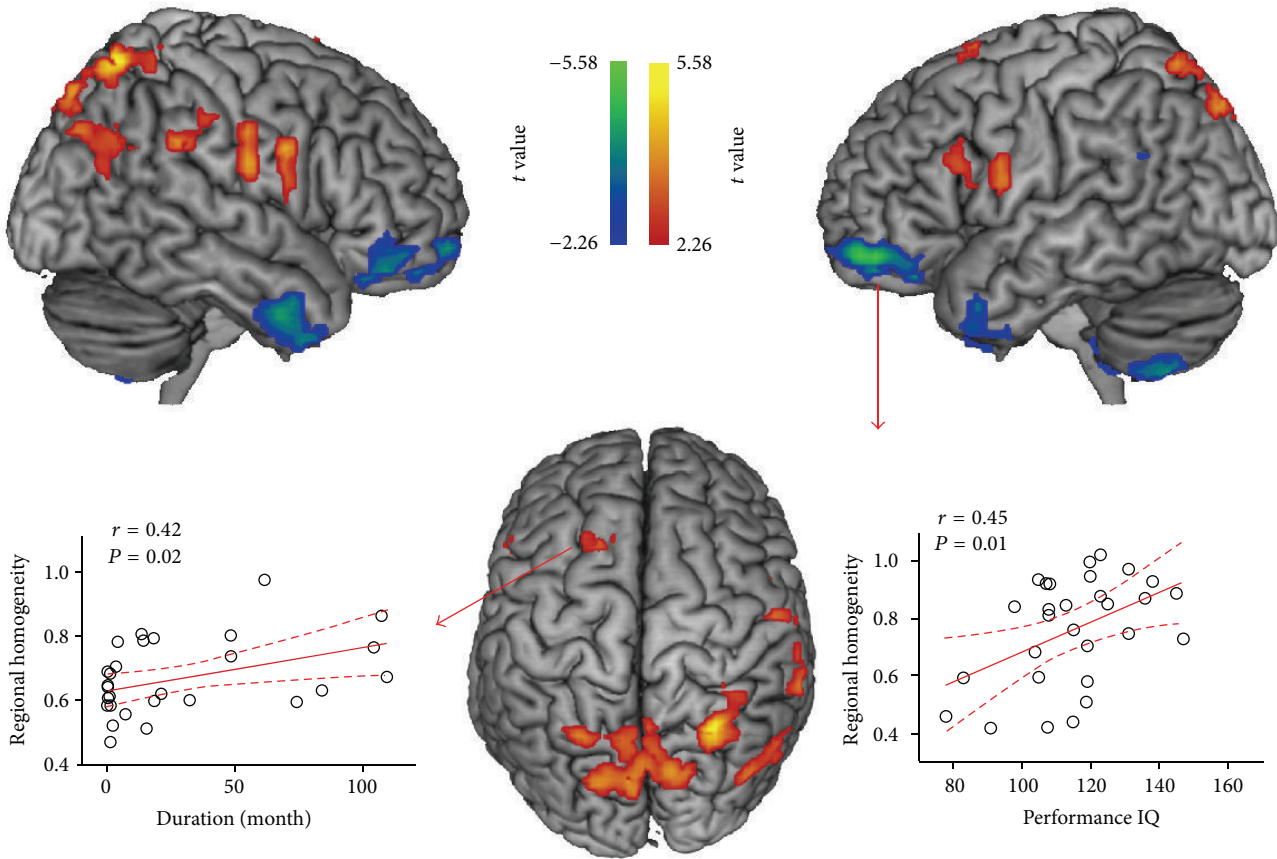
FIGURE 1: Brain regions showing abnormal regional homogeneity in children with rolandic epilepsy. Two-line graph indicated the local synchronization in left superior gyrus and left orbitofrontal area showing significant correlation with disease duration and performance IQ, respectively. The warm and cool colors indicate brain regions with increased and decreased regional homogeneity in children with RE, respectively.

correlation with disease severity provide evidence for a neural correlation of RE. In addition to the motor and premotor area, the cerebellum and striatum also play important roles in motor control. The decreased ReHo of these regions revealed their dysfunction in RE patients. It also suggested that the abnormal cortico-striato-cerebellar circuit might be related to the clinical syndrome of these patients.

We also observed increased ReHo in superior parietal lobule (SPL), which related to the posterior part of attention system [57]. Since SPL is posterior to the central area, we speculated that the increase might be a result of the propagation of the epileptic discharges [58]. Behavior study has revealed the impairment of spatial attention in RE patients [59]. Our findings complementally implicated the brain functional mechanism of this cognitive impairment. Future studies correlating with neurophysiology measurements with ReHo, the local neural synchronization, are warranted to validate such behavior-neuroimaging association.

The most remarkable finding in this study was the significant decrease in local synchronization in the limbic system (including bilateral orbitofrontal area and temporal pole) in the children with RE (Figure 1 and Table 2). A previous structural MRI study found subtle cortical abnormality in

orbitofrontal region, suggesting the pathomorphology in the active phase of brain development in patients with RE [9]. However, this EEG-fMRI study did not find IED-related BOLD hemodynamic changes in this brain region, which could be attributed to a possibility that this might be a form of RE epilepsy with signs of cortical hyperexcitability that vary with time in terms of rate and side [19, 20]. The study results first provide the evidence of BOLD synchronization that the children with RE have disturbed orbitofrontal area functions. The human orbitofrontal cortex receives information from motor, limbic, and sensory cortices, reflecting sensory integration for executive motor control [60]. It could be speculated that sensory integration dysfunction in RE might be attributed to any harmful causes, for example, ictal epileptic activity, in addition to the neuronal inhibition induced by the IED activity. Moreover, this dysfunction was associated with performance IQ (Figure 1), which could imply an underlying neural correlation of neuropsychological deficiencies in children with RE.

The present work involved several limitations. First, the antiepileptic medication taken by some patients might confound the results; in future studies, homogeneous patients should be grouped more appropriately and the medication

dose should be detailed. Second, the sample size used was modest; larger sample size may provide further insights. Third, we observed the IDE in only several patients. In this case, we did not analyze the IED-related BOLD hemodynamic changes in this group. Finally, the local synchronization was measured at a low sampling rate, which impeded investigating high rhythm alternation in RE. Future study should use advanced data acquisition sequences to enable whole brain fMRI scanning at subsecond temporal resolution [61].

5. Conclusions

The present study examined the local synchronization of BOLD fluctuation, providing a description of the pathology mechanism of RE. Children with RE showed increased regional homogeneity in central, premotor, and prefrontal regions, and the findings were consistent with the location of typical epileptic focus of RE. Children with RE also showed decreased regional homogeneity in the limbic system, not strictly related to primary site of the typical focus, suggesting impaired sensory integration in RE. The present results may shed new light on the understanding of neural correlation of neuropsychological deficiencies in children with RE.

Conflict of Interests

The authors declare that there is no conflict of interests regarding the publication of this paper.

Acknowledgments

References

[1] E. C. Wirrell, "Benign epilepsy of childhood with centrotemporal spikes," *Epilepsia*, vol. 39, no. 4, pp. S32–S41, 1998.

[2] C. P. Panayiotopoulos, M. Michael, S. Sanders, T. Valeta, and M. Koutroumanidis, "Benign childhood focal epilepsies: assessment of established and newly recognized syndromes," *Brain*, vol. 131, no. part 9, pp. 2264–2286, 2008.

[3] R. Guerrini and S. Pellacani, "Benign childhood focal epilepsies," *Epilepsia*, vol. 53, no. 4, pp. 9–18, 2012.

[4] U. Stephani and G. Carlsson, "The spectrum from BCECTS to LKS: the rolandic EEG trait—impact on cognition," *Epilepsia*, vol. 47, supplement 2, pp. 67–70, 2006.

[5] S. Chan and W. Lee, "Benign epilepsy in children," *Journal of the Formosan Medical Association*, vol. 110, no. 3, pp. 134–144, 2011.

[6] C. S. Camfield and P. R. Camfield, "Rolandic epilepsy has little effect on adult life 30 years later: a population-based study," *Neurology*, vol. 82, no. 13, pp. 1162–1166, 2014.

[7] R. Sarkis, E. Wyllie, R. C. Burgess, and T. Loddenkemper, "Neuroimaging findings in children with benign focal epileptiform discharges," *Epilepsy Research*, vol. 90, no. 1-2, pp. 91–98, 2010.

[8] H. Kanemura, S. Hata, K. Aoyagi, K. Sugita, and M. Aihara, "Serial changes of prefrontal lobe growth in the patients with benign childhood epilepsy with centrotemporal spikes presenting with cognitive impairments/behavioral problems," *Brain and Development*, vol. 33, no. 2, pp. 106–113, 2011.

[9] G. M. Overvliet, R. M. H. Besseling, J. F. A. Jansen et al., "Early onset of cortical thinning in children with rolandic epilepsy," *NeuroImage: Clinical*, vol. 2, no. 1, pp. 434–439, 2013.

[10] J. J. Lin, J. D. Riley, D. A. Hsu et al., "Striatal hypertrophy and its cognitive effects in new-onset benign epilepsy with centrotemporal spikes," *Epilepsia*, vol. 53, no. 4, pp. 677–685, 2012.

[11] H. R. Pardoe, A. T. Berg, J. S. Archer, R. K. Fulbright, and G. D. Jackson, "A neurodevelopmental basis for BECTS: evidence from structural MRI," *Epilepsy Research*, vol. 105, no. 1-2, pp. 133–139, 2013.

[12] C. Ciumas, M. Saignavongs, F. Ilski et al., "White matter development in children with benign childhood epilepsy with centro-temporal spikes," *Brain*, vol. 137, part 4, pp. 1095–1106, 2014.

[13] S. E. Kim, J. H. Lee, H. K. Chung, S. M. Lim, and H. W. Lee, "Alterations in white matter microstructures and cognitive dysfunctions in benign childhood epilepsy with centrotemporal spikes," *European Journal of Neurology*, vol. 21, no. 5, pp. 708–717, 2014.

[14] R. M. Besseling, J. F. Jansen, G. M. Overvliet et al., "Reduced structural connectivity between sensorimotor and language areas in rolandic epilepsy," *PLoS ONE*, vol. 8, no. 12, Article ID e83568, 2013.

[15] F. Xiao, Q. Chen, X. Yu et al., "Hemispheric lateralization of microstructural white matter abnormalities in children with active benign childhood epilepsy with centrotemporal spikes (BECTS): a preliminary DTI study," *Journal of the Neurological Sciences*, vol. 336, no. 1-2, pp. 171–179, 2014.

[16] M. Siniatchkin, F. Moeller, J. Jacobs et al., "Spatial filters and automated spike detection based on brain topographies improve sensitivity of EEG-fMRI studies in focal epilepsy," *NeuroImage*, vol. 37, no. 3, pp. 834–843, 2007.

[17] R. Boor, J. Jacobs, A. Hinzmann et al., "Combined spike-related functional MRI and multiple source analysis in the non-invasive spike localization of benign rolandic epilepsy," *Clinical Neurophysiology*, vol. 118, no. 4, pp. 901–909, 2007.

[18] S. Boor, G. Vucurevic, C. Pfleiderer, P. Stoeter, G. Kutschke, and R. Boor, "EEG-related functional MRI in benign childhood epilepsy with centrotemporal spikes," *Epilepsia*, vol. 44, no. 5, pp. 688–692, 2003.

[19] R. A. J. Masterton, A. S. Harvey, J. S. Archer et al., "Focal epileptiform spikes do not show a canonical BOLD response in patients with benign rolandic epilepsy (BECTS)," *NeuroImage*, vol. 51, no. 1, pp. 252–260, 2010.

[20] R. A. J. Masterton, G. D. Jackson, and D. F. Abbott, "Mapping brain activity using event-related independent components analysis (eICA): specific advantages for EEG-fMRI," *NeuroImage*, vol. 70, pp. 164–174, 2013.

[21] U. Lengler, I. Kafadar, B. A. Neubauer, and K. Krakow, "fMRI correlates of interictal epileptic activity in patients with idiopathic benign focal epilepsy of childhood: a simultaneous EEG-functional MRI study," *Epilepsy Research*, vol. 75, no. 1, pp. 29–38, 2007.

[22] J. S. Archer, R. S. Briellman, D. F. Abbott, A. Syngeniotis, R. M. Wellard, and G. D. Jackson, "Benign epilepsy with centro-temporal spikes: Spike triggered fMRI shows somato-sensory cortex activity," *Epilepsia*, vol. 44, no. 2, pp. 200–204, 2003.

[23] W. Liao, Z. Zhang, D. Mantini et al., "Dynamical intrinsic functional architecture of the brain during absence seizures," *Brain Structure and Function*, 2013.

[24] W. Liao, Z. Zhang, D. Mantini et al., "Relationship between large-scale functional and structural covariance networks in idiopathic generalized epilepsy," *Brain Connect*, vol. 3, no. 3, pp. 240–254, 2013.

[25] W. Liao, Z. Zhang, Z. Pan et al., "Altered functional connectivity and small-world in mesial temporal lobe epilepsy," *PLoS ONE*, vol. 5, no. 1, Article ID e8525, 2010.

[26] W. Liao, Z. Zhang, Z. Pan et al., "Default mode network abnormalities in mesial temporal lobe epilepsy: a study combining fMRI and DTI," *Human Brain Mapping*, vol. 32, no. 6, pp. 883–895, 2011.

[27] Z. Zhang, W. Liao, Z. Wang et al., "Epileptic discharges specifically affect intrinsic connectivity networks during absence seizures," *Journal of the Neurological Sciences*, vol. 336, no. 1-2, pp. 138–145, 2014.

[28] Z. Zhang, G. Lu, Y. Zhong et al., "fMRI study of mesial temporal lobe epilepsy using amplitude of low-frequency fluctuation analysis," *Human Brain Mapping*, vol. 31, no. 12, pp. 1851–1861, 2010.

[29] Z. Zhang, G. Lu, Y. Zhong et al., "Impaired perceptual networks in temporal lobe epilepsy revealed by resting fMRI," *Journal of Neurology*, vol. 256, no. 10, pp. 1705–1713, 2009.

[30] Z. Zhang, G. Lu, Y. Zhong et al., "Altered spontaneous neuronal activity of the default-mode network in mesial temporal lobe epilepsy," *Brain Research*, vol. 1323, pp. 152–160, 2010.

[31] Z. Zhang, G. Lu, Y. Zhong et al., "Impaired attention network in temporal lobe epilepsy: a resting FMRI study," *Neuroscience Letters*, vol. 458, no. 3, pp. 97–101, 2009.

[32] Y. Zang, T. Jiang, Y. Lu, Y. He, and L. Tian, "Regional homogeneity approach to fMRI data analysis," *NeuroImage*, vol. 22, no. 1, pp. 394–400, 2004.

[33] L. Jiang, T. Xu, Y. He et al., "Toward neurobiological characterization of functional homogeneity in the human cortex: regional variation, morphological association and functional covariance network organization," *Brain Structure and Function*, 2014.

[34] X. N. Zuo, T. Xu, L. Jiang et al., "Toward reliable characterization of functional homogeneity in the human brain: preprocessing, scan duration, imaging resolution and computational space," *NeuroImage*, vol. 65, pp. 374–386, 2013.

[35] Y. He, L. Wang, Y. Zang et al., "Regional coherence changes in the early stages of Alzheimer's disease: a combined structural and resting-state functional MRI study," *NeuroImage*, vol. 35, no. 2, pp. 488–500, 2007.

[36] C. Zhu, Y. Zang, Q. Cao et al., "Fisher discriminative analysis of resting-state brain function for attention-deficit/hyperactivity disorder," *NeuroImage*, vol. 40, no. 1, pp. 110–120, 2008.

[37] Y. Liu, K. Wang, C. YU et al., "Regional homogeneity, functional connectivity and imaging markers of Alzheimer's disease: a review of resting-state fMRI studies," *Neuropsychologia*, vol. 46, no. 6, pp. 1648–1656, 2008.

[38] Z. Liu, C. Xu, Y. Xu et al., "Decreased regional homogeneity in insula and cerebellum: A resting-state fMRI study in patients with major depression and subjects at high risk for major depression," *Psychiatry Research—Neuroimaging*, vol. 182, no. 3, pp. 211–215, 2010.

[39] Q. Z. Wu, D. M. Li, W. H. Kuang et al., "Abnormal regional spontaneous neural activity in treatment-refractory depression revealed by resting-state fMRI," *Human Brain Mapping*, vol. 32, no. 8, pp. 1290–1299, 2011.

[40] T. Wu, X. Long, Y. Zang et al., "Regional homogeneity changes in patients with parkinson's disease," *Human Brain Mapping*, vol. 30, no. 5, pp. 1502–1510, 2009.

[41] J. Paakki, J. Rahko, X. Long et al., "Alterations in regional homogeneity of resting-state brain activity in autism spectrum disorders," *Brain Research*, vol. 1321, pp. 169–179, 2010.

[42] D. K. Shukla, B. Keehn, and R. A. Müller, "Regional homogeneity of fMRI time series in autism spectrum disorders," *Neuroscience Letters*, vol. 476, no. 1, pp. 46–51, 2010.

[43] T. Yang, Z. Fang, J. Ren et al., "Altered spontaneous activity in treatment-naive childhood absence epilepsy revealed by regional homogeneity," *Journal of the Neurological Sciences*, vol. 340, no. 1-2, pp. 58–62, 2014.

[44] K. E. Weaver, W. A. Chaovalitwongse, E. J. Novotny, A. Poliakov, T. G. Grabowski, and J. G. Ojemann, "Local functional connectivity as a pre-surgical tool for seizure focus identification in non-lesion, focal epilepsy," *Frontiers in Neurology*, vol. 4, article 43, 2013.

[45] Y. Zhong, G. Lu, Z. Zhang, Q. Jiao, K. Li, and Y. Liu, "Altered regional synchronization in epileptic patients with generalized tonic-clonic seizures," *Epilepsy Research*, vol. 97, no. 1-2, pp. 83–91, 2011.

[46] H. Zeng, R. Pizarro, V. A. Nair, C. La, and V. Prabhakaran, "Alterations in regional homogeneity of resting-state brain activity in mesial temporal lobe epilepsy.," *Epilepsia*, vol. 54, no. 4, pp. 658–666, 2013.

[47] K. Mankinen, X. Long, J. Paakki et al., "Alterations in regional homogeneity of baseline brain activity in pediatric temporal lobe epilepsy," *Brain research*, vol. 1373, pp. 221–229, 2011.

[48] ILAE, "Proposal for revised classification of epilepsies and epileptic syndromes. Commission on Classification and Terminology of the International League Against Epilepsy," *Epilepsia*, vol. 30, no. 4, pp. 389–399, 1989.

[49] Y. Chao-Gan and Z. Yu-Feng, "DPARSF: a MATLAB toolbox for "pipeline" data analysis of resting-state fMRI," *Frontiers in Systems Neuroscience*, vol. 4, p. 13, 2010.

[50] J. D. Power, K. A. Barnes, A. Z. Snyder, B. L. Schlaggar, and S. E. Petersen, "Spurious but systematic correlations in functional connectivity MRI networks arise from subject motion," *NeuroImage*, vol. 59, no. 3, pp. 2142–2154, 2012.

[51] X. Song, Z. Dong, X. Long et al., "REST: a Toolkit for resting-state functional magnetic resonance imaging data processing," *PLoS ONE*, vol. 6, no. 9, Article ID e25031, 2011.

[52] R. A. B. Badawy, D. R. Freestone, A. Lai, and M. J. Cook, "Epilepsy: ever-changing states of cortical excitability," *Neuroscience*, vol. 222, pp. 89–99, 2012.

[53] O. David, I. Guillemain, S. Saillet et al., "Identifying neural drivers with functional MRI: an electrophysiological validation," *PLoS Biology*, vol. 6, no. 12, article e315, pp. 2683–2697, 2008.

[54] C. A. Schevon, J. Cappell, R. Emerson et al., "Cortical abnormalities in epilepsy revealed by local EEG synchrony," *NeuroImage*, vol. 35, no. 1, pp. 140–148, 2007.

[55] F. Moeller, J. Moehring, I. Ick et al., "EEG-fMRI in atypical benign partial epilepsy," *Epilepsia*, vol. 54, no. 8, pp. e103–e108, 2013.

[56] B. J. Shannon, M. E. Raichle, A. Z. Snyder et al., "Premotor functional connectivity predicts impulsivity in juvenile offenders," *Proceedings of the National Academy of Sciences of the United States of America*, vol. 108, no. 27, pp. 11241–11245, 2011.

[57] M. D. Fox, M. Corbetta, A. Z. Snyder, J. L. Vincent, and M. E. Raichle, "Spontaneous neuronal activity distinguishes human dorsal and ventral attention systems," *Proceedings of the National Academy of Sciences of the United States of America*, vol. 103, no. 26, pp. 10046–10051, 2006.

[58] K. Y. Jung, J. M. Kim, and D. W. Wook Kim, "Patterns of interictal spike propagation across the central sulcus in benign rolandic epilepsy," *Clinical Electroencephalography*, vol. 34, no. 3, pp. 153–157, 2003.

[59] L. Deltour, L. Querné, M. Vernier-Hauvette, and P. Berquin, "Deficit of endogenous spatial orienting of attention in children with benign epilepsy with centrotemporal spikes (BECTS)," *Epilepsy Research*, vol. 79, no. 2-3, pp. 112–119, 2008.

[60] E. T. Rolls, "The functions of the orbitofrontal cortex," *Brain and Cognition*, vol. 55, no. 1, pp. 11–29, 2004.

[61] D. A. Feinberg, S. Moeller, S. M. Smith et al., "Multiplexed echo planar imaging for sub-second whole brain fmri and fast diffusion imaging," *PLoS ONE*, vol. 5, no. 12, Article ID e15710, 2010.